Fakultät für Mathematik, Informatik und Naturwissenschaften | RWTH AACHEN UNIVERSITY

“Novel Manganese Catalytic Systems in the Activation of Si–H and H–H bonds”

Von der Fakultät für Mathematik, Informatik und Naturwissenschaften der RWTH Aachen University zur Erlangung des akademischen Grades eines Doktors der Naturwissenschaften genehmigte Dissertation

vorgelegt von

Emanuele Antico, M. Sc.

aus

Macerata, Italien.

Berichter:

Prof. Dr. rer. nat. Walter Leitner

Prof. Dr. rer. nat. Jürgen Klankermayer

Tag der mündlichen Prüfung: 18.03.2024

Diese Dissertation ist auf den Internetseiten der Universitätsbibliothek verfügbar.

To my family

Declaration of Authorship

I, Emanuele Antico,

declare that this thesis and the work presented in it are my own and has been generated by me

as the result of my own original research.

Hiermit erkläre ich an Eides statt/I do solemnly swear that:

1. This work was done wholly or mainly while in candidature for the doctoral degree at this faculty and university;

2. Where any part of this thesis has previously been submitted for a degree or any other qualification at this university or any other institution, this has been clearly stated;

3. Where I have consulted the published work of others or myself, this is always clearly attributed;

4. Where I have quoted from the work of others or myself, the source is always given. This thesis is entirely my own work, with the exception of such quotations;

5. I have acknowledged all major sources of assistance;

6. Where the thesis is based on work done by myself jointly with others, I have made clear

exactly what was done by others and what I have contributed myself;

7. Parts of this work have been published before as:

- Antico, E.; Schlichter, P.; Werlé, C.; Leitner, W. *JACS Au* **2021**, *1* (6), 742–749.

- Antico, E.; Leutzsch, M.; Wessel, N.; Weyhermüller, T.; Werlé, C.; Leitner, W. *Chem. Sci.* **2023**, *14* (1), 54–60.

This thesis was prepared at the MAX PLANCK INSTITUTE FOR CHEMICAL ENERGY CONVERSION between January 2020 and September 2023 under the scientific supervision of Prof. Dr. WALTER LEITNER.

Acknowledgements

Scientific work, in its rigorous structure, can be a very lonely journey. In this pages, I wish to take a moment to express my appreciation to all the people that made my Ph.D. experience significantly more enjoyable and manageable through their presence and support.

I would like to begin thanking Dr. Jacopo de Bellis and Dr. Souha Kacem for their early inclusion of me in various social activities, even before my arrival, when I shortly came to visit the institute. Their actions quickly helped me to expand my social involvement with people across multiple departments.

I am also deeply appreciative of my friends Peter Schlichter, Michał Mrozowicz and Beatrice Lansbergen that I got to know during my first weeks here in Mülheim an der Ruhr. We all started our Ph.D. basically at the same time, and through these four years they have been a constant and refreshing presence that added a lot of color to my time.

My gratitude also goes to Jeroen Vossen and Johannes Zenner, who significantly assisted me in navigating the initial challenges of transitioning from Italy to Germany, allowing me to reach a comfort zone in Mülheim pretty soon. Johannes, in particular, has been a patient and invaluable friend in moments of fragility and personal uncertainty.

I would also like to acknowledge the individuals who made the time in the institute more pleasant. Alexander Schmitz, friend and official disk jockey of the lab, has been a constant source of smiles, jokes and help inside and outside the lab. Dr. Lisa Goclik, always positive and eager to organize team-events, has been able to make the challenging times of the move to the new building significantly smoother and light-hearted. Additionally, I extend my thanks to all the people (that I will not list) that shared with me the working environment, the conference trips, the group trip and the laboratory space, for the nice times together.

On a more scientific note, I particularly enjoyed collaborating with Peter Schlichter, with whom I co-first-authored the publication arising from the first chapter of this work. I also value the brief period I spent working with my friend and chemical engineer Niklas Wessel, who allowed me to work with his miniplant under his supervision. We measured together the flow FT-IR reported in Chapter 3, which helped us to identify the "$Mn(CO)_3$" as the active framework. Working with him elbow to elbow, gave me very interesting insights on the approach of engineers towards chemistry. Also, many thanks to Dr. Thomas Weyhermüller, Bernd Mienert and Helena Randel that took care of selecting single crystals for XRD, performed the measurements and refined the structures. Moreover, thanks to our analytical team for facilitating use of routine instrumentation. In particular, a special thank you goes to Alina Jakubowski, who

injected manually all the gaseous samples for GC-TCD analysis that are present in the work, and created the calibration curves for the TCD detector.

A thank you goes to Dr. Christophe Werlé, who taught me to conduct research independently and entrusted me with enjoying the beauty of research with a significant degree of freedom, that is a rare privilege for which I am very thankful. Moreover, I am very grateful for his determined commitment to promoting the visibility and recognition of our co-authored work, and I have always appreciated his hard-working and approachable attitude. Throughout my stay I also found very engaging the scientific discussions with Dr. Alexis Bordet, Dr. Nicolas Kaeffer and Dr. Andreas Vorholt, who shared with me very precious insights in magnetically heated heterogeneous catalysis, organometallic electrochemistry and biphasic homogeneous catalysis. I had little prior knowledge of these topics before arriving at the institute, and I now consider them almost familiar thanks to their encouraging attitude towards my curiosities.

Among the scientists who profoundly influenced my learning during my time here, I need to thank Dr. Markus Leutzsch: a brilliant scientist in the NMR department at the neighboring Max Planck Institute. He guided me with patience towards learning extremely useful skills to use in mechanistic investigations. His contribution was crucial for obtaining reliable and reproducible kinetic data displayed in the Chapter 3 of this work.

A heartfelt thank you goes to Prof. Leitner for several reasons. Firstly, for offering me the opportunity to pursue my Ph.D. in his group at the Max Planck Institute for Chemical Energy Conversion. Secondly for his guidance and precious input on my scientific projects, which has been crucial in the very early stages of my Ph.D.; I am also very appreciative of the constructive feedbacks he has been providing me for improving my presentation skills in preparation for conferences, and for improving this manuscript which, thanks to his suggestions, is currently in a significantly better shape. Additionally, his efforts in generating learning opportunities inside the institute were also highly appreciated: the regular presence of guests sharing their research provided me with important insights towards the frontiers of catalysis, both from an industrial and academic perspective. And, in this regard, thanks again to Dr. Kaeffer and Dr. Vorholt also for their efforts in the same direction.

Now, I wish to express my deepest gratitude to my partner, Melina Müller, who provided me with endless support on various fronts during the drafting of this manuscript. She supported me both on the emotional level in difficult times, and on the logistic level to allow me to invest more time into this work. Moreover, she also helped me significantly in improving the thesis itself thanks to her several rounds of proofreading on the manuscript. In this regard, also many thanks to Jeroen Vossen, Dr. Gabriel Durin, Johannes Zenner and Michał Mrozowicz, that have also put a significant amount of effort in giving me feedback about this document and made precious suggestions to improve its quality.

Last but not least, I would like to thank my parents Alessandro Antico and Daniela Corvatta. They maintained in constant contact with me during these years with sweet attentions. Moreover, they have been investing a lot into my education in terms of personal and financial effort, that is something invaluable to me. They encouraged me to move away from my hometown to study in a more stimulating environment, the University of Pisa, where I got a very strong fundamental chemical knowledge. They also encouraged me to do an experience abroad, leading me to Helsinki, where I learned to work independently in a laboratory and where I had the chance to attend my very first conference, EuCOMC2019. It is at that conference that I ultimately met Prof. Leitner, with whom I talked for the first time discussing potential Ph.D. opportunities in his group.

While we often emphasize individual achievements in the context of meritocracy, it must also be acknowledged the substantial impact of external factors on our success. Thanks to the approach that my parents always had towards my education, I had the privilege to focus exclusively on my studies without the burden of financial concerns. This allowed me to build a very solid basic knowledge, which made the early steps of my Ph.D. life significantly easier. Moreover, I have greatly benefited from the scientific exchange in our MPI-campus, that also helped me to keep the research move forward. Therefore, even though at the end I will be the only one getting a title from this dissertation, the results here can be considered, in a broad sense, definitely a TEAM EFFORT for which I am very grateful.

Thank you all,

Emanuele

Abstract

In the recent efforts towards a greener chemical industry, the development of new catalytic systems based on earth-abundant metals is of particular importance. In fact, when compared to noble metals, the economic and environmental burden for their mining is generally lower and their supply chain is overall more resilient to geopolitical events. However, it is challenging to substitute highly catalytically active metals such as Ru, Rh, Ir, or Pd while obtaining similar performances. A promising approach is the substitution of Ru(II) pincer complexes with their Mn(I) analogues in hydrogenation and dehydrogenation reactions: the employment of ligands able to engage in Metal–Ligand Cooperation improved the activity of Mn(I) pincer complexes to levels able to compete with (and sometimes outperform) similar Ru(II) complexes, widely applied in homogeneous hydrogenation and dehydrogenation catalysis. This discovery revived a lot of interest towards Mn(I) chemistry, that has been living a true renaissance since 2016. In the first chapter of this work, the freshly discovered catalytic potential of Metal-Ligand Cooperative Mn(I) pincer complexes will be described. Then, an historical excursion into Mn(I) organometallic chemistry will highlight how important mechanistic aspects of coordination chemistry could be investigated by studying, among complexes of other metals, some Mn(I) complexes (*e.g.* the study of alkyl migration into M–CO bonds, the discovery and definition of agostic interaction, and the coordination of σ-bonds such as Si–H and H–H bonds to metal centers). Finally, in the last part of Chapter 1, some recent examples of a novel class of Mn(I) complexes catalytically active in hydrogenation and dehydrogenation reactions will be presented.

After the introductory part, Chapter 2 and Chapter 3 will focus on the Mn(I) activation of Si–H bonds. In particular, the σ-coordination of Si–H bond to a Mn(I) center will be of key importance in dehydrogenation catalysis, showing that [$MnBr(CO)_5$], due to its readiness to dissociate CO, is able to outperform both unactivated and *in-situ* activated pincer complexes in this type of catalysis. More in detail, in Chapter 2 of this work, the catalytic properties of the commercial and bench stable [$MnBr(CO)_5$] will be exploited in the dehydrogenative hydrosilylation of free carboxylic acids to alcohols. Initial mechanistic insights that point towards the necessity for an unsaturated complex as an active catalyst will be provided. In Chapter 3, the same catalyst [$MnBr(CO)_5$], will be utilized for the dehydrogenative coupling of Si–H bonds with H_2O to access a scope of different silanols. Besides the scope of the reaction, showing excellent selectivity towards the silanols, the mechanism of the reaction will be presented in detail. Kinetic data obtained *via* quantitative ^{1}H-NMR, data from GC-TCD analysis, flow FT-IR studies on the reaction will provide clear mechanistic insights into both the activation of [$MnBr(CO)_5$] in the presence of Si–H bonds, and the overall catalytic cycle. The results point towards a coordinatively unsaturated Mn(I) tricarbonyl complex as active species in the reaction. Finally, in Chapter 4, the knowledge acquired on unsaturated Mn(I) carbonyl complexes will be used to design a cost-effective Mn(I) 1,2-bis(diphenylphosphino)ethane complex capable of activating

H_2 upon σ-coordination in the absence of pristine base-activation. The complex will be able to catalyze the hydrogenation of indoles, including some unprotected ones, which has never been reported using a Mn-based non-pincer catalyst. Mechanistic insights will be provided thanks to studies on the yield-time profile of the reaction (utilizing both H_2 and D_2), single crystal X-Ray diffraction of potential *off-cycle species* of the catalytic cycle, and the synthesis of plausible active species. Again, a coordinatively unsaturated Mn(I) carbonyl complex will be presented as a potential active species. In Chapter 5, the conclusions arising from the work will be summarized.

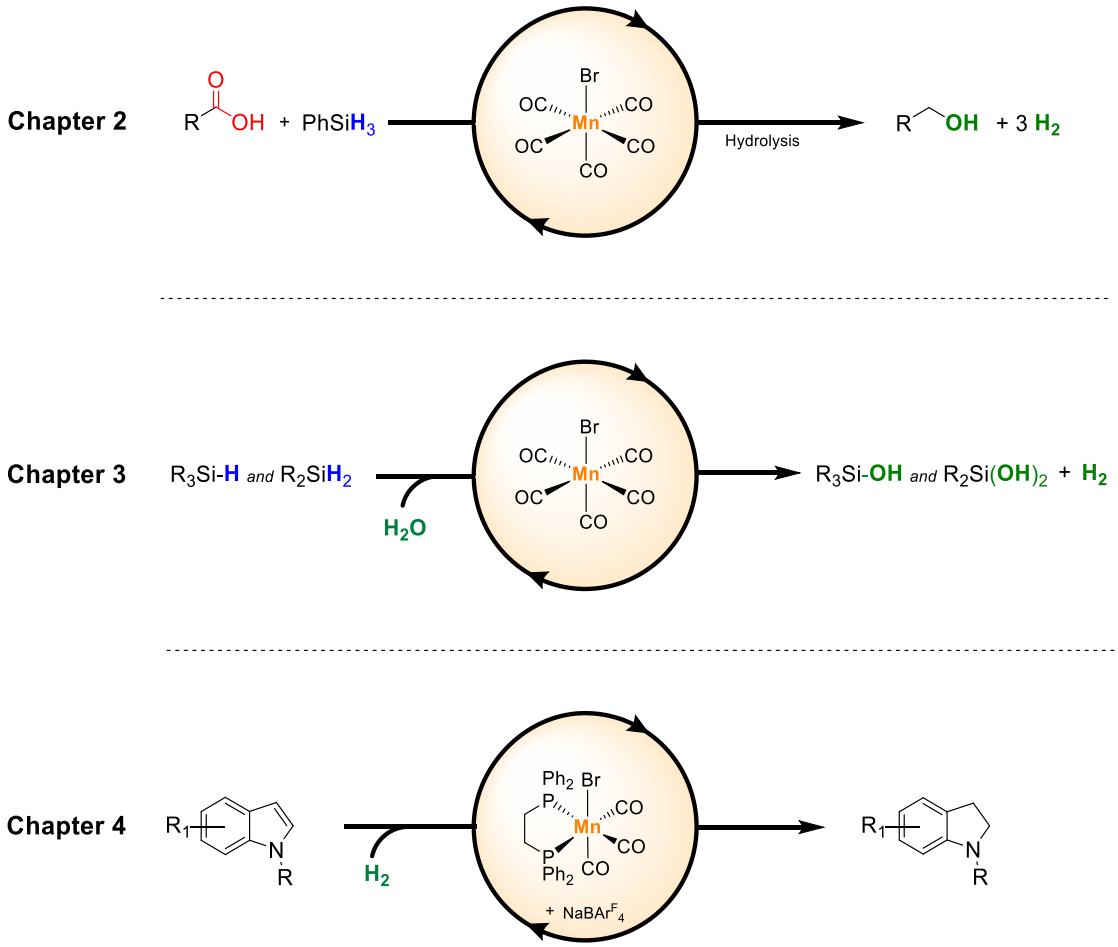


Figure 1: Schematic organization of the thesis content, arranged by chapter.

Zusammenfassung

In Anbetracht der jüngsten Bemühungen um eine umweltfreundlichere chemische Industrie, ist die Entwicklung neuer katalytischer Systeme auf der Grundlage natürlich verfügbarer 3d-Metalle von besonderer Bedeutung. Im Vergleich zu Edelmetallen ist die wirtschaftliche und ökologische Belastung durch ihren Abbau in der Regel geringer und die im Zusammenhang stehende Lieferkette insgesamt widerstandsfähiger gegenüber geopolitischen Ereignissen. Es ist jedoch eine Herausforderung, katalytisch hochaktive Metalle wie Ru, Rh, Ir oder Pd zu ersetzen und dabei ähnliche Leistungen zu erzielen. Ein vielversprechender Ansatz ist die Substitution von Ru(II)-Pincerkomplexen durch ihre Mn(I)-Analoga bei Hydrierungs- und Dehydrierungsreaktionen: Durch die Verwendung von des Konzepts der Metall-Ligand-Kooperation an Mn(I)-Pincerkomplexen wird deren Aktivität so weit verbessert, dass sie mit vergleichbaren Ru(II)-Komplexen konkurrieren können (und diese manchmal sogar übertreffen), welche in der homogenen Hydrierungs- und Dehydrierungskatalyse häufig eingesetzt werden. Diese Entdeckung hat das Interesse an der Mn(I)-Chemie geweckt, die seit 2016 eine wahre Renaissance erlebt. Im ersten Kapitel dieser Arbeit wird das neu entdeckte katalytische Potenzial von Metall-Ligand-kooperativen Mn(I)-Pincerkomplexen beschrieben. Anschließend wird die historische Entwicklung der metallorganischen Mn(I)-Chemie zusammengefasst. Ein Fokus liegt dabei auf den wichtigen mechanistischen Aspekten der Koordinationschemie, die mittels Mn(I)-Komplexen untersucht wurden (z. B. die Untersuchung der Alkylmigration in M–CO-Bindungen, die Entdeckung und Definition der agostischen Wechselwirkung und die Koordination von σ-Bindungen wie Si–H- und H–H-Bindungen an Metallzentren). Schließlich werden im letzten Teil von Kapitel 1 einige neuere Beispiele für Mn(I)-Komplexe ohne Metal-Ligand-Kooperation vorgestellt, die bei Hydrierungs- und Dehydrierungsreaktionen katalytisch aktiv sind. Nach dem einleitenden Teil konzentrieren sich Kapitel 2 und Kapitel 3 auf die Mn(I)-Aktivierung von Si–H-Bindungen. Insbesondere die σ-Koordination der Si–H-Bindung an ein Mn(I)-Zentrum wird bei der Dehydrierungskatalyse von zentraler Bedeutung sein, wobei gezeigt wird, dass $[MnBr(CO)_5]$ aufgrund seiner Fähigkeit, CO zu dissoziieren, in der Lage ist, sowohl nicht aktivierte als auch in-situ aktivierte Pincer-Komplexe bei dieser Art von Katalyse zu übertreffen. In Kapitel 2 dieser Arbeit werden die katalytischen Eigenschaften des komerziellen und vergleichsweise stabilen $[MnBr(CO)_5]$ bei der dehydrierenden Hydrosilylierung ungeschützter Carbonsäuren zu Alkoholen genutzt. Erste mechanistische Erkenntnisse, die darauf hindeuten, dass ein ungesättigter Komplex als aktiver Katalysator erforderlich ist, werden vorgestellt. In Kapitel 3 wird derselbe Katalysator $[MnBr(CO)_5]$ für die dehydrierende Kupplung von Si–H-Bindungen mit H_2O verwendet, um eine Reihe verschiedener Silanole mit ausgezeichnete Selektivität zu erhalten. Kinetische Daten, die mittels q-^{1}H-NMR, GC-TCD-Analysen und Flow FT-IR-Studien zur Reaktion gewonnen wurden, werden klare mechanistische Einblicke in sowohl die Aktivierung

von [MnBr(CO)$_5$] in Gegenwart von Si–H-Bindungen als auch in den gesamten katalytischen Zyklus liefern. Die Daten deuten auf einen koordinativ ungesättigten Mn(I)-Tricarbonylkomplex als aktive Spezies in der Reaktion hin. In Kapitel 4 werden schließlich die gewonnenen Erkenntnisse über ungesättigte Mn(I)-Carbonylkomplexe genutzt, um einen kostengünstigen Mn(I)-1,2-Bis(diphenylphosphino)ethan-Komplex zu entwickeln, der in der Lage ist, H_2 bei σ-Koordination zu aktivieren, ohne dass eine initiale Basenaktivierung benötigt wird. Der Komplex ist in der Lage, die Hydrierung von Indolen, einschließlich einiger ungeschützter Indole, zu katalysieren, was bisher noch nie mit einem Mn-Katalysator, der nicht auf Pincerliganden basiert, beschrieben wurde. Mechanistische Einblicke werden dank Studien zum Ausbeute-Zeit-Profil der Reaktion (unter Verwendung von H_2 und D_2), der Einkristall-Röntgenbeugung potenzieller Off-Cycle-Spezies des katalytischen Zyklus und der Synthese plausibler aktiver Spezies gewonnen. Auch hier wird ein koordinativ ungesättigter Mn(I)-Carbonylkomplex als potenziell aktive Spezies vorgestellt. In Kapitel 5 werden die Schlussfolgerungen aus dieser Arbeit zusammengefasst.

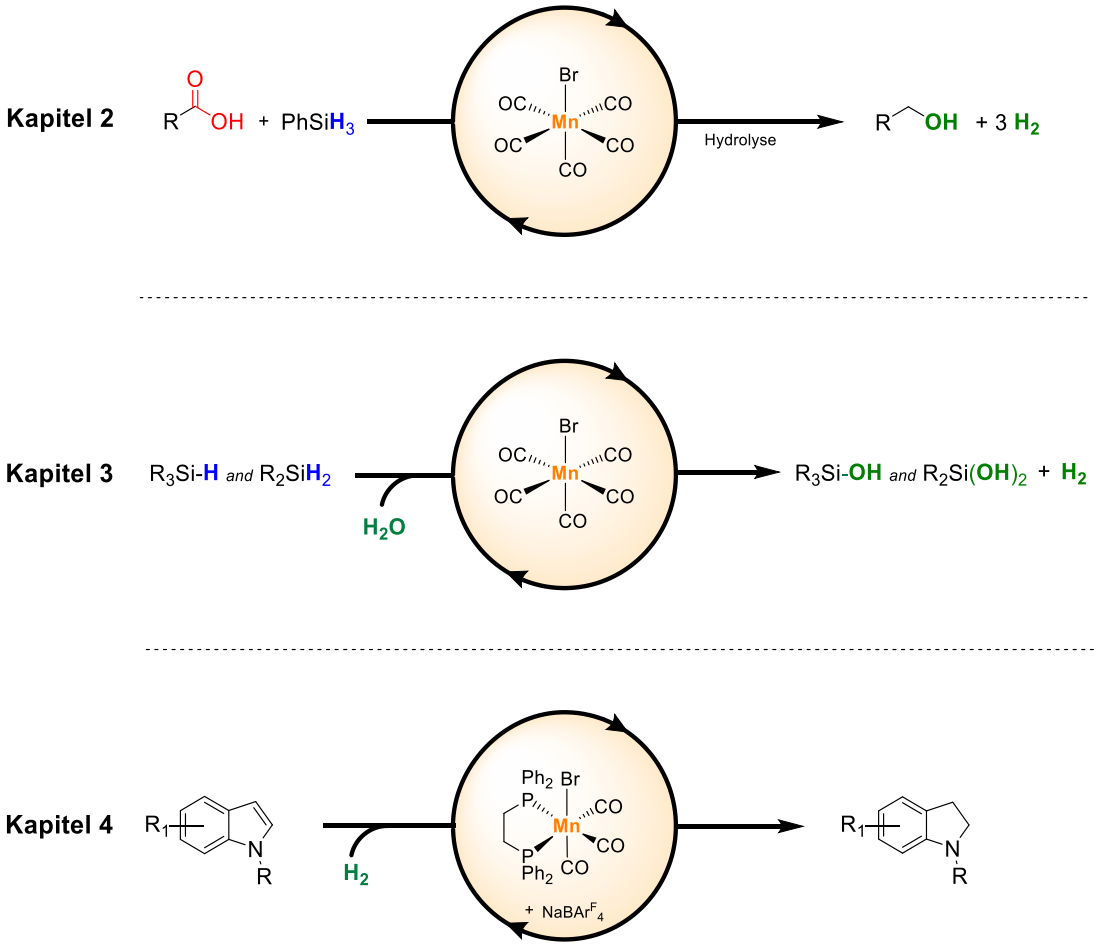


Abbildung 1: Schematischer Aufbau des Inhalts der Dissertation, geordnet nach Kapiteln.

Table of Contents

1. Background and Motivation 1

1.1. Manganese: an Emerging Player in the (De)-hydrogenation Arena 1

1.2. Mn(I) and Coordination of σ-bonds: Still Unexploited Catalytic Potential? 12

1.3. Aim of the Thesis 22

1.4. References 23

2. [MnBr(CO)$_5$] Catalyzed Reduction of Carboxylic Acids to Alcohols 29

2.1. Introduction 29

2.2. Objective 30

2.3. Initial Screening and Optimization 30

2.4. Reaction Scope and Catalytic Performances 32

2.5. Mechanistic Insights 34

2.5.1. The formation of a silyl ester as first reaction step 34

2.5.2. The need for a coordinatively unsaturated complex as a catalyst 35

2.5.3. The nature of the Si–based species during the reaction 36

2.6. Suggested Mechanistic Cycle 38

2.7. Conclusion and Outlook 39

2.8. Experimental Procedure and Characterization Data 40

2.8.1. General consideration 40

2.8.2. General procedure for the optimization 40

2.8.3. General procedure for the substrate scope 41

2.8.4. Procedure for the GC-TCD studies 41

2.8.5. Synthesis and isolation of the silyl ester 42

2.8.6. Procedure for $^{31}P\{^1H\}$-NMR analysis of crude reaction mixtures 42

2.8.7. Procedure for the reaction where hydrogen was released 42

2.8.8. Procedure for the crude NMR analysis of the polysiloxane byproducts 43

2.8.9. Procedure for the isolation of the polysiloxane byproducts after hydrolysis 43

2.8.10. Characterization data 44

2.9. References 50

3. [MnBr(CO)$_5$] as an Active Precatalyst for the Selective Oxidation of Silanes to Silanols 54

3.1. Introduction 54

3.1. Objectives 57

3.2. Initial Screening and Optimization 58

3.3. Reaction Scope and Catalytic Performances 60

3.4. Mechanistic Investigation 62

3.4.1. Reaction between [MnBr(CO)$_5$] and PhSiMe$_2$H 62

3.4.2. Kinetic studies 64

3.4.3. Investigating the coordination sphere of the active species 66

3.5. Mechanistic Proposal 68

3.6. Conclusion and Outlook 69

3.7. Experimental Procedure and Characterization Data 70

3.7.1. General considerations 70

3.7.2. General procedure for the reaction optimization 70

3.7.3. General procedures for the substrate scope 71

3.7.4. Procedure followed for the kinetic studies 73

3.7.5. Synthesis and characterization of PhMe$_2$Si-D 75

3.7.6. Procedure for the stoichiometric experiments between [MnBr(CO)$_5$] and PhMe$_2$SiH 75

3.7.7. Procedure for the reaction between PhMe$_2$SiH and Br$_2$ 75

3.7.8. Procedure for the gas phase analysis studies on the headspace of the reaction 75

3.7.9. Procedure for the IR studies 76

3.7.10. Procedure for the isolation of Mn-7 and its test in catalytic studies 76

3.7.11. Procedure for the low catalyst loading reaction 77

3.7.12. Procedure for the gram scale reaction 78

3.7.13. Characterization data 79

3.8. References 84

4. [Mn(CO)$_3$(dppe)]-Derivatives as Catalysts for the Hydrogenation of Indoles 88

4.1. Introduction 88

4.2. Objective 90

4.3. Initial Screening and Optimization 90

4.4. Preliminary Reaction Scope 93

4.5. Mechanistic Investigation 94

4.5.1. Yield-time profile 94

4.5.2. Deuteration analysis 96

4.5.3. Stoichiometric reactions 98

4.5.4. Towards a candidate for the active species 100

4.6. Suggested Mechanism 101

4.7. Conclusions and Outlook 102

4.8. Experimental Procedure and Characterization Data 103

4.8.1. General considerations 103

4.8.2. Synthesis of the non-commercial manganese complexes 103

4.8.3. Handling of the autoclaves 105

4.8.4. General procedure for the optimization 105

4.8.5. General procedure for the substrate scope 106

4.8.6. General procedure for the yield-time profile using H_2 or D_2 106

4.8.7. Synthesis of complex *fac*-[$Mn(CO)_3$(dppe)H] 107

4.8.8. Procedure for the reaction between *fac*-[$Mn(CO)_3$(dppe)H] and 1-methylindole 107

4.8.9. Procedure for the reaction between *fac*-[$MnBr(CO)_3$(dppe)] and $NaBAr^F{}_4$ 107

4.8.10. Procedure for the reaction between *fac*-[$MnBr(CO)_3$(dppe)] and $NaBAr^F{}_4$ under H_2 pressure 107

4.8.11. Synthesis of Brookhart's acid 108

4.8.12. Synthesis of complex Mn-13 108

4.8.13. Characterization data of isolated compounds 109

4.9. References 111

5. Conclusion and Outlook 114

6. Appendix 117

6.1. Analytical Instrumentation 117

6.1.1. NMR spectrometers 117

6.1.2. GC for headspace analysis 117

6.1.3. FT-IR spectrometers 117

6.1.4. Polarimeter 117

6.1.5. Photochemistry setup 117

6.1.6. X-Ray Diffraction 117

6.1.7. Mass spectrometry 118

6.2. Supplementary Electronic Characterization Data 119

6.3. Supplementary NMR Data for Section 3.4.1 131

6.4. Novel Crystal Structures of Compounds Reported in the Work 132

6.4.1. Procedure for the X-Ray crystallography and the refinement of structures 132

6.4.2. Crystallographic data and structure refinement for the molecule 2o 133

6.4.3. Crystallographic data and structure refinement for the molecule 2p 134

6.4.4. Crystallographic data and structure refinement for the complex Mn-7 135

6.4.5. Crystallographic data and structure refinement for the complex Mn-10 136

6.4.6. Crystallographic data and structure refinement for the complex Mn-12 137

6.4.7. Graphical representation of the molecular structures of the crystallized compounds 138

6.5. Supplementary Kinetic Section 142

6.5.1. Order in $[MnBr(CO)_5]$ 143

6.5.2. Order in $PhMe_2SiH$ 145

6.5.3. Order in H_2O 147

6.6. Relevant Spectra for Flow FT-IR 149

6.7. Supplementary Spectra for the Deuteration of 1-methylindole and 1-methylindoline 151

6.8. Characterization Data of the Complex Mn-13 153

6.9. References 154

Glossary

2-MTHF = 2-Methyltetrahydrofuran

APCI-MS = Atmospheric-pressure chemical ionization mass spectrometry

2-BuOH = 2-butanol

COD = Cyclooctadiene

CO_2-eq. = CO_2 equivalent

Cp = Cyclopentadienyl anion

DETA = Diethylenetriamine

DIBAL-H = Diisobutylaluminium hydride

dppe = 1,2-Bis(diphenylphosphino)ethane

dmpe = 1,2-Bis(dimetylphosphino)ethane

depe = 1,2-Bis(dietylphosphino)ethane

dcpe = 1,2-Bis(dicyclohexylphosphino)ethane

dr = diastereoisomeric ratio

ee = enantiomeric excess

equiv. = equivalent

FT-IR = Fourier-Transform Infrared Spectroscopy

GC = Gas Chromatography

GC-TCD = Gas Chromatography employing a Thermal Conductivity Detector

HR-MS = High Resolution Mass Spectrometry

HOMO = Highest Occupied Molecular Orbital

KIE = Kinetic Isotope Effect

LUMO = Lowest Unoccupied Molecular Orbital

MS = Mass Spectrometry

M = Molar

mg = milligram

mmol = millimole

μmol = micromole

mM = milliMolar

MMT = Methylcyclopentadienyl Manganese Tricarbonyl

μM = microMolar

MLC = Metal–Ligand Cooperation

MLCve = Metal–Ligand Cooperative

N = Normal

$NaBAr^{F}_{4}$ = Sodium Tetrakis(3,5-bis(trifluoromethyl)phenyl)borate

NMR = Nuclear Magnetic Resonance

$O^{i}Pr$ = *iso*-Propoxide

$O^{t}Bu$ = *tert*-Butoxide

OTf = Trifluoromethanesulfonate

P(A) = Unspecified Pressure of gas A

ppm = parts per millon

q-NMR = quantitative Nuclear Magnetic Resonance

R.T. = Room Temperature

T = Temperature

TCD = Thermal Conductivity Detector

TBA = Tetrabutylammonium

THF = Tetrahydrofuran

t = time

TOF = Turnover frequency = $\frac{n\,(product)}{n\,(catalyst) * time}$

TON = Turnover number = $\frac{n\,(product)}{n\,(catalyst)}$

TMS = Tetramethylsilane

Vol = Volume

VTNA = Variable Time Normalization Analysis

XRD = X-Ray Diffraction

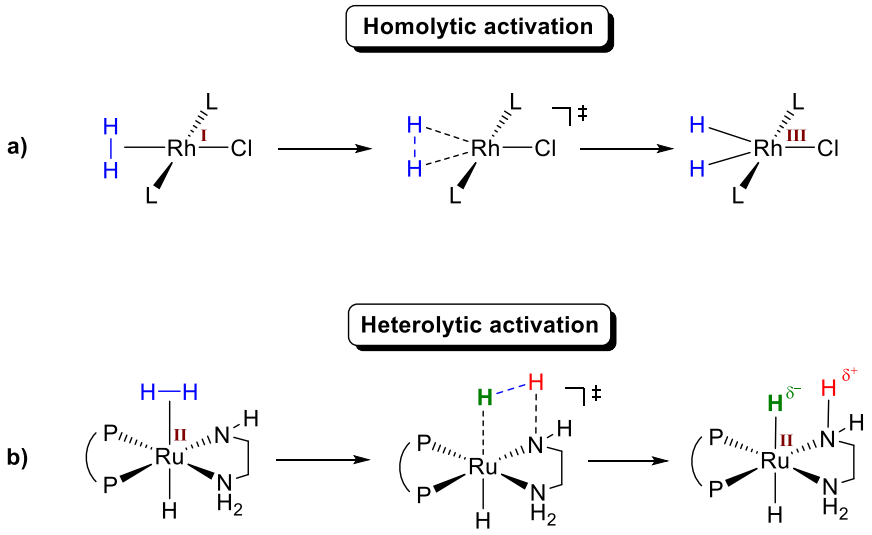
Xyl = 3,5-dimethylphenyl substituent

δ = Chemical shift

1. Background and Motivation

1.1. Manganese: an Emerging Player in the (De)-hydrogenation Arena

Hydrogenation and dehydrogenation are key reactions in modern chemical industry, and are used for the production of important intermediates such as unsaturated hydrocarbons at a pace of millions of tons per year. Historically, homogenous catalysis witnessed an important innovation with the advent of Rh- and Ru-based Wilkinson-type catalysts in the 1960s. These metal complexes started to show improved selectivity and milder reaction conditions in reactions such as hydroformylation and hydrogenation,[1] growing the interest of the community for 4d and 5d metal-based homogenous catalysts. The research in the field led to other important breakthroughs, such as the development and mechanistic understanding of the asymmetric hydrogenation reactions, led by Ryoji Noyori, which resulted in him receiving the Nobel Prize in Chemistry in 2001 (alongside William S. Knowles and K. Barry Sharpless). A key point of Noyori's work laid in the innovative activation mode of the H_2 molecule: the cleavage of H_2 was facilitated from a N–H functionality in the ligand backbone, formally cleaved as H^- and H^+, as an alternative pathway respect to the oxidative addition/reductive elimination popular at that time (**Scheme 1**).

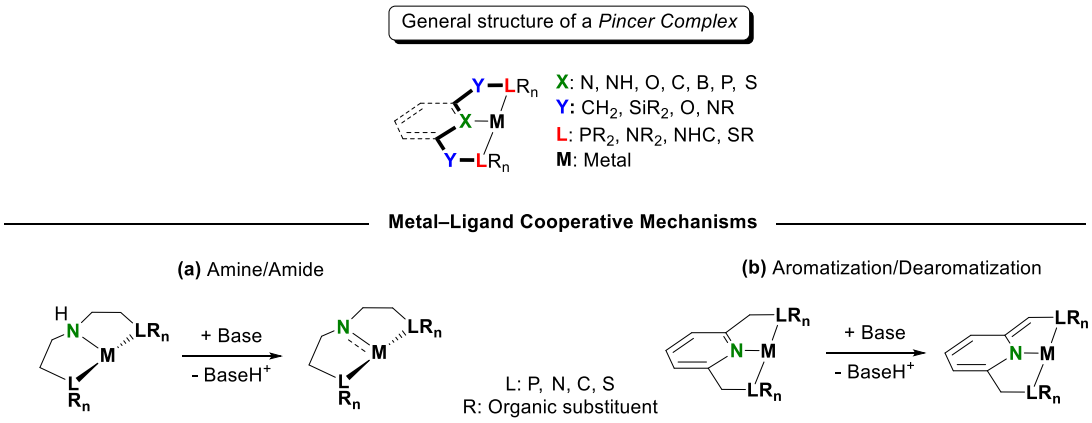


Scheme 1: a) Homolytic activation of the H_2 molecule at a Rh center *via* an oxidative addition mechanism; b) Heterolytic activation of the H_2 molecule in the presence of a Noyori-type catalyst, in which the metal retains its formal oxidation state.[2] Scheme inspired from reference 3.[3]

Already in 1995, Leitner and Dedieu demonstrated the energetic convenience of this heterolytic activation mode of the H–H bond, where the metal retains its formal oxidation state, over an oxidative addition/reductive elimination cycle.[4] In their computational investigation, they examined the Rh-catalyzed hydrogenation of CO_2 using *cis*-[$RhH(PH_3)_2$] as the model compound. Their study revealed that, following the initial formation of the formate complex [$Rh(O_2CH)(PH_3)_2$], heterolytic cleavage of the H–H bond was

facilitated by the coordinated formate (referred to as "*σ methatesis*" in their work), and was energetically more favorable than the corresponding oxidative addition. Researchers, recognizing that heterolytic activation of H_2 can significantly enhance the performances of hydrogenation catalysts, developed ligands containing a non-innocent functional group positioned in close proximity to the metal center to aid in the bond activation. This concept, in which the ligand "*cooperates*" with the metal in the activation of the substrate, took the name of *Metal-Ligand Cooperation* (MLC). A large variety of ligand backbones which are able to engage in this MLC mechanism have been developed so far,[5-8] but some well-defined tridentate frameworks have gained growing popularity due to their simple structure, remarkable stability and synthetic versatility. This class of ligands has been called *pincer ligand*.[9] When a *pincer ligand* coordinates to a metal center, it generates a *pincer complex*. In **Scheme 2**, the general structure of a pincer complex is illustrated, showing the tunability that can be achieved in the electro-steric properties of the ligand around the metal center.

In the same figure, it is also possible to observe the two most common MLCve mechanisms for two emblematic classes of pincer complexes, which proved to be particularly fruitful in the fields of hydrogenation and de-hydrogenation chemistry: the so-called MACHO-type-PNP system, and the lutidine-based pincer complex.



Scheme 2: Top: the general structure of pincer complexes and their potential variability is represented. (a) Base promoted MLC amine/amide mechanism for the MACHO-type pincer complex; (b) Base promoted MLC aromatization/dearomatization mechanism for the lutidine-based pincer complex.

Both ligands require the presence of a base for the activation of the MLCve mechanism. For the MACHO-type-PNP ligand (**Scheme 2**, **(a)**), the increased acidity of the N-H group coordinated to the metal center facilitates the deprotonation from a base to form the corresponding *amido complex*, similarly to the case of Noyori's catalyst. In the case of the lutidine-based pincer ligand instead (**Scheme 2**, **(b)**), which has been developed and extensively used by Milstein and co-workers,[10, 11] the mode of cooperativity follows the so called *aromatization/de-aromatization mechanism*,[6, 7] where a -CH_2 of the lutidine backbone is the active

cooperative site. Both ligands have been used to prepare a series of pincer complexes of various noble metals. In particular, pincer complexes of Ru employing these two backbones were proved to be particularly effective in hydrogen transfer reactions, delivering some of the first examples ever reported for the hydrogenation of challenging substrates such as carbonates[12, 13] or carbamates and ureas,[14] and achieving high turnovers in the hydrogenation of CO_2 to both formate[15] and MeOH.[16-20] These Ru(II) complexes have also been very successful in the dehydrogenation field (especially in the formal conversion of alcohols to aldehydes), facilitating both the formation of C–C, C–O and C–N bonds *via* a hydrogen borrowing mechanism, and the oxidative dehydrogenation of alcohols and other functional groups.[21]

However, ruthenium and other 4d and 5d metals (on which these complexes are normally based on) present some intrinsic problems: their scarcity makes the cost for their supply and the environmental burden for their mining quite high, especially when compared to the more abundant 3d metals (**Figure 2**). Moreover, their generally higher toxicity creates additional costs in the downstream production of fine chemicals, for which the cost of the metal catalyst and its removal from the final product can easily overcome more than half of the total cost of the raw materials.[22] Earth-abundant metals can instead be more biocompatible, less expensive and generally more uniformly distributed on earth's crust, making their provision more resilient to geopolitical instabilities.

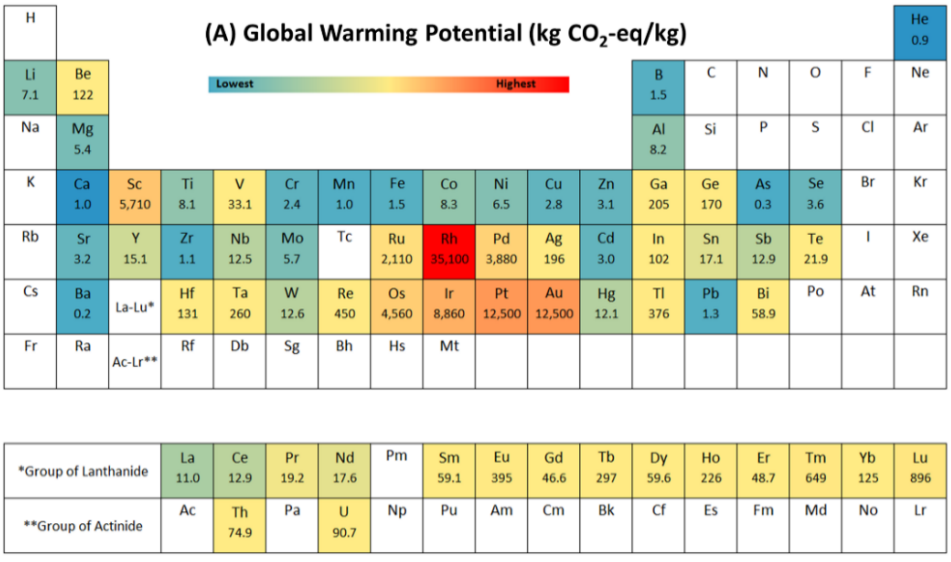
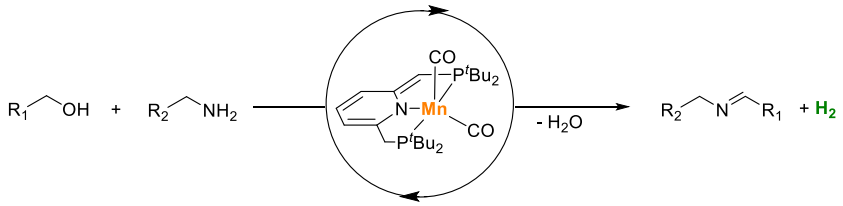


Figure 2: The cradle-to-gate Global Warming Potential per kilogram of each element (kg CO_2-eq. per kg) colored according to the corresponding color ramp. Reprinted from reference 23.[23]

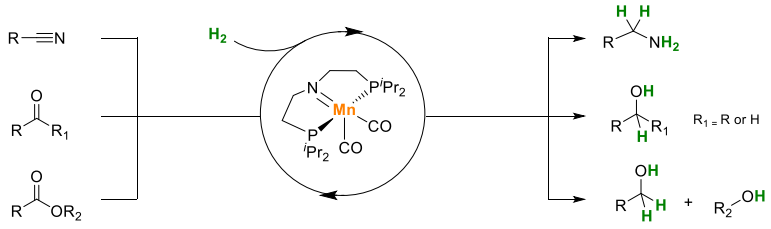
While trying to exploit the full catalytic potential of noble metals, research has been also investigating how to improve the catalytic performances of 3d metals. A key factor to boost their activity turned out to be the use of tailor-made ligands, which allowed for continuously improved reactivity and stability, pushing the

performances of 3d metal catalysts close (and sometimes beyond) what can be achieved with noble metals.[11,24] The widespread success of Fe catalysis led Wills to entitle it "Ruthenium lite" in 2011.[25] However, in recent years, Mn(I) pincer complexes emerged as a possible alternative to Fe(II) in the field of catalytic hydrogenation and dehydrogenation, being now among the favorite substitutes for their Ru(II) analogues. The initial realization dates back to 2016, when the group of Milstein tested out the catalytic performances of a Mn(I) complex coordinating their characteristic lutidine-based pincer ligand in the dehydrogenative coupling of alcohols and amines, obtaining very good catalytic performances (**Scheme 3**).[26]



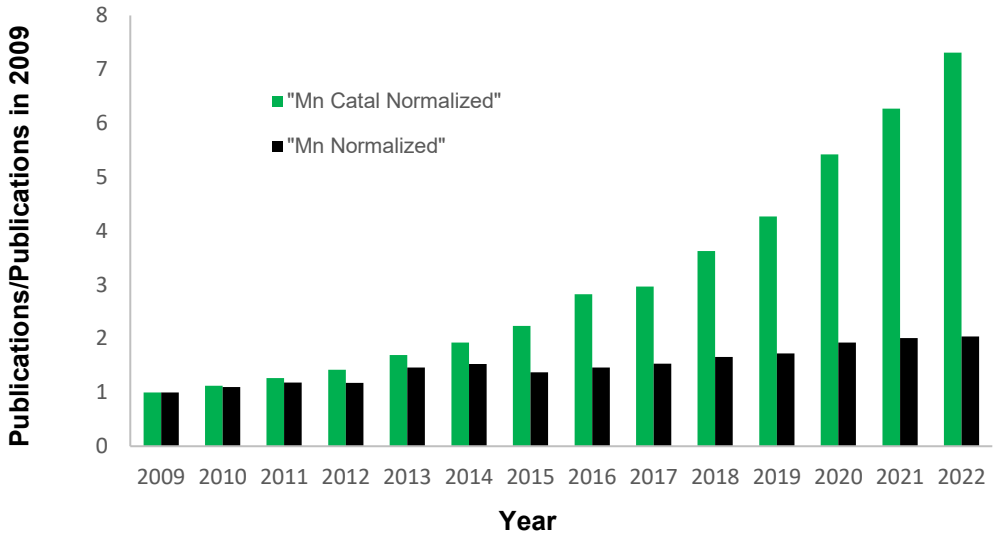
Scheme 3: Dehydrogenative coupling of alcohols and amine reported by Milstein and coworkers using a Mn(I) pincer complex in 2016.

A few months later, the group of Beller also reported that a Mn(I) pincer complex, this time bearing the MACHO ligand, was highly active in the hydrogenation of organic substrates. Functional groups such as aldehydes, ketones and nitriles could all be successfully hydrogenated to the corresponding alcohols and amines (**Scheme 4**).[27] The example was immediately followed by two other reports from the same group, in which the same catalyst successfully hydrogenated esters to alcohols,[28] and catalyzed the dehydrogenative N-alkylation of amines with alcohols.[29]



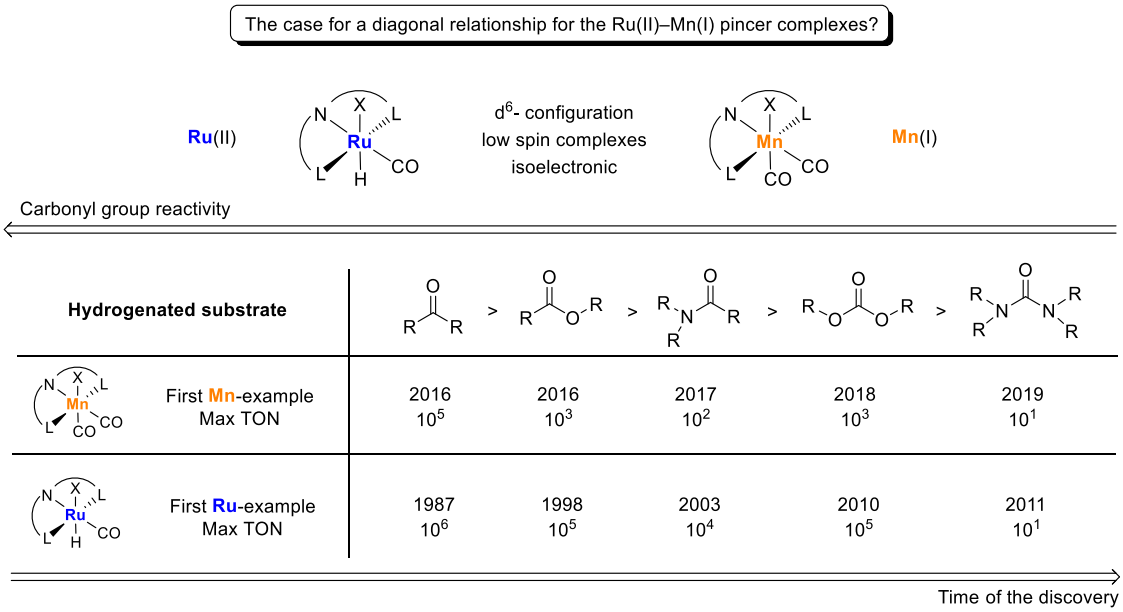
Scheme 4: Hydrogenation of several organic substrates using a Mn(I) pincer complex reported by Beller and coworkers in 2016.

Many more examples kept following, and, in just a few years, the reports using manganese for hydrogenation and dehydrogenation reactions rose dramatically both in number (**Graph 1**) and in degree of reaction difficulty (**Scheme 5**). Manganese(I)-based pincer complexes, with small variations from the aforementioned lutidine and MACHO backbones, soon became able to hydrogenate the same challenging functional groups such as carbonates,[30-32] carbamates and ureas.[33]



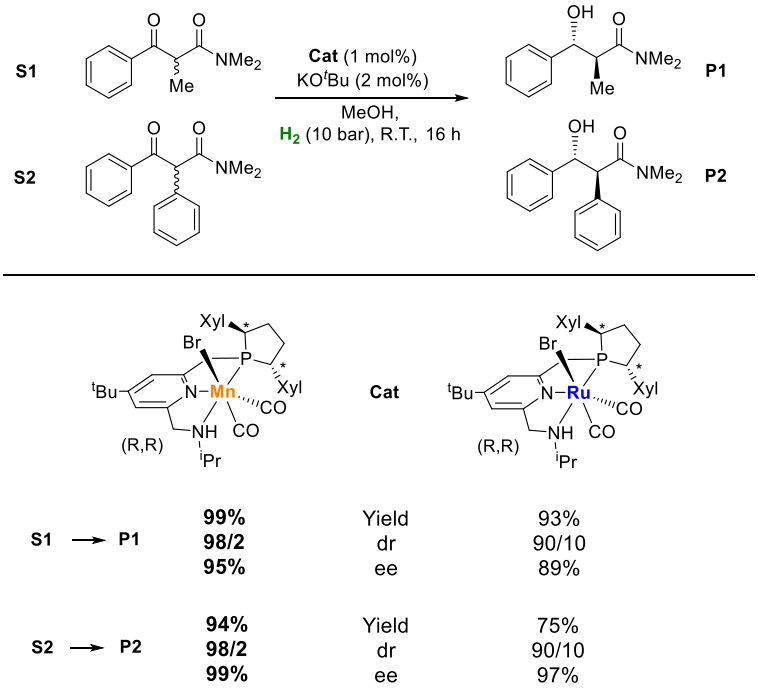
Graph 1: Relative growth, respect to the 2009 level, in the number of publications with either the term "Mn" (in black) or both "Mn" and "catal" (in green) in their title of abstract. Data from reference 34.[34]

These similarities pose the base for a potential "diagonal relationship" between the two metals: it compares the chemical behavior of an element in the oxidation state n^+ with a congener in the period above and the group to the left in the oxidation state $(n-1)^+$. While this analogy is mainly applied to main group metals, it seems to well rationalize the chemical similarities between Mn(I) and Ru(II), which have been harnessed with a certain success also in our research group, as illustrated in forthcoming examples.



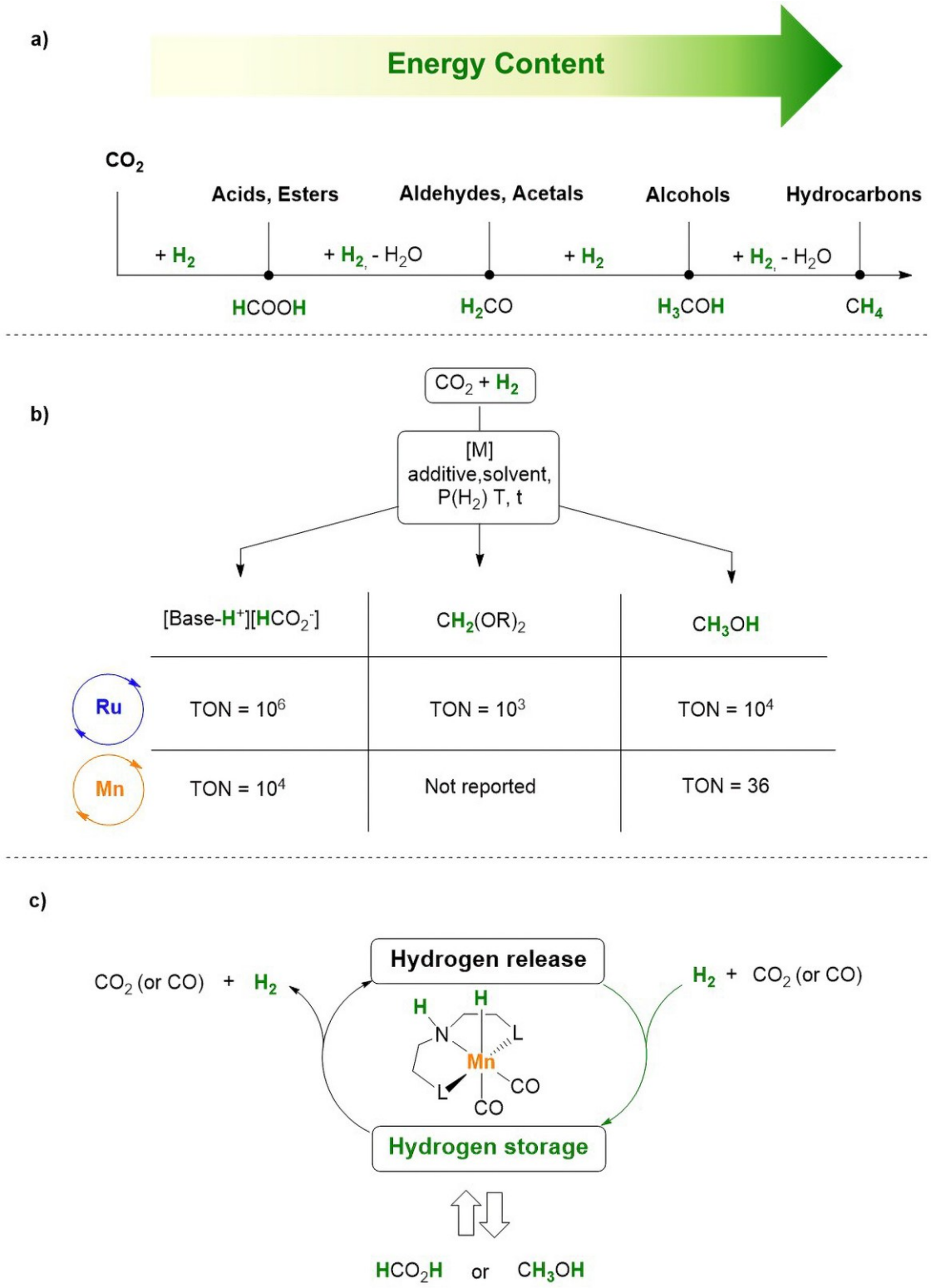
Scheme 5: Comparison of characteristics of Ru(II) and Mn(I) pincer complexes. In the table, the historical development in the hydrogenation of various organic substrates is reported, together with the respective best performances achieved in terms of turnover number.

Mn(I) pincer complexes were in fact proven to mimic the (re)activity of their Ru(II) analogues in hydrogenation reactions, and in some cases even outperform them. In 2019 Ding and coworkers, while studying the chiral derivative of a lutidine based pincer ligand, tested both the Mn(I) and a Ru(II) versions of the same pincer complex in the hydrogenation of racemic β-ketoamides under dynamic kinetic resolution conditions (**Scheme 6**). They could observe that the Mn-based complex was outperforming its Ru(II) counterpart both in terms of yield and enantioselectivity. Not only this example constituted the first case of a manganese-catalyzed dynamic kinetic resolution, but it reached a TON up to 10^4 which represents, according to the authors, the highest TON reported for any transition metal-catalyzed reaction of this type with racemic α-substituted-β-ketoamides.[35]



Scheme 6: Reaction conditions and results obtained for the dynamic kinetic resolution reported by Ding and co-workers, testing both manganese and ruthenium based catalysts with the same ligand framework (dr = diastereoisomeric ratio; ee = enantiomeric excess).

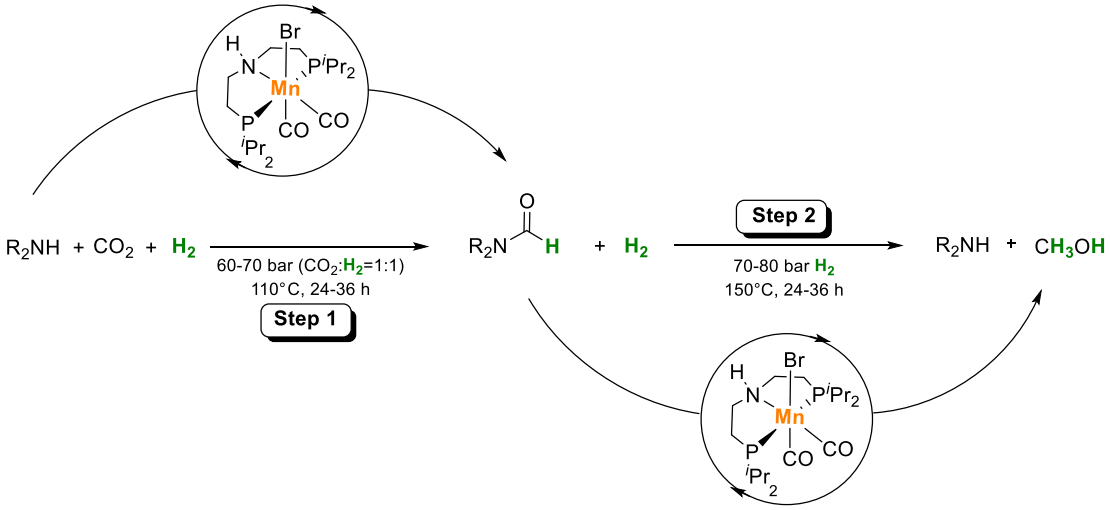
This example, despite showing the high activity which Mn(I) pincer complexes can reach as hydrogenation catalysts in the area of organic synthesis, is not representative of their full catalytic potential. Their performances were explored also in (de)hydrogenation chemistry with small molecules such as CO_2, for potential applications in the field of chemical energy storage. The hydrogenation of CO_2 to produce reduced forms of carbon increases its energy content for future utilization. As shown in **Scheme 7**, the first reduction step of a CO_2 molecule is its hydrogenation to the formic acid/formate level. For this reaction, several examples using Mn(I) catalysts have been reported for both the hydrogenation of CO_2 to formate,[36-38] and for the corresponding dehydrogenation of formic acid back to CO_2 and H_2.[39, 40]



Scheme 7: (a) Qualitative representation of the increase in energy content of CO_2-derived molecules upon reduction with H_2; (b) current state of the art for the best catalytic performances in CO_2 hydrogenation for ruthenium and manganese complexes; (c) graphical representation of the use of CO_2 and CO as potential chemical energy carriers upon reduction with H_2.

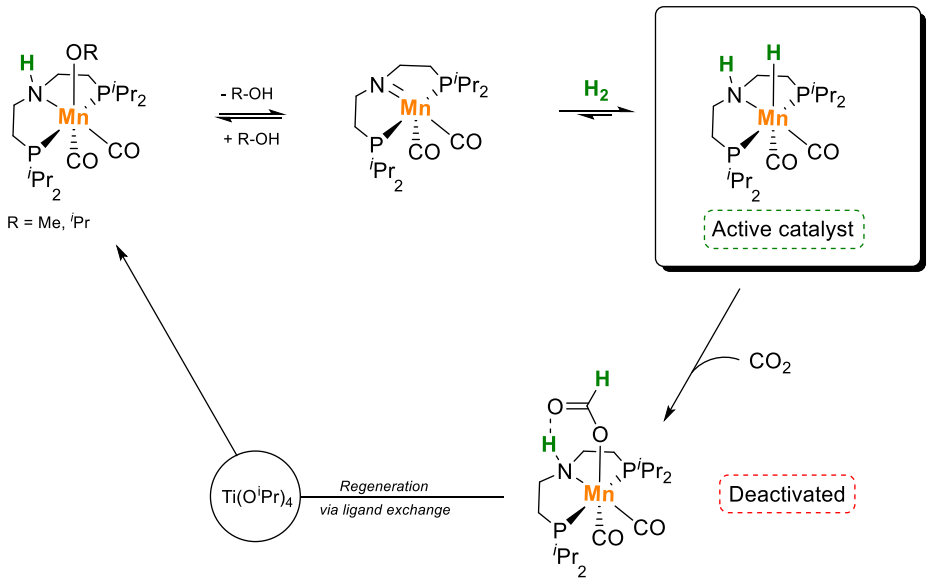
Only one example so far, reported by the Beller group, was shown to effectively catalyze both reactions in the presence of an α-amino acid as a promoter.[41] Another important reduction step in the hydrogenation of CO_2, is the one affording methanol as the product. The small alcohol, because of its high energy density and liquid physical state at room temperature, is particularly attractive as chemical energy carrier.[42]

However, the hydrogenation of CO_2 to CH_3OH has been to proven to be significantly more challenging for Mn(I) pincer complexes compared to Ru(II) ones: early reports from Prakash and coworkers in 2017 showed that, in order to carry out the hydrogenation of CO_2 to CH_3OH, it is necessary to use secondary amines as promoters. Their role is to enable the indirect hydrogenation of CO_2 through the initial formation of formamides intermediates, followed by the hydrogenation of their carbonyl group to CH_3OH together with the regeneration of the free amine (**Scheme 8**).[43]



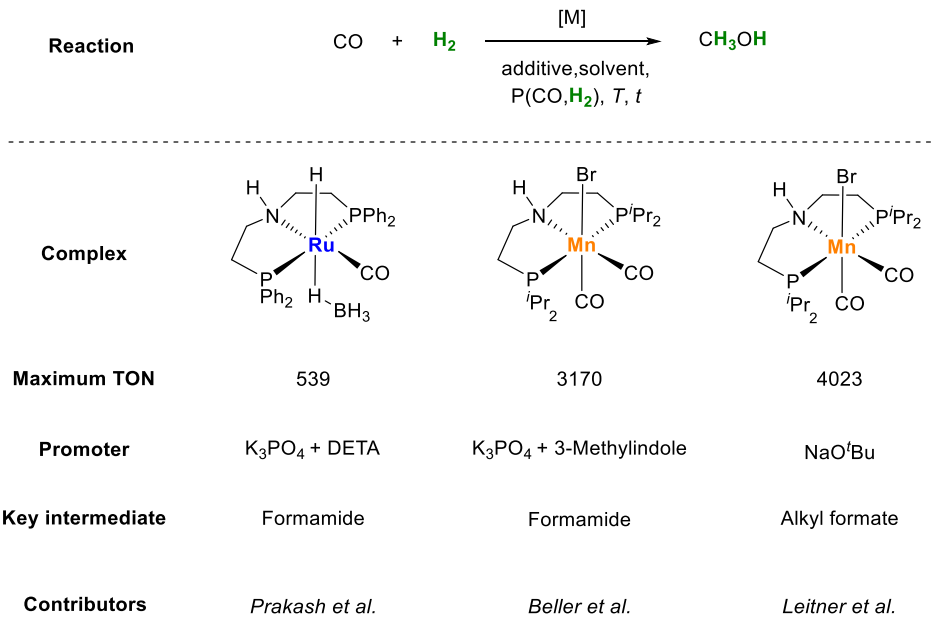
Scheme 8: Strategy followed by Prakash and coworkers for the manganese catalyzed sequential *"one pot – two steps"* hydrogenation of CO_2 to CH_3OH.

To overcome the hurdle of a multistep process, our group investigated the same reaction trying to develop a direct hydrogenation of CO_2 to CH_3OH. The mechanism was studied in detail, and it was found that the turnover was inhibited by the formation of a very stable and catalytically inert formate complex of Mn formed during the catalytic cycle (**Scheme 9**).[44, 45] The addition of a sub-stoichiometric amount of sacrificial $Ti(O^iPr)_4$ as a Lewis acid could regenerate the catalyst, abstracting the formate from the Mn center. This example represents the only Mn-catalyzed direct hydrogenation of CO_2 to CH_3OH reported to date. However, better results in the quest to methanol could be obtained when using CO as C1 synthon in the presence of Mn catalysts.



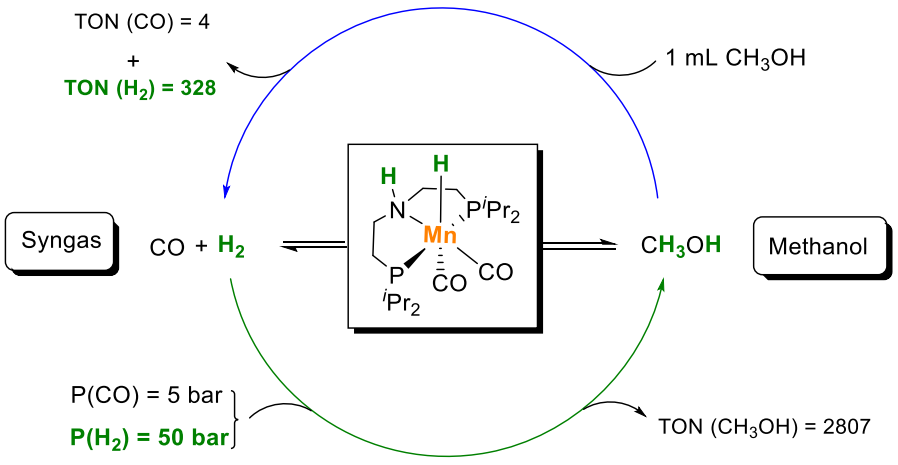
Scheme 9: The use of $Ti(O^iPr)_4$ as a Lewis acid for the regeneration of the active form of the Mn-MACHO complex. The regeneration proceeds *via* ligand exchange between $Ti(O^iPr)_4$ and the Mn-formate complex.

While the hydrogenation of CO to CH_3OH is a very well established reaction in heterogeneous catalysis, it poses significant challenges in homogeneous catalysis: the strong coordination bond between CO and metal complexes, associated with its unfavorable thermodynamics of insertion into the M-H bonds,[46-49] make CO a particularly demanding substrate to hydrogenate for transition metal complexes. Additionally, these metal complexes often form catalytically inactive species under CO pressure, further complicating the process. A strategy to promote the turnover is represented by the addition of nucleophilic additives like amines or alkoxydes to the reaction mixture. They can, in fact, form intermediates such as formamides or organic formates that can be easier to hydrogenate. After two examples where a Mn(I) or Ru(II) pincer complexes were used together with an amine or an indole as promoters in this reaction (**Scheme 10**),[50, 51] our group showed that the use of an alcohol as solvent in the presence of sub-stoichiometric amount of NaO^tBu promotes very effectively the hydrogenation of CO to CH_3OH *via* the formation of an alkyl formate intermediate.[52]



Scheme 10: Selected examples of Ru(II) and Mn(I) catalysts for the selective CO hydrogenation to CH_3OH.

This result opened the possibility to use methanol itself as a solvent, which was demonstrated in the work as a possibility to develop a true liquid phase methanol process without any additional co-reagent. Another significant advantage of this reaction, enabled by the Mn-MACHO complex, is the excellent selectivity towards methanol, which represents a major limitation of the heterogeneous process. Our group has also been working on the reverse reaction, proving that it is possible to use the same catalyst for the dehydrogenation of methanol back to syngas (**Scheme 11**). In the work, it was also shown that the reaction proceeds *via* a methyl-formate intermediate.[53]



Scheme 11: Schematic representation of the CO/CH_3OH cycle mediated by the Mn-MACHO complex for hydrogen storage purposes.

This section of Chapter 1 gave a glimpse on the enormous potential that Mn(I) pincer complexes have in the field of (de-)hydrogenation catalysis. The area is in continuous development, with research groups trying to improve the activity and robustness of the ligand frameworks supporting the metal.[54] However, the use of these pincer ligands also comes at a cost. In fact, the economic advantage of using Mn instead of Ru as a metal gets partially lost, as the ligand framework is often accountable for the majority of the overall cost of the catalyst, regardless of the metal chosen. Both academia and industry are at work to improve the affordability of some MLCve backbones, such as the MACHO-system, in order to enable some promising discoveries to be tested in an industrial setting. At the same time, there is another active research field trying to create a novel category of Mn(I) complexes with diverse ligand frameworks based on a different bond activation approach. In fact, a characteristic of Mn(I) carbonyl complexes that has received relatively less attention within the catalysis field, is their capacity to coordinate σ-bonds. In the historical advancement of Mn(I) organometallic chemistry, there are numerous and well-documented instances of Mn(I) complexes coordinating E–H bonds (where E = C, Si or H). However, the use of this coordination mode has been somewhat overlooked in catalysis, with only a few sporadic examples taking advantage of it. As Mn(I) catalysis is experiencing a resurgence, σ-bond activation is becoming increasingly more common in catalytic applications. The historical development of this branch of research and its present evolution in the field of de(hydrogenation) catalysis will be examined in the upcoming sub-chapter of this work.

1.2. Mn(I) and Coordination of σ-bonds: Still Unexploited Catalytic Potential?

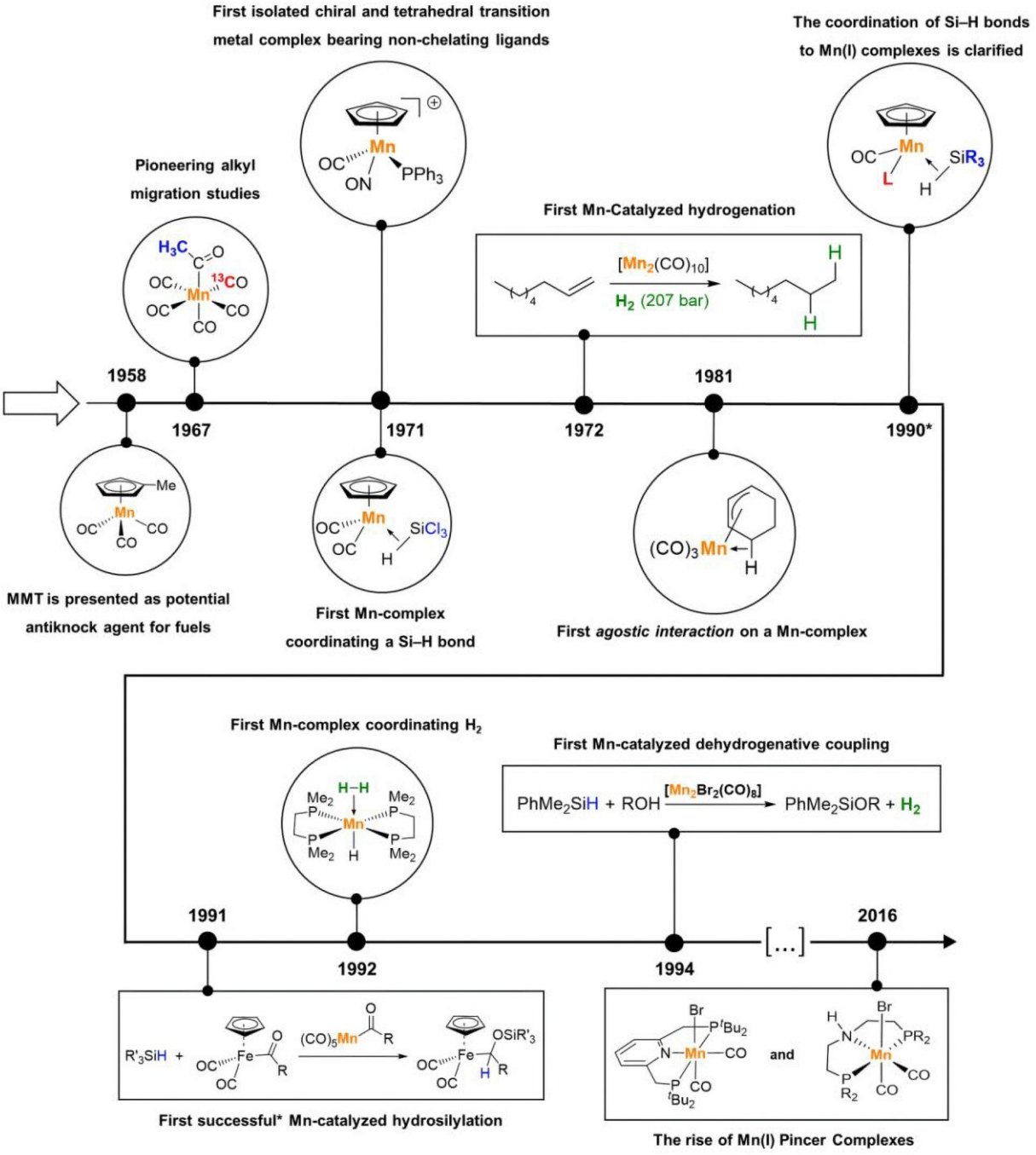
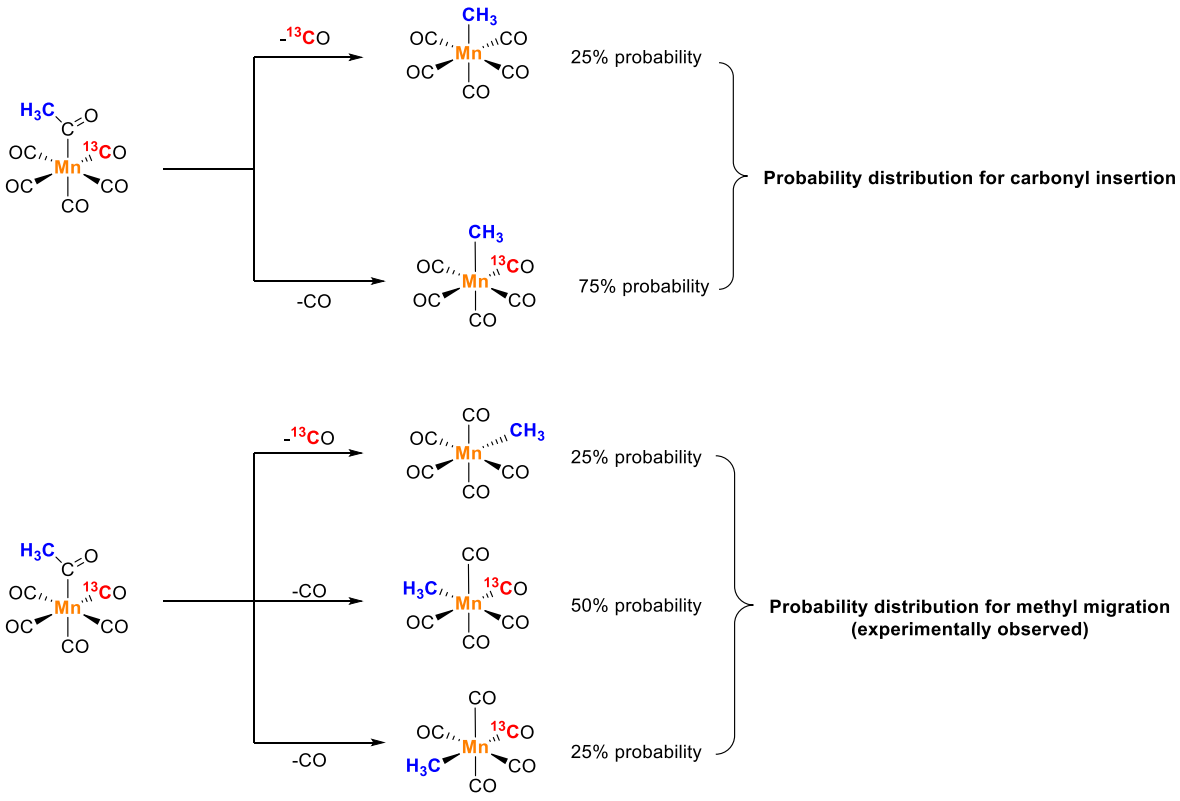


Figure 3: Historical steps in manganese organometallic chemistry concerning key σ-coordination modes and hydrogenation/dehydrogenation catalysis. *According to the opinion of the author.

In the 1950s, triggered by the isolation of ferrocene, chemists started to investigate the synthesis of organometallic compounds of different metals.[55] In particular, research focused also on manganese-based

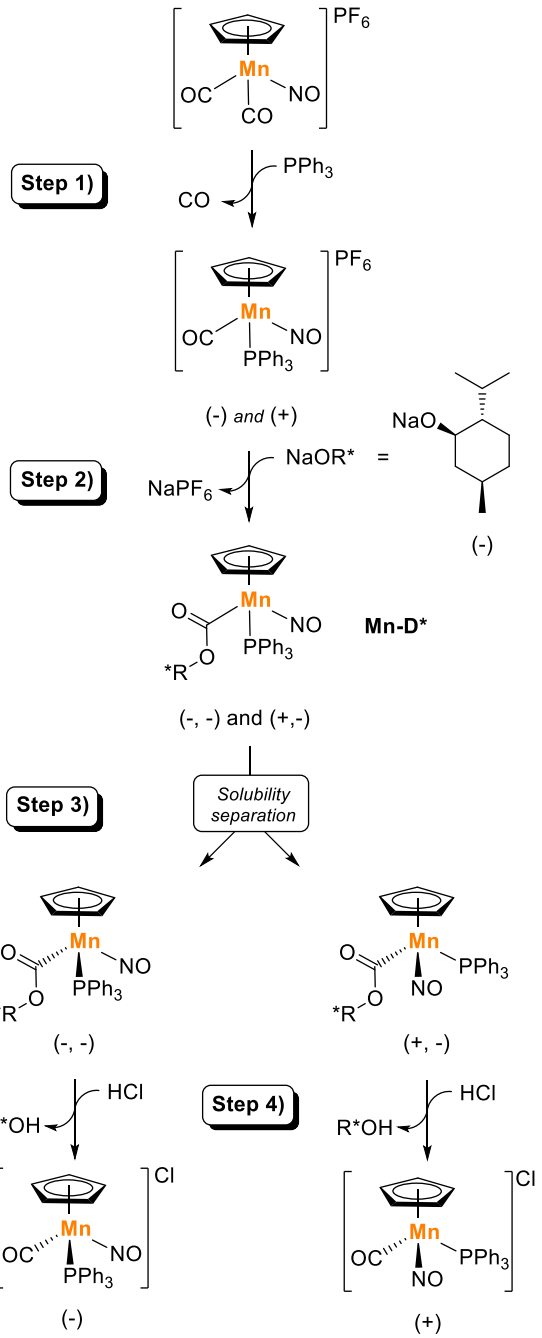
organometallic compounds that, over the course of history, significantly contributed to the development of the field. Already in 1958, Brown and Lovell from the laboratories of *Ethyl Corporation* introduced methylcyclopentadyenyl manganese tricarbonyl (MMT) as a potential antiknock agent for fuels.[56] A decade later, in 1967, Mn(I) alkyl carbonyl complexes were used to shed light on the debated mechanism of alkyl migration / CO insertion at the metal center. The labelling study was performed by Calderazzo and coworkers on $[Mn(CO)_5CH_3]$. After proving the microscopic reversibility of the reaction, the authors studied the labelling pattern of the decomposition product of the complex $[Mn(CO)_4(^{13}CO)(COCH_3)]$, that led to the conclusion that it is the methyl group which migrates on the CO ligand, and not the CO which inserts in the Mn-CH_3 bond. (**Scheme 12**).[49, 57]



Scheme 12: Reproduction of the results obtained by Calderazzo and coworkers in the controlled decomposition of a ^{13}C-labelled Mn-acetyl pentacarbonyl complex. After proving the microscopic reversibility of the reaction, the statistical pattern of the controlled decompositions showed that it is the -CH_3 which migrates on the CO, and not the CO to insert in the Mn-CH_3 bond.

Shortly after, in 1971, Brunner's work on a Mn(I) piano-stool complex achieved a landmark in asymmetric organometallic synthesis.[58] The complex $[CpMn(CO)(NO)(PPh_3)]Cl$ was the first tetrahedral transition metal complex to be isolated in both its enantioenriched enantiomers while being chiral at the metal and bearing four different ligands at the same time. The synthesis started from $[CpMn(CO)_2(NO)]PF_6$, where the substitution of one CO ligand with triphenylphosphine afforded a racemic mixture of the two complexes with formula $[CpMn(CO)(NO)(PPh_3)]PF_6$ (**Scheme 13**). The racemic mixture was reacted with (-)-menthol

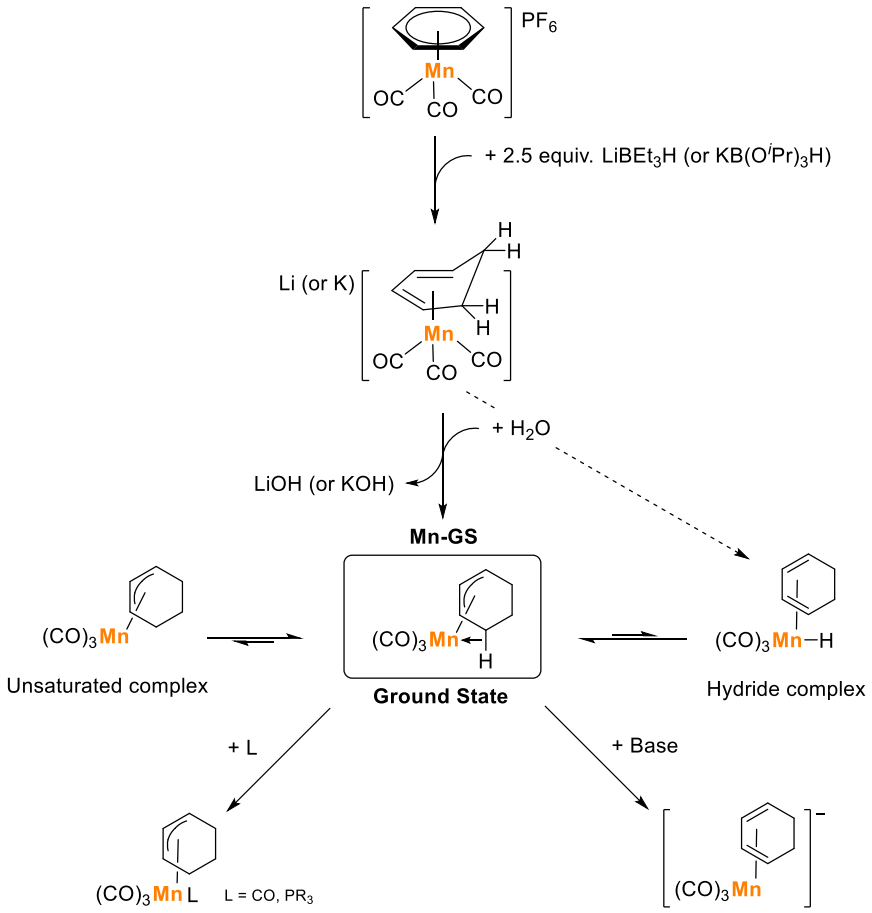
to afford the two corresponding diasteroisomeric acyl complexes **Mn-D***, which were separated due to their notable differences in solubility in organic solvents. The treatment of each diasteroisomer with HCl removed the (-)-menthol, regenerating the carbonyl ligand and affording the two enatioenriched enantiomers of [CpMn(CO)(NO)(PPh_3)]Cl.



Scheme 13: Strategy followed by Brunner and coworkers for the synthesis and isolation of the first tetrahedral transition metal complex chiral at the metal and bearing four different ligands.

Another important milestone that was set with the participation of a Mn(I) carbonyl complex is the definition of *agostic interaction*. In 1981, Brookhart and coworkers were studying the reactivity of nucleophiles

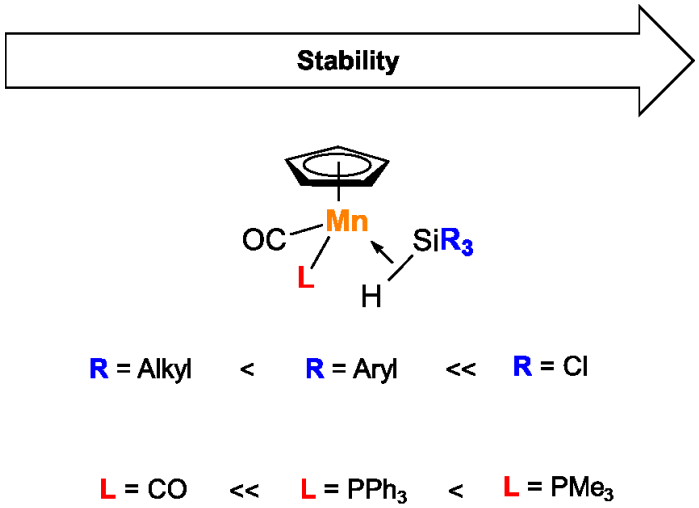
towards arenes coordinated to transition metals. While studying the cationic complex $[Mn(benzene)(CO)_3]PF_6$ in the presence of borohydrides, they obtained the allyl complex **Mn-GS** (**Scheme 14**), containing the peculiar coordination of a C–H bond *via* a "*3 centers - 2 electrons bond*".[59] The remarkable stability of the complex allowed for a detailed investigation of the bonding situation between the C–H bond and the metal. The results of this investigation, along with many other examples, were documented in the seminal report by Brookhart and Green in which they defined the fascinating coordination mode as *agostic interaction.*[60] The term comes from the greek "*αγοστώ"*, meaning "*to hold close to oneself*", and is still in use today in organometallic chemistry.



Scheme 14: Key steps in the work of Brookhart and coworkers that led to the isolation of the manganese complex **Mn-GS**, one of the first manganese complexes exhibiting an agostic interaction acknowledged as such.

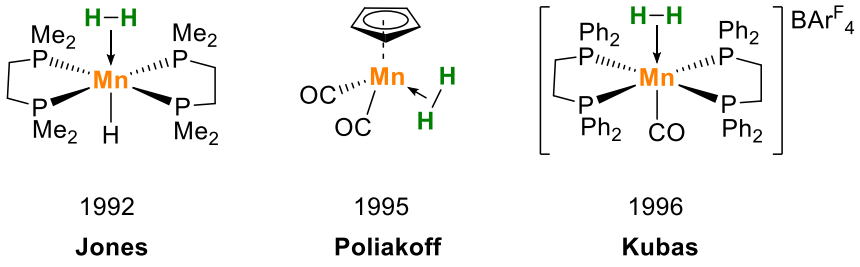
A similar bonding situation was also found between Si–H bonds and Mn(I) carbonyl complexes. This time, we owe the findings to the efforts of Schubert and other groups.[61] The very first derivatives of methylcyclopentadienyl manganese tricarbonyl coordinating Si–H bonds were prepared already in 1971.[62] However, it wasn't until the 80s that they served as model complexes for a detailed investigation of the σ-coordination of different Si–H bonds. The studies involved systematic variations on both the ligand

environment of the complex and the substitution on the hydrosilane, showing that it is possible to finely tune the degree of oxidative addition of the Si–H bond at the Mn(I) center.



Scheme 15: Influence of the electronic properties of both the substituents at the silicon and the ligands at the Mn have on the stability of the Si–H bond coordination.

The strength of the σ-coordination is strongly influenced by the electronic properties of both the metal and the silicon atom. In fact, it was experimentally observed that the stability of the resulting σ-complex increases as the substituents at the silicon become more electron-withdrawing, and as the ligands at the metal become more electron-donating (**Scheme 15**).[61] Computational studies confirmed that contribution of the π-backdonation of the metal to the LUMO of the corresponding Si–H bond is crucial for the stability of the coordination bond.[61]

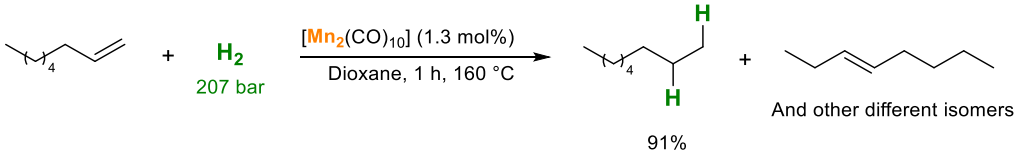


Scheme 16: Selected pioneering examples of Mn(I) dihydrogen complexes.

These detailed pioneering studies on the σ-coordination of C–H and Si–H bonds paved the way to the challenging η^2-σ-coordination of a neutral H_2 molecule to Mn(I) carbonyl complexes (**Scheme 16**). In 1992, Jones studied and characterized a manganese complex bearing the 1,2-bis(dimethylphosphino)ethane scaffold, $[Mn(dmpe)_2H(H_2)]$, proposing it as a potential model substrate for C–H activation;[63] a different

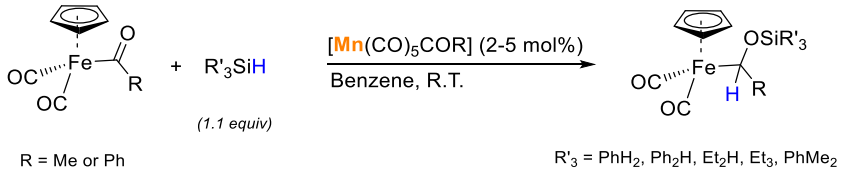
dihydrogen complex was prepared by Poliakoff in 1995 starting from the manganese cyclopentadienyl tricarbonyl [$CpMn(CO)_3$]. They showed that [$CpMn(CO)_3$] can be reacted with H_2 under photochemical irradiation in supercritical CO_2, to generate the complex [$CpMn(CO)_2(H_2)$].[64] A few years later, Kubas has also contributed to the field reporting in 1996 the synthetic procedure for the 16 electrons complex [$Mn(CO)(dppe)_2$]BAr^F_4, together with its reactivity towards H_2. The coordinatively unsaturated Mn(I) complex, generated by the reaction of [$MnBr(CO)(dppe)_2$] with $NaBAr^F_4$, could in fact reversibly coordinate N_2 and H_2.[65] This example was followed by another one in 2000 from the same group.[66]

In parallel to the steps forward taken in the coordination chemistry of σ-bonds, Mn(I) and Mn(0) carbonyl complexes started to be tested out as catalysts already in the 1970s. The first instances focused on reactions popular at the time, such as hydrogenation and hydroformylation. The first contribution to the field dates back to 1972, when Metlin and coworkers showed that [$Mn_2(CO)_{10}$] is able to catalyze the hydrogenation and hydroformylation of simple olefins such as, 1-octene and cyclohexene at 160 °C (**Scheme 17**).[67]



Scheme 17: First reported example for a Mn catalyzed hydrogenation reaction.

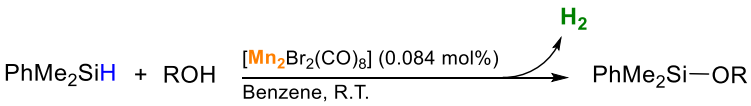
This constitutes the first example for a hydrogenation reaction catalyzed by a manganese complex. Subsequently, Fish and coworkers presented another example demonstrating that Mn(0) carbonyl complexes such as [$Mn_2(CO)_8(PBu_3)_2$] can catalyze the hydrogenation of some N-based heterocycles. To achieve this goal, they employed the catalyst in 5 mol% loading, a reaction temperature of 200 °C and 24 bar of syngas pressure.[68] Atwood followed the steps of these two examples, reporting the first instance of a Mn(I)-catalyzed photocatalytic reaction involving the hydrogenation and isomerization of alkenes, employing cis-[$Mn(CO)_4H(PPh_3)$] as the catalyst, again focusing on 1-octene as the substrate.[69]



Scheme 18: First reported example for a successful Mn catalyzed hydrosilylation reaction.

While evidence on the peculiar coordination mode between Mn(I) and Si–H bonds were collected, manganese carbonyl complexes were also studied as catalysts for their activation, marking some early examples of Mn(I) hydrosilylation catalysis promoted *via* σ-coordination. Following a pioneering report from Yates in 1982, where [$Mn_2(CO)_{10}$] could catalyze the hydrosilylation of ketones under UV irradiation

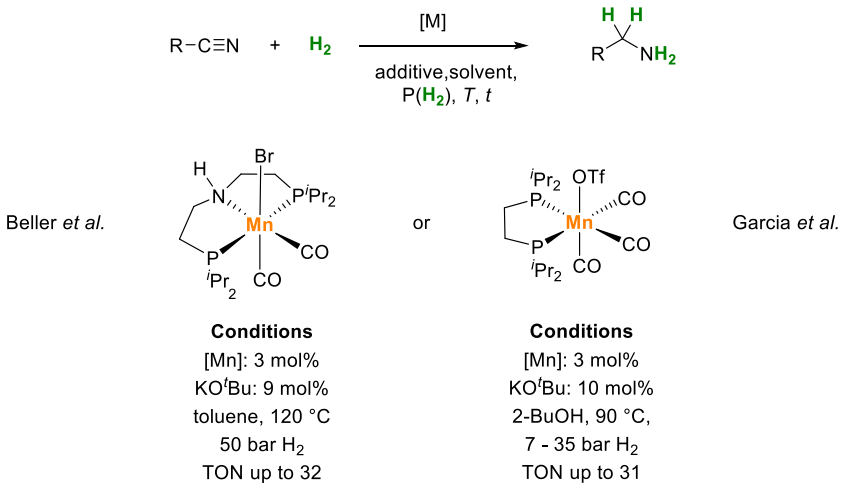
in 5% yield,[70] significant contributions to the field of Mn(I) hydrosilylation catalysis were made by the group of Cutler: in 1991 they used the Mn(I) acyl complexes [$Mn(CO)_5COMe$] and [$Mn(CO)_5COPh$] to hydrosilylate organoiron acyl complexes in very good yields (**Scheme 18**).[71] The same or similar acyl Mn(I) carbonyl complexes were used also by the same group to catalyze the hydrosilylation of esters in 1995,[72] of ketones in 1996,[73] and of other organometallic complexes.[74, 75]



Scheme 19: Pioneering work of Cutler and coworkers in the dehydrogenative coupling of $PhMe_2SiH$ with different alcohols catalyzed by [$Mn_2Br_2(CO)_8$].

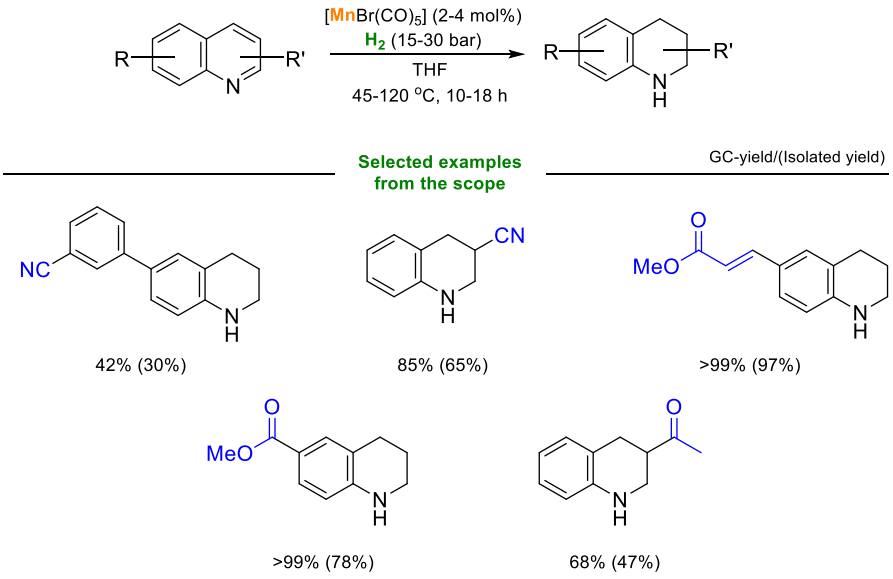
Another example of Mn(I) catalyzed Si–H bond activation that comes from the same group, using a different complex, was published in 1994. The dimeric version of [$MnBr(CO)_5$], [$Mn_2Br_2(CO)_8$], was used as a catalyst to perform the dehydrogenative coupling between $PhMe_2SiH$ and a range of different alcohols to the corresponding silyl-ethers (**Scheme 19**).[76]

With the exception of a few rare reports that utilized manganese carbonyl complexes in catalysis,[77, 78] their overall weaker performance in (de)hydrogenation catalysis when compared to other metals resulted in a relative lack of interest in Mn-based catalysts until 2016. However, the recent advancements in the chemistry of Mn(I) pincer complexes have revitalized interest in this metal, sparking a true *renaissance* in this area of manganese catalysis. Following the initial breakthroughs researchers began to develop novel Mn(I) catalysts that could show comparable or improved activity without the need for MLC. García and coworkers were successful in this task by using a very simple Mn(I) tricarbonyl complex to hydrogenate nitriles under basic conditions in the absence of a cooperative N-H functionality coordinated to the metal center.[79] Despite the absence of a MLCve site, it is possible to observe overall improved catalytic performances of the complex, that could even catalyze the hydrogenation of nitriles under milder conditions when compared to the Mn-MACHO from 2016 (**Scheme 20**).



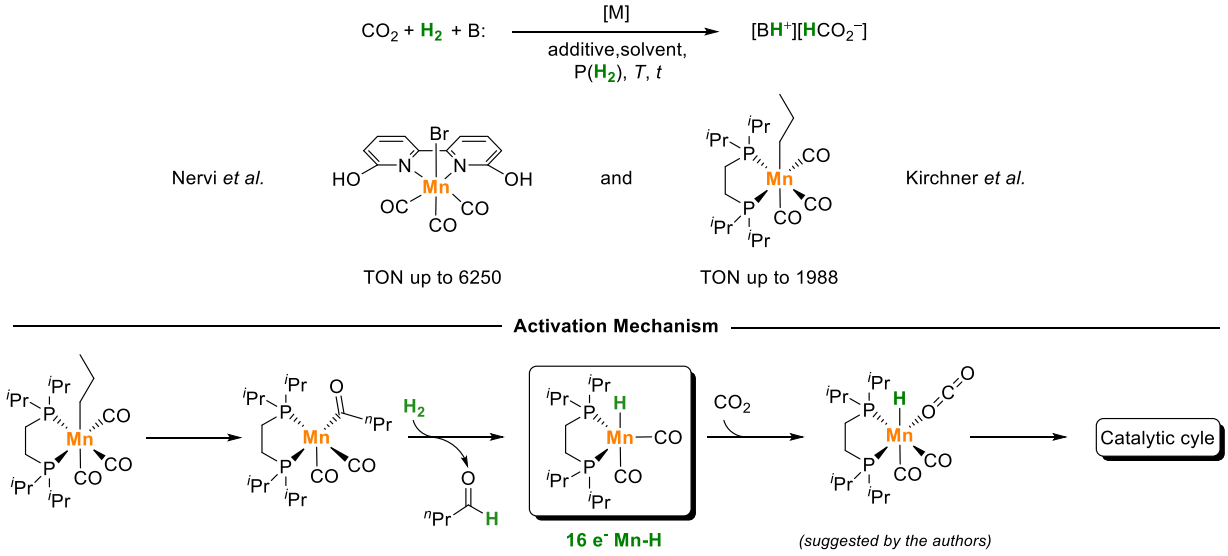
Scheme 20: Selected examples for the hydrogenation of nitriles using Mn(I) complexes.

Another interesting example comes from the Beller group, in which they used the simplest commercially available Mn(I) complex, $[MnBr(CO)_5]$, as a catalyst for the hydrogenation of quinolines.[80] The reaction conditions for the hydrogenation can be as mild as 45 °C and 15 bar of H_2. Several functional groups (including functionalities that can be hydrogenated by MLCve Mn(I) pincer complexes) were perfectly retained during the reaction. Ketones, esters (including α,β-unsaturated ones) and nitriles remained unreacted, allowing the synthesis of the corresponding tetrahydroquinolines in very good yields. This is a good example for the potential chemoselectivity that can be achieved with Mn(I) complexes not employing MLC (**Scheme 21**).



Scheme 21: General reaction scheme for the hydrogenation of quinolines to tetrahydroquinolines with H_2 catalyzed by $[MnBr(CO)_5]$ reported by Beller and coworkers. A selection of products from the substrate scope is reported with the corresponding yields.

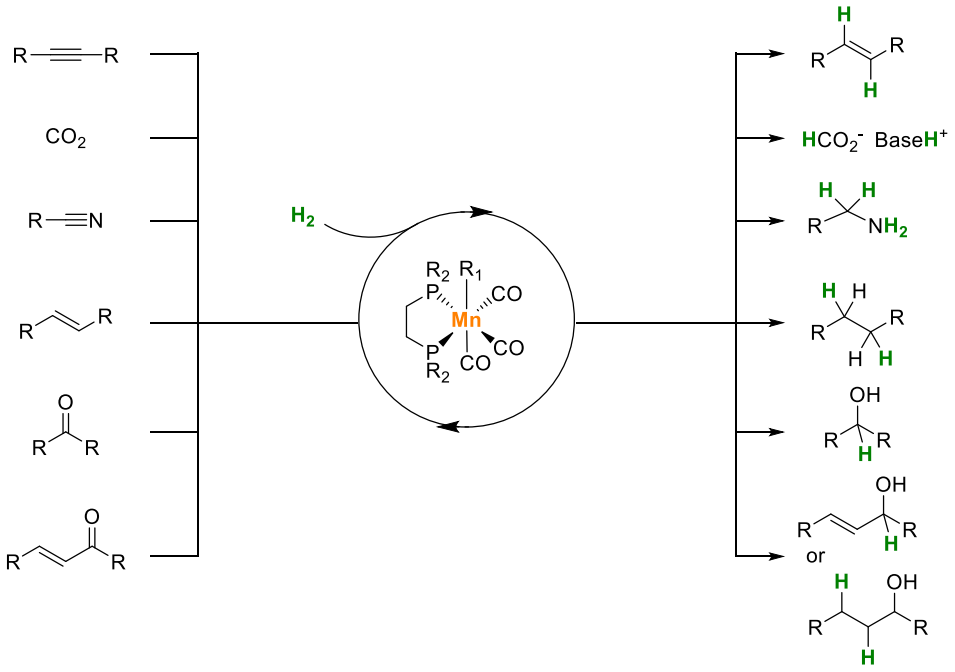
Other interesting contributions in this direction come from the field of CO_2 hydrogenation. Specifically, two non-pincer Mn(I) complexes which demonstrated the ability to hydrogenate CO_2 to formate upon base-activation.[81, 82] Among the two, the example of Weber and Kirchner is particularly interesting, since the activation mechanism of the complex draws inspiration from the insertion chemistry of Calderazzo (**Scheme 12**). The precatalyst for the reaction is a 1,2-bis(diisopropylphosphino) Mn(I) propyl tricarbonyl complex. The propyl chain is able to migrate on the CO ligand on the Mn already at room temperature. This insertion generates a very unstable 16 electrons acyl complex (**Scheme 22**), able to coordinate H_2 and activate it *via* a controlled decomposition. The products of this decompositions are another 16-electrons manganese complex with a hydride ligand, and butanal. The vacant coordination site can coordinate CO_2, that reacts with the hydride to form the first equivalent of formate and continues in the catalytic cycle. The resulting acyl complex generated *via* alkyl migration has been proven to be a very effective catalyst in hydrogenation and dehydrogenation reactions, as shown by the Kirchner group which used different variants of these 1,2-bis(dialkylphosphino)ethane-Mn-alkyl complexes as precatalyst to hydrogenate different organic substrates.[83]



Scheme 22: Top: selected examples for the hydrogenation of CO_2 to formate in the presence of base catalyzed by non-pincer Mn(I) complexes. Bottom: activation mechanism of the 1,2-bis(diisopropylphosphino)ethane Mn(I) propyl tricarbonyl complex reported by Kirchner and coworkers.

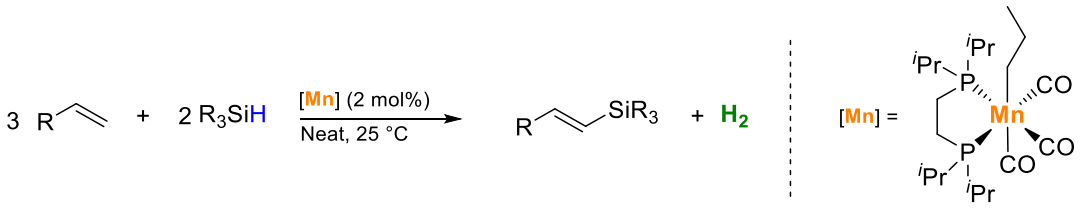
Ketones,[84, 85] nitriles[84, 86] and alkenes[87] can all been successfully hydrogenated to the desired products, even alkynes could be selectively semi-hydrogenated to E-alkenes (**Scheme 23**).[88] These unsaturated Mn(I) complexes were also able to successfully activate Si–H bonds in a dehydrogenative fashion: Kirchner and Weber developed the dehydrogenative coupling of different silanes with terminal alkenes to afford selectively E-vinylsilanes.[89] The reaction, carried out at R.T., opens an interesting synthetic pathway to

vinylsilanes, traditionally prepared *via* the nucleophilic substitution of a silyl-halide or an silyl-alkoxyde with a Grignard reagent (**Scheme 24**).



Scheme 23: Summary of the hydrogenation reactions catalyzed by Mn(I) alkyl tricarbonyl complexes so far.

The examples presented in this sub-chapter show that it is possible to move away from Metal–Ligand Cooperation for the development of simple and effective Mn-based catalytic systems. It was shown that Mn(I) complexes are able to perform both hydrogenation and dehydrogenation chemistry, without the need for a basic environment to trigger the MLCve mechanism. Especially, the progress made in the 20th-century Mn(I) coordination chemistry provides the foundation for the creation of a new generation of catalytic systems able to activate Si–H and H–H bonds *via* σ-coordination at the Mn(I) center. The research undertaken in this Ph.D. thesis will also focus towards this direction, placing particular emphasis on the investigation of both the mechanistic aspects and coordination attributes required to facilitate an efficient σ-bond activation. This approach will help in identifying the least elaborated catalyst for each desired transformation, and will ease the design of future homogenous Mn(I) organometallic catalysts for novel reactions.



Scheme 24: Scheme for the dehydrogenative coupling between silanes and olefines catalyzed by a Mn(I) alkyl complex.

1.3. Aim of the Thesis

The development of active, simple and scalable earth-abundant catalysts for hydrogenation and dehydrogenation reactions is a major challenge in the field of homogeneous catalysis. Initially, noble metals were predominantly used, but the introduction of pincer ligands employing Metal-Ligand Cooperation mechanisms significantly improved the catalytic performance of earth-abundant metals. Pincer complexes based on earth-abundant metals quickly gained popularity, as they could match or even outperform noble metals in certain cases. Metal-Ligand Cooperative Mn(I) pincer complexes have emerged as strong contenders for similar Ru(II) complexes, mimicking their reactivity and competing with them in activity. This resurgence in Mn catalysis renewed the interest of the catalysis community in this metal, prompting researchers to explore different Mn(I) catalysts.

The work of this Ph.D. thesis aims to develop novel Mn(I) catalytic systems drawing inspiration from the well-established coordination chemistry of Mn(I) with σ-bonds, rarely investigated in catalysis. More specifically, the thesis will mainly focus on the activation of Si–H and H–H bonds at Mn(I) fragments for the development of original reactions relevant to the field of chemical energy conversion. Particular attention will be placed to the elucidation of the mechanistic aspects of the catalytic systems, to obtain a clear picture of the coordination requirements of the Mn(I) center for the catalytic activation of Si–H and H–H bonds *via* σ-coordination. Such knowledge would facilitate the design of improved or novel catalytic systems while keeping the catalyst complexity to its minimum, promoting an easy scalability and reproducibility of the work.

1.4. References

1. Evans, D.; Osborn, J. A.; Jardine, F. H.; Wilkinson, G., Homogeneous Hydrogenation and Hydroformylation using Ruthenium Complexes. *Nature* **1965**, *208* (5016), 1203-1204.

2. Dub, P. A.; Gordon, J. C., The role of the metal-bound N–H functionality in Noyori-type molecular catalysts. *Nat. Rev. Chem.* **2018,** *2* (12), 396-408.

3. Liu, Y.; Yue, X.; Luo, C.; Zhang, L.; Lei, M. Mechanisms of Ketone/Imine Hydrogenation Catalyzed by Transition-Metal Complexes. *Energy Environ. Mater.* **2019**, *2* (4), 292–312.

4. Hutschka, F.; Dedieu, A.; Leitner, W., σ Metathesis as a Critical Step for the Transition Metal Catalyzed Formation of Formic Acid from CO_2 and H_2? An Ab Initio Investigation. *Angew. Chem. Int. Ed.* **1995**, *34* (16), 1742–1745.

5. Khusnutdinova, J. R.; Milstein, D., Metal–Ligand Cooperation. *Angew. Chem. Int. Ed.* **2015**, *54* (42), 12236-12273.

6. Gunanathan, C.; Milstein, D., Metal–Ligand Cooperation by Aromatization–Dearomatization: A New Paradigm in Bond Activation and "Green" Catalysis. *Acc. of Chem. Res.* **2011,** *44* (8), 588-602.

7. Milstein, D., Metal–ligand cooperation by aromatization–dearomatization as a tool in single bond activation. *Phil. Trans. R. Soc. A.* **2015**, *373* (2037), 20140189.

8. Higashi, T.; Kusumoto, S.; Nozaki, K., Cleavage of Si–H, B–H, and C–H Bonds by Metal–Ligand Cooperation. *Chem. Rev.* **2019,** *119* (18), 10393-10402.

9. Peris, E.; Crabtree, R. H., Key factors in pincer ligand design. *Chem. Soc. Rev.* **2018,** *47* (6), 1959-1968.

10. Gunanathan, C.; Milstein, D., Bond Activation and Catalysis by Ruthenium Pincer Complexes. *Chem. Rev.* **2014,** *114* (24), 12024-12087.

11. Zell, T.; Milstein, D., Hydrogenation and Dehydrogenation Iron Pincer Catalysts Capable of Metal–Ligand Cooperation by Aromatization/Dearomatization. *Acc. of Chem. Res.* **2015,** *48* (7), 1979-1994.

12. Balaraman, E.; Gunanathan, C.; Zhang, J.; Shimon, L. J.; Milstein, D., Efficient hydrogenation of organic carbonates, carbamates and formates indicates alternative routes to methanol based on CO_2 and CO. *Nat. Chem.* **2011,** *3* (8), 609-14.

13. Han, Z. B.; Rong, L. C.; Wu, J.; Zhang, L.; Wang, Z.; Ding, K. L., Catalytic Hydrogenation of Cyclic Carbonates: A Practical Approach from CO_2 and Epoxides to Methanol and Diols. *Angew. Chem. Int. Edit.* **2012,** *51* (52), 13041-13045.

14. Balaraman, E.; Ben-David, Y.; Milstein, D., Unprecedented catalytic hydrogenation of urea derivatives to amines and methanol. *Angew. Chem. Int. Ed.* **2011,** *50* (49), 11702-5.

15. Filonenko, G. A.; van Putten, R.; Schulpen, E. N.; Hensen, E. J. M.; Pidko, E. A., Highly Efficient Reversible Hydrogenation of Carbon Dioxide to Formates Using a Ruthenium PNP-Pincer Catalyst. *ChemCatChem* **2014**, *6* (6), 1526–1530.

16. Rezayee, N. M.; Huff, C. A.; Sanford, M. S., Tandem amine and ruthenium-catalyzed hydrogenation of CO_2 to methanol. *J. Am. Chem. Soc.* **2015,** *137* (3), 1028-31.

17. Kothandaraman, J.; Goeppert, A.; Czaun, M.; Olah, G. A.; Prakash, G. K. S., Conversion of CO_2 from Air into Methanol Using a Polyamine and a Homogeneous Ruthenium Catalyst. *J. Am. Chem. Soc.* **2016,** *138* (3), 778-781.

18. Kar, S.; Sen, R.; Goeppert, A.; Prakash, G. K. S., Integrative CO_2 Capture and Hydrogenation to Methanol with Reusable Catalyst and Amine: Toward a Carbon Neutral Methanol Economy. *J. Am. Chem. Soc.* **2018,** *140* (5), 1580-1583.

19. Sen, R.; Goeppert, A.; Kar, S.; Prakash, G. K. S., Hydroxide Based Integrated CO_2 Capture from Air and Conversion to Methanol. *J. Am. Chem. Soc.* **2020,** *142* (10), 4544-4549.

20. Everett, M.; Wass, D. F., Highly productive CO_2 hydrogenation to methanol - a tandem catalytic approach via amide intermediates. *Chem. Commun.* **2017,** *53* (68), 9502-9504.

21. Gunanathan, C.; Milstein, D., Applications of Acceptorless Dehydrogenation and Related Transformations in Chemical Synthesis. *Science* **2013,** *341* (6143), 1229712.

22. Remmel, A., Why Chemists Can't Quit Palladium. *Nature News Feature* **2022,** *606* (7914), 448-451.

23. Nuss, P.; Eckelman, M. J., Life Cycle Assessment of Metals: A Scientific Synthesis. *PLOS ONE* **2014,** *9* (7), e101298.

24. Fürstner, A., Iron Catalysis in Organic Synthesis: A Critical Assessment of What It Takes To Make This Base Metal a Multitasking Champion. *ACS Cent. Sci.* **2016,** *2* (11), 778-789.

25. Darwish, M.; Wills, M., Asymmetric catalysis using iron complexes – 'Ruthenium Lite'? *Catal. Sci. & Technol.* **2012,** *2* (2), 243-255.

26. Mukherjee, A.; Nerush, A.; Leitus, G.; Shimon, L. J.; Ben David, Y.; Espinosa Jalapa, N. A.; Milstein, D., Manganese-Catalyzed Environmentally Benign Dehydrogenative Coupling of Alcohols and Amines to Form Aldimines and H_2: A Catalytic and Mechanistic Study. *J. Am. Chem. Soc.* **2016,** *138* (13), 4298-301.

27. Elangovan, S.; Topf, C.; Fischer, S.; Jiao, H.; Spannenberg, A.; Baumann, W.; Ludwig, R.; Junge, K.; Beller, M., Selective Catalytic Hydrogenations of Nitriles, Ketones, and Aldehydes by Well-Defined Manganese Pincer Complexes. *J. Am. Chem. Soc.* **2016,** *138* (28), 8809-14.

28. Elangovan, S.; Garbe, M.; Jiao, H.; Spannenberg, A.; Junge, K.; Beller, M., Hydrogenation of Esters to Alcohols Catalyzed by Defined Manganese Pincer Complexes. *Angew. Chem. Int. Ed.* **2016,** *55* (49), 15364-15368.

29. Elangovan, S.; Neumann, J.; Sortais, J. B.; Junge, K.; Darcel, C.; Beller, M., Efficient and selective N-alkylation of amines with alcohols catalysed by Manganese pincer complexes. *Nat. Commun.* **2016,** *7*, 12641.

30. Kaithal, A.; Holscher, M.; Leitner, W., Catalytic Hydrogenation of Cyclic Carbonates using Manganese Complexes. *Angew. Chem. Int. Ed.* **2018,** *57* (41), 13449-13453.

31. Kumar, A.; Janes, T.; Espinosa-Jalapa, N. A.; Milstein, D., Manganese Catalyzed Hydrogenation of Organic Carbonates to Methanol and Alcohols. *Angew. Chem. Int. Ed.* **2018,** *57* (37), 12076-12080.

32. Zubar, V.; Lebedev, Y.; Azofra, L. M.; Cavallo, L.; El-Sepelgy, O.; Rueping, M., Hydrogenation of CO_2 -Derived Carbonates and Polycarbonates to Methanol and Diols by Metal-Ligand Cooperative Manganese Catalysis. *Angew. Chem. Int. Ed.* **2018,** *57* (41), 13439-13443.

33. Das, U. K.; Kumar, A.; Ben-David, Y.; Iron, M. A.; Milstein, D., Manganese Catalyzed Hydrogenation of Carbamates and Urea Derivatives. *J. Am. Chem. Soc.* **2019,** *141* (33), 12962-12966.

34. Webpage *Dimensions AI* - "Mn" or "Mn Catal" as free text in title or abstract. (accessed September 4th, 2023) https://app.dimensions.ai/discover/publication?search_mode=content&search_text=Mn&search_type=kws&search_field=text_search.

35. Zhang, L.; Wang, Z.; Han, Z.; Ding, K., Manganese-Catalyzed anti-Selective Asymmetric Hydrogenation of α-Substituted β-Ketoamides. *Angew. Chem. Int. Ed.* **2020,** *59* (36), 15565-15569.

36. Bertini, F.; Glatz, M.; Gorgas, N.; Stoger, B.; Peruzzini, M.; Veiros, L. F.; Kirchner, K.; Gonsalvi, L., Carbon dioxide hydrogenation catalysed by well-defined Mn(I) PNP pincer hydride complexes. *Chem. Sci.* **2017,** *8* (7), 5024-5029.

37. Kumar, A.; Daw, P.; Espinosa-Jalapa, N. A.; Leitus, G.; Shimon, L. J.; Ben-David, Y.; Milstein, D., CO_2-activation by Manganese pincer complexes through different modes of metal–ligand cooperation. *Dalton Trans.* **2019,** *48* (39), 14580-14584.

38. Schlenker, K.; Christensen, E. G.; Zhanserkeev, A. A.; McDonald, G. R.; Yang, E. L.; Lutz, K. T.; Steele, R. P.; VanderLinden, R. T.; Saouma, C. T., Role of Ligand-Bound CO_2 in the Hydrogenation of CO_2 to Formate with a (PNP)Mn Catalyst. *ACS Catal.* **2021,** *11* (13), 8358-8369.

39. Tondreau, A. M.; Boncella, J. M., 1,2-Addition of Formic or Oxalic Acid to $^{-}N\{CH_2CH_2(PiPr_2)\}_2$ -Supported Mn (I) dicarbonyl complexes and the Manganese-mediated decomposition of formic acid. *Organometallics* **2016,** *35* (12), 2049-2052.

40. Anderson, N. H.; Boncella, J.; Tondreau, A. M. Manganese-Mediated Formic Acid Dehydrogenation. *Chem. Eur. J.* **2019,** *25* (45), 10557-10560.

41. Wei, D.; Sang, R.; Sponholz, P.; Junge, H.; Beller, M., Reversible hydrogenation of carbon dioxide to formic acid using a Mn-pincer complex in the presence of lysine. *Nat. Energy* **2022,** *7* (5), 438-447.

42. Olah, G. A., Beyond Oil and Gas: The Methanol Economy. *Angew. Chem. Int. Ed.* **2005,** *44* (18), 2636-2639.

43. Kar, S.; Goeppert, A.; Kothandaraman, J.; Prakash, G. K. S., Manganese-Catalyzed Sequential Hydrogenation of CO_2 to Methanol via Formamide. *ACS Catal.* **2017,** *7* (9), 6347-6351.

44. Kuß, D. A.; Hölscher, M.; Leitner, W., Hydrogenation of CO_2 to Methanol with Mn-PNP-Pincer Complexes in the Presence of Lewis Acids: the Formate Resting State Unleashed. *ChemCatChem* **2021***, 13* (14), 3319–3323.

45. Kuß, D. A.; Hölscher, M.; Leitner, W., Combined Computational and Experimental Investigation on the Mechanism of CO_2 Hydrogenation to Methanol with Mn-PNP-Pincer Catalysts. *ACS Catal.* **2022,** *12* (24), 15310-15322.

46. Gladysz, J. A., Transition Metal Formyl Complexes. In *Advances in Organometallic Chemistry*, Stone, F. G. A.; West, R., Eds. Academic Press: 1982; Vol. 20, pp 1-38.

47. Berke, H.; Hoffmann, R., Organometallic migration reactions. *J. Am. Chem. Soc.* **1978,** *100* (23), 7224-7236.

48. Ziegler, T.; Versluis, L.; Tschinke, V., Migratory aptitude of hydride and methyl towards carbon monoxide, thiocarbonyl, and carbene in $RMn(CO)_4XY$ (XY = CO, CS, CH_2; R = H, Me). A theoretical study by the Hartree-Fock-Slater transition-state method. *J. Am. Chem. Soc.* **1986,** *108* (4), 612-617.

49. Noack, K.; Calderazzo, F., Carbon monoxide insertion reactions V. The carbonylation of methylmanganese pentacarbonyl with ^{13}CO. *J. Organomet. Chem.* **1967,** *10* (1), 101-104.

50. Kar, S.; Goeppert, A.; Prakash, G. K. S., Catalytic Homogeneous Hydrogenation of CO to Methanol via Formamide. *J. Am. Chem. Soc.* **2019**, *141* (32), 12518-12521.

51. Ryabchuk, P.; Stier, K.; Junge, K.; Checinski, M. P.; Beller, M., Molecularly Defined Manganese Catalyst for Low-Temperature Hydrogenation of Carbon Monoxide to Methanol. *J. Am. Chem. Soc.* **2019**, *141* (42), 16923-16929.

52. Kaithal, A.; Werlé, C.; Leitner, W., Alcohol-Assisted Hydrogenation of Carbon Monoxide to Methanol Using Molecular Manganese Catalysts. *JACS Au* **2021**, *1* (2), 130-136.

53. Kaithal, A.; Chatterjee, B.; Werlé, C.; Leitner, W., Acceptorless Dehydrogenation of Methanol to Carbon Monoxide and Hydrogen using Molecular Catalysts. *Angew. Chem. Int. Ed.* **2021**, *60* (51), 26500-26505.

54. Yang, W.; Chernyshov, I. Y.; van Schendel, R. K. A.; Weber, M.; Müller, C.; Filonenko, G. A.; Pidko, E. A., Robust and efficient hydrogenation of carbonyl compounds catalysed by mixed donor Mn(I) pincer complexes. *Nat. Commun.* **2021**, *12* (1), 12.

55. Reynolds, L. T.; Wilkinson, G., Some Methylcyclopentadienyl-Metal Compounds. *J. Inorg. Nucl. Chem.* **1959,** *9* (1), 86-92.

56. Brown, J. E.; Lovell, W. G. A New Manganese Antiknock. *Ind. Eng. Chem.* **1958**, *50* (10), 1547–1550.

57. Maitlis, P. M.; Belli Dell'Amico, D., Fausto Calderazzo: Pioneer in Mechanistic Organometallic Chemistry. *Organometallics* **2014,** *33* (24), 6989-7006.

58. Brunner, H. Optical Activity from Asymmetric Transition Metal Atoms. *Angew. Chem. Int. Ed.* **1971**, *10* (4), 249–260.

59. Lamanna, W.; Brookhart, M., Preparation and reactivity of the (cyclohexadiene)Manganese tricarbonyl anion. Potentially useful methods of arene and carbon-hydrogen bond activation. *J. Am. Chem. Soc.* **1981,** *103* (4), 989-991.

60. Brookhart, M., Green, M. L. H., Carbon-hydrogen-transition metal bonds. *J. Organomet. Chem.* **1983,** *250* (1), 395-408.

61. Schubert, U., η^2 Coordination of Si–H σ Bonds to Transition Metals. In *Advances in Organometallic Chemistry*, Stone, F. G. A.; West, R., Eds. Academic Press: 1990; Vol. 30, pp 151-187.

62. Graham, W. A. G.; Jetz, W., Silicon-transition metal chemistry. I. Photochemical preparation of silyl(transition metal) hydrides. *Inorg. Chem.* **1971,** *10* (1), 4-9.

63. Perthuisot, C.; Fan, M.; Jones, W. D., Catalytic thermal carbon-hydrogen activation with Manganese complexes: evidence for .η^2-H_2 coordination in a neutral Manganese complex and its role in carbon-hydrogen activation. *Organometallics* **1992,** *11* (11), 3622-3629.

64. Banister, J. A.; Lee, P. D.; Poliakoff, M., Flow Reactors for Preparative Chemistry in Supercritical Fluid Solution: "Solvent-Free" Synthesis and Isolation of $Cr(CO)_5(C_2H_4)$ and $(.\eta^5\text{-}C_5H_5)Mn(CO)_2(.\eta^2\text{-}H_2)$. *Organometallics* **1995,** *14* (8), 3876-3885.

65. King, W. A.; Luo, X.-L.; Scott, B. L.; Kubas, G. J.; Zilm, K. W., Cationic Manganese(I) Dihydrogen and Dinitrogen Complexes Derived from a Formally 16-Electron Complex with a Bis-Agostic Interaction, $[Mn(CO)(Ph_2PC_2H_4PPh_2)_2]^+$. *J. Am. Chem. Soc.* **1996,** *118* (28), 6782-6783.

66. Fang, X.; Huhmann-Vincent, J.; Scott, B. L.; Kubas, G. J., H2 binding to and silane alcoholysis on an electrophilic Mn(I) fragment with tied-back phosphite ligands. X-ray structure of a $Mn–CH_2Cl_2$ complex. *J. Organomet. Chem.* **2000,** *609* (1), 95-103.

67. Weil, T. A.; Metlin, S.; Wender, I., The $Mn_2(CO)_{10}$ catalyzed hydrogenation and hydroformylation of olefins. *J. Organomet. Chem.* **1973,** *49* (1), 227-232.

68. Fish, R. H.; Thormodsen, A. D.; Cremer, G. A., Homogeneous catalytic hydrogenation. 1. Regiospecific reductions of polynuclear aromatic and polynuclear heteroaromatic nitrogen compounds catalyzed by transition metal carbonyl hydrides. *J. Am. Chem. Soc.* **1982,** *104* (19), 5234-5237.

69. Bogdan, P. L.; Sullivan, P. J.; Donovan, T. A.; Atwood, J. D., Photocatalysis of hydrogenation and isomerization of alkenes by cis-$HMn(CO)_4PPh_3$. *J. Organomet. Chem.* **1984,** *269* (3), c51-c54.

70. Yates, R. L., Photoactivated homogeneous catalytic hydrosilylation of carbonyl compounds. *Journal of Catalysis* **1982,** *78* (1), 111-115.

71. Hanna, P. K.; Gregg, B. T.; Cutler, A. R., Manganese carbonyl compounds as hydrosilation catalysts for organoiron acyl complexes. *Organometallics* **1991,** *10* (1), 31-33.

72. Mao, Z.; Gregg, B. T.; Cutler, A. R., Catalytic hydrosilylation of organic esters using Manganese carbonyl acetyl complexes. *J. Am. Chem. Soc.* **1995,** *117* (40), 10139-10140.

73. DiBiase Cavanaugh, M.; Gregg, B. T.; Cutler, A. R., Manganese Carbonyl Complexes as Catalysts for the Hydrosilation of Ketones: Comparison with $RhCl(PPh_3)_3$. *Organometallics* **1996,** *15* (12), 2764-2769.

74. DiBiase Cavanaugh, M.; Gregg, B. T.; Chiulli, R. J.; Cutler, A. R., The reactions of hydrosilanes with the methoxycarbonyl complexes $Cp(L)(CO)MCO_2Me$(M = Fe, Ru; L = CO, PPh_3) and $(L)(CO)_xMCO_2Me$(M = Co, Mn; L = CO, PPh_3; x = 3,4, with and without catalysis. *Journal of Organometallic Chemistry* **1997,** *547* (1), 173-182.

75. Mao, Z.; Gregg, B. T.; Cutler, A. R., Manganese- and Rhodium-Catalyzed Phenylsilane Hydrosilation−Deoxygenation of Iron Acyl Complexes $Cp(L)(CO)FeC(O)R$ (L = CO, PPh_3, $P(OMe)_3$, $P(OPh)_3$; R = CH_3, Ph, $CHMe_2$, CMe_3). *Organometallics* **1998,** *17* (10), 1993-2002.

76. Gregg, B. T.; Cutler, A. R., Manganese Carbonyl Bromide-Catalyzed Alcoholysis of the Monohydrosilane $HSiMe_2Ph$. *Organometallics* **1994,** *13* (3), 1039-1043.

77. Zheng, J.; Chevance, S.; Darcel, C.; Sortais, J.-B., Selective reduction of carboxylic acids to aldehydes through Manganese catalysed hydrosilylation. *Chem. Commun.* **2013,** *49* (85), 10010-10012.

78. Zheng, J.; Elangovan, S.; Valyaev, D. A.; Brousses, R.; César, V.; Sortais, J.-B.; Darcel, C.; Lugan, N.; Lavigne, G., Hydrosilylation of Aldehydes and Ketones Catalyzed by Half-Sandwich Manganese(I) N-Heterocyclic Carbene Complexes. *Adv. Synth. Catal.* **2014,** *356* (5), 1093-1097.

79. Garduño, J. A.; García, J. J., Non-Pincer Mn(I) Organometallics for the Selective Catalytic Hydrogenation of Nitriles to Primary Amines. *ACS Catal.* **2019,** *9* (1), 392-401.

80. Papa, V.; Cao, Y.; Spannenberg, A.; Junge, K.; Beller, M., Development of a practical non-noble metal catalyst for hydrogenation of N-heteroarenes. *Nat. Catal.* **2020,** *3* (2), 135-142.

81. Dubey, A.; Nencini, L.; Fayzullin, R. R.; Nervi, C.; Khusnutdinova, J. R., Bio-Inspired Mn(I) Complexes for the Hydrogenation of CO_2 to Formate and Formamide. *ACS Catal.* **2017,** *7* (6), 3864-3868.

82. Kostera, S.; Weber, S.; Peruzzini, M.; Veiros, L. F.; Kirchner, K.; Gonsalvi, L., Carbon Dioxide Hydrogenation to Formate Catalyzed by a Bench-Stable, Non-Pincer-Type Mn(I) Alkylcarbonyl Complex. *Organometallics* **2021,** *40* (9), 1213-1220.

83. Weber, S.; Kirchner, K., Manganese Alkyl Carbonyl Complexes: From Iconic Stoichiometric Textbook Reactions to Catalytic Applications. *Acc. Chem. Res.* **2022,** *55* (18), 2740-2751.

84. Weber, S.; Stoger, B.; Kirchner, K., Hydrogenation of Nitriles and Ketones Catalyzed by an Air-Stable Bisphosphine Mn(I) Complex. *Org. Lett.* **2018,** *20* (22), 7212-7215.

85. Weber, S.; Brünig, J.; Veiros, L. F.; Kirchner, K., Manganese-Catalyzed Hydrogenation of Ketones under Mild and Base-free Conditions. *Organometallics* **2021,** *40* (9), 1388-1394.

86. Weber, S.; Veiros, L. F.; Kirchner, K., Old Concepts, New Application – Additive-Free Hydrogenation of Nitriles Catalyzed by an Air Stable Alkyl Mn(I) Complex. **2019,** *361* (23), 5412-5420.

87. Weber, S.; Stöger, B.; Veiros, L. F.; Kirchner, K., Rethinking Basic Concepts—Hydrogenation of Alkenes Catalyzed by Bench-Stable Alkyl Mn(I) Complexes. *ACS Catal.* **2019,** *9* (11), 9715-9720.

88. Farrar-Tobar, R. A.; Weber, S.; Csendes, Z.; Ammaturo, A.; Fleissner, S.; Hoffmann, H.; Veiros, L. F.; Kirchner, K., E-Selective Manganese-Catalyzed Semihydrogenation of Alkynes with H_2 Directly Employed or In Situ-Generated. *ACS Catal.* **2022,** *12* (4), 2253-2260.

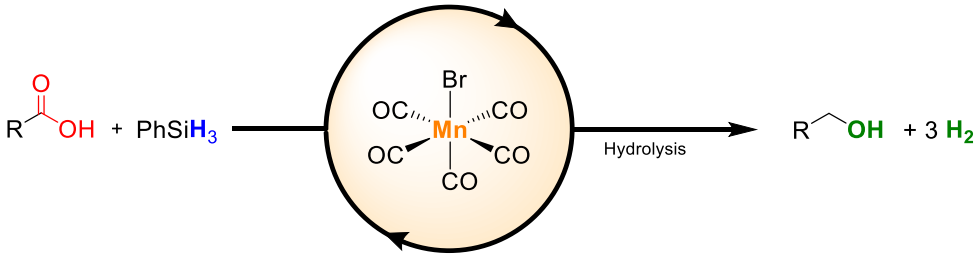
89. Weber, S.; Glavic, M.; Stöger, B.; Pittenauer, E.; Podewitz, M.; Veiros, L. F.; Kirchner, K., Manganese-Catalyzed Dehydrogenative Silylation of Alkenes Following Two Parallel Inner-Sphere Pathways. *J. Am. Chem. Soc.* **2021,** *143* (42), 17825-17832.

2. [MnBr(CO)$_5$] Catalyzed Reduction of Carboxylic Acids to Alcohols

Parts of this chapter have been published in:

Antico, E.; Schlichter, P.; Werlé, C.; Leitner, W. *JACS Au* **2021**, *1* (6), 742–749.

The work included in this chapter has been conducted in close cooperation with Peter Schlichter, whose data have been exclusively included in his Ph.D. thesis and are not part of the current chapter.



Scheme 25: Graphical abstract of Chapter 2.

2.1. Introduction

Carboxylic acids are widely available molecules that can be produced from different renewable sources, such as CO_2 or biomass. This makes carboxylic acids a very appealing class of substrates for the synthesis of intermediates applied in the chemical industry, such as alcohols. Alcohols can, in fact, serve as starting materials in the synthesis of surfactants,[1] or be applied as additives in diesel engines.[2, 3] Instead of relying on stoichiometric strong reducing agents such as diborane, $LiAlH_4$, or DIBAL-H, it would be desirable to develop a catalytic direct reduction of carboxylic acids, in accordance with the principles of green chemistry.[4] However, the free carboxylic acid functionality is particularly challenging to reduce catalytically, especially when employing a transition metal catalyst: the Brønsted acidity of the $–CO_2H$ group is often incompatible with MLC-pathways (normally activated *via* base), and its remarkable coordinative capabilities can deactivate the catalyst *via* formation of very stable coordination bonds.[5] These are among the reasons for which only very few examples are reported in the literature for the direct hydrogenation of carboxylic acids,[6-11] even though this methodology offers a highly atom economical approach to perform the reaction. The examples reported make mostly use of noble metals in combination with tailor-made ligands, requiring high reaction temperatures and H_2 pressures, reflecting the challenge associated with the reaction. In fact, there is only one example for this reaction reported with an earth-abundant metal catalyst so far, employing a system based on a Cobalt complex.[12]

A possible alternative route to perform the reduction, is by making use of silanes as reducing agents instead of molecular hydrogen. Silanes are non-toxic, widely available, easy to handle and the exothermic formation of Si–O bonds facilitates the reduction of polar C–O bonds.[13] While hydrosilylation is common in the

reduction of ketones, esters and amides,[14] the examples for the reduction of free carboxylic acids are quite scarce. Moreover, they often require a large excess of silane, need specialized equipment[19, 20] or make use of a catalyst based on noble metals such as Ru,[15, 16] Rh[17] or Ir.[18] In fact, there is just a handful of instances making use of earth-abundant catalysts for the hydrosilylation of carboxylic acids: Lemaire reported that the simple copper salt $Cu(OTf)_2$ can perform the reaction using a high catalyst loading.[21] Sortais and Darcel showed that carbonyl complexes of iron and manganese, respectively $[Fe(COD)(CO)_3]$ and $[Mn_2(CO)_{10}]$, can also catalyze the reaction, but only under photochemical conditions.[19, 20] Based on the previous work conducted on Mn(I) hydrosilylation chemistry,[22-29] it was decided to further investigate the work initiated in our group, where it was shown that a Mn(I) pincer complex bearing a triazole backbone can perform the hydrosilylation of ketones, esters and a small scope of carboxylic acids.[30]

2.2. Objective

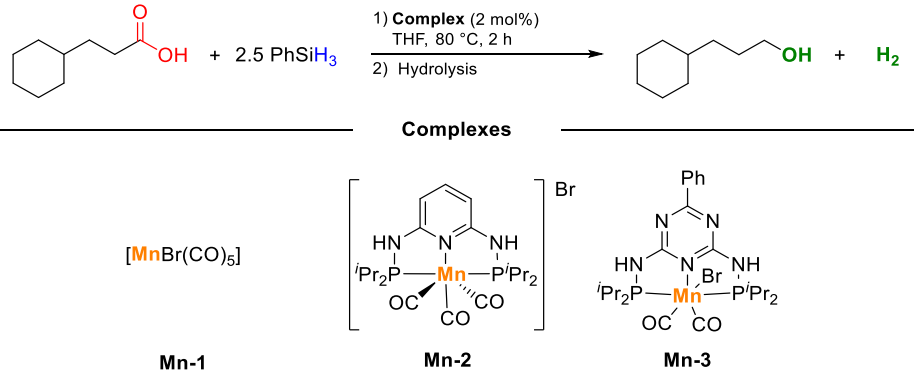
The development of a simple and bench-stable procedure for a dehydrogenative direct reduction of carboxylic acids to alcohols is the main objective of this work. After the seminal work performed in our group,[30] a simplification of the procedure and a significant cost-reduction of the catalytic system are among the main targets of this investigation. The gain of mechanistic insights is also among the goals of the study, with the aim of applying the results from the simplified catalytic system to other reactions.

2.3. Initial Screening and Optimization

3-Cyclohexylpropanoic acid was chosen as a model substrate to optimize the reaction. The initial conditions were chosen based on what was reported in the literature for similar Mn(I) complexes.[30] At first, different manganese complexes were screened in the reaction employing THF as a solvent and choosing a temperature of 80 °C (the results are summarized in **Table 1**). Interestingly, among all the Mn(I) complexes screened, it was $[MnBr(CO)_5]$ to afford the highest yield in 3-cyclohexyl-1-propanol (83%), performing better than both the complexes **Mn-2** (whose ligand framework has been recently reported by Kirchner and co-workers as an active catalyst for the hydrosilylation of carbon dioxide)[31] and **Mn-3** (a manganese-triazine pincer complex previously reported in hydrogenation reactions).[32] Preliminary activation of the MLCve complexes **Mn-2** and **Mn-3** was also performed by testing them out in the reaction in the presence of KO^{t}Bu as base. The experiment led **Mn-2** to form a solid gel, and **Mn-3** to successfully convert the starting acid into 3-cyclohexyl-1-propanol in 42% of yield. Other commercial complexes of manganese in different oxidation states were successively screened in the reaction, leading to no conversion of the starting material. KO^{t}Bu alone was also tested, resulting in the formation of an untreatable gel. Then, different solvents were screened in the reaction keeping $[MnBr(CO)_5]$ at a constant loading, in order to further improve its catalytic performances. Since all the solvents screened improved the results obtained in the neat reaction, in accordance with the principles of *green chemistry*,[33, 34] 2-MTHF was selected as the solvent of

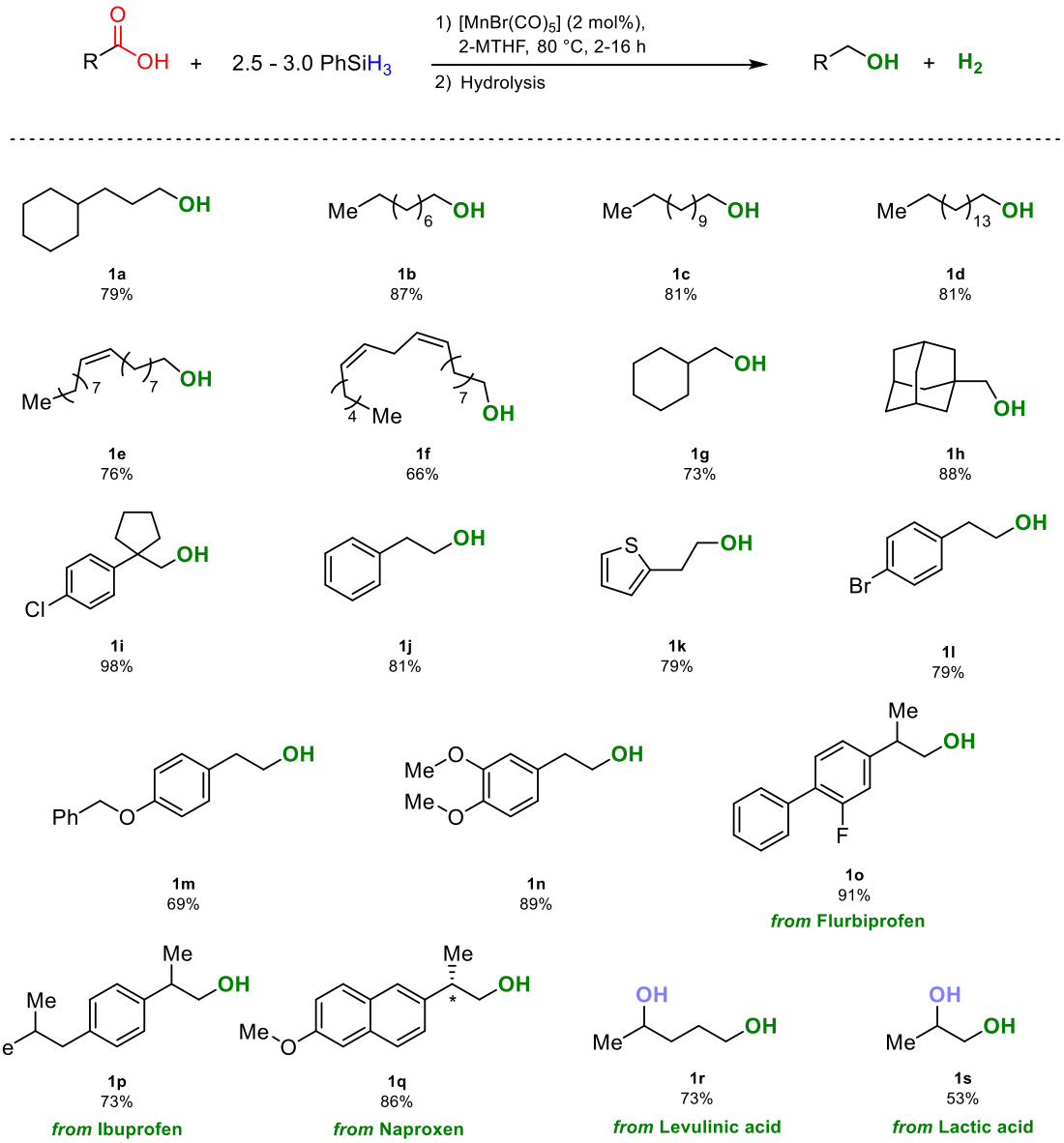
choice. Different silanes were also screened by Peter Schlichter, and $PhSiH_3$ performed the best. This knowledge was used to test the reaction in a scope of different carboxylic acids, whose results are reported in the following *sub-chapter*.

Table 1: Comparison of different complexes screened under identical conditions at a catalyst loading of 2 mol % with 2.5 equiv. of $PhSiH_3$ in THF at 80 °C. The ^{1}H-NMR yields after hydrolysis were determined with respect to ferrocene as internal standard.



Complex	Additive	Solvent	NMR Yield (%)
Mn-1	–	THF	83
Mn-2	–	THF	<5
Mn-3	–	THF	0
Mn-2	KO^{t}Bu (6 mol%)	THF	Solid gel
Mn-3	KO^{t}Bu (6 mol%)	THF	42
$MnCl_2$	–	THF	0
$MnBr_2$	–	THF	0
$Mn(acetate)_2(H_2O)_4$	–	THF	0
$Mn(OAc)_3(H_2O)_2$	–	THF	Trace
–	TBABr (2 mol%)	THF	0
–	KO^{t}Bu (2 mol%)	THF	Solid Gel
–	–	THF	0
Mn-1	–	Neat	87
Mn-1	–	2-MTHF	**96**
Mn-1	–	Toluene	92
Mn-1	–	Heptane	92
Mn-1	–	Cyclohexane	95
Mn-1	–	$CHCl_3$	>99

2.4. Reaction Scope and Catalytic Performances



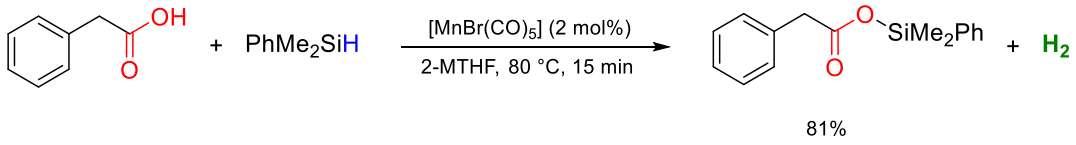
Scheme 26: Scope of the hydrosilylation of different carboxylic acids to their respective alcohols. The reaction conditions for each substrate are reported in Section 2.8.3.

Different carboxylic acids were tested in the optimized reaction conditions, employing a general reaction time of 4 hours (**Scheme 26**). Aliphatic terminal acids such as nonanoic acid, dodecanoic acid and hexadecanoic acid all produced the respective alcohols **1b**, **1c** and **1d** in very good yield. The presence of unsaturations along the chain, such as in the case of oleic and linoleic acid, was tolerated, allowing for retention of the respective alkene functionality in the alcohols **1e** and **1f** (even though [MnBr(CO)5] has been reported as an active hydrosilylation catalyst for alkenes).[25] Substrates of higher bulkiness, such as 1-adamantanecarboxylic acid and 1-(4-chlorophenyl)-1-cyclopentanecarboxylic acid required a longer reaction time, but they were also successfully reduced to their respective alcohols **1h** and **1i**. 2-Phenylacetic

acid derivatives proved to be particularly successful substrates for the reaction, regardless of the electronic and steric properties of the substituents on the aromatic ring. The presence of an oxygen (in the form of a methoxy- or benzyloxy- group), a halogen (such as a fluoride or a bromide) or a heterocycle in place of the phenyl substituent (such as thiophene) were all tolerated without incurring in side reactions, affording the alcohols **1j** to **1n**. Next, biologically active 2-phenylacetic acid derivatives such as Flurbiprofen, Ibuprofen and Naproxen were tested out in the reaction, affording very good yields in the products **1o**, **1p** and **1q**. The stereochemistry of the chiral center of the Naproxen alcohol was also examined. By measuring the specific optical rotation, it was confirmed that the (S)-configuration of the chiral center of **1q** was completely retained from the starting material (S)-2-(6-methoxynaphthalen-2-yl)propanoic acid. Finally, the reaction was extended to acids potentially derivable from biomass such as levulinic acid and lactic acid, which were successfully converted to their respective diols **1r** and **1s**. Furthermore, aromatic carboxylic acids were also effectively reduced using slightly modified conditions, with detailed results documented in Peter Schlichter's thesis. After investigating the reaction scope, phenylacetic acid was used as a model substrate for studying the catalytic performances of [$MnBr(CO)_5$] in a loading of 0.5 mol%. A maximum TON of 156 was achieved.

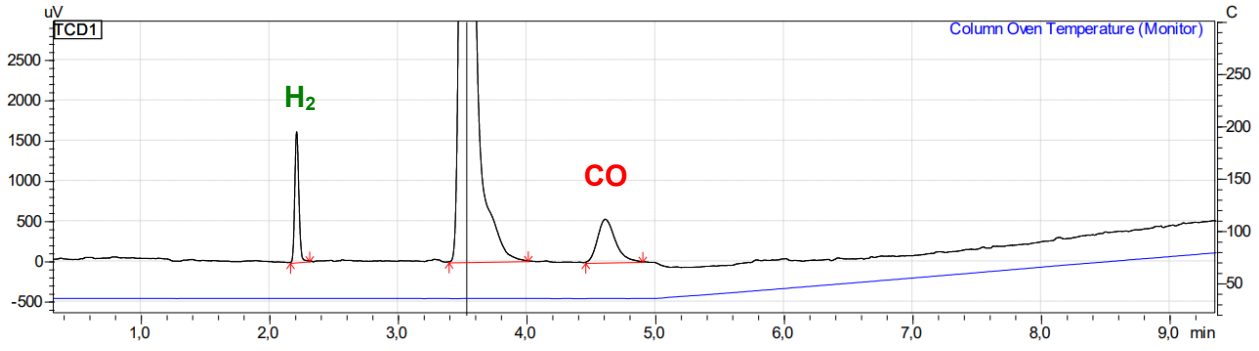
2.5. Mechanistic Insights

2.5.1. The formation of a silyl ester as first reaction step



Scheme 27: Reaction between 2-phenylacetic acid and dimethylphenylsilane.

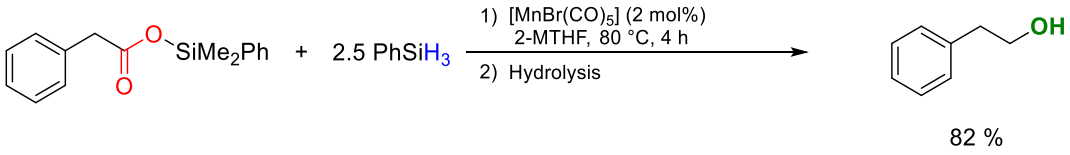
The synthesis of plausible reaction intermediates was targeted in order to gain insights into the reaction mechanism. 2-Phenylacetic acid was reacted with $PhMe_2SiH$ (a tertiary silane bearing only one hydridic hydrogen) in a 1:1 ratio under standard reaction conditions. In the absence of [MnBr(CO)$_5$], no reaction took place. However, the presence of 2 mol% of [MnBr(CO)$_5$] could lead to the formation of the corresponding silyl ester, isolated *via* distillation in 81% yield (**Scheme 27**). During the reaction it was possible to observe vigorous gas evolution, suggesting that the formation of the silyl-ester is the dehydrogenative step in the reaction. To confirm the dehydrogenative nature of the coupling, the reaction was repeated and its headspace was analyzed. Besides Ar, it was possible to detect H_2 and CO in a ratio of 25:1, indicating that [MnBr(CO)$_5$] is also dissociating an average of 2 CO molecules in the reaction (**Figure 4**).



Gas identified	Retention time (min)	Volume (%)
H_2	2.22	66.5
Ar	3.53	30.4
CO	4.61	3.1

Figure 4: GC-TCD data for the reaction between 2-phenylacetic acid and dimethylphenylsilane reported in Scheme 27.

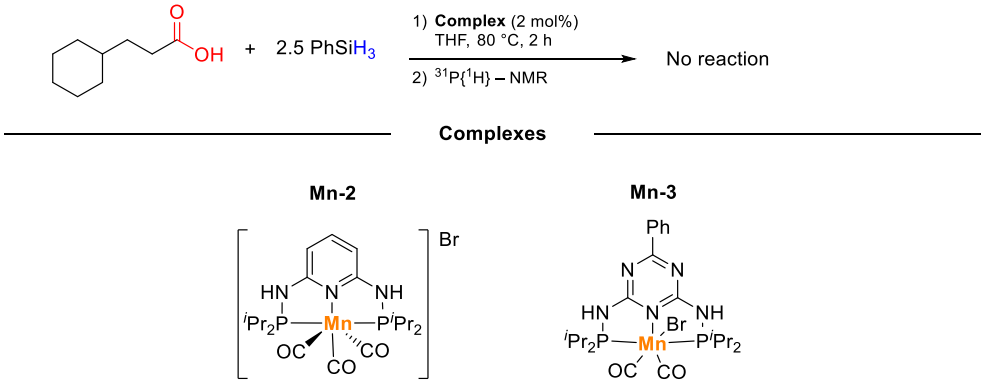
The silyl ester was then reacted with $PhSiH_3$ under standard reaction conditions, and 2-phenylethanol was obtained as the reaction product in 82% yield. This outcome supports the hypothesis that silyl esters are plausible reaction intermediates, which can be further reduced to the corresponding silyl ether, affording the alcohol after hydrolysis (**Scheme 28**). This result also shows that the hydrogen formed during the reaction is not playing a significant role in the reduction.



Scheme 28: Reaction of the silyl ester with $PhSiH_3$ in standard reaction conditions.

To further support the latter claim, a reaction using 2-phenylacetic acid as the substrate was repeated, allowing for the hydrogen to evolve out of the reaction vessel and exchanging its atmosphere with Ar. This experiment led to the same yield obtained in the scope in 2-phenylethanol, thus confirming that hydrogen does not play any major role in the catalysis.

2.5.2. The need for a coordinatively unsaturated complex as a catalyst



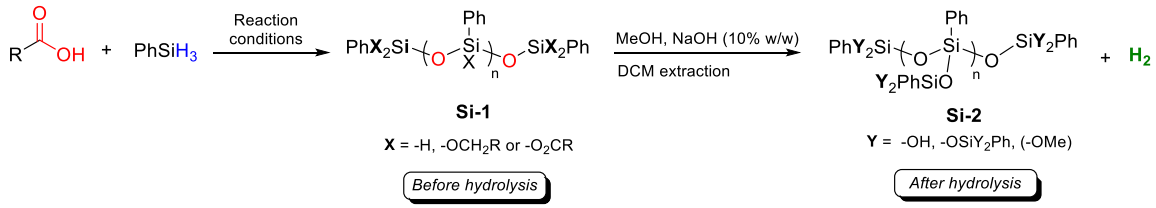
	Mn-2	Mn-3
$^{31}P\{^{1}H\}$-NMR (ppm) after reaction	133.7	136.3
Literature value (ppm) for the complex	133.9	135.5

Table 2: Representation of the $^{31}P\{^{1}H\}$ data collected on the complexes screened in the reaction. The references for the values can be found in section 2.8.10, together with the characterization data of the complexes.

The results obtained during the optimization, together with the detection of CO in the headspace of a reaction using $[MnBr(CO)_5]$ as a catalyst (Section 2.5.1), suggest that a manganese complex should be in the oxidation state +I and should be able to access a free coordination site in order to be catalytically active (**Table 1**). The complexes **Mn-2** and **Mn-3** were further investigated in the reaction to examine whether

their inactivity can be attributed to the inability to generate a free coordination site under reaction conditions. First, the absence of CO in the gas phase of the reaction carried out in the presence of **Mn-2** and **Mn-3** was confirmed via GC-TCD. Subsequently, the $^{31}P\{^{1}H\}$-NMR of the crude reaction mixture before hydrolysis was analyzed. The ^{31}P chemical shift for the two complexes indicates that the ligand is still coordinated to the metal center (**Table 2**). Therefore, their inactivity in catalysis when employed as such can be imputed to their inertness towards generating a free coordination site.

2.5.3. The nature of the Si–based species during the reaction



Scheme 29: Reaction products and byproducts containing silicon formed during the different steps of the reaction.

The Si-based products formed during the reaction were investigated by studying the crude reaction mixture of two different substrates prior to hydrolysis. The selected substrates for the analysis were 3-cyclohexylpropanoic acid and 4-trifluoromethylbenzoic acid. The crude reaction mixtures of these substrates with $PhSiH_3$ were directly analyzed respectively *via* ^{1}H- and $^{19}F\{^{1}H\}$-NMR. In the ^{1}H-NMR, it is possible to observe the formation of various singlets on a broad peak in the range 5.5 to 4.0 ppm (**Figure 5**). The singlets in this region (typical for Si–H bonds) likely correspond to the polysiloxanes formed during the reaction still bearing unreacted Si–H bonds.

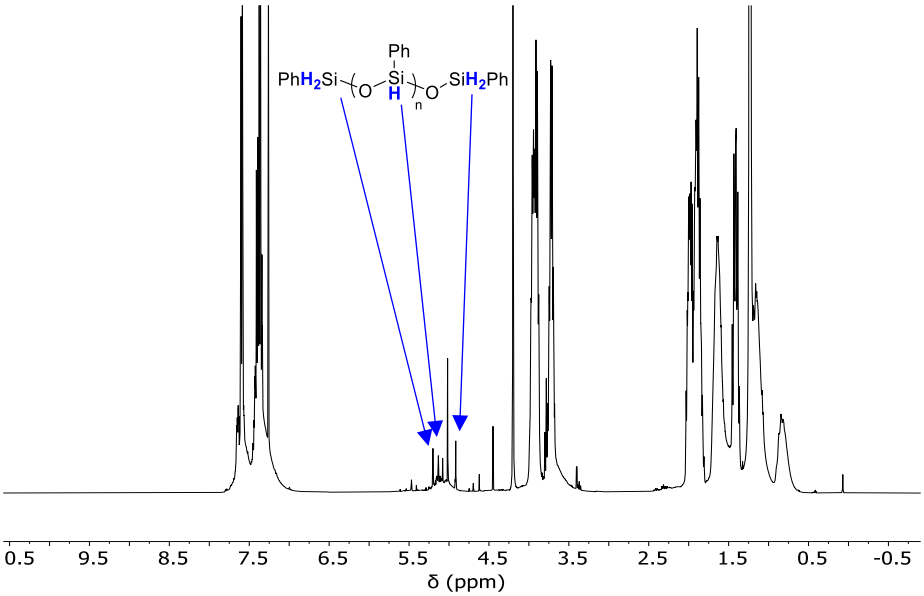


Figure 5: ^{1}H-NMR (400 MHz, $CDCl_3$, 296 K) of the crude mixture of a reaction between 3-cyclohexylpropanoic acid and $PhSiH_3$ before hydrolysis.

The $^{19}F\{^1H\}$-NMR shows instead a broad peak corresponding to the -CF_3 in para position respect to the pristine carboxylic acid functionality (**Figure 6**). The broadness of the signal, which was observed in a similar report,[39] suggests that the fluorine atoms are in a similar but non–identical chemical environment, pointing towards the presence of different siloxane species bound to the protected alcohol.

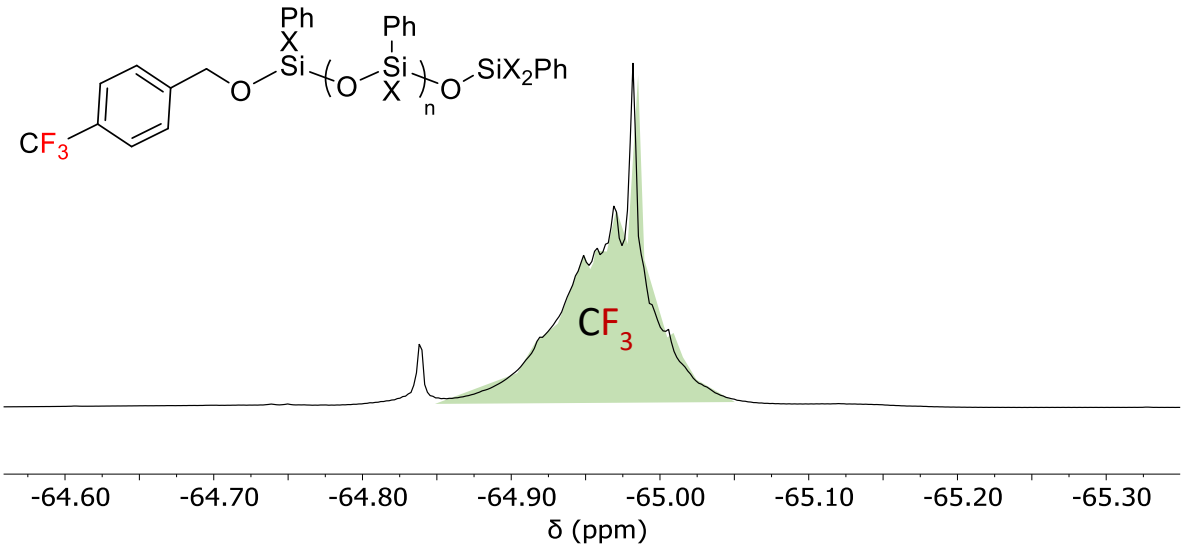
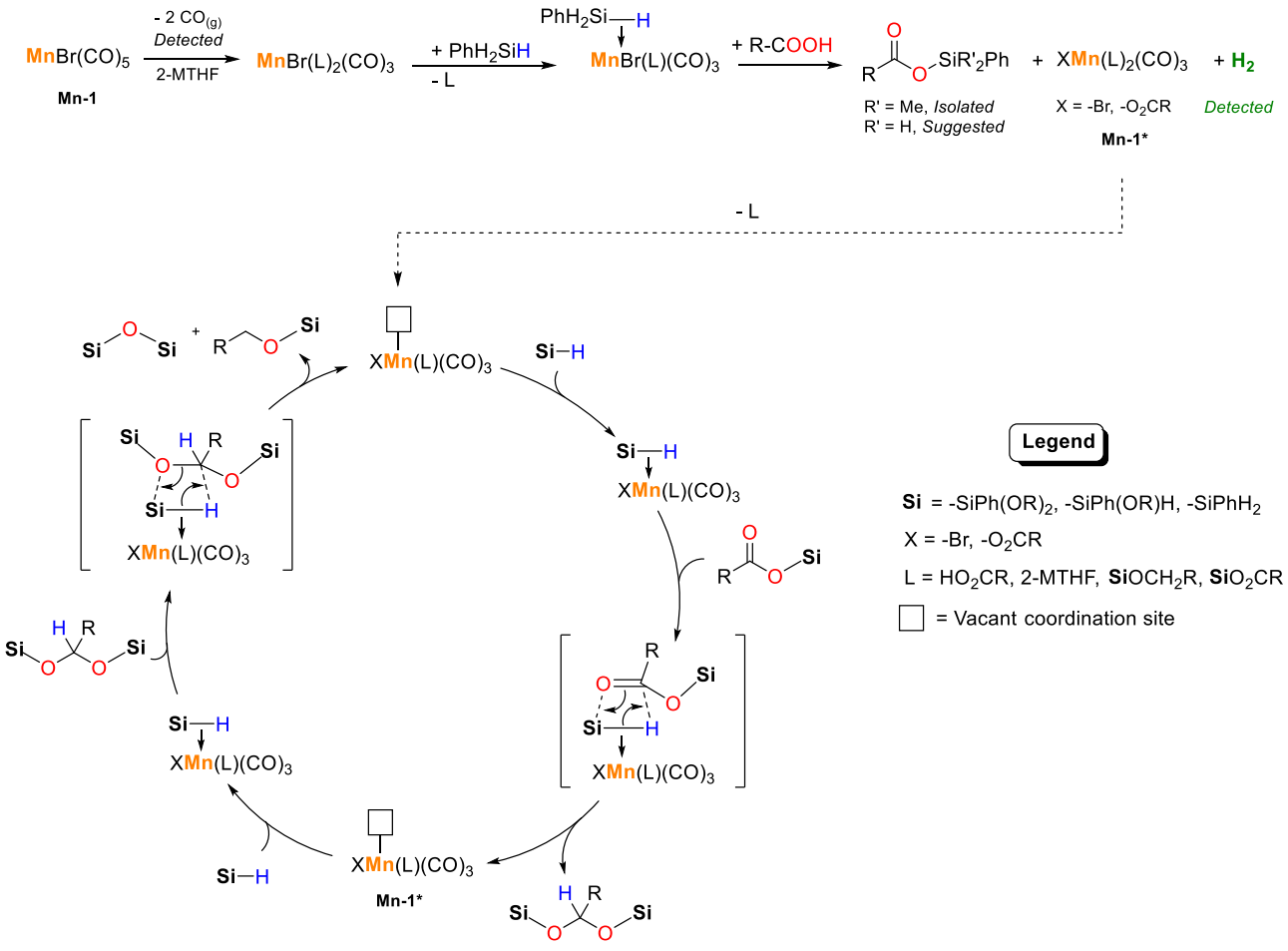


Figure 6: $^{19}F\{^1H\}$-NMR (376 MHz, THF-d_8, 296 K) of the crude reaction mixture of a reaction between 4-trifluoromethylbenzoic acid and phenylsilane before hydrolysis.

2.6. Suggested Mechanistic Cycle

A reaction mechanism consistent with the experimental data is suggested in **Scheme 30**. The reaction begins with the dissociation of CO from the [MnBr(CO)$_5$] center, allowing for the formation of an unsaturated complex able to activate the Si–H bond of PhSiH$_3$ *via* σ-coordination. The activated Si–H bond can readily react with the carboxylic acid *via* the dehydrogenative formation of the silyl ester as the first step of the reaction. The unsaturated catalytically active species can again activate Si–H bonds, according to the same mechanism, and further reduce the silyl ester ultimately leading to the silyl ether (or protected alcohol) and the corresponding polysiloxane species as byproducts. Conclusively, upon hydrolysis, the alcohol is desilylated and recovered from the aqueous phase.



Scheme 30 : Suggested mechanistic cycle for the hydrosilylation of carboxylic acids catalyzed by [MnBr(CO)$_5$].

2.7. Conclusion and Outlook

In conclusion, the improved catalytic performances of the bench stable and commercially available [$MnBr(CO)_5$], when compared to more elaborated Mn(I) complexes, could be demonstrated in this chapter. [$MnBr(CO)_5$] can catalyze the challenging reduction of a wide variety of carboxylic acids to their respective alcohols in high yields. The reaction proceeds first *via* the formation of silyl ester intermediates, followed by their hydrosilylation. The good catalytic performances of [$MnBr(CO)_5$] can be attributed to its ability to readily access a coordinatively unsaturated complex *via* dissociation of CO, allowing for a maximum TON of 156. This pathway for the generation of a free coordination site, precluded to the other complexes examined in this reaction, allowed for the resulting coordinatively unsaturated Mn(I) species to activate the Si–H bonds *via* σ-coordination. A more in-depth investigation of the Mn species participating in the catalytic activation of Si–H bonds will be provided in the next chapter with the subsequent findings.

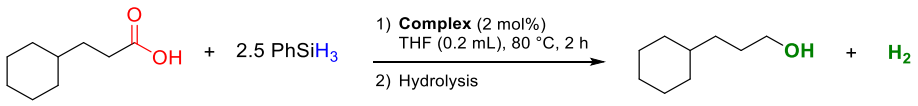
2.8. Experimental Procedure and Characterization Data

To enhance the readability and comprehension of the experimental procedures for this chapter, a detailed list of all the devices employed for measurements is provided in the Appendix, Section 6.1.

2.8.1. General considerations

Unless otherwise stated, all air-sensitive experiments were conducted under argon atmosphere in 10 mL Schlenk tubes using standard Schlenk techniques or an MBraun inert-gas glovebox. Solvents for air- and moisture-sensitive experiments were purified through a MBraun-SPS-7 system, or dried over activated 4Å molecular sieves and degassed according to standard laboratory procedure. The carboxylic acids used as starting materials, and the commercial Mn salts tested in catalysis were purchased from Sigma Aldrich, Alfa Aesar or TCI Europe and used as received. $PhSiH_3$ was purchased from Sigma Aldrich and used as received. [MnBr(CO)$_5$] has been used as received from Alfa Aesar and it was also used for the synthesis of the complexes **Mn-2**[40] and **Mn-3**[41] according to the respective reported literature procedures. The chemical shifts (δ) are given in ppm relative to TMS, and were assigned taking as a reference the residual solvent signals ($CDCl_3$: δH = 7.26 ppm, δC = 77.16 ppm; DMSO-d_6: δ_H = 2.50 ppm, δ_C = 39.52 ppm). ^{13}C spectra were generally acquired with broadband proton decoupling. The chemical shift (δ) for ^{19}F-NMR spectra is given in ppm with respect to $CFCl_3$ as a reference ($\delta_{^{19}F}$ = 0 ppm). The chemical shift (δ) for ^{31}P-NMR spectra is given in ppm with respect to H_3PO_4 (85% in H_2O) as a reference ($\delta_{^{31}P}$ = 0 ppm). The peak patterns are indicated as follows: s = singlet; d = doublet; t = triplet; q = quartet; p = quintet: m = multiplet, dd = doublet of doublets, td = triplet of doublets. The signal of –OH group of the alcohol, when assigned, is indicated with "OH". The values for the optical rotation are given as *specific optical rotation*, with exact temperature, concentration (c/(10 mg/mL)) and solvent.

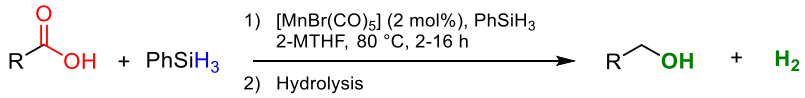
2.8.2. General procedure for the optimization



The complex of choice (0.01 mmol) and the corresponding additive (0.02 – 0.06 mmol) were weighed under air in a Schlenk tube equipped with a magnetic stirrer, and the reaction vessel was evacuated and refilled with argon 3 times (in the case of KO^{t}Bu as the additive, everything was weighed in the glovebox). Phenylsilane (135.3 mg, 1.25 mmol), 3-cyclohexylpropanoic acid (78.1 mg, 0.5 mmol) and the solvent of choice (0.2 mL) were added under argon flow. The Schlenk tube was closed and placed in a pre-heated oil bath at 80 °C for 2 h. Subsequently, The reaction vessel was cooled down to R.T. and opened in air before dropwise addition of CH_3OH (3 mL) and aqueous NaOH (10% w/w, 2 mL). The reaction mixture was left stirring overnight at R.T.; the crude product was extracted from the aqueous phase with DCM (3 × 10 mL). The combined organic layers were dried over $MgSO_{4(s)}$ for 30 min, filtered, and then concentrated under

reduced pressure. Prior to the extraction, ferrocene (18.6 mg, 0.1 mmol) was dissolved in DCM (4 mL) and added as an internal NMR standard. Yields were obtained by setting the integral value for the ferrocene singlet (4.16 ppm, 10 H) as 1.00, and integrating the characteristic methylene signal of the 3-cyclohexyl-1-propanol (3.62 ppm, 2H).

2.8.3. General procedure for the substrate scope



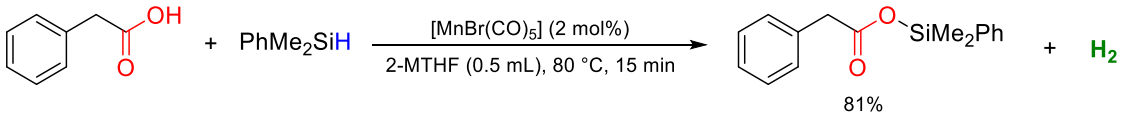
[MnBr(CO)$_5$] (5.5 mg, 0.02 mmol) and the chosen carboxylic acid (1.0 mmol) were weighed under air in a Schlenk tube equipped with a magnetic stirrer, and the reaction vessel was evacuated and refilled with argon 3 times. Phenylsilane (270.5 mg, 2.5 mmol; or 324.6 mg, 3.0 mmol for substrates **1r** and **1s**), and 2-MTHF (0.5 mL) were added under argon flow (in the case of the silyl ester of Section 2.5.1, or the carboxylic acids liquid at R.T., they were weighed in the Schlenk tube under inert gas before addition of $PhSiH_3$ and the solvent). The mixture was then heated in an oil bath set to 80 °C for 4 h (2 h in the case of substrate **1a** and 16 h in the case of **1h** and **1i**). The reaction vessel was cooled down to R.T. and opened in air before dropwise addition of MeOH (6 mL) and aqueous NaOH (10% w/w, 4 mL). Subsequently the reaction mixture was left stirring overnight at R.T.; the crude product was extracted from the aqueous phase with DCM (3 × 10 mL). The combined organic layers were dried over $MgSO_{4(s)}$ for 30 min, filtered, and the solvent was removed under reduced pressure. For NMR yields, Ferrocene (37.2 mg, 0.2 mmol) was dissolved in 4 mL of DCM and added as internal NMR standard prior to extraction. NMR yields were obtained setting the integral value for the ferrocene singlet (4.16 ppm, 10 H) as 1.00, and integrating the characteristic methylene R-CH_2-OH signal of the respective product (typically ≈ 3.5 ppm, 2H). The products which were isolated were purified through bulb to bulb distillation under reduced pressure (Kugelrohr distillation). The alcohols obtained from the reduction of Flurbiprofen, Ibuprofen, Naproxen, levulinic acid and lactic acid (respectively **1o**, **1p** **1q**, **1r**, **1s**) were purified *via* column chromatography (the elution mixture used is given together with the respective characterization data 2.8.10).

2.8.4. Procedure for the GC-TCD studies

An oven dried Schlenk tube equipped with a magnetic stirrer was evacuated and filled with argon 3 times. The proper amount of Silane (2.5 mmol for $PhSiH_3$, 1.0 mmol for $PhMe_2SiH$) was added to the Schlenk tube under argon flow. The stoichiometric amount of phenylacetic acid (1.0 mmol) and the respective manganese catalyst (0.02 mmol) were weighed in air on a weighing boat and transferred to the Schlenk tube in argon flow, followed by dry and degassed 2-MTHF (0.5 mL). The Schlenk tube was closed with a cap equipped with a septum, and placed in a pre-heated oil bath at 80 °C for the required amount of time. The reaction mixture was cooled down to R.T., and 100 µL of the gas phase were analyzed *via* GC-TCD. The

quantification of $H_{2(g)}$ and $CO_{(g)}$ has been performed using calibration curves to obtain the corresponding value in Vol (%) with respect to the integrated areas of the two gases.

2.8.5.Synthesis and isolation of the silyl ester



Scheme 31: Experimental details for the synthesis of the silyl ester.

Dimethylphenylsilane (141.0 mg, 1.03 mmol) has been weighed in an oven dried Schlenk tube equipped with a magnetic stirrer inside the glovebox. The stoichiometric amount of 2-phenylacetic acid (141.2 mg, 1.04 mmol) and [MnBr(CO)5] (5.6 mg, 0.02 mmol) were weighed in air on a weighing boat, and added to the Schlenk tube in argon flow followed by dry and degassed 2-MTHF (0.5 mL). The Schlenk tube was closed and placed at 80 °C in a pre-heated oil bath for 15 minutes. The reaction mixture was cooled down, and the solvent was removed under reduced pressure. The concentrated reaction mixture was then transferred into an oven dried Kugelrohr distillation flask and the product was isolated through bulb to bulb distillation under reduced pressure (Kugelrohr distillation). This procedure, similar to others described in literature for the isolation of similar compounds,[42] allowed the recovery of 221.3 mg of product (yield = 81 %).

2.8.6. Procedure for $^{31}P\{^{1}H\}$-NMR analysis of crude reaction mixtures

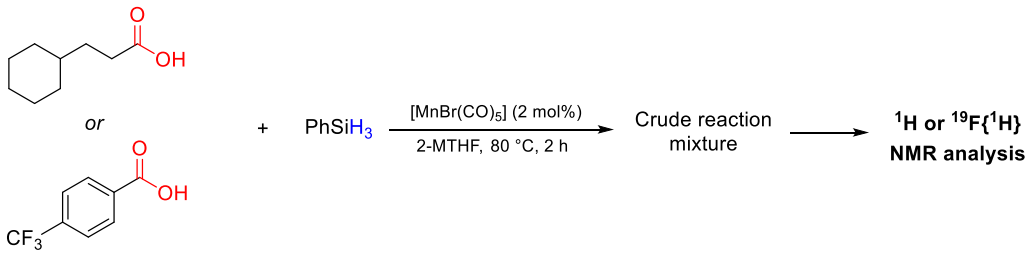
The complexes **Mn-2** and **Mn-3** (0.01 mmol) were weighed under air in a Schlenk tube equipped with a magnetic stirrer, and the reaction vessel was evacuated and refilled with argon 3 times. Phenylsilane (135.3 mg, 1.25 mmol), 3-cyclohexylpropanoic acid (78.1 mg, 0.5 mmol) and THF (0.2 mL) were added in argon flow. The reaction mixture was heated in an oil bath set to 80 °C for 2 hours. Subsequently the reaction mixture was cooled down to room temperature and transferred to the glovebox. 0.25 mL of the crude reaction mixture was transferred into an oven-dried NMR tube under argon. The respective dry and degassed NMR solvent (DMSO-d_6 for **Mn-2** and $CDCl_3$ for **Mn-3**) was added to the NMR tube, to reach a volume of approximately 0.5 mL. A $^{31}P\{^{1}H\}$-NMR spectrum was then recorded at 296 K.

2.8.7. Procedure for the reaction where hydrogen was released

[MnBr(CO)5] (5.5 mg, 0.02 mmol) and 2-phenylacetic acid (136.1 mg, 1.0 mmol) were weighed under air in a Schlenk tube equipped with a magnetic stirrer, and the reaction vessel was evacuated and refilled with argon 3 times. Phenylsilane (270.5 mg, 2.5 mmol) and 2-MTHF (0.5 mL) were added in argon flow. The Schlenk tube was closed and placed in an oil bath set to 80 °C while being connected to the Schlenk line. As soon as the bubbling of H_2 ceased, the atmosphere of the Schlenk tube has been exchanged with argon, and the reaction was run for a total of 4 h. The reaction vessel was cooled down to R.T, and the reaction

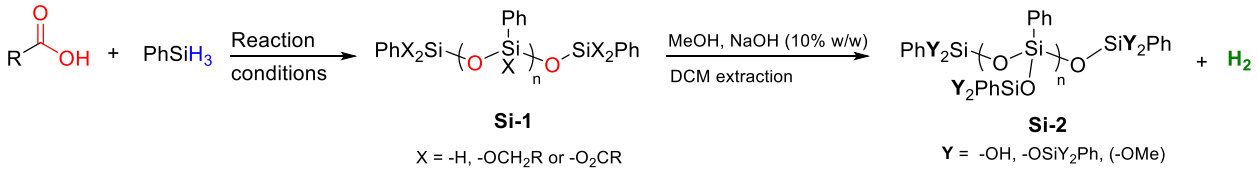
mixture was left stirring in air overnight at R.T. after dropwise addition of MeOH (6 mL) and aqueous NaOH (10% w/w, 4 mL). The crude product was extracted from the aqueous phase with DCM (3 × 10 mL). The combined organic layers were dried over $MgSO_{4(s)}$ for 30 min, filtered, and the solvents removed under reduced pressure. Before performing the extraction, ferrocene (21.2 mg, 0.1 mmol) was dissolved in DCM (4 mL) and added as internal NMR standard. The yield was obtained setting the integral value for the ferrocene singlet (4.16 ppm, 10 H) as 1.00, and integrating the characteristic methylene signal of 2-phenylethanol (2.88 ppm, 2 H). Yield = 87%.

2.8.8. Procedure for the crude NMR analysis of the polysiloxane byproducts



$[MnBr(CO)_5]$ (5.7 mg, 0.02 mmol) was weighed under air in a Schlenk tube equipped with a magnetic stirrer, and the reaction vessel was evacuated and refilled with argon 3 times. Subsequently, 3-cyclohexylpropanoic acid (163.3 mg, 1.0 mmol, in the case of the ^1H crude NMR) or 4-trifluoromethylbenzoic acid (94.5 mg, 0.5 mmol, in the case of the $^{19}F\{^1H\}$-NMR), $PhSiH_3$ (respectively 279.2 mg, 2.6 mmol, and 108.2 mg, 1.0 mmol) and 2-MTHF (respectively 0.5 mL and 0.25 mL) were added in argon flow. The mixture was heated in an oil bath set to 80 °C for 2 h. The reaction vessel was cooled down to R.T. and transferred into the glovebox. 0.1 mL of the crude reaction mixture was transferred into an oven dried J-Young tube and added with 0.4 mL of dry and degassed $CDCl_3$. The corresponding crude NMR spectra were then recorded at R.T.

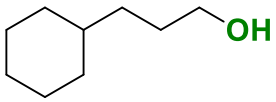
2.8.9. Procedure for the isolation of the polysiloxane byproducts after hydrolysis



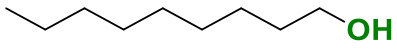
After a Kugelrohr distillation performed to isolate a product of the scope, the residue of the distillation was dissolved in DCM (0.5 mL), transferred in a vial and dried under reduced pressure. A ^1H-NMR and an anionic APCI-MS of the compound have been recorded and are reported in Section 6.2.

2.8.10. Characterization data

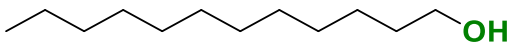
All spectra of previously existent substances are consistent with reported NMR spectra.



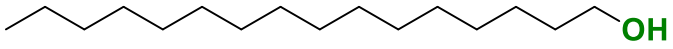
Cyclohexane propanol (**1a**)[43]; $C_9H_{18}O$, colorless oil. **^{1}H NMR** (400 MHz, $CDCl_3$, 296 K) δ 3.62 (t, *J* = 6.7 Hz, 2H), 1.77 – 1.49 (m, 7H), 1.31 (s, 1H), 1.26 – 1.10 (m, 6H), 0.96 – 0.80 (m, 2H). **^{13}C{^{1}H} NMR** (101 MHz, $CDCl_3$, 296 K) δ 63.6, 37.6, 33.6, 33.5 (2C), 30.3, 26.8, 26.5 (2C).



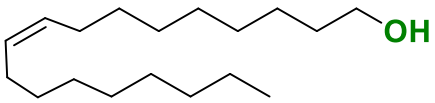
Nonanol (**1b**)[44]; $C_9H_{20}O$, colorless oil. **^{1}H NMR** (400 MHz, $CDCl_3$, 296 K) δ 3.63 (t, *J* = 6.7 Hz, 2H), 1.61-1.52 (p, *J* = 6.7 Hz, 2H), 1.39 – 1.17 (m, 13 H), 0.88 (t, *J* = 6.7 Hz, 3H). **^{13}C{^{1}H} NMR** (101 MHz, $CDCl_3$, 296 K) δ 63.3, 32.9, 32.0, 29.7, 29.6, 29.4, 25.9, 22.8, 14.3.



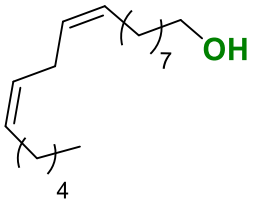
Lauryl alcohol (**1c**)[45]; $C_{12}H_{26}O$, colorless oil. **^{1}H NMR** (400 MHz, $CDCl_3$, 296 K) δ 3.64 (t, *J* = 6.6 Hz, 2H), 1.62 – 1.51 (p, *J* = 6.6 Hz, 2H), 1.38 - 1.18 (m, 19H), 0.88 (t, *J* = 6.8 Hz, 3H). **^{13}C{^{1}H} NMR** (101 MHz, $CDCl_3$, 296 K) δ 63.3, 32.4, 32.1, 29.8, 29.8, 29.8, 29.8, 29.6, 29.5, 25.9, 22.8, 14.3.



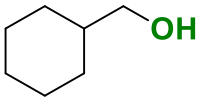
Cetyl alcohol (**1d**)[45]; $C_{16}H_{34}O$, white solid. **^{1}H NMR** (400 MHz, $CDCl_3$, 296 K) δ 3.67 – 3.60 (t, *J* = 6.4, 2H), 1.60-1.52 (m, 2H), 1.39-1.18 (m, 27H), 0.88 (t, *J* = 6.5 Hz, 3H). **^{13}C{^{1}H} NMR** (101 MHz, $CDCl_3$, 297 K) δ 63.2, 32.9, 32.1, 29.8 (4C), 29.8 (2C), 29.8, 29.8, 29.6, 29.5, 25.9, 22.8, 14.3.



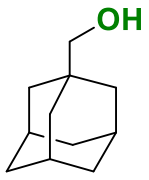
Oleyl alcohol (**1e**)[45]; $C_{18}H_{36}O$, colorless oil. **^{1}H NMR** (400 MHz, $CDCl_3$, 296 K) δ 5.37 – 5.32 (m, 2H), 3.64 (t, *J* = 6.6 Hz, 2H), 2.02 (m, 4H), 1.65 – 1.48 (m, 2H), 1.39-1.20 (m, 23H), 0.93 – 0.78 (t, *J* = 6.6 Hz, 3H). **^{13}C{^{1}H} NMR** (101 MHz, $CDCl_3$, 296 K) δ 130.0, 129.9, 63.3, 32.9, 32.1, 29.9, 29.9, 29.6, 29.6, 29.6, 29.5 (2C), 29.4, 27.4, 27.4, 25.6, 22.8, 14.3.



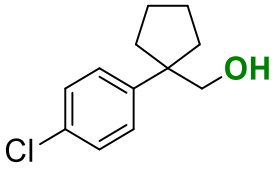
Linoleyl alcohol (**1f**)[46]; $C_{18}H_{34}O$, colorless oil. **^{1}H NMR** (400 MHz, $CDCl_3$, 296 K) δ 5.50 – 5.27 (m, 4H), 3.72 – 3.57 (t, *J* = 6.8 Hz, 2H), 2.77 (t, *J* = 6.5 Hz, 2H), 2.05 (m, 4H), 1.56 (m, 2H), 1.32 (m, 17H), 0.89 (t, *J* = 6.8 Hz, 3H). **^{13}C{^{1}H} NMR** (101 MHz, $CDCl_3$, 296 K) δ 130.3, 130.3, 128.1, 128.1, 63.2, 32.9, 31.7, 29.8, 29.6, 29.5, 29.5, 29.4, 27.4, 27.4, 25.9, 25.8, 22.7, 14.2.



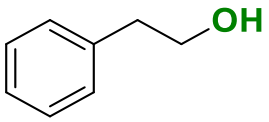
Cyclohexane methanol (**1g**)[47]; $C_7H_{14}O$, colorless oil. **^{1}H NMR** (400 MHz, $CDCl_3$, 296 K) δ 3.44 (d, *J* = 3.6 Hz, 2H), 1.73-1.63 (m, 5H), 1.53-1.42 (m, OH, 1H), 1.32-1.09 (m, 4H), 0.99-0.87 (m, 2H). **^{13}C{^{1}H} NMR** (101 MHz, $CDCl_3$, 296 K) δ 68.9, 40.6, 29.7 (2C), 26.7, 25.9 (2C).



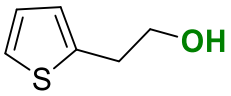
1-Adamantane methanol (**1h**)[48]; $C_{11}H_{18}O$, white solid. **^{1}H NMR** (400 MHz, $CDCl_3$, 296 K) δ 3.20 (d, *J* = 5.3 Hz, 2H), 1.99 (s, 3H), 1.77 – 1.61 (m, 6H), 1.51 (d, *J* = 2.2 Hz, 6H), 1.25 (m, OH, 1H).**^{13}C{^{1}H} NMR** (101 MHz, $CDCl_3$, 296 K) δ 74.0, 39.2 (3C), 37.3 (3C), 34.6, 28.3 (3C).



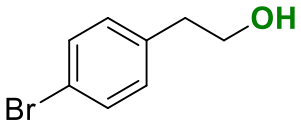
1-(4-Chlorophenyl)-1-cyclopentane methanol (**1i**)[49]; $C_{12}H_{15}ClO$, white solid. **^{1}H NMR** (400 MHz, $CDCl_3$, 296 K) δ 7.35 – 7.19 (m, 4H), 3.51 (d, *J* = 6.2 Hz, 2H), 2.00 (m, 2H), 1.83 (m, 2H), 1.73 (m, 4H), 1.20 (m, OH, 1H). **^{13}C{^{1}H} NMR** (101 MHz, $CDCl_3$, 296 K) δ 145.5, 132.1, 128.9 (2C), 128.5(2C), 70.2, 53.1, 34.5 (2C), 23.9 (2C).



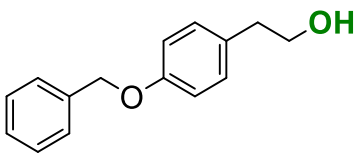
2-Phenylethanol (**1j**)[47]; $C_8H_{10}O$, colorless oil. **^{1}H NMR** (400 MHz, $CDCl_3$, 296 K) δ 7.37 – 7.29 (m, 2H), 7.24 (m, 3H), 3.87 (q, *J* = 5.9 Hz, 2H), 2.88 (t, *J* = 6.6 Hz, 2H), 1.42 (m, OH, 1H). **^{13}C{^{1}H} NMR** (101 MHz, $CDCl_3$, 296 K) δ 138.6, 129.2 (2C), 128.7 (2C), 126.6, 63.8, 39.3.



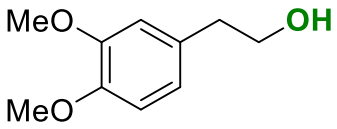
2-Thiopheneethanol (**1k**)[50]; C_6H_8OS, colorless oil. **^{1}H NMR** (400 MHz, $CDCl_3$, 296 K) δ 7.18 (dd, *J* = 5.1, 1.2 Hz, 1H), 6.96 (dd, *J* = 5.1, 3.4 Hz, 1H), 6.88 (m, 1H), 3.87 (t, *J* = 6.3 Hz, 2H), 3.09 (t, *J* = 5.8 Hz, 2H), 1.58 (s, 1H). **^{13}C{^{1}H} NMR** (101 MHz, $CDCl_3$, 296 K) δ 140.9, 127.1, 125.8, 124.2, 63.7, 33.4.



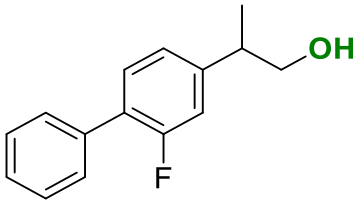
4-Bromophenyl ethanol (**1l**)[51]; C_8H_9OBr, colorless oil. **^{1}H NMR** (400 MHz, $CDCl_3$, 296 K) δ 7.43 (d, *J* = 8.3 Hz, 2H), 7.11 (d, *J* = 8.3 Hz, 2H), 3.85 (q, *J* = 6.0 Hz, 2H), 2.83 (t, *J* = 6.5 Hz, 2H), 1.38 (m, OH, 1H). **^{13}C{^{1}H} NMR** (101 MHz, $CDCl_3$, 297 K) δ 137.7, 131.7 (2C), 130.9 (2C), 120.4, 63.5, 38.7.



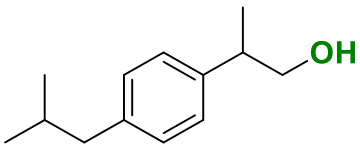
(4-Benzyloxyphenyl)ethanol (**1m**)[52]; $C_{15}H_{16}O_2$, white solid. **^{1}H NMR** (400 MHz, $CDCl_3$, 296 K) δ 7.48 – 7.29 (m, 5H), 7.15 (d, *J* = 8.6 Hz, 2H), 6.94 (d, *J* = 8.6 Hz, 2H), 5.05 (s, 2H), 3.83 (td, *J* = 6.4 Hz, 6.0 Hz, 2H), 2.82 (t, *J* = 6.5 Hz, 2H), 1.36 (t, *J* = 6.0 Hz, OH, 1H). **^{13}C{^{1}H} NMR** (101 MHz, $CDCl_3$, 296 K) δ 157.7, 137.2, 130.8, 130.1 (2C), 128.7 (2C), 128.1, 127.6 (2C), 115.2 (2C), 70.2, 63.9, 38.4.



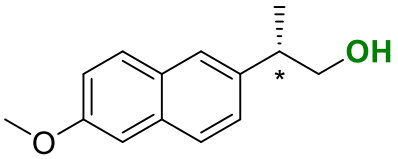
3,4-Dimethoxy-benzyl ethanol (**1n**)[53]; $C_{10}H_{14}O_3$, colorless oil. **^{1}H NMR** (400 MHz, $CDCl_3$, 296 K) δ 6.83 (d, *J* = 8.0 Hz, 1H), 6.80 – 6.74 (m, 2H), 3.91 – 3.80 (m, 8H), 2.82 (t, *J* = 6.5 Hz, 2H), 1.41 (s, 1H). **^{13}C{^{1}H} NMR** (101 MHz, $CDCl_3$, 297 K) δ 149.1, 147.8, 131.1, 121.1, 112.3, 111.5, 63.9, 56.0, 55.9, 38.9.



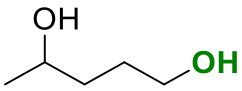
Flurbiprofen alcohol (**1o**)[54]; $C_{15}H_{15}OF$, white solid. This compound was purified from the crude by column chromatography, using an elution mixture of 4:1 pentane: ethyl acetate. **^{1}H** NMR (400 MHz, $CDCl_3$, 296 K) δ 7.57 – 7.51 (m, 2H), 7.48 – 7.32 (m, 4H), 7.15 – 7.01 (m, 2H), 3.75 (m, 2H), 3.00 (m, 1H), 1.38 (t, *J* = 6.1 Hz, OH, 1H), 1.31 (d, *J* = 7.0 Hz, 3H). **^{13}C{^{1}H}** NMR (101 MHz, $CDCl_3$, 296 K) δ 160.0 (d, *J* = 248.1 Hz), 145.7 (d, *J* = 7.2 Hz), 135.8, 130.9 (d, *J* = 4.0 Hz), 129.1 (d, *J* = 2.9 Hz, 2C), 128.6 (2C), 127.7, 127.4 (d, *J* = 13.5 Hz), 123.7 (d, *J* = 3.2 Hz), 115.1 (d, *J* = 22.8 Hz), 68.6, 42.2 (d, *J* = 1.5 Hz), 17.6. **^{19}F{^{1}H} NMR** (376 MHz, $CDCl_3$, 296 K) δ 117.9.



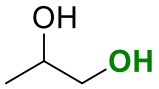
Ibuprofen alcohol (**1p**)[54]; $C_{13}H_{20}O$, colorless oil. This compound was purified from the crude by column chromatography, using an elution mixture of 15:1 pentane: ethyl acetate. **^{1}H NMR** (400 MHz, $CDCl_3$, 296 K) δ 7.13 (m, 4H), 3.69 (d, *J* = 6.8 Hz, 2H), 2.93 (m, 1H), 2.45 (d, *J* = 7.2 Hz, 2H), 1.85 (m, 1H), 1.30 (s, 1H), 1.27 (d, *J* = 7.0 Hz, 3H), 0.90 (d, *J* = 6.7 Hz, 6H). **^{13}C{^{1}H} NMR** (101 MHz, $CDCl_3$, 296 K) δ 140.7, 140.1, 129.4 (2C), 127.2 (2C), 68.8, 45.1, 42.1, 30.2, 22.4 (2C), 17.6.



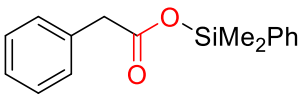
Naproxen alcohol (**1q**)[54]; $C_{14}H_{16}O_2$, white solid. This compound was purified from the crude by column chromatography, using an elution mixture of 3:1 Pentane: Ethyl Acetate. $[\alpha]_D^{20}$ = –18.7 (c = 1, $CHCl_3$). $[\alpha]_D^{25}$ = –18.5 (c = 1, $CHCl_3$). The specific optical rotation values obtained for (S)-Naproxen alcohol at the given temperatures and concentration, are in agreement with what reported in the literature[55]. **^{1}H NMR** (400 MHz, $CDCl_3$, 296 K) δ 7.71 (dd, *J* = 8.5, 7.0 Hz, 2H), 7.61 (d, *J* = 1.8 Hz, 1H), 7.35 (dd, *J* = 8.5, 1.8 Hz, 1H), 7.17 – 7.10 (m, 2H), 3.92 (s, 3H), 3.78 (t, *J* = 6.4 Hz, 2H), 3.09 (m, 1H), 1.35 (d, *J* = 7.0 Hz, 3H), 1.32 (m, OH, 1H). **^{13}C{^{1}H} NMR** (101 MHz, $CDCl_3$, 296K) δ 157.5, 138.6, 133. 6, 129.1, 129.1, 127.3, 126.3, 125.93, 118.9, 105.6, 68.7, 55.3, 42.4, 17.7.



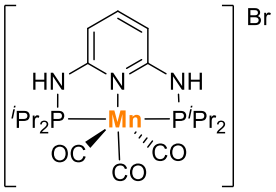
Pentan-1,4-diol (**1r**)[56]; $C_5H_{12}O_2$, colorless oil. **^{1}H NMR** (400 MHz, $CDCl_3$, 296 K) δ 3.85 (m, 1H), 3.74-3.58 (m, 2H), 2.45 (s, 2H), 1.75-1.57 (m, 3H), 1.57-1.44 (m, 1H), 1.21 (d, *J* = 6.2 Hz, 3H). **^{13}C{^{1}H} NMR** (101 MHz, $CDCl_3$, 297 K) δ 67.8, 62.8, 36.1, 29.0, 23.5.



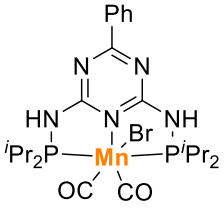
Propylene Glycol (**1s**); $C_3H_8O_2$, colorless oil. **^{1}H NMR** (400 MHz, $CDCl_3$, 296 K) δ 3.83 (m, 1H), 3.55 (dd, J = 11.2, 3.0 Hz, 1H), 3.32 (dd, J = 11.2, 7.8 Hz, 1H), 2.87 (br s, 2H), 1.09 (d, J = 6.3 Hz, 3H). **^{13}C{^{1}H} NMR** (101 MHz, $CDCl_3$, 297 K) δ 68.3, 68.0, 18.8.



Dimethylphenylsilyl benzeneacetate, colorless oil. **^{1}H NMR** (400 MHz, $CDCl_3$, 296 K) δ 7.56 – 7.42 (m, 2H), 7.41 – 7.17 (m, 8H), 3.58 (s, 2H), 0.47 (s, 6H). **^{13}C{^{1}H} NMR** (101 MHz, THF-d_8, 296 K) δ 171.9, 136.9, 135.9, 134.5, 130.9 (d), 130.3, 129.2 (d), 128.7 (d), 127.6 (d), 43.4 (d), -1.3 (d). HR-MS: m/z calculated for $[C_{16}H_{18}O_2SiNa]^+$ = 293.09683, found = 293.09679



$C_{20}H_{33}BrMnN_3O_3P_2$,[40] white solid. **^{1}H NMR** (400 MHz, DMSO-d_6) δ 8.97 (s, 2H), 7.48 (t, J = 8.0 Hz, 1H), 6.37 (d, J = 8.0 Hz, 2H), 2.75 (m, 4H), 1.40 (dd, J = 15.9, 6.9 Hz, 12H), 1.27 (dd, J = 16.3, 7.1 Hz, 12H). **^{31}P NMR** (162 MHz, DMSO-d_6) δ 133.69.



$C_{23}H_{35}BrMnN_5O_2P_2$,[41] yellow solid. **^{1}H NMR** (400 MHz, $CDCl_3$) δ 8.28 (d, J = 7.7 Hz, 2H), 7.60 – 7.37 (m, 3H), 6.11 (s, 2H), 3.63 (m, 2H), 2.77 (m, 2H), 1.62 – 1.18 (m, 24H). **^{31}P NMR** (162 MHz, $CDCl_3$) δ 135.63.

2.9. References

1. Handbook of Detergents, Part F, Production; Zoller, U.; Sosis, P., CRC Press: Boca Raton, 2008.

2. Leitner, W.; Klankermayer, J.; Pischinger, S.; Pitsch, H.; Kohse-Höinghaus, K., Advanced Biofuels and Beyond: Chemistry Solutions for Propulsion and Production. *Angew. Chem. Int. Ed.* **2017,** *56* (20), 5412-5452.

3. Yesilyurt, M. K.; Cakmak, A., An extensive investigation of utilization of a C8 type long-chain alcohol as a sustainable next-generation biofuel and diesel fuel blends in a CI engine – The effects of alcohol infusion ratio on the performance, exhaust emissions, and combustion characteristics. *Fuel* **2021,** *305*, 121453.

4. Funk, M.; Ash, C., A cleaner, greener future for chemicals. *Science* **2020,** *367* (6476), 378-379.

5. Kuß, D. A.; Hölscher, M.; Leitner, W., Hydrogenation of CO_2 to Methanol with Mn-PNP-Pincer Complexes in the Presence of Lewis Acids: the Formate Resting State Unleashed. *ChemCatChem* **2021,** *13* (14), 3319–3323.

6. Geilen, F. M. A.; Engendahl, B.; Hölscher, M.; Klankermayer, J.; Leitner, W., Selective Homogeneous Hydrogenation of Biogenic Carboxylic Acids with $[Ru(TriPhos)H]^+$: A Mechanistic Study. *J. Am. Chem. Soc.* **2011,** *133* (36), 14349-14358.

7. Brewster, T. P.; Miller, A. J. M.; Heinekey, D. M.; Goldberg, K. I., Hydrogenation of Carboxylic Acids Catalyzed by Half-Sandwich Complexes of Iridium and Rhodium. *J. Am. Chem. Soc.* **2013,** *135* (43), 16022-16025.

8. vom Stein, T.; Meuresch, M.; Limper, D.; Schmitz, M.; Hölscher, M.; Coetzee, J.; Cole-Hamilton, D. J.; Klankermayer, J.; Leitner, W., Highly Versatile Catalytic Hydrogenation of Carboxylic and Carbonic Acid Derivatives using a Ru-Triphos Complex: Molecular Control over Selectivity and Substrate Scope. *J. Am. Chem. Soc.* **2014,** *136* (38), 13217-13225.

9. Naruto, M.; Saito, S., Cationic mononuclear ruthenium carboxylates as catalyst prototypes for self-induced hydrogenation of carboxylic acids. *Nat Commun* **2015,** *6* (1), 8140.

10. Cui, X.; Li, Y.; Topf, C.; Junge, K.; Beller, M., Direct Ruthenium-Catalyzed Hydrogenation of Carboxylic Acids to Alcohols. *Angew. Chem. Int. Ed.* **2015,** *54* (36), 10596-10599.

11. Saito, A.; Yoshioka, S.; Naruto, M.; Saito, S., Catalytic Hydrogenation of N-protected α-Amino Acids Using Ruthenium Complexes with Monodentate Phosphine Ligands. *Adv. Synth. Catal.* **2020,** *362* (2), 424-429.

12. Korstanje, T. J.; Ivar van der Vlugt, J.; Elsevier, C. J.; de Bruin, B., Hydrogenation of carboxylic acids with a homogeneous cobalt catalyst. *Science* **2015,** *350* (6258), 298-302.

13. Addis, D.; Das, S.; Junge, K.; Beller, M., Selective Reduction of Carboxylic Acid Derivatives by Catalytic Hydrosilylation. *Angew. Chem. Int. Ed.* **2011,** *50* (27), 6004-6011.

14. Bhunia, M.; Sreejyothi, P.; Mandal, S. K., Earth-abundant metal catalyzed hydrosilylative reduction of various functional groups. *Coordination Chemistry Reviews* **2020,** *405*, 213110.

15. Matsubara, K.; Iura, T.; Maki, T.; Nagashima, H., A Triruthenium Carbonyl Cluster Bearing a Bridging Acenaphthylene Ligand: An Efficient Catalyst for Reduction of Esters, Carboxylic Acids, and Amides by Trialkylsilanes. *J. Org. Chem.* **2002,** *67* (14), 4985-4988.

16. Fernández-Salas, J. A.; Manzini, S.; Nolan, S. P., Chemoselective Ruthenium-Catalysed Reduction of Carboxylic Acids. *Adv. Synth. Catal.* **2014,** *356* (2-3), 308-312.

17. Nguyen, T. V. Q.; Yoo, W.-J.; Kobayashi, S., Chelating Bis(1,2,3-triazol-5-ylidene) Rhodium Complexes: Versatile Catalysts for Hydrosilylation Reactions. *Adv. Synth. Catal.* **2016,** *358* (3), 452-458.

18. Corre, Y.; Rysak, V.; Trivelli, X.; Agbossou-Niedercorn, F.; Michon, C., A Versatile Iridium(III) Metallacycle Catalyst for the Effective Hydrosilylation of Carbonyl and Carboxylic Acid Derivatives. *Eur. J. Org. Chem.* **2017,** *2017* (32), 4820-4826.

19. Misal Castro, L. C.; Li, H.; Sortais, J.-B.; Darcel, C., Selective switchable iron-catalyzed hydrosilylation of carboxylic acids. *Chem. Commun.* **2012,** *48* (85), 10514-10516.

20. Zheng, J.; Chevance, S.; Darcel, C.; Sortais, J.-B., Selective reduction of carboxylic acids to aldehydes through Manganese catalysed hydrosilylation. *Chem. Commun.* **2013,** *49* (85), 10010-10012.

21. Zhang, Y.-J.; Dayoub, W.; Chen, G.-R.; Lemaire, M., Copper(II) triflate-catalyzed reduction of carboxylic acids to alcohols and reductive etherification of carbonyl compounds. *Tetrahedron* **2012,** *68* (36), 7400-7407.

22. Mao, Z.; Gregg, B. T.; Cutler, A. R., Catalytic hydrosilylation of organic esters using Manganese carbonyl acetyl complexes *J. Am. Chem. Soc.* **1995,** *117* (40), 10139-10140.

23. Zheng, J.; Elangovan, S.; Valyaev, D. A.; Brousses, R.; César, V.; Sortais, J.-B.; Darcel, C.; Lugan, N.; Lavigne, G., Hydrosilylation of Aldehydes and Ketones Catalyzed by Half-Sandwich Manganese(I) N-Heterocyclic Carbene Complexes. *Inorg. Chem.* **2014,** *356* (5), 1093-1097.

24. Valyaev, D. A.; Wei, D.; Elangovan, S.; Cavailles, M.; Dorcet, V.; Sortais, J.-B.; Darcel, C.; Lugan, N., Half-Sandwich Manganese Complexes Bearing Cp Tethered N-Heterocyclic Carbene Ligands: Synthesis and Mechanistic Insights into the Catalytic Ketone Hydrosilylation. *Organometallics* **2016,** *35* (24), 4090-4098.

25. Yang, X.; Wang, C., Diverse Fates of β-Silyl Radical under Manganese Catalysis: Hydrosilylation and Dehydrogenative Silylation of Alkenes. *Chin. J. Chem.* **2018,** *36* (11), 1047-1051.

26. Yang, X.; Wang, C., Dichotomy of Manganese Catalysis via Organometallic or Radical Mechanism: Stereodivergent Hydrosilylation of Alkynes. *Angew. Chem. Int. Ed.* **2018,** *57* (4), 923-928.

27. Sousa, S. C. A.; Realista, S.; Royo, B., Bench-Stable Manganese NHC Complexes for the Selective Reduction of Esters to Alcohols with Silanes. *Adv. Synth. Cat*. **2020,** *362* (12), 2437-2443.

28. Behera, R. R.; Ghosh, R.; Panda, S.; Khamari, S.; Bagh, B., Hydrosilylation of Esters Catalyzed by Bisphosphine Manganese(I) Complex: Selective Transformation of Esters to Alcohols. *Org. Lett.* **2020,** *22* (9), 3642-3648.

29. Dong, J.; Yuan, X.-A.; Yan, Z.; Mu, L.; Ma, J.; Zhu, C.; Xie, J., Manganese-catalysed divergent silylation of alkenes. *Nat. Chem.* **2021,** *13* (2), 182-190.

30. Martínez-Ferraté, O.; Chatterjee, B.; Werlé, C.; Leitner, W., Hydrosilylation of carbonyl and carboxyl groups catalysed by Mn(I) complexes bearing triazole ligands. *Cat. Sci.Technol.* **2019,** *9* (22), 6370-6378.

31. Bertini, F.; Glatz, M.; Stöger, B.; Peruzzini, M.; Veiros, L. F.; Kirchner, K.; Gonsalvi, L., Carbon Dioxide Reduction to Methanol Catalyzed by Mn(I) PNP Pincer Complexes under Mild Reaction Conditions. *ACS Catal.* **2019,** *9* (1), 632-639.

32. Kallmeier, F.; Irrgang, T.; Dietel, T.; Kempe, R., Highly Active and Selective Manganese C=O Bond Hydrogenation Catalysts: The Importance of the Multidentate Ligand, the Ancillary Ligands, and the Oxidation State. *Angew. Chem. Int. Ed.* **2016,** *55* (39), 11806-11809.

33. Anastas, P.; Eghbali, N. Green Chemistry: Principles and Practice. *Chem. Soc. Rev.* **2010**, *39* (1), 301–312.

34. Zimmerman, J. B.; Anastas, P. T.; Erythropel, H. C.; Leitner, W., Designing for a green chemistry future. *Science* **2020,** *367* (6476), 397-400.

35. Kaplaneris, N.; Kaltenhäuser, F.; Sirvinskaite, G.; Fan, S.; De Oliveira, T.; Conradi, L.-C.; Ackermann, L., Late-stage stitching enabled by Manganese-catalyzed C─H activation: Peptide ligation and access to cyclopeptides. **2021,** *7* (9), eabe6202.

36. Wang, D.; Dong, J.; Fan, W.; Yuan, X.-A.; Han, J.; Xie, J., Dimeric Manganese-Catalyzed Hydroarylation and Hydroalkenylation of Unsaturated Amides. **2020,** *59* (22), 8430-8434.

37. Wang, H.; Choi, I.; Rogge, T.; Kaplaneris, N.; Ackermann, L., Versatile and robust C–C activation by chelation-assisted Manganese catalysis. *Nat. Catal.* **2018,** *1* (12), 993-1001.

38. Yang, W.; Chernyshov, I. Y.; van Schendel, R. K. A.; Weber, M.; Müller, C.; Filonenko, G. A.; Pidko, E. A., Robust and efficient hydrogenation of carbonyl compounds catalysed by mixed donor Mn(I) pincer complexes. *Nat Commun* **2021,** *12* (1), 12.

39. Stoll, E. L.; Tongue, T.; Andrews, K. G.; Valette, D.; Hirst, D. J.; Denton, R. M., A practical catalytic reductive amination of carboxylic acids. *Chem. Sci.* **2020,** *11* (35), 9494-9500.

40. Bruneau-Voisine, A.; Wang, D.; Roisnel, T.; Darcel, C.; Sortais, J.-B., Hydrogenation of ketones with a Manganese PN^{3}P pincer pre-catalyst. *Catal. Commun.* **2017,** *92*, 1-4.

41. Gawali, S. S.; Pandia, B. K.; Gunanathan, C., Manganese(I)-Catalyzed alpha-Alkenylation of Ketones Using Primary Alcohols. *Org. Lett.* **2019,** *21* (10), 3842-3847.

42. Ojima, Y.; Yamaguchi, K.; Mizuno, N., An Efficient Solvent-Free Route to Silyl Esters and Silyl Ethers. *Adv. Synth. Catal.* **2009,** *351* (9), 1405-1411.

43. Kumar, A.; Goyal, V.; Sarki, N.; Singh, B.; Ray, A.; Bhaskar, T.; Bordoloi, A.; Narani, A.; Natte, K., Biocarbon Supported Nanoscale Ruthenium Oxide-Based Catalyst for Clean Hydrogenation of Arenes and Heteroarenes. *ACS Sustain. Chem. Eng.* **2020,** *8* (41), 15740-15754.

44. Brunel, J. M., Scope, limitations and mechanistic aspects in the selective homogeneous palladium-catalyzed reduction of alkenes under transfer hydrogen conditions. *Tetrahedron* **2007,** *63* (18), 3899-3906.

45. Barman, M. K.; Das, K.; Maji, B., Selective Hydroboration of Carboxylic Acids with a Homogeneous Manganese Catalyst. *J. Org. Chem.* **2019,** *84* (3), 1570-1579.

46. Bender, T. A.; Bergman, R. G.; Raymond, K. N.; Toste, F. D., A Supramolecular Strategy for Selective Catalytic Hydrogenation Independent of Remote Chain Length. *J. Am. Chem. Soc.* **2019,** *141* (30), 11806-11810.

47. Chakraborty, S.; Dai, H.; Bhattacharya, P.; Fairweather, N. T.; Gibson, M. S.; Krause, J. A.; Guan, H., Iron-based catalysts for the hydrogenation of esters to alcohols. *J. Am. Chem. Soc.* **2014,** *136* (22), 7869-72.

48. Bodnar, B. S.; Vogt, P. F., An improved Bouveault-Blanc ester reduction with stabilized alkali metals. *J. Org. Chem.* **2009,** *74* (6), 2598-600.

49. Roberts, D. D.; Arant, M. E., Solvolysis Reactions: Relative Abilities of Cyclopentyl/Phenyl Groups To Stabilize an Electron-Deficient Carbon. *J. Org. Chem.* **1994,** *59* (21), 6464-6469.

50. Sakai, N.; Kawana, K.; Ikeda, R.; Nakaike, Y.; Konakahara, T., $InBr_3$-Catalyzed Deoxygenation of Carboxylic Acids with a Hydrosilane: Reductive Conversion of Aliphatic or Aromatic Carboxylic Acids to Primary Alcohols or Diphenylmethanes. *Eur. J. Org. Chem.* **2011,** *2011* (17), 3178-3183.

51. Schupbach, B.; Terfort, A., A divergent synthesis of oligoarylalkanethiols with Lewis-basic N-donor termini. *Org. Biomol. Chem.* **2010,** *8* (15), 3552-62.

52. Zhou, F. Y.; She, J.; Wang, Y. G., Synthesis of a benzyl-protected analog of arenarioside, a trisaccharide phenylpropanoid glycoside. *Carbohydr. Res.* **2006,** *341* (15), 2469-77.

53. Shahane, S.; Louafi, F.; Moreau, J.; Hurvois, J.-P.; Renaud, J.-L.; van de Weghe, P.; Roisnel, T., Synthesis of Alkaloids of Galipea officinalisby Alkylation of an α-Amino Nitrile. *Eur. J. Org. Chem.* **2008,** *2008* (27), 4622-4631.

54. Friest, J. A.; Maezato, Y.; Broussy, S.; Blum, P.; Berkowitz, D. B., Use of a robust dehydrogenase from an archael hyperthermophile in asymmetric catalysis-dynamic reductive kinetic resolution entry into (S)-profens. *J. Am. Chem. Soc.* **2010,** *132* (17), 5930-5931.

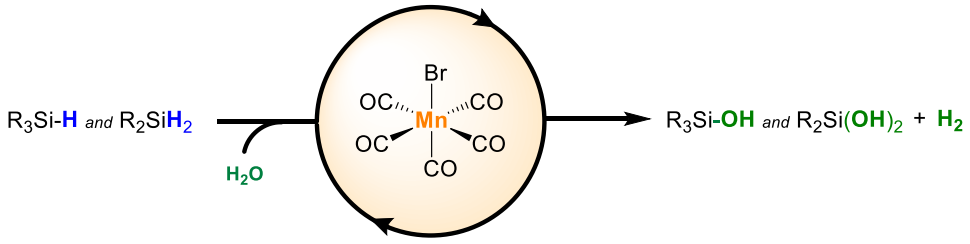
55. Koul, S.; Koul, J. L.; Singh, B.; Kapoor, M.; Parshad, R.; Manhas, K. S.; Taneja, S. C.; Qazi, G. N., Trichosporon beigelli esterase (TBE): a versatile esterase for the resolution of economically important racemates. *Tetrahedron: Asymmetry* **2005,** *16* (15), 2575-2591.

56. Shao, Z.; Zhong, R.; Ferraccioli, R.; Li, Y.; Liu, Q., General and Phosphine-Free Cobalt-Catalyzed Hydrogenation of Esters to Alcohols. *Chin. J. Chem.* **2019,** *37* (11), 1125-1130.

3. [MnBr(CO)$_5$] as an Active Precatalyst for the Selective Oxidation of Silanes to Silanols

Parts of this chapter have been published in:

Antico, E.; Leutzsch, M.; Wessel, N.; Weyhermüller, T.; Werlé, C.; Leitner, W. *Chem. Sci.* **2023**, *14* (1), 54–60.



Scheme 32: Graphical abstract of Chapter 3.

3.1. Introduction

Silanols are molecules containing at least one silicon atom bound to a free hydroxyl group. Over the years, silanols were found to have a wide variety of applications in several fields: in medicinal chemistry, it has been shown that the substitution of a carbon atom with a silicon atom can vary the properties of known pharmaceutical products (**Figure 7**).[1] Moreover, silanediols have been shown to be active inhibitors of different viruses' proteases.[2] In synthetic organic chemistry, silanols can be used as cross coupling partners,[3] and in the synthesis of polymers and other materials, silanediols play an important role as building blocks.[4]

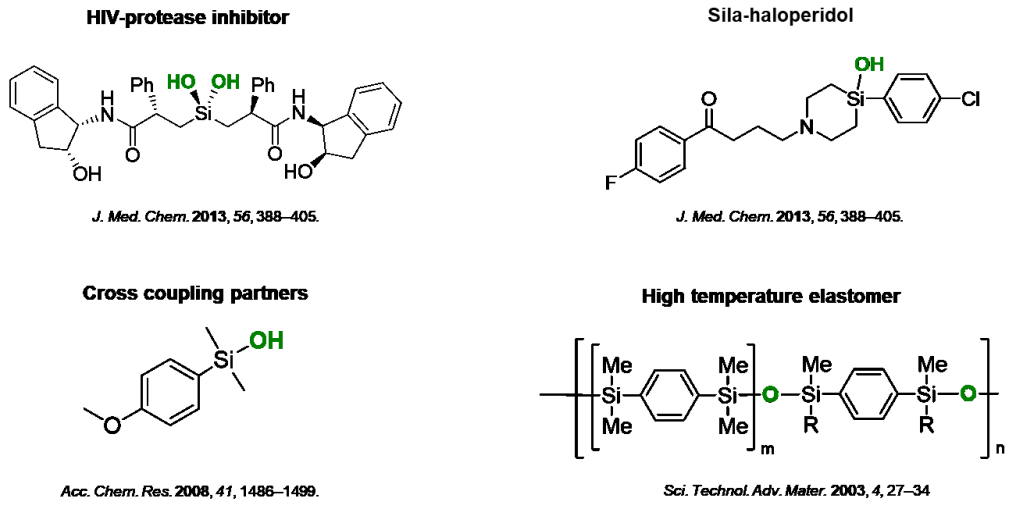


Figure 7: Selected examples of silanols and their application in the respective fields.

Among the possible synthetic pathways to obtain silanols, traditional procedures rely either on the hydrolysis of halo- or alkoxy-silanes (requiring strictly buffered conditions and a stoichiometric amount of base),[5-7] or the oxidation of hydrosilanes with strong oxidants like OsO_4[8] or $KMnO_4$,[9] which also leads to

stoichiometric amounts of byproducts (**Figure 8**). Therefore, there is an interest in developing alternative catalytic protocols based on the principles of *green chemistry,*[10] making use of green oxidants such as H_2O_2, molecular oxygen or H_2O. In particular, the use of H_2O as the oxidant is consensually considered to be the ideal choice for this reaction, leading to valuable H_2 as the only reaction byproduct and making the isolation of the product particularly simple.[7, 11] Nevertheless, the use of H_2O often introduces selectivity challenges arising from the formation of siloxane side products, which represents a significant limitation for the procedure.

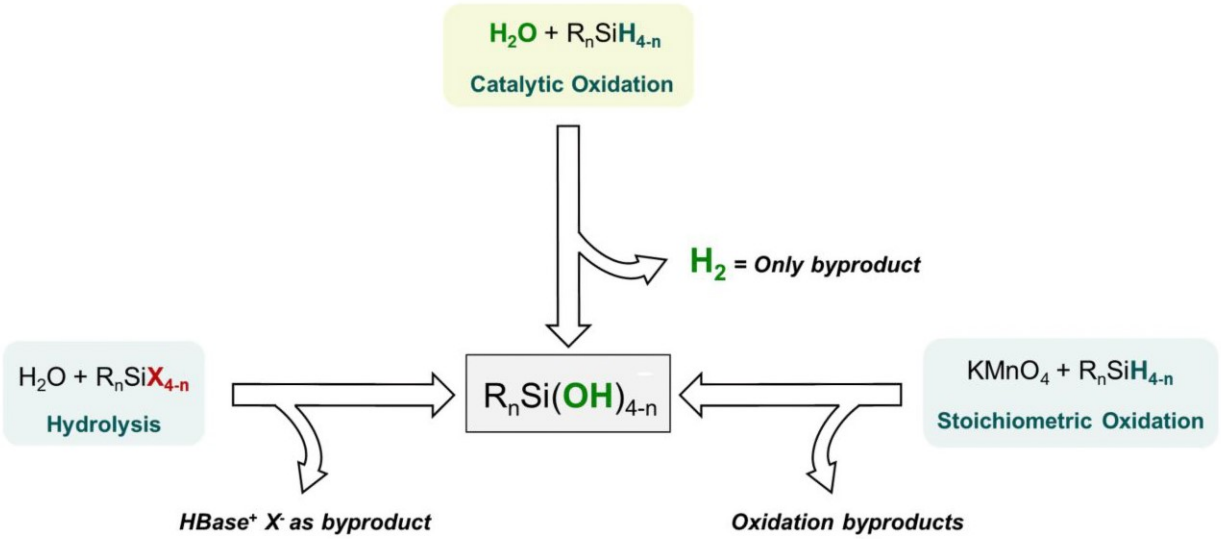
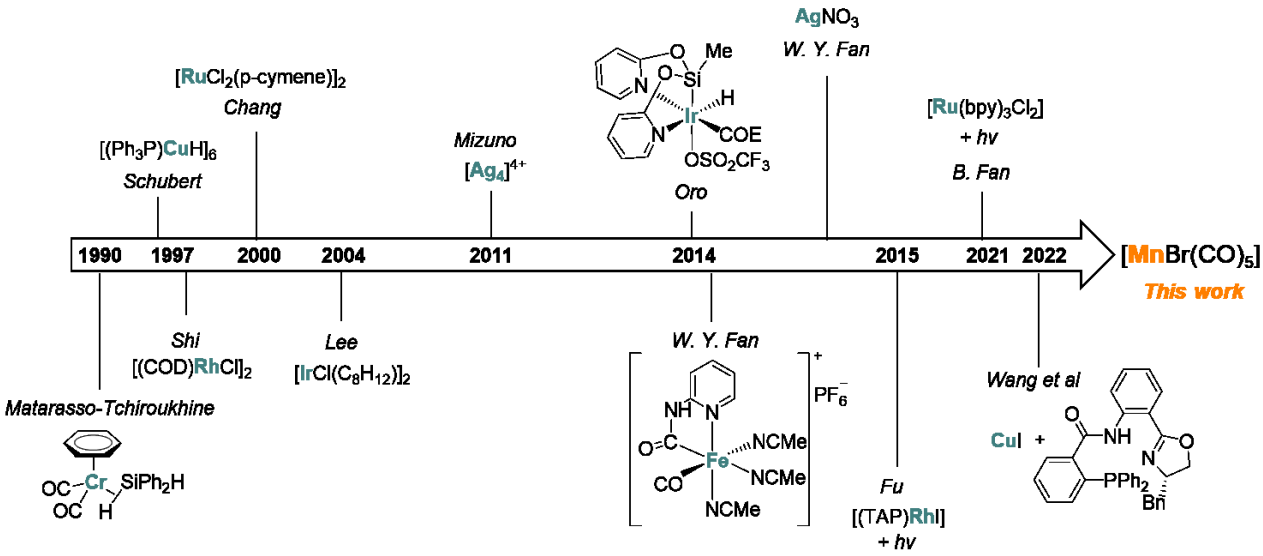


Figure 8: Most common synthetic pathways for the synthesis of silanols along with the corresponding byproducts.

Most synthetic procedures reported to date for the oxidation of hydrosilanes with H_2O, both with homogeneous and heterogeneous catalysts, are based on metals of group 9-11. In fact, metals such as Rh,[12, 13] Ir,[14, 15] Pd,[16, 17] Pt,[18] Au,[19-21] or Ag[22-24] can easily activate Si–H bonds in their reaction with nucleophiles. When focusing on homogeneous examples, the use of 3d metals is comparatively underrepresented. Among the same groups in the periodic table, Cu has been an early example of a homogeneous catalyst for this reaction. The copper cluster $[(Ph_3P)CuH]_6$, which was reported by Schubert in 1997,[25] was able to convert a narrow scope of tertiary silanes to their respective silanols with a significant amount of siloxane side products. A more recent example also using copper is the one reported by Wang, Gu and Liu. Their catalysts, prepared *in situ* from CuI in 10 mol% loading and an equimolar amount of a chiral pincer ligand, could catalyze an enantioselective hydroxylation of secondary silanes.[26] Moving to group 8, a number of Ru systems have been developed for silane oxidation,[27-30] with its 3d congener iron also showing promising activity, as demonstrated by Fan's report on a highly active Fe(II) carbonyl complex optimized for the generation of H_2 using a large excess of water.[31]



Scheme 33: Selected examples of homogeneous catalysts for the dehydrogenative oxidation of silanes to silanols with H_2O.

Looking at examples from groups 6 and 7, their use as homogenous catalysts for this reaction is comparatively rare. A very early example in 1990 was reported from Matarasso-Tchiroukhine, who showed that a chromium(0) carbonyl complex is able to σ-coordinate a Si–H bond of Ph_2SiH_2 to the metal, activating it towards the reaction with water and other nucleophiles.[32] Later, thanks to the work of Abu-Omar and Wei, it was discovered that also rhenium-oxo complexes can catalyze the same reaction.[33,34] Surprisingly instead, despite its good historical performances in Si–H bond activation, manganese is an under-represented element in the field of silane oxidation: as shown in the previous chapter, simple Mn(I) carbonyl complexes such as [MnBr(CO)$_5$] are able to perform the dehydrogenative coupling between Si–H bonds and carboxylic acids. Moreover, as reported in Section 1.2 (**Scheme 19**), Cutler and coworkers could demonstrate already in 1994 that the dimeric version of [MnBr(CO)$_5$], [$Mn_2Br_2(CO)_8$], is active in the dehydrogenative coupling of $PhMe_2SiH$ and several alcohols.[35] However, apart from research that will be presented in this chapter, there is only one documented instance in the literature where a manganese-based catalyst has been used for the oxidation of silanes to silanols. The work was performed by Xiao, Li, and their team, employing a Mn(II) bipyridinde derivative as a catalyst with an excess of the much stronger oxidant H_2O_2 to carry on the reaction.[11] Due to the discovery of the good catalytic properties of [MnBr(CO)$_5$] in the activation of Si–H bonds observed in the previous chapter, the possibility of a Mn(I) dehydrogenative coupling of silanes and H_2O mediated by [MnBr(CO)$_5$] was investigated in this chapter.

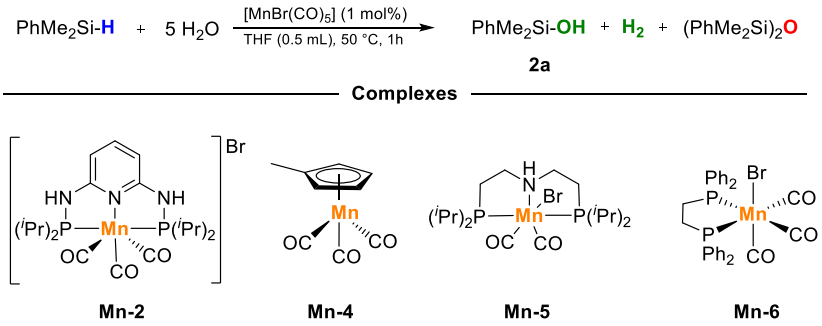
3.1. Objectives

The development of a reliable catalytic procedure for the Mn(I) catalyzed dehydrogenative synthesis of silanols from hydrosilanes, using H_2O as the oxidant, is the main objective of this work. Ideally, the procedure should limit the formation of siloxane side products and employ the simplest manganese catalyst to ensure cost-effectiveness and scalability. Building upon the initial mechanistic insights from the previous chapter, a more comprehensive understanding of the Si–H bond activation mechanism at the Mn center would be desirable. A clearer picture of key mechanistic aspects could in fact enable the design of novel manganese based catalytic systems able to activate Si–H and other bonds *via* σ-coordination.

3.2. Initial Screening and Optimization

Dimethylphenylsilane was chosen as the model substrate to test for activity and to identify suitable reaction conditions, because of its high reactivity towards the formation of siloxane dimers. Several manganese complexes in different oxidation states have been tested out in THF at 50 °C with 5 equivalents of H_2O and a loading of 1 mol%. It was possible to observe that, among the complexes screened, only [MnBr(CO)$_5$] is catalytically active in these conditions (similarly to what observed in the previous chapter; **Table 3**).

Table 3: Testing for the catalytic activity of different manganese complexes in the oxidation of dimethylphenylsilane with H_2O. The ^{1}H-NMR yields were determined with respect to mesitylene as internal standard.

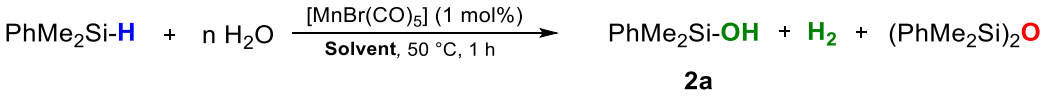


Additive (mol %)	Yield (%)	Conversion (%)
[MnBr(CO)$_5$] (1 mol%)	>99	>99
MnF_3 (1 mol%)*	0	0
$MnBr_2$ (1 mol%)	0	0
[Mn(OAc)$_3$(H$_2$O)$_2$] (1 mol%)	0	0
$MnCl_2$ (1 mol%)	0	0
$MnBr_2$ (1 mol%) + 3 LiCl	0	0
$MnCl_2$ (2 mol%) + 3 LiCl	0	0
Mn-4 (2 mol%)	0	0
Mn-2 (1 mol%)	0	0
Mn-2* (1 mol%)	0	0
Mn-5 (1 mol%)	0	0
Mn-6 (1 mol%)	0	0
Mn-6** (1 mol%)	0	0

*Repeated in DMSO at 50 °C
**Repeated in 2-MTHF at 80 °C

While the dehydrogenative coupling was successful in a wide range of solvents of different polarity (**Table 4**), the best results in terms of selectivity were obtained in solvents of medium coordination strength: ethyl acetate, THF, and 2-MTHF. Interestingly, the use of acetone and ethyl acetate did not lead to hydrosilylated side-products, although manganese carbonyl complexes are known to be active catalysts in the hydrosilylation of carbonyl groups.[36] Even with a ratio silane to water equal to 1:1, the reaction shows complete conversion and a selectivity of 78%, indicating that the coupling of $PhMe_2SiH$ with H_2O is preferred over the one with $PhMe_2SiOH$. However, a 3:1 ratio of H_2O to silane was found to give the best selectivity. The reaction was then tested on a scope of different silanes, with the outcomes reported in the next section of the chapter.

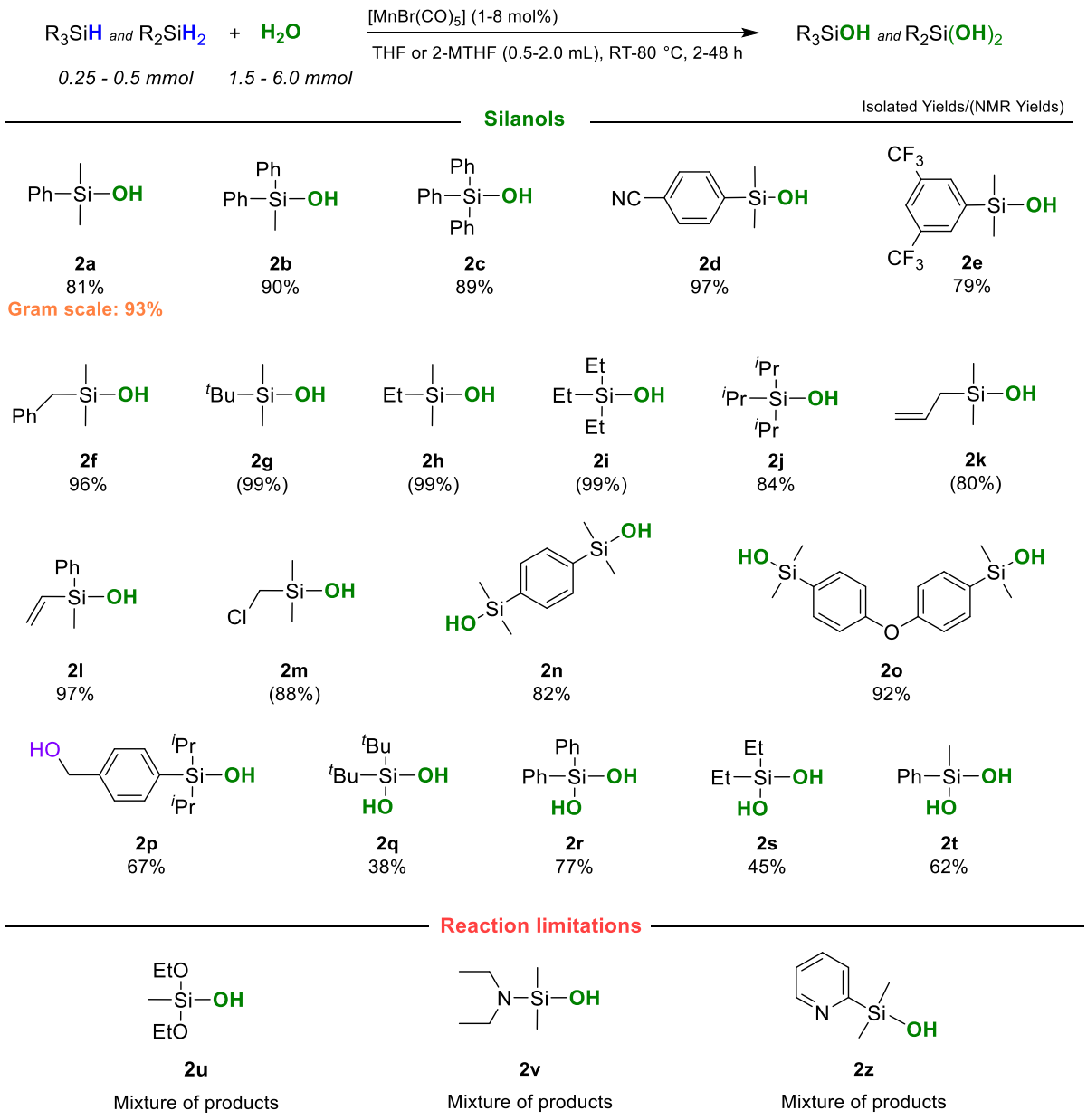
Table 4: Optimization of the reaction between $PhMe_2SiH$ and H_2O using [MnBr(CO)$_5$] as a catalyst. The ^{1}H-NMR yields were determined with respect to mesitylene as internal standard.



Solvent	H_2O equiv.	NMR Yield of 2a (%)	Conversion (%)
Acetone	5	89	>99
THF	5	>99	>99
Heptane	5	40	>99
Toluene	5	55	>99
Chloroform	5	74	>99
Acetonitrile	5	27	>99
2-MTHF	5	99	>99
DMSO	5	62	>99
EtOAc	5	96	>99
THF	4	>99	>99
THF	**3**	**>99**	**>99**
THF	2	90	>99
THF	1	78	>99

3.3. Reaction Scope and Catalytic Performances

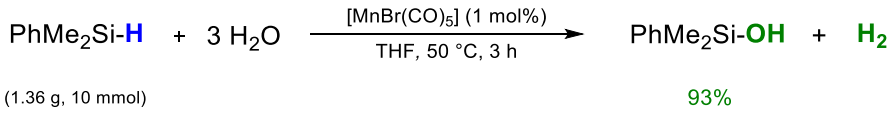
The parameters highlighted in **Table 4** were adopted as standard conditions, but they have been significantly varied from substrate to substrate in order to obtain the best selectivity and yield for each of them. The results of the substrate scope are summarized in **Scheme 34**, while the reaction conditions for each individual substrate are summarized in the experimental section (**Table 5**, Section 3.7.3).



Scheme 34: Scope of the oxidation of different silanes to their respective silanols and silanediols with H_2O as the oxidant. The ^{1}H-NMR yields were determined with respect to mesitylene as internal standard.

The catalytic oxidation gave good to excellent yields across a span of silanes bearing different functionalities. Small variations from $PhMe_2SiH$, like the substitution of methyl groups in **2a** with phenyl

rings (**2b**, **2c**) or substituted phenyl rings (either carrying a nitrile- (**2d**) or trifluoromethyl-(**2e**) functionality) was fully tolerated affording yields up to 97%. Silanes containing purely aliphatic substituents were converted to their respective silanols with excellent outcomes (**2f–j**), allowing for the presence of unsaturated groups like allyl- or vinyl-groups, that remained fully intact. In this way, it was possible to obtain the respective silanols **2k** and **2l** in high yields, which would have been difficult with the standard synthetic procedures based on stoichiometric oxidants.[8, 9] Then, even silanes carrying a functional group able to further react towards the formation of siloxanes were successfully converted to the silanols **2m–p** in excellent yields, performing the catalytic reactions either at milder temperatures, or employing a higher dilution and a larger excess of H_2O. Finally, it was also possible to react secondary silanes to obtain the respective silanediols, such as di-*tert*-butylsilanediol (**2q**), diphenylsilanediol (**2r**), diethyl-(**2s**) and methylphenylsilanediol (**2t**), albeit the yields for some of these very challenging substrates were slightly lower. Unfortunately, it was not possible to obtain the silanols **2u** and **2v** with this procedure, since the reaction led to an inseparable mixture of products in various reaction conditions.

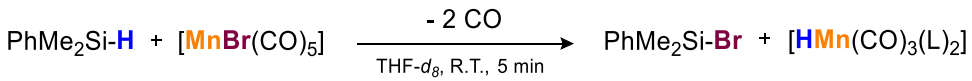


Scheme 35: Conversion of dimethylphenylsilane to dimethylphenylsilanol performed on a gram scale.

Finally, a gram-scale reaction was performed with $PhMe_2SiH$ as a substrate, affording $PhMe_2SiOH$ in 93% isolated yield, with a slightly modified experimental procedure adapted to run the reaction on a bigger scale (**Scheme 35**). Turnover studies were performed on the same substrate, leading [MnBr(CO)$_5$] to achieve a maximum TOF of 4088 h^{-1}. This value is rather uncommon for [MnBr(CO)$_5$], that in most reactions is used in loadings at least ten times higher, in the range 5-10 mol%.[35-37]

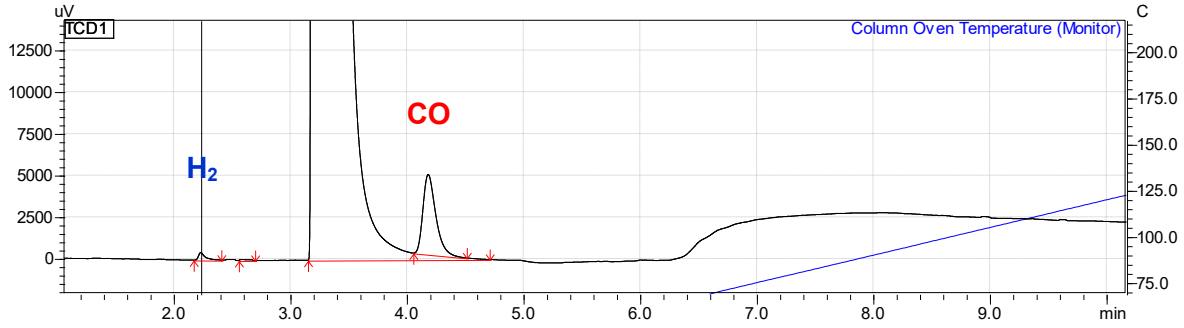
3.4. Mechanistic Investigation

3.4.1. Reaction between [MnBr(CO)$_5$] and PhSiMe$_2$H



Scheme 36: Results obtained from a stoichiometric reaction between dimethylphenylsilane and [MnBr(CO)$_5$].

In order to shed light on the activation mechanism of [MnBr(CO)$_5$], a stoichiometric reaction between [MnBr(CO)$_5$] and PhMe$_2$SiH was followed in THF-d$_8$. First, after observing immediate development of gas from the solution, a gaseous sample was taken from the headspace and analyzed *via* GC-TCD after a reaction time of 5 minutes. This analysis showed the presence of CO in the gas phase (**Figure 9**), confirming release of CO from [MnBr(CO)$_5$] as the very first step (**Scheme 36**), which aligns with what was observed in the previous chapter. Subsequently, a sample of the reaction was analyzed *via* ^{1}H- and ^{29}Si-NMR.



Gas identified	Retention time	Vol%
Hydrogen	2.234	2.584
Argon	3.215	96.581
CO	4.185	0.834

Figure 9: GC-TCD data for the headspace of the reaction in **Scheme 36**.

Already after 15 minutes, it is possible to observe the formation of two singlets arising at 0.81 and – 7.85 ppm in the ^{1}H-NMR (**Figure 10**), which correspond respectively to PhMe$_2$SiBr and a manganese hydride of likely composition [HMn(CO)$_3$(L)$_2$] (where L = THF-d_8). The identity of PhMe$_2$SiBr was also confirmed by ^{29}Si-NMR, and by comparing both spectra with the ones obtained reacting PhMe$_2$SiH with Br$_2$ (**Figure 11**). The experimental evidences for the amount of CO coordinated to the metal instead are

provided later in the chapter (Section 3.4.3). The results therefore suggest that [MnBr(CO)$_5$] is a precatalyst, and that it is activated after the release of CO *via* a "*hydride-bromide exchange*" mechanism with PhMe$_2$SiH.

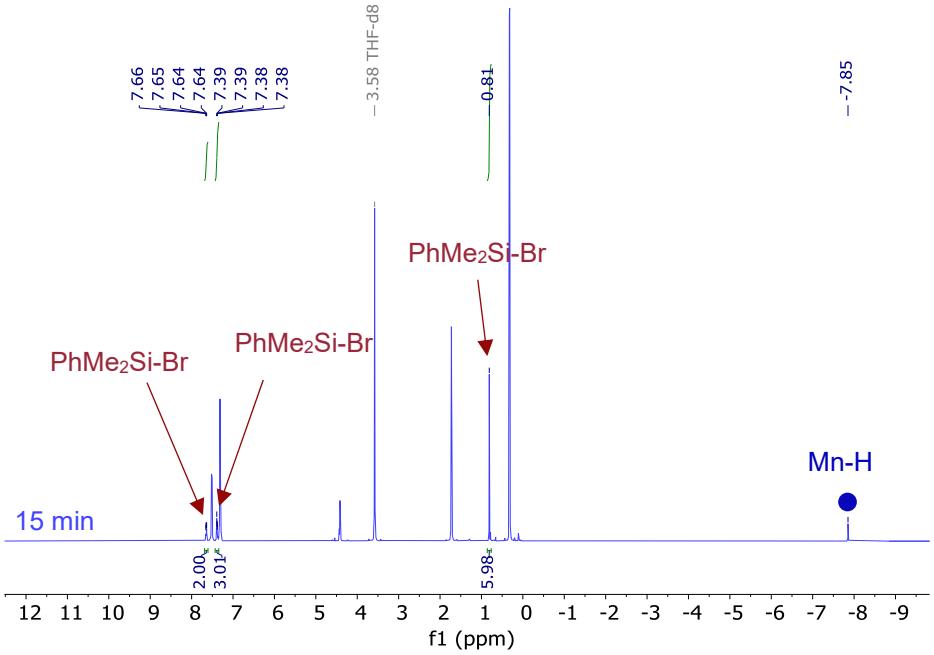


Figure 10: ^{1}H-NMR spectrum (500 MHz, THF-d_8, 296 K) of the reaction reported in Scheme 36 after 15 minutes. The signals highlighted by a red arrow correspond to PhMe$_2$SiBr, and the one highlighted with a blue dot to the manganese hydride.

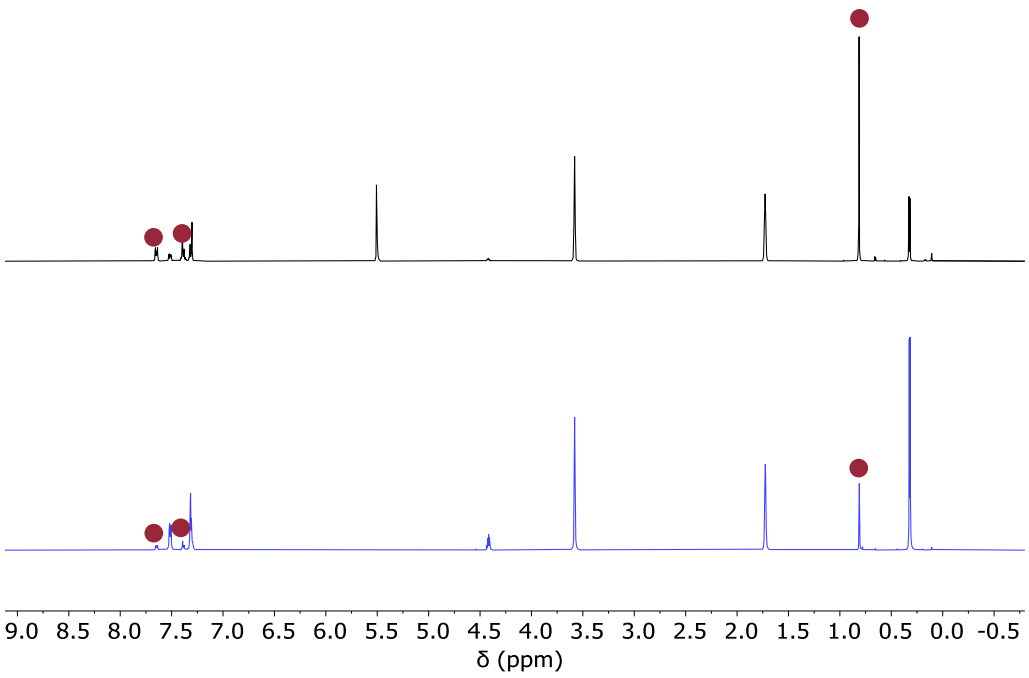


Figure 11: Comparison of the ^{1}H-NMR spectra of the crude reaction mixture between PhMe$_2$SiH and Br$_2$ (black, on top) with the reaction reported in Scheme 36 after 15 minutes (blue, below). Details of this spectrum and the corresponding ^{29}Si-NMR data can be found in section 6.3 of the Appendix.

3.4.2. Kinetic studies

After initial insights into the activation of [MnBr(CO)$_5$], kinetic studies were performed on the reaction in order to obtain more details on the nature of the active species. The rate of the reaction was studied in THF-d_8 at 35 °C by variation of the relevant concentration of silane, H_2O, and [MnBr(CO)$_5$], while following both the formation of $PhMe_2SiOH$ and consumption of $PhMe_2SiH$ *via* quantitative ^{1}H-NMR. The concentration values chosen to study the reaction rate are reported in **Table 6**. The data obtained were collected and analyzed both according to the Variable Time Normalization Analysis (VTNA) method[37-39] (described in in Section 6.5), and with the initial rates methods which led to consistent results (reported also in Section 6.5). The concentration profiles obtained by ^{1}H-NMR spectroscopy were utilized to determine the overall reaction orders of the reaction components. The best curve overlaps (**Figure 12**) show a reaction order of 0.9 in [MnBr(CO)$_5$] and 0.85 in $PhMe_2SiH$, and a significant inhibiting effect of in H_2O with a negative reaction order -0.6.

$$K_{obs} = K\,[MnBr(CO)_5]^{0.9}\,[H_2O]^{-0.6}\,[PhMe_2SiH]^{0.8}$$

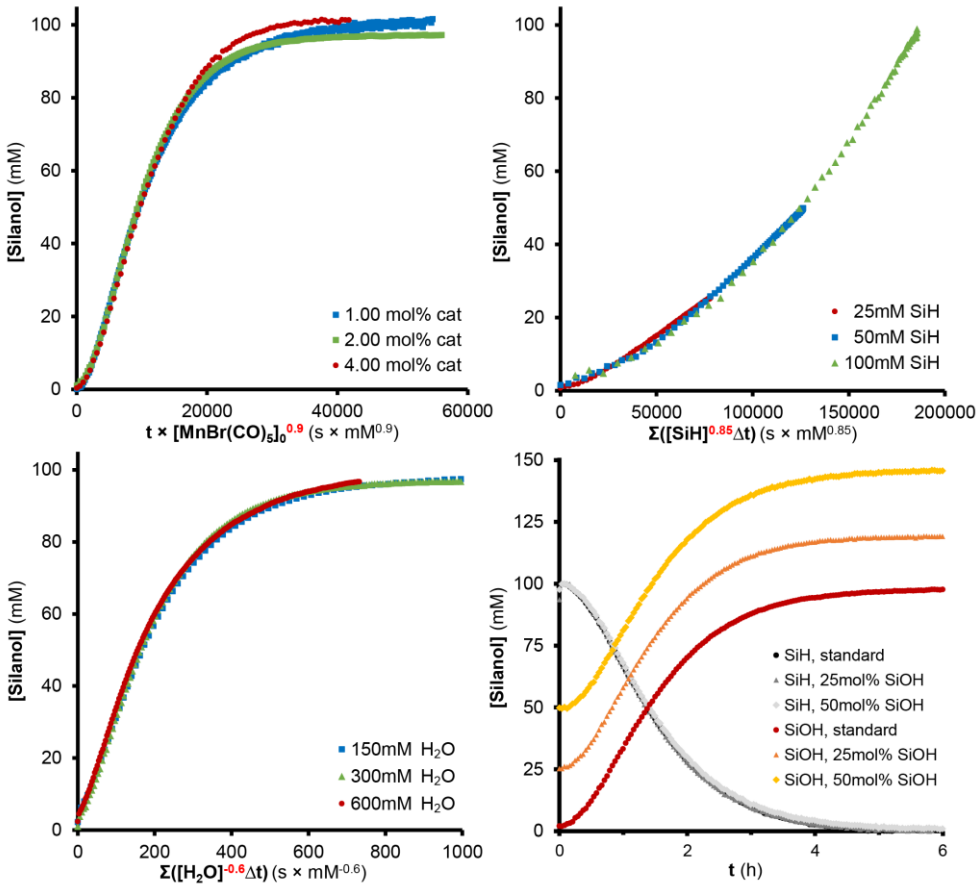
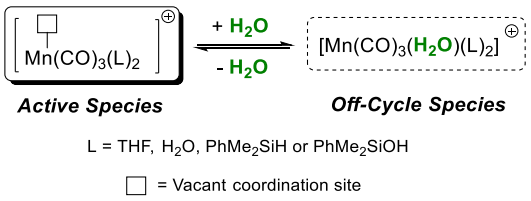


Figure 12: Kinetic plots for the reaction obtained using VTNA analysis of the NMR data plotted with the coefficients affording the best overlap: the formation of $PhMe_2SiOH$ shows 0.9th order dependence in [MnBr(CO)$_5$] (top-left), 0.85th in [$PhMe_2SiH$] (top-right), -0.6th in [H_2O] (bottom-left) and does not show product inhibition (bottom-right).

This finding, together with the catalytic inertness of other Mn(I) carbonyl complexes unable to generate a free coordination site in the reaction conditions (**Table 3**, similarly to what observed in the previous chapter), points towards an unsaturated complex as the catalytic active species. In fact, the reaction order in H_2O of -0.6 is consistent with a reversible inhibition effect of water, in which the catalytically active species is involved in a coordinative pre-equilibrium with H_2O (**Scheme 37**).



Scheme 37: Influence of H_2O on the reversible inhibition of the catalytically active species.

In order to verify if $PhMe_2SiOH$ could have a similar inhibiting effect on the reaction rate, one kinetic experiment was repeated with starting concentrations of $PhMe_2SiOH$ between 25 and 50 mol% with respect to $PhMe_2SiH$. The experiment did not show any inhibiting activity of $PhMe_2SiOH$ in these concentrations, in line what was observed in terms of chemoselectivity during the optimization (**Figure 12**). Therefore, from the kinetic studies the first evidence for a coordinatively unsaturated active species in catalysis was obtained. Next, $PhMe_2SiD$ and D_2O were studied in the reaction in order to detect a measurable KIE (**Figure 13**). Both the combinations of D_2O with $PhMe_2SiH$, and $PhMe_2SiD$ with H_2O did not show any KIE, suggesting that the cleavage of Si–H or O–H bonds are not involved in the rate-determining step of the reaction.

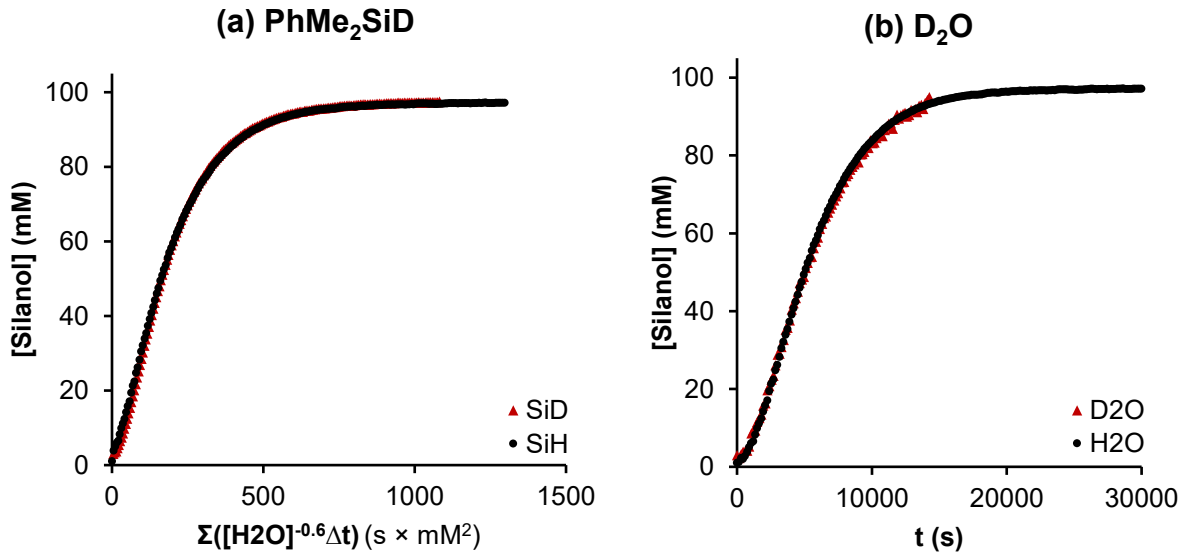
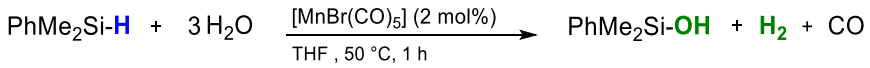


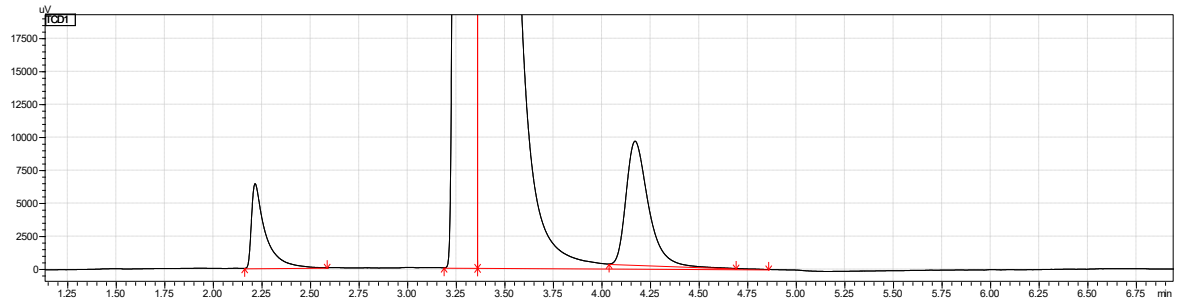
Figure 13: Concentration profiles of $PhMe_2SiOH$ arising respectively from the reactions between: (a) $PhMe_2SiD$ and H_2O (time scale normalized with respect to the water content); (b) $PhMe_2SiH$ and D_2O.

3.4.3. Investigating the coordination sphere of the active species



Scheme 38: Reaction between $PhMe_2SiH$ and H_2O catalyzed by [MnBr(CO)$_5$] and analyzed *via* GC-TCD.

The coordination sphere of the potential active species was further investigated. In a first attempt to figure out how many CO ligands are still coordinated to the metal center, the gas phase analysis of a reaction between $PhMe_2SiH$ and H_2O was analyzed at complete conversion. The GC-TCD data show again a ratio of H_2/CO = 25. This value indicates that, on average, each [MnBr(CO)$_5$] dissociates 2 CO (**Error! Reference source not found.**).



Gas identified	Retention time	Vol%
Hydrogen	2.217	18.01
Argon	3.270	81.26
CO	4.173	0.73

Another reaction between $PhMe_2SiH$ and H_2O at 2 mol% catalyst loading was followed *via* flow FT-IR. It was possible to observe that, at 35 °C, the majority of [MnBr(CO)$_5$] is converted within 1 hour. Simultaneously with the consumption of [MnBr(CO)$_5$] it is possible to observe the formation of new bands arising in the area 1950-1900 cm^{-1}, characteristic region for Mn(I) species comprising a tricarbonyl unit. (**Figure 14**).[40]

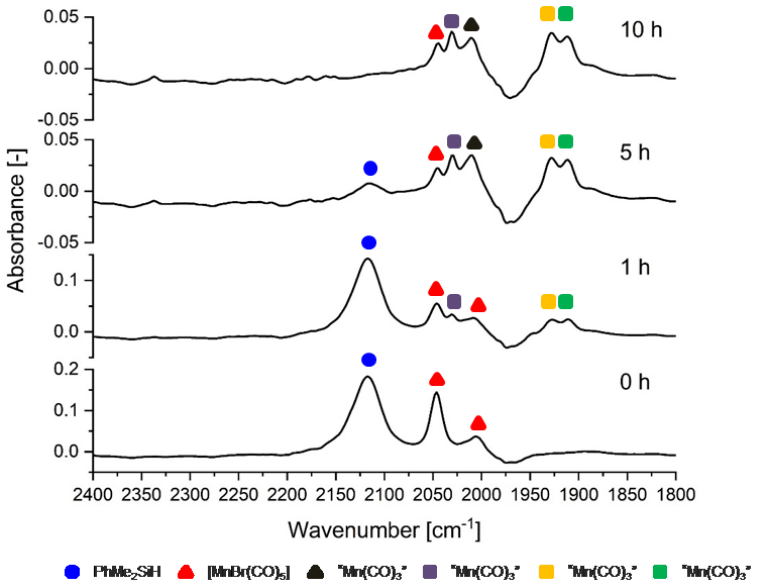


Figure 14: Selected FT-IR spectra at different time intervals of the reaction above (Scheme 38) performed under flow conditions.

Further evidence about the coordination sphere of the Mn(I) complexes formed during the reaction was obtained from analysis of the solid material obtained after water extraction of the reaction mixture, and subsequent evaporation of all volatiles from the aqueous phase at the end of the reaction.

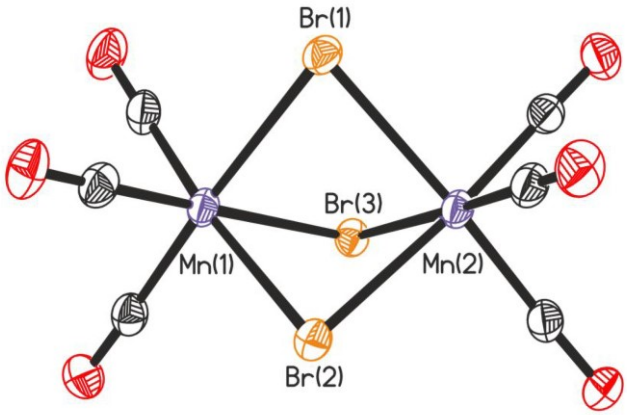


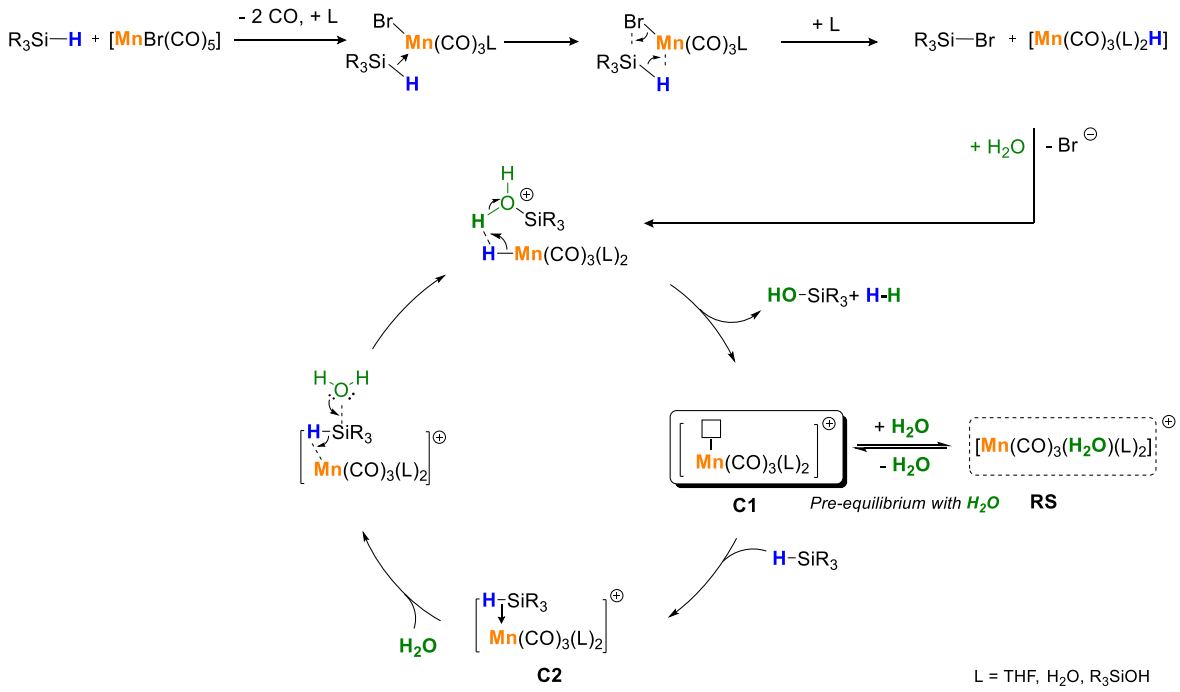
Figure 15: Anion $[(CO)_6Mn_2(\mu\text{-}Br)_3]^-$ of the species **Mn-7** (*trans*-$[Mn(II)(THF)_4(OH_2)_2][(CO)_6Mn_2(\mu\text{-}Br)_3]_2$), crystallized from a crude reaction mixture. The procedure is reported in section 3.7.10. The crystallographic data and the full crystal structure are reported respectively in Section 6.4.4 and Section 6.4.7.

From the solid obtained it was possible to grow a single crystal suitable for X-Ray diffraction, which revealed the presence of a cationic mononuclear *trans*-$[Mn(II)(THF)_4(OH_2)_2]^{2+}$ and two dinuclear anions $[(CO)_6Mn_2(\mu\text{-}Br)_3]^-$ as counterions (**Mn-7**, **Figure 15**; the crystallographic data and the full crystal structure are reported respectively in Section 6.4.4 and Section 6.4.7). The solid was also found to retain some of the

initial catalytic activity upon reuse in a second reaction with fresh solvent and substrate (61% conversion after 1 h). This suggests a potential role of *off-cycle species* for **Mn-7**, and confirms the key role of these "Mn(CO)$_3$" fragments for the catalytic activity in the reaction.

3.5. Mechanistic Proposal

A plausible reaction mechanism consistent with the experimental data collected in this chapter is presented below in **Scheme 39**. In the initial activation step, [MnBr(CO)$_5$] dissociates 2 CO ligands, allowing for σ-coordination of the silane R_3SiH to the metal center. This coordination leads to the formation of the corresponding bromosilane R_3SiBr, and a hydride complex [MnH(CO)$_3$(L)$_2$]. Hydrolysis of the Si–Br unit leads to the protonated silanol, which subsequently protonates the Mn–H liberating H_2 as the second desired product. The resulting unsaturated complex of the type $[Mn(CO)_3(L)_2]^+$ (**C1**, **Scheme 39**; L = solvent, H_2O, or R_3SiOH) can be suggested as the active species carrying the catalytic cycle on. In fact, coordination of additional water as L converts **C1** into a octahedral *off-cycle species* **RS**, explaining the negative reaction order in H_2O. Alternatively, re-coordination of Br^- would also seem conceivable despite being less likely, due to the large excess of water under turnover conditions. In competition with the other neutral ligands, σ-coordination of R_3SiH (possibly, the rate determining step of the reaction) generates the adduct **C2** as the next productive species activating the silane for the nucleophilic attack of H_2O. In line with this suggestion, cationic and monomeric Mn(I) complexes such as $[Mn(CO)_3(L)_2]^+$ are known to perform heterolytic cleavage of Si–H bonds already at R.T.,[41, 42] and constitute, therefore, plausible candidates as active species in agreement with the absence of H/D kinetic isotope effects. The slight deviations in the reaction orders for [MnBr(CO)$_5$] and $PhMe_2SiH$ from unity may indicate that the silane could also be involved in slow degradation of the catalyst to inactive species.



Scheme 39: Suggested mechanistic cycle for the dehydrogenative oxidation of silanes catalyzed by [MnBr(CO)5] using H_2O as the green oxidant.

3.6. Conclusion and Outlook

In this chapter it was shown that [MnBr(CO)5] is an active precatalyst for the selective oxidation of silanes to silanols using H_2O as the oxidant. The reaction evolves stoichiometric amounts of hydrogen and can be performed under neutral conditions. The newly developed protocol allowed the preparation of primary and secondary silanols, including also di-silanols, some of which would be incompatible with traditional synthetic procedures. The reaction showed excellent selectivity for a wide scope of products, was able to avoid the undesired formation of siloxanes and could easily be gram-scaled. The reaction mechanism has been thoroughly investigated with several analytical techniques, being most consistent with a catalytic cycle mediated by a Mn(I) tricarbonyl unit of general formula $[Mn(CO)_3(L)_2]^+$ (L = solvent, H_2O, or $R_nSi(OH)_{4-n}$), as the active species. In line with the objectives of the thesis, the knowledge acquired in this chapter on the reaction mechanism will lead us to investigate, in the next chapter, whether it is be possible to design an active catalyst bearing the "$[Mn(CO)_3]^+$" framework for catalytic hydrogenation reactions, as an alternative possibility to the well-established Mn(I)-based MLC-pincer catalysts.

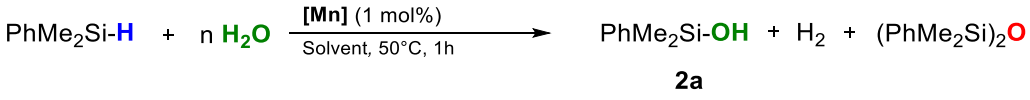
3.7. Experimental Procedure and Characterization Data

To enhance the readability and comprehension of the experimental procedures for this chapter, a detailed list of all the devices employed for measurements is provided in the Appendix, Section 6.1.

3.7.1. General considerations

Unless otherwise stated, all air-sensitive experiments were conducted under an argon atmosphere using standard Schlenk techniques or an MBraun inert-gas glovebox. Solvents for air- and moisture-sensitive experiments were purified through a MBraun-SPS-7 system or dried over activated molecular sieves (3 or 4Å) and degassed according to standard laboratory procedure. All the silanes used as starting materials and and the commercial Mn salts tested in catalysis were purchased from Sigma Aldrich, abcr, Alfa Aesar, or TCI Europe and used as received. [MnBr(CO)$_5$] has been used as received from Sigma Aldrich or Alfa Aesar and it was also used for the synthesis of the complexes **Mn-2**,[43] **Mn-5**,[44] and **Mn-6**[45] according to reported literature procedures. **Mn-4** was purchased from Sigma Aldrich and was used as received. The chemical shifts (δ) are given in ppm (parts per million) relative to TMS and were assigned taking as a reference the residual solvent signals ($CDCl_3$: δ_H = 7.26 ppm, δ_C = 77.16 ppm; DMSO-d_6: δ_H = 2.50 ppm, δ_C = 39.52 ppm; THF-d_8: δ_H = 3.58 ppm, δ_C = 25.31 ppm; C_6D_6: δ_H = 7.16 ppm, δ_C = 128.06 ppm). ^{13}C spectra were generally acquired with broadband proton decoupling. The chemical shift (δ) for ^{19}F-NMR spectra is given in ppm with respect to $CFCl_3$ as a reference ($\delta_{^{19}F}$ = 0 ppm). ^{29}Si-NMR spectra were recorded using a DEPT pulse sequence, and the chemical shifts are reported in ppm with respect to TMS (δ_{Si} = 0 ppm). The chemical shift (δ) for ^{31}P-NMR spectra is given in ppm with respect to H_3PO_4 (85% in H_2O) as a reference ($\delta_{^{31}P}$ = 0 ppm). The peak patterns for NMR spectra are indicated as follows: s = singlet; d = doublet; t = triplet; q = quartet; m = multiplet; dd = doublet of doublets; br = broad. The IR data are given in wavenumbers (cm^{-1}), and the intensity of the bands is indicated as follows: st = strong; me = medium; w = weak.

3.7.2. General procedure for the reaction optimization



The selected Mn complex (5 x 10^{-3} mmol), mesitylene (20 µL, 0.14 mmol), and dimethylphenylsilane (68.1 mg, 0.5 mmol) were weighed in a 4 mL vial equipped with a screw cap and a magnetic stirrer inside the glovebox. The reaction vessel was taken outside the glovebox, and placed in a 25 mL Schlenk tube under inert gas. H_2O and the solvent of choice were added to the vial under argon stream. The reaction mixture was heated at 50 °C for 1 hour. The reaction vessel was cooled down to R.T.; ca 0.05 mL of the crude reaction mixture was transferred to an oven dried NMR tube, and was added with and 0.5 mL of DMSO-d_6. Quantitative ^{1}H-NMR spectroscopy was conducted to determine the conversion and yield of the reaction.

The Si-OH integral (5.88 ppm, 1H) was set at 1.00 and compared with the characteristic peak value of mesitylene (6.76 ppm, 3H).

3.7.3. General procedures for the substrate scope

The indicated silane (0.5 mmol) was weighed in a 4 mL vial equipped with a screw cap and a magnetic stirrer inside the glovebox (in the case of NMR yields, 20 μL of Mesitylene were also weighed together with the silane). The reaction vessel was taken outside the glovebox and placed in a 25 mL Schlenk tube under inert gas. H_2O (27 μL, 1.5 mmol) and THF or 2-MTHF (0.25 mL) were added to the vial in argon flow. A freshly prepared solution of [MnBr(CO)$_5$] (0.25 mL, 0.02 M in THF or 2-MTHF) was added. The reaction mixture was heated at the indicated temperature and time. The reaction vessel was cooled down to R.T.; the vial was carefully opened to release the H_2 overpressure. In the case of NMR yields, an NMR tube was filled with the crude mixture (ca 0.05 mL), DMSO-*d*$_6$ (0.5 mL), and quantitative ^{1}H-NMR spectroscopy was conducted to determine the conversion and yield of the reaction. The Si-OH proton signal integral (5.88 ppm, 1H) was set to 1.00 and compared to the characteristic peak value in mesitylene (6.76 ppm, 3H). For the isolated yields, at the end of the reaction the reaction vessel was stirred open under air for 10-15 min, then closed and irradiated with blue light (450 nm) until the color of the solution changed from yellow to colorless, with brown particles of $MnO_{2(s)}$. Activated 3Å molecular sieves were added to the reaction mixture to remove the excess water. The reaction mixture was filtered through a syringe filter, and the vial was washed with DCM (5 mL). The solvent was removed under reduced pressure to provide the target compound.

The substrates studied in the scope have undergone individual optimization in order to maximize the yield. The conditions used may vary significantly for each individual substrate and they are summarized in **Table 5**.

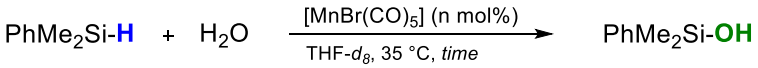
Table 5: Summary of the reaction conditions used for each individual substrate for the scope of **Scheme 34**.

Product	Silane (mmol)	Solvent (volume)	T (°C)	Time (h)	[MnBr(CO)$_5$]	H_2O (mmol).
2a	0.5	THF (0.5 mL)	50	1	1 mol%	1.5
2b	0.5	2-MTHF (0.5 mL)	80	1	1 mol%	1.5
2c	0.5	2-MTHF (0.5 mL)	80	1	1 mol%	1.5
2d	0.5	THF (0.5 mL)	60	4	1 mol%	1.5
2e	0.5	2-MTHF (0.5 mL)	80	1	2 mol%	1.5
2f	0.5	THF (0.5 mL)	50	2	1 mol%	1.5
2g	0.5	THF (0.5 mL)	50	24	1 mol%	1.5
2h	0.5	THF (0.5 mL)	R.T.	24	1 mol%	1.5
2i	0.5	THF (0.5 mL)	50	24	1 mol%	1.5
2j	0.5	2-MTHF(0.5 mL)	80	5	2 mol%	1.5
2k	0.5	THF (0.5 mL)	R.T.	24	1 mol%	1.5
2l	0.5	THF (0.5 mL)	50	4	1 mol%	1.5
2m	0.5	THF (0.5 mL)	R.T.	24	1 mol%	1.5
2n	0.25	THF (2.0 mL)	50	4	2 mol%	6
2o	0.25	THF (2.0 mL)	50	4	2 mol%	6
2p	0.25	THF (2.0 mL)	50	48	2 mol%	6
2q	0.25	THF (1.0 mL)	50	48	4 mol%	6
2r	0.25	THF (1.0 mL)	R.T.	48	8 mol%	6
2s	0.25	THF (1.0 mL)	50	48	4 mol%	6
2t	0.25	THF (1.0 mL)	R.T.	48	8 mol%	6
2u	0.5	THF (0.5 mL)	R.T.	24	1 mol%	1.5
2v	0.5	THF (0.5 mL)	R.T.	24	1 mol%	1.5
2z	0.5	THF (0.5 mL)	50	4	1 mol%	1.5

3.7.4. Procedure followed for the kinetic studies

Stock solutions of H_2O, $PhMe_2SiH$ added with mesitylene as internal NMR standard, and [MnBr(CO)$_5$] in THF-d_8 were prepared in oven-dried volumetric flasks under an inert atmosphere (either by the use of Schlenk techniques or inside the glovebox). An oven-dried J-Young tube was placed in a Schlenk tube, and it was evacuated and refilled with argon three times. To reach the desired concentration in all the three components (reported in **Table 6**), the chosen volume of H_2O solution in dry and degassed THF-d_8 was added with a Hamilton syringe to the J-Young tube under argon flow. The J-Young tube was closed, brought to the glovebox, and the chosen volume of stock solutions of $PhMe_2SiH$ and [MnBr(CO)$_5$] were also added using Hamilton syringes. The volume of the solution has been brought to 500 µL by further addition of dry and degassed THF-d_8. The J-Young tube was closed, and the sample was taken outside the glovebox and immediately placed in a Dewar filled with dry ice. The tube was inserted in the probe-head of an NMR spectrometer pre-heated at 35 °C, and ^{1}H-NMR spectra were recorded every 150 s until full conversion of $PhMe_2SiH$ was achieved. The order with respect to each component was determined both by the initial rate method and *via* VTNA.[37-39] The KIE was determined by preparing the samples according to the same procedure, but using stock solutions of D_2O or $PhMe_2SiD$ in dry and degassed THF-d_8. The product inhibition was studied with 25 mol% and 50 mol% of $PhMe_2SiOH$ with respect to the initial concentration of $PhMe_2SiH$ added to the J-Young tube together with the other reagents. The main signals used for monitoring the course of the reaction were the septet at 4.42 ppm for $PhMe_2SiH$ (1H), and the singlet at 0.27 ppm for $PhMe_2SiOH$ (6H)

Table 6: Initial concentrations of each component for each run of the kinetic analysis.

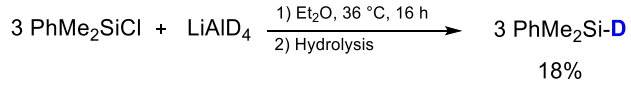


Run	[PhMe$_2$SiH]	[H$_2$O]	[MnBr(CO)$_5$]	[PhMe$_2$SiOH]
1	100 mM	300 mM	1 mM	0 mM
2*	100 mM	300 mM	2 mM	0 mM
3	100 mM	300 mM	4 mM	0 mM
4	25 mM	300 mM	2 mM	0 mM
5	50 mM	300 mM	2 mM	0 mM
6*	100 mM	150 mM	2 mM	0 mM
7	100 mM	600 mM	2 mM	0 mM
8	25 mM	150 mM	2 mM	0 mM
9	50 mM	150 mM	2 mM	0 mM
10**	100 mM	300 mM	2 mM	0 mM
11***	100 mM	300 mM	2 mM	0 mM
12	100 mM	300 mM	2 mM	25 mM
13	100 mM	300 mM	2 mM	50 mM

*Repeated twice
** PhMe$_2$SiD used instead of PhMe$_2$SiH
*** D$_2$O used instead of H$_2$O

3.7.5. Synthesis and characterization of PhMe$_2$Si-D

The synthesis was carried out based on slightly modified literature procedures.[46,47]



Scheme 40: Reaction conditions for the synthesis of PhMe$_2$SiD.

$LiAlD_4$ (44.9 mg, 1.0 mmol) was weighed in a 25 mL Schlenk tube equipped with a magnetic stirrer and a screw cap. $PhMe_2SiCl$ (494.6 mg, 2.9 mmol) was weighed in a vial inside the glovebox. Et_2O (3 mL) was added to $LiAlD_4$ to form a suspension. $PhMe_2SiCl$ was added dropwise to the suspension. The vial was washed with Et_2O (4 x 0.5 mL) and added to the Schlenk tube. The resulting mixture was heated at 36 °C for 16 hours. A $NaOH_{(aq)}$ solution (3 mL, 10% w/w) was added dropwise to the crude reaction mixture and stirred for 15 min. The aqueous phase turned into an emulsion and was extracted with Et_2O (4 x 5 mL). The solvent was evaporated, and $PhMe_2SiD$ was isolated *via* vacuum transfer as a colorless oil (69.6 mg, 0.51 mmol, 18%).

3.7.6. Procedure for the stoichiometric experiments between [MnBr(CO)$_5$] and PhMe$_2$SiH

[MnBr(CO)$_5$] (10.9 mg, 0.04 mmol) and $PhMe_2SiH$ (5.5 mg, 0.04 mmol) were weighed in a vial inside the glovebox, dissolved in THF-d_8 (0.6 mL) and transferred in an oven-dried J-Young tube. ^{1}H- and ^{29}Si- NMR were recorded over time.

3.7.7. Procedure for the reaction between PhMe$_2$SiH and Br$_2$

Br_2 (74.9 mg, 0.5 mmol) was added to a 10 mL Schlenk tube under an argon atmosphere. 2 mL of DCM were added to Br_2 in argon flow. The Schlenk tube was cooled down to 0 °C in an ice bath, and $PhMe_2SiH$ (157.2 µL, 1.0 mmol) was added dropwise under argon flow to the dark red solution vigorously stirred. The solution turned colorless and was stirred at 0 °C for 30 min. The Schlenk tube was warmed up to R.T. over 15 min, and 0.25 mL of the reaction mixture were transferred to a J-Young tube under Ar. The solvent was removed under reduced pressure, and 0.5 mL of THF-d_8 were added to the J-Young tube in Ar flow. The crude reaction mixture (^{1}H- and ^{29}Si-NMR) is shown in black in Section 3.4.1 (**Figure 11**) for comparison with the reaction between [MnBr(CO)$_5$] and $PhMe_2SiH$.

3.7.8. Procedure for the gas phase analysis studies on the headspace of the reaction

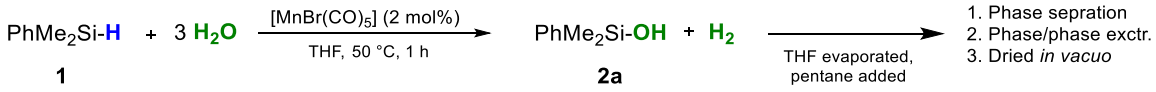
[MnBr(CO)$_5$] (5.5 mg, 0.02 mmol) and dimethylphenylsilane (133.8 mg, 1.0 mmol) were weighed in a 10 mL Schlenk tube inside the glovebox. The reaction vessel was taken outside the glovebox and covered with aluminum foil. H_2O (36 µL, 2.0 mmol) and THF (1 mL) were added to the vial in argon flow. The reaction mixture was heated in an oil bath set to 50 °C for 1 h. Subsequently, the reaction vessel was allowed to cool down to R.T., and 100 µL of the headspace of the reaction was injected into the GC-TCD. The

quantification of $H_{2(g)}$ and $CO_{(g)}$ has been performed using calibration curves to obtain the corresponding value in Vol (%) with respect to the integrated areas of the two gases.

3.7.9. Procedure for the IR studies

[MnBr(CO)$_5$] (5.5 mg, 0.02 mmol) and dimethylphenylsilane (136.3 mg, 1.0 mmol) were weighed in two separate 4 mL vials inside the glovebox, dissolved in THF and transferred to a volumetric flask of 10 mL that was brought to volume with THF. The solution was transferred to a syringe, brought outside the glovebox and added to a 25 mL Schlenk tube under inert gas already containing 54 µL of H_2O (3.0 mmol). The reaction mixture was manually stirred, and transferred with a syringe to a Fischer-Porter bottle in Ar flow. The Fischer-Porter bottle was already equipped with a stirring bar and a flow system (already under inert gas), and already pre-heated by an oil bath set to 35 °C. Subsequently, the flow apparatus was sealed and started with a rate of 3 mL min^{-1}, and the FT-IR recorded with a frequency of 1 spectrum/min.

3.7.10. Procedure for the isolation of Mn-7 and its test in catalytic studies



Scheme 41: Schematic representation of the steps followed for the isolation of the solid leading to **Mn-8**.

[MnBr(CO)$_5$] (27.0 mg, 0.1 mmol) and $PhMe_2SiH$ (689.2 mg, 5.1 mmol) were weighed in a 25 mL Schlenk tube inside the glovebox. The reaction vessel was taken outside the glovebox, added with H_2O (270 µL, 15.0 mmol) and THF (5 mL) in Ar flow. The reaction mixture was placed in a pre-heated oil bath set to 50 °C for 1 h. Subsequently, the reaction vessel cooled down to R.T., and THF was removed under reduced pressure. Pentane (2 mL) was added to the crude reaction mixture leading to phase separation of the residual H_2O (**Figure 16**, panels A and B). 1 mL of degassed H_2O was added to the Schlenk tube, and the yellow aqueous phase was extracted with pentane (3 x 2 mL) and Et_2O (1 x 2 mL, **Figure 16**, panel C). The water of the residual yellow aqueous phase was removed under reduced pressure, leading to a dark orange solid. From this orange solid, it was possible to crystallize **Mn-7**.

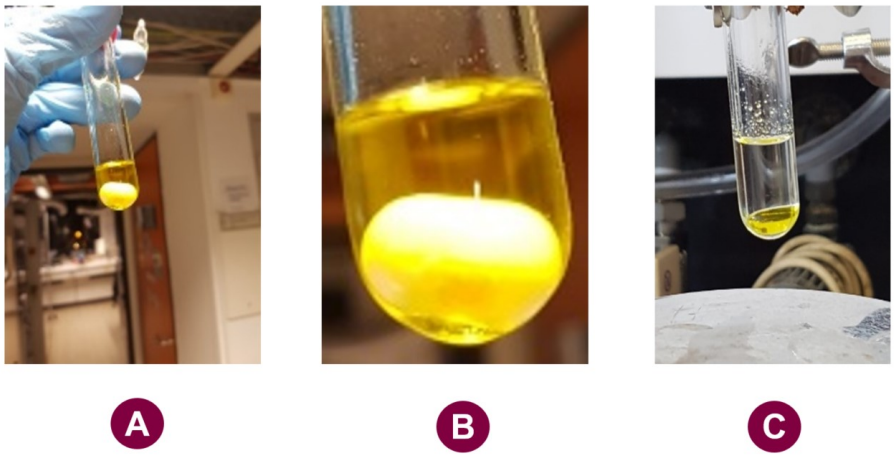


Figure 16: Pictures of the reaction mixture illustrating the separation process.

The orange solid obtained (3.8 mg, 2.7 x 10^{-3} mmol)*****, mesitylene (44.7 mg, 0.37 mmol) and $PhMe_2SiH$ (141.3 mg, 1.0 mmol) were weighed in a 4 mL vial inside the glovebox. The reaction vessel was taken outside the glovebox and placed in a 25 mL Schlenk tube under inert gas. H_2O (54 µL, 3.0 mmol) and THF (1.0 mL) were added to the vial in argon flow. The vial was placed in a pre-heated oil bath at 50 °C, and the reaction mixture was stirred for 1 h. Subsequently, the reaction vessel cooled down to R.T;. a NMR tube was filled with the crude mixture (ca. 0.05 mL), DMSO-d_6 (0.5 mL), and quantitative ^{1}H-NMR spectroscopy was conducted to determine the conversion and yield of the reaction. The yield of 61% was obtained by setting the integral value for the mesitylene singlet (6.76 ppm, 3H) as 1.00 and integrating the characteristic Si-OH signal of the product.

* Calculated assuming that the solid is entirely composed of **Mn-7** and dividing 3.8 mg by the F.W. of **Mn-7**.

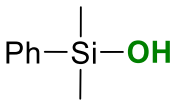
3.7.11. Procedure for the low catalyst loading reaction

Dimethylphenylsilane (67.1 mg, 0.5 mmol) and mesitylene (20 µL, 0.14 mmol) were weighed in a 4 mL vial inside the glovebox equipped with a screw cap and a magnetic stirrer. A solution of [MnBr(CO)$_5$] in 2-MTHF (5 mM) was prepared in the glovebox in a 2 mL volumetric flask and transferred to a 10 mL Schlenk tube. The vial was taken outside the glovebox, placed in a 25 mL Schlenk tube under inert gas and added with H_2O (18 µL, 2 mmol) under Ar flow. 500 µL of the [MnBr(CO)$_5$] solution was added to the vial in argon flow and the reaction mixture was heated in an oil bath set to 80 °C for 163 s. Subsequently, the reaction vessel was cooled down to R.T.; 0.05 mL of the crude mixture were transferred to an NMR tube and added with 0.5 mL of DMSO-d_6. The yield of 92% in $PhMe_2SiOH$ was obtained by setting the integral value for the characteristic signal of the product (Si-OH, 5.88 ppm, 1H) as 1.00 and integrating the corresponding mesitylene singlet (6.76 ppm, 3H). The resulting TOF for this reaction was found to be 4088 h^{-1}.

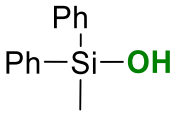
3.7.12. Procedure for the gram scale reaction

[MnBr(CO)$_5$] (27.5 mg, 0.1 mmol) was dissolved in THF (13 mL) in a 50 mL Schlenk tube equipped with a screw cap and a magnetic stirrer inside the glovebox. PhMe$_2$SiH (1.36 g, 10.0 mmol) was dissolved in THF (13 mL) in a different 50 mL Schlenk tube inside the glovebox. Both Schlenk tubes were taken outside the glovebox and connected to the Schlenk line. H_2O (540 µL, 30 mmol) was added to the [MnBr(CO)$_5$] solution in THF under argon flow using an Eppendorf pipette, followed by dropwise addition of the PhMe$_2$SiH solution in THF (over 15 min) to the vigorously stirred solution of [MnBr(CO)$_5$] and H_2O. The Schlenk tube containing PhMe$_2$SiH was rinsed with 5 mL more of THF and added to the reaction vessel, which was placed in a pre-heated oil bath at 50 °C for 3 hours (while being connected to the Schlenk line to prevent the development of overpressure). At the end of the reaction, the Schlenk tube was cooled down to room temperature, and the solvent was evaporated under reduced pressure. The resulting mixture was purified by silica gel column chromatography with Pentane:EtOAc = 9:1 as eluent to afford PhMe$_2$SiOH as a colorless oil (1.41 g, 9.26 mmol, 93%).

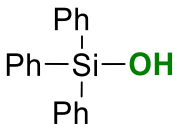
3.7.13. Characterization data



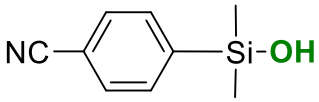
Dimethylphenylsilanol **(2a)**,[11] $C_8H_{12}OSi$, colorless oil: **^{1}H NMR** (400 MHz, $CDCl_3$, 296 K) δ 7.69 – 7.50 (m, 2H), 7.39 (m, 3H), 1.78 (s, 1H), 0.42 (s, 6H). **^{13}C{^{1}H} NMR** (101 MHz, $CDCl_3$, 296 K) δ 139.23, 133.18, 129.81, 128.06, 0.14. **^{29}Si NMR** (79 MHz, $CDCl_3$, 296 K) δ 7.95.



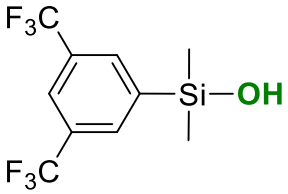
Methyldiphenylsilanol **(2b)** [11] $C_{13}H_{14}OSi$, colorless oil. **^{1}H NMR** (400 MHz, $CDCl_3$, 296 K) δ 7.70 – 7.56 (m, 4H), 7.52 – 7.30 (m, 6H), 2.24 – 2.05 (s, br, 1H), 0.68 (s, 3H). **^{13}C{^{1}H} NMR** (101 MHz, $CDCl_3$, 296 K) δ 137.19, 134.11, 130.06, 128.08, -1.09.**^{29}Si NMR** (79 MHz, $CDCl_3$) δ -2.42.



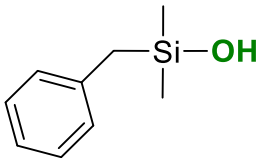
Triphenylsilanol **(2c),**[11] $C_{18}H_{16}OSi$, white solid: **^{1}H NMR** (400 MHz, $CDCl_3$, 296 K) δ 7.93 – 7.55 (m, 6H), 7.53 – 7.28 (m, 9H), 2.51 (s, br, 1H). **^{13}C{^{1}H} NMR** (101 MHz, $CDCl_3$, 296 K) δ 135.25, 135.13, 130.29, 128.08. **^{29}Si NMR** (79 MHz, $CDCl_3$) δ -12.53.



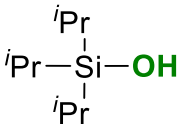
4-(Hydroxydimethylsilyl)benzonitrile **(2d)**,[51] $C_9H_{11}NOSi$, colorless oil. **^{1}H NMR** (400 MHz, $CDCl_3$) δ 7.86 – 7.49 (m, 4H), 1.98 (s, br, 1H), 0.43 (s, 6H). **^{13}C{^{1}H} NMR** (101 MHz, $CDCl_3$) δ 145.73, 133.68, 131.31, 119.03, 113.25, 0.08. **^{29}Si NMR** (79 MHz, $CDCl_3$) δ 7.45.



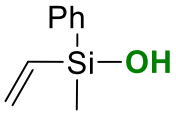
(3,5-Bis(trifluoromethyl)phenyl)dimethylsilanol **(2e)** $C_{10}H_{10}F_6OSi$, white solid. HR-MS: m/z calculated for $[C_{10}H_{10}F_6OSi]^+$ = 288.03996, found = 288.03957. **^{1}H NMR** (400 MHz, $CDCl_3$) δ 8.01 (s, 2H), 7.89 (s, 1H), 2.01 (s, 1H), 0.47 (s, 6H). **^{13}C{^{1}H} NMR** (101 MHz, $CDCl_3$) δ 142.63, 133.06, 131.03 (q, *J* = 32.9 Hz), 124.18-122.77 (m), 123.70 (q, J = 272.9 Hz), 0.20. **^{19}F NMR** (376 MHz, $CDCl_3$) δ -62.83. **^{29}Si NMR** (79 MHz, $CDCl_3$) δ 7.40.



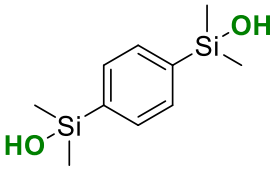
Benzyldimethylsilanol **(2f)** [11] $C_9H_{14}OSi$, colorless oil. **^{1}H NMR** (400 MHz, $CDCl_3$, 296 K) δ 7.26 – 7.19 (m, 2H), 7.15 – 6.99 (m, 3H), 2.18 (s, 2H), 1.58 (s, 1H), 0.14 (s, 6H).**^{13}C{^{1}H} NMR** (101 MHz, $CDCl_3$, 296 K) δ 139.11, 128.59, 128.29, 124.46, 28.17, -0.55.**^{29}Si NMR** (79 MHz, $CDCl_3$) δ 14.42.



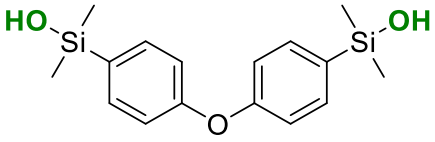
Triisopropylsilanol **(2j)**[48] $C_9H_{22}OSi$, colorless oil. **^{1}H NMR** (400 MHz, $CDCl_3$, 296 K) δ 1.30 (s, 1H), 1.05 (m, 21H). ^{13}C NMR (101 MHz, $CDCl_3$, 296 K) **^{13}C{^{1}H} NMR** (101 MHz, $CDCl_3$) δ 17.85, 12.42. **^{29}Si NMR** (79 MHz, $CDCl_3$) δ 15.11.



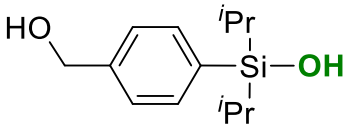
Methyl(phenyl)(vinyl)silanol **(2l)**[49] $C_9H_{12}OSi$, colorless oil. **^{1}H NMR** (400 MHz, $CDCl_3$, 296 K) δ 7.65 – 7.55 (m, 2H), 7.45 – 7.34 (m, 3H), 6.31 (dd, *J* = 20.2, 14.8 Hz, 1H), 6.14 (dd, *J* = 14.9, 3.8 Hz, 1H), 5.89 (dd, *J* = 20.2, 3.8 Hz, 1H), 1.94 (s, 1H), 0.49 (s, 3H).**^{13}C{^{1}H} NMR** (101 MHz, $CDCl_3$, 296 K) 137.36, 136.65, 134.75, 133.75, 130.00, 128.07, -1.55. **^{29}Si NMR** (79 MHz, $CDCl_3$) δ -4.12.



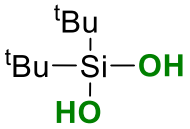
1,4-Phenylenebis(dimethylsilanol) **(2n)**, $C_{10}H_{18}O_2Si_2$, white solid.**^{1}H NMR** (400 MHz, $CDCl_3$, 296 K) δ 7.62 (s, 4H), 1.80 (s, 2H), 0.41 (s, 12H).**^{13}C{^{1}H} NMR** (101 MHz, $CDCl_3$, 296 K) δ 140.80, 132.59, 0.11. **^{29}Si NMR** (79 MHz, $CDCl_3$) δ 7.85.



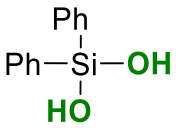
(Oxybis(4,1-phenylene))bis(dimethylsilanol) **(2o)** $C_{16}H_{22}O_3Si_2$, white solid. **^{1}H NMR** (400 MHz, $CDCl_3$, 296 K) δ 7.70 – 7.43 (m, 4H), 7.12 – 6.93 (m, 4H), 1.78 (s, 2H), 0.41 (s, 12H). **^{13}C{^{1}H} NMR** (101 MHz, $CDCl_3$, 296 K) δ 158.43, 134.98, 133.71, 118.62, 0.26. **^{29}Si NMR** (79 MHz, $CDCl_3$) δ 7.86.



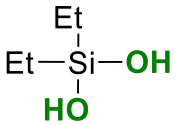
(4-(Hydroxymethyl)phenyl)diisopropylsilanol **(2p)** $C_{13}H_{22}O_2Si$, white solid. HR-MS: m/z calculated for $[C_{13}H_{21}O_2Si]^-$ = 237.131634, found = 237.131660.**^{1}H NMR** (400 MHz, $CDCl_3$, 296 K) δ 7.56 (d, *J* = 7.9 Hz, 2H), 7.38 (d, *J* = 7.6 Hz, 2H), 4.72 (d, *J* = 5.9 Hz, 2H), 1.70 (s, 1H), 1.65 (t, *J* = 6.0 Hz, OH, 1H), 1.22 (hept, *J* = 7.3 Hz, 2H), 1.05 (d, *J* = 7.3 Hz, 6H), 0.97 (d, *J* = 7.4 Hz, 6H).**^{13}C{^{1}H} NMR** (101 MHz, $CDCl_3$, 296 K) 142.05, 134.86, 134.54, 126.37, 65.52, 17.27, 17.02, 12.53. **^{29}Si NMR** (79 MHz, $CDCl_3$) δ 7.52.



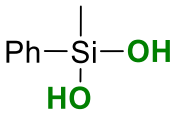
Di-*tert*-butylsilanediol **(2q)**[51] $C_8H_{20}O_2Si$, white solid. **^{1}H NMR** (400 MHz, DMSO-d_6) δ 5.50 (s, 2H), 0.93 (s, 18H). **^{13}C NMR** (101 MHz, DMSO-d_6) δ 27.66, 19.74. **^{29}Si NMR** (79 MHz, DMSO-d_6) δ -14.07.



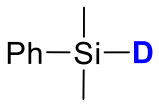
Diphenylsilanediol **(2r)**,[11] $C_{12}H_{12}O_2Si$, white solid. **^{1}H NMR** (400 MHz, DMSO-d_6) δ 7.66 – 7.54 (m, 4H), 7.40 – 7.28 (m, 6H), 6.94 (s, 2H). **^{13}C{^{1}H} NMR** (101 MHz, DMSO-d_6) δ 137.80, 134.07, 129.35, 127.48. **^{29}Si NMR** (79 MHz, DMSO-d_6) δ -34.90.



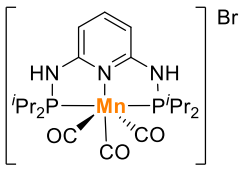
Diethylsilanediol **(2s)** [11] $C_4H_{12}O_2Si$, white solid. **^{1}H NMR** (400 MHz, DMSO-d_6) δ 5.66 (s, 2H), 0.88 (t, J = 8.0 Hz, 6H), 0.37 (q, J = 8.0 Hz, 4H). **^{13}C{^{1}H} NMR** (101 MHz, DMSO-d_6) δ 6.84, 6.59. **^{29}Si NMR** (79 MHz, DMSO-d_6) δ -8.61.



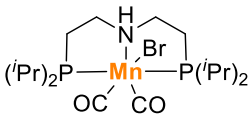
Methylphenylsilanediol **(2t)**,[11] $C_7H_{10}O_2Si$, white solid. **^{1}H NMR** (400 MHz, DMSO-d_6) δ 7.61 – 7.53 (m, 2H), 7.39 – 7.29 (m, 3H), 6.33 (s, 2H), 0.15 (s, 3H). **^{13}C{^{1}H} NMR** (101 MHz, DMSO-d_6) δ 139.41, 133.38, 129.10, 127.42, -0.53. **^{29}Si NMR** (79 MHz, DMSO-d_6) δ -21.60.



Dimethylphenylsilane-*d* [46, 47], $C_8H_{11}SiD$, colorless oil. **^{1}H NMR** (400 MHz, $CDCl_3$) δ 7.60 – 7.50 (m, 2H), 7.43 – 7.31 (m, 3H), 0.34 (s, 6H). **^{13}C{^{1}H} NMR** (101 MHz, $CDCl_3$) δ 137.57 (t, *J* = 1.0 Hz), 134.15, 129.33, 128.00, -3.70 – -3.75 (t, J = 1.1 Hz). **^{29}Si NMR** (79 MHz, $CDCl_3$) δ -17.47 (t, J = 28.7 Hz).

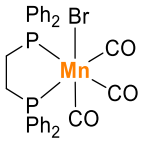


$C_{20}H_{33}BrMnN_3O_3P_2$,[43] white solid. **^{1}H NMR** (400 MHz, DMSO-d_6) δ 8.97 (s, 2H), 7.48 (t, *J* = 8.0 Hz, 1H), 6.37 (d, *J* = 8.0 Hz, 2H), 2.75 (m, 4H), 1.40 (dd, *J* = 15.9, 6.9 Hz, 12H), 1.27 (dd, *J* = 16.3, 7.1 Hz, 12H). **^{31}P NMR** (162 MHz, DMSO-d_6) δ 133.69.



$C_{18}H_{37}BrMnNO_2P_2$, yellow solid.[44]

^{1}H NMR (400 MHz, Benzene-d_6) δ 3.26 (m, 2H), 2.86 (t, *J* = 12.8 Hz, 1H), 2.61 – 2.39 (m, 2H), 2.22 (m, 2H), 2.03 – 1.86 (m, 2H), 1.66 (m, 2H), 1.56 – 1.47 (m, 6H), 1.38 – 1.18 (m, 14H), 1.07 (m, 6H). **^{31}P{^{1}H} NMR** (162 MHz, Benzene-d_6) δ 81.21.



$C_{29}H_{24}BrMnO_3P_2$, yellow solid.[45]

^{1}H NMR (400 MHz, $CDCl_3$) δ 7.74 – 7.61 (m, 4H), 7.55 (m, 4H), 7.48 – 7.30 (m, 12H), 3.14 (m, 2H), 2.78 (m, 2H). **^{31}P NMR** (162 MHz, $CDCl_3$) δ 70.21. **FT-IR** (solid, $\tilde{\nu}$, cm^{-1}) 3055 w, 2011 st, 1949 st, 1905 st, 1483 w, 1434 me, 1097 me, 690 me.

3.8. References

1. Tacke, R.; Heinrich, T.; Bertermann, R.; Burschka, C.; Hamacher, A.; Kassack, M. U., Sila-haloperidol: A Silicon Analogue of the Dopamine (D2) Receptor Antagonist Haloperidol. *Organometallics* **2004,** *23* (19), 4468-4477.

2. Franz, A. K.; Wilson, S. O., Organosilicon Molecules with Medicinal Applications. *J. Med. Chem.* **2013,** *56* (2), 388-405.

3. Denmark, S. E.; Ambrosi, A., Why You Really Should Consider Using Palladium-Catalyzed Cross-Coupling of Silanols and Silanolates. *Org. Process Res. Dev.* **2015,** *19* (8), 982-994.

4. Liu, Y.; Imae, I.; Makishima, A.; Kawakami, Y., Synthesis and characterization of poly(silphenylenesiloxane)s containing functional side groups, a study to high-temperature elastomer. *Sci. Technol. Adv. Mater.* **2003,** *4* (1), 27-34.

5. Cella, J. A.; Carpenter, J. C., Procedures for the preparation of silanols. *J. Organomet. Chem.* **1994,** *480* (1), 23-26.

6. Chandrasekhar, V.; Boomishankar, R.; Nagendran, S., Recent Developments in the Synthesis and Structure of Organosilanols. *Chem. Rev.* **2004,** *104* (12), 5847-5910.

7. Jeon, M.; Han, J.; Park, J., Catalytic Synthesis of Silanols from Hydrosilanes and Applications. *ACS Catal.* **2012,** *2* (8), 1539-1549.

8. Valliant-Saunders, K.; Gunn, E.; Shelton, G. R.; Hrovat, D. A.; Borden, W. T.; Mayer, J. M., Oxidation of Tertiary Silanes by Osmium Tetroxide. *Inorg. Chem.* **2007,** *46* (13), 5212-5219.

9. Lickiss, P. D.; Lucas, R., Oxidation of sterically hindered organosilicon hydrides using potassium permanganate. *J. Organomet. Chem.* **1996,** *521* (1), 229-234.

10. Zimmerman, J. B.; Anastas, P. T.; Erythropel, H. C.; Leitner, W., Designing for a green chemistry future. *Science*, **2020,** *367* (6476), 397-400.

11. Wang, K.; Zhou, J.; Jiang, Y.; Zhang, M.; Wang, C.; Xue, D.; Tang, W.; Sun, H.; Xiao, J.; Li, C., Selective Manganese-Catalyzed Oxidation of Hydrosilanes to Silanols under Neutral Reaction Conditions. *Angew. Chem. Int. Ed.* **2019,** *58* (19), 6380-6384.

12. Shi, M.; M. Nicholas, K., Catalytic Dehydrocoupling of Silane by a Homogenous Rhodium Complex with Water. *J. Chem. Res. (S)* **1997,** (11), 400-401.

13. Yu, M.; Jing, H.; Liu, X.; Fu, X., Visible-Light-Promoted Generation of Hydrogen from the Hydrolysis of Silanes Catalyzed by Rhodium(III) Porphyrins. *Organometallics* **2015,** *34* (24), 5754-5758.

14. Lee, Y.; Seomoon, D.; Kim, S.; Han, H.; Chang, S.; Lee, P. H., Highly Efficient Iridium-Catalyzed Oxidation of Organosilanes to Silanols. *J. Org. Chem.* **2004,** *69* (5), 1741-1743.

15. Garcés, K.; Fernández-Alvarez, F. J.; Polo, V.; Lalrempuia, R.; Pérez-Torrente, J. J.; Oro, L. A., Iridium-Catalyzed Hydrogen Production from Hydrosilanes and Water. *ChemCatChem* **2014,** *6* (6), 1691-1697.

16. Barnes, G. H.; Daughenbaugh, N. E., The Preparation of Organosilanols via the Metal-Catalyzed Reaction of Organosilicon Hydrides with Water. *J. Org. Chem.* **1966,** *31* (3), 885-887.

17. Shimizu, K.-i.; Kubo, T.; Satsuma, A., Surface Oxygen-Assisted Pd Nanoparticle Catalysis for Selective Oxidation of Silanes to Silanols. *Chem. Eur. J.* **2012,** *18* (8), 2226-2229.

18. Chauhan, B. P. S.; Sarkar, A.; Chauhan, M.; Roka, A., Water as green oxidant: a highly selective conversion of organosilanes to silanols with water. *Appl. Organometal. Chem.* **2009,** *23* (10), 385-390.

19. Mitsudome, T.; Noujima, A.; Mizugaki, T.; Jitsukawa, K.; Kaneda, K., Supported gold nanoparticlecatalyst for the selective oxidation of silanes to silanols in water. *Chem. Commun.* **2009,** (35), 5302-5304.

20. Asao, N.; Ishikawa, Y.; Hatakeyama, N.; Menggenbateer; Yamamoto, Y.; Chen, M.; Zhang, W.; Inoue, A., Nanostructured Materials as Catalysts: Nanoporous-Gold-Catalyzed Oxidation of Organosilanes with Water. *Angew. Chem. Int. Ed.* **2010,** *49* (52), 10093-10095.

21. John, J.; Gravel, E.; Hagège, A.; Li, H.; Gacoin, T.; Doris, E., Catalytic Oxidation of Silanes by Carbon Nanotube–Gold Nanohybrids. *Angew. Chem. Int. Ed.* **2011,** *50* (33), 7533-7536.

22. Mitsudome, T.; Arita, S.; Mori, H.; Mizugaki, T.; Jitsukawa, K.; Kaneda, K., Supported Silver-Nanoparticle-Catalyzed Highly Efficient Aqueous Oxidation of Phenylsilanes to Silanols. *Angew. Chem. Int. Ed.* **2008,** *47* (41), 7938-7940.

23. Kikukawa, Y.; Kuroda, Y.; Yamaguchi, K.; Mizuno, N., Diamond-Shaped $[Ag_4]^{4+}$ Cluster Encapsulated by Silicotungstate Ligands: Synthesis and Catalysis of Hydrolytic Oxidation of Silanes. *Angew. Chem. Int. Ed.* **2012,** *51* (10), 2434-2437.

24. Teo, A. K. L.; Fan, W. Y., Catalytic hydrogen evolution from hydrolytic oxidation of organosilanes with silver nitrate catalyst. *RSC Adv.* **2014,** *4* (71), 37645-37648.

25. Schubert, U.; Lorenz, C., Conversion of Hydrosilanes to Silanols and Silyl Esters Catalyzed by $[Ph_3PCuH]_6$. *Inorg. Chem.* **1997,** *36* (6), 1258-1259.

26. Yang, W.; Liu, L.; Guo, J.; Wang, S.-G.; Zhang, J.-Y.; Fan, L.-W.; Tian, Y.; Wang, L.-L.; Luan, C.; Li, Z.-L.; He, C.; Wang, X.; Gu, Q.-S.; Liu, X.-Y., Enantioselective Hydroxylation of Dihydrosilanes to Si-Chiral Silanols Catalyzed by In Situ Generated Copper(II) Species. *Angew. Chem. Int. Ed.* **2022,** *61,* e202205743.

27. Lee, M.; Ko, S.; Chang, S., Highly Selective and Practical Hydrolytic Oxidation of Organosilanes to Silanols Catalyzed by a Ruthenium Complex. *J. Am. Chem. Soc.* **2000,** *122* (48), 12011-12012.

28. Choi, E.; Lee, C.; Na, Y.; Chang, S., $[RuCl_2(p\text{-cymene})]_2$ on Carbon: An Efficient, Selective, Reusable, and Environmentally Versatile Heterogeneous Catalyst. *Org. Lett.* **2002,** *4* (14), 2369-2371.

29. Mori, K.; Tano, M.; Mizugaki, T.; Ebitani, K.; Kaneda, K., Efficient heterogeneous oxidation of organosilanes to silanols catalysed by a hydroxyapatite-bound Ru complex in the presence of water and molecular oxygen. *New J. Chem.* **2002,** *26* (11), 1536-1538.

30. Lv, H.; Laishram, R. D.; Chen, J.; Khan, R.; Zhu, Y.; Wu, S.; Zhang, J.; Liu, X.; Fan, B., Photocatalyzed cross-dehydrogenative coupling of silanes with alcohols and water. *Chem. Commun.* **2021,** *57* (30), 3660-3663.

31. Liang Teo, A. K.; Fan, W. Y., A novel iron complex for highly efficient catalytic hydrogen generation from the hydrolysis of organosilanes. *Chem. Commun.* **2014,** *50* (54), 7191-7194.

32. Matarasso-Tchiroukhine, E., $AreneCr(CO)_2(\eta^2\text{-}HSiHPh_2)$ complexes as catalysts for the Si–H bond activation. Hydrolysis of the Si–H bond and dehydrogenative coupling between diphenylsilane and nucleophiles. *J. Chem. Soc., Chem. Commun.* **1990,** (9), 681-682.

33. Ison, E. A.; Corbin, R. A.; Abu-Omar, M. M., Hydrogen Production from Hydrolytic Oxidation of Organosilanes Using a Cationic Oxorhenium Catalyst. *J. Am. Chem. Soc.* **2005,** *127* (34), 11938-11939.

34. Wang, W.; Wang, J.; Huang, L.; Wei, H., Mechanistic insights into hydrogen generation for catalytic hydrolysis and alcoholysis of silanes with high-valent oxorhenium(v) complexes. *Cat. Sci. Technol.* **2015,** *5* (4), 2157-2166.

35. Gregg, B. T.; Cutler, A. R., Manganese Carbonyl Bromide-Catalyzed Alcoholysis of the Monohydrosilane $HSiMe_2Ph$. *Organometallics* **1994,** *13* (3), 1039-1043.

36. DiBiase Cavanaugh, M.; Gregg, B. T.; Cutler, A. R., Manganese Carbonyl Complexes as Catalysts for the Hydrosilation of Ketones: Comparison with $RhCl(PPh_3)_3$. *Organometallics* **1996,** *15* (12), 2764-2769.

37. Burés, J., Variable Time Normalization Analysis: General Graphical Elucidation of Reaction Orders from Concentration Profiles. *Angew. Chem. Int. Ed.* **2016,** *55* (52), 16084-16087.

38. Burés, J., A Simple Graphical Method to Determine the Order in Catalyst. *Angew. Chem. Int. Ed.* **2016,** *55* (6), 2028-2031.

39. Nielsen, C. D. T.; Burés, J., Visual kinetic analysis. *Chem. Sci.* **2019,** *10* (2), 348-353.

40. Connor, J. A.; Hudson, G. A., Studies of chelation: II. Phosphine complexes of molybdenum and Manganese. *J. Organomet. Chem.* **1974,** *73* (3), 351-358.

41. Fang, X.; Huhmann-Vincent, J.; Scott, B. L.; Kubas, G. J., H2 binding to and silane alcoholysis on an electrophilic Mn(I) fragment with tied-back phosphite ligands. X-ray structure of a Mn–CH2Cl2 complex. *J. Organomet. Chem.* **2000,** *609* (1), 95-103.

42. Weber, S.; Glavic, M.; Stöger, B.; Pittenauer, E.; Podewitz, M.; Veiros, L. F.; Kirchner, K., Manganese-Catalyzed Dehydrogenative Silylation of Alkenes Following Two Parallel Inner-Sphere Pathways. *J. Am. Chem. Soc.* **2021,** *143* (42), 17825-17832.

43. Bruneau-Voisine, A.; Wang, D.; Roisnel, T.; Darcel, C.; Sortais, J.-B., Hydrogenation of ketones with a Manganese PN^3P pincer pre-catalyst. *Catal. Commun.* **2017,** *92*, 1-4.

44. Kaithal, A.; Holscher, M.; Leitner, W., Catalytic Hydrogenation of Cyclic Carbonates using Manganese Complexes. *Angew. Chem. Int. Ed.* **2018,** *57* (41), 13449-13453.

45. J. A. Pope, S.; Reid, G., Phosphine, arsine and stibine complexes of Manganese(I) carbonyl halides: synthesis, multinuclear NMR spectroscopic studies, redox properties and crystal structures. *J. Chem. Soc, Dalton Trans.* **1999,** (10), 1615-1622.

46. Gandhamsetty, N.; Park, S.; Chang, S., Selective Silylative Reduction of Pyridines Leading to Structurally Diverse Azacyclic Compounds with the Formation of sp(3) C-Si Bonds. *J. Am. Chem. Soc.* **2015,** *137* (48), 15176-84.

47. Dai, Q.; Liu, L.; Qian, Y.; Li, W.; Zhang, J., Construction of P-Chiral Alkenylphosphine Oxides through Highly Chemo-, Regio-, and Enantioselective Hydrophosphinylation of Alkynes. *Angew. Chem., Int. Ed.* **2020,** *59* (46), 20645-20650.

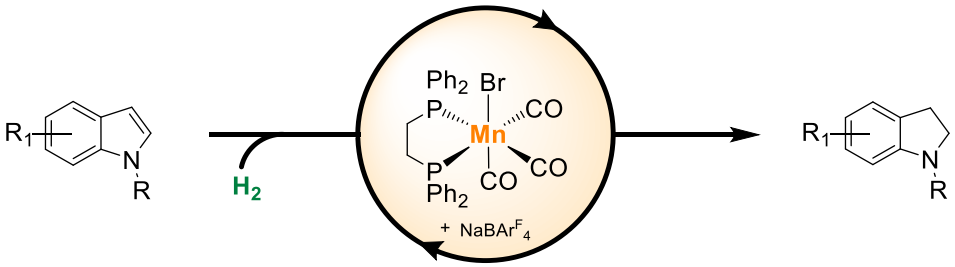
48. Liang, H.; Wang, L. J.; Ji, Y. X.; Wang, H.; Zhang, B., Selective Electrochemical Hydrolysis of Hydrosilanes to Silanols via Anodically Generated Silyl Cations. *Angew. Chem., Int. Ed.* **2021,** *60* (4), 1839-1844.

49. Bahr, S.; Brinkmann-Chen, S.; Garcia-Borras, M.; Roberts, J. M.; Katsoulis, D. E.; Houk, K. N.; Arnold, F. H., Selective Enzymatic Oxidation of Silanes to Silanols. *Angew. Chem., Int. Ed.* **2020,** *59* (36), 15507-15511.

50. Lickiss, P. D.; Lucas, R., Oxidation of sterically hindered organosilicon hydrides using potassium permanganate. *J. Organomet. Chem.* **1996**, *521* (1-2), 229-234.

51. Denmark, S. E.; Kallemeyn, J. M. Palladium-Catalyzed Silylation of Aryl Bromides Leading to Functionalized Aryldimethylsilanols. *Org. Lett.* **2003**, *5* (19), 3483–3486.

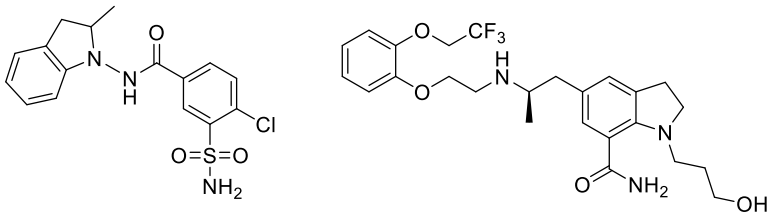
4. [Mn(CO)$_3$(dppe)]-Derivatives as Catalysts for the Hydrogenation of Indoles



Scheme 42: Graphical abstract of Chapter 4.

4.1. Introduction

Indolines hold considerable importance in medicinal chemistry due to their unique structural properties, which combine hydrophobicity with a non-coplanar hydrogen bonding site.[1] As a result, these properties give indolines remarkable biological activity, making them widely applied in medicinal chemistry (**Scheme 43**), both as marketed or investigated drug candidates.[1-4]



Indapamide

Silodosin

a)

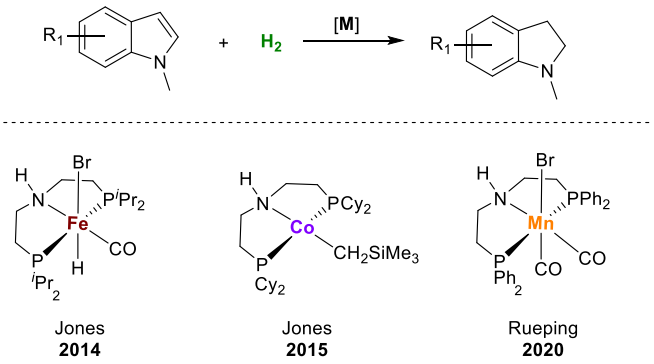
b)

Scheme 43: Selected examples of indolines as marketed drugs: a) Indapamide, a diuretic drug used in the treatment of hypertension.[5] b) Silodosin, used in the treatment of prostatic hyperplasia.[6]

It is possible to prepare indolines *via* a large variety of methods,[1, 7] including the Diels-Alder cyclization, multicomponent/multistep synthesis, or the hydrogenation of indoles. The latter option is particularly attractive because of its potential for late-stage functionalization on the indole moiety. However, the reaction presents several difficulties. As the activation of the indole ring is challenging due to its stabilization by resonance,[7] it often requires pristine protonation at the C-3 position with an external Brønsted acid.[8-10] In addition to that, when the nitrogen is unprotected, the hydrogenation leads to the formation of a cyclic secondary aniline, that can coordinate and interfere with the catalytic cycle and engage in other reactions. Due to these factors, the reported examples of indoles in this reaction are notably fewer compared to other N-based heterocycles. Additionally, the majority of these examples involves the utilization of noble metal

catalysts, such as Ru,[10, 12, 13] Rh,[14] Pd[8, 15-19] and Ir,[9, 20] with some instances catalyzing the asymmetric versions of the reaction.

When it comes to earth-abundant metals, there have been very few reported examples so far for the hydrogenation of indoles, and all of them utilize a MLCve backbone.[21] For instance, Jones and coworkers reported in 2014 and 2015 that Fe and Co pincer complexes were able to both hydrogenate and dehydrogenate various N-based heterocycles, including 2-methylindole, which was the only indole in their scope.[22, 23] Moving on to Mn instead, while there are already in the literature examples of commercial carbonyl complexes able to hydrogenate N-heterocycles,[24] the only example reported to date able to hydrogenate indoles is the one reported by Rueping and Co-workers.[25] They showed that the pincer complex Mn-MACHO could hydrogenate a scope of different indoles at 100 °C, using 50 bar of H_2 over 24 to 36 h (**Scheme 44**).



Scheme 44: Selected examples for the hydrogenation of indoles to indolines using an earth-abundant metal catalyst.

Given the limited number of examples available, it was decided to explore the feasibility of the reaction with a non-MLCve Mn catalyst. Building on the favorable catalytic performances showed in the previous chapters by [MnBr(CO)$_5$] in a base-free environment, the investigation was started from testing [MnBr(CO)$_5$] in the hydrogenation of indoles.

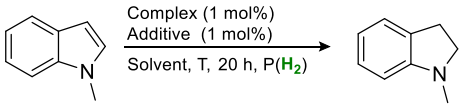
4.2. Objective

In the previous chapters the potential of Mn(I) carbonyl complexes with a coordinatively unsaturated site was demonstrated in the catalytic activation of Si–H bonds *via* σ-coordination. The development of a Mn(I) based catalyst able to activate H_2 *via* the same mechanism for the challenging hydrogenation of indoles, is the main objective of this work. In particular, due to the good performances obtained in a base-free environment, the newly developed catalytic system should be suitable to hydrogenate substrates that are normally hydrogenated under acidic and/or base-free conditions like indoles. One of the secondary objectives of this chapter is to demonstrate that non-MLCve catalysts can perform the reaction under milder conditions and with enhanced chemoselectivity than already existing Mn(I) catalysts.

4.3. Initial Screening and Optimization

We began our investigation screening several manganese complexes in the hydrogenation of 1-methylindole in cyclohexane (**Table 7**). [MnBr(CO)$_5$] and [Mn$_2$(CO)$_{10}$] showed no activity in the reaction at 100 °C and 50 bar of H_2. Inspired by the work of Kubas (Section 1.2),[26] [MnBr(CO)$_5$] was tested for catalytic activity together with NaBAr$^F_4$ as an activator, in an attempt to abstract the bromide from the coordination sphere of the manganese complex. Even in this case, [MnBr(CO)$_5$] showed no catalytic activity. However, the complex *fac*-[MnBr(CO)$_3$(dppe)] (**Mn-6**), more similar to the one reported by Kubas, yielded an almost quantitative amount of 1-methylindoline **3a** when employed as a catalyst together with an equimolar amount of NaBAr$^F_4$ as activator (**Table 7**). **Mn-6** was then also tested in the presence of other activators, commonly used for MLCve Mn-complexes.[25] However, the use of a base such as KO^{t}Bu or Et$_3$N poisoned the catalytic activity. As a result, only the formation of small amounts of the respective Mn-H (in the case of Et$_3$N) was observed, without any conversion of the starting material. To support the hypothesis that NaBAr$^F_4$ acts as a bromide scavenger, AgSbF$_6$ was also tested as an activator for **Mn-6**. This resulted in the corresponding 1-methylindoline being obtained in 26% yield. Several reaction conditions were tested, and it was possible to reduce the temperature and the hydrogen pressure of the reaction to 60 °C and 20 bar without significant losses in yield. At 40 °C however, the yield and conversion dropped to only 40%. Different solvents were screened at 40 °C in an attempt to observe improvement in the conversion: the use of coordinating solvents such as methanol, DMSO, or CH$_3$CN resulted in no conversion of the starting material, whereas the use of solvents of more moderate or low coordination strength like toluene, THF and CHCl$_3$ only produced 1-methylindoline in a yield lower than 5%.

Table 7: Testing for the catalytic activity of different manganese complexes in the hydrogenation of 1-methylindole to 1-methylindoline and subsequent optimization of the reaction. ^{1}H-NMR yields were determined with respect to 1,3,5-trimethoxybenzene as internal standard. [a] = 2.5 equiv. respective to the Mn complex.

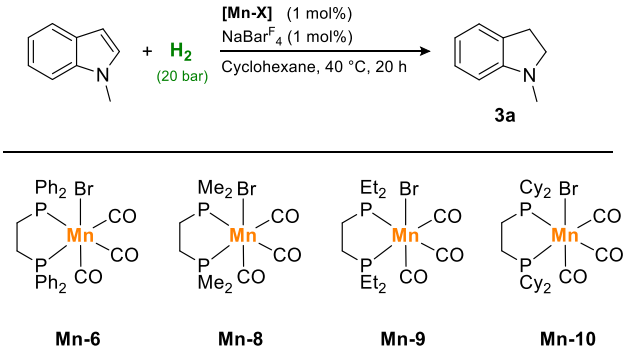


3a

Solvent	Temperature (°C)	H_2 pressure (bar)	Complex (1 mol%)	Additive (1 mol%)	NMR Yield (%)
Cyclohexane	100	50	$[MnBr(CO)_5]$	–	0
Cyclohexane	100	50	$[Mn_2(CO)_{10}]$	–	0
Cyclohexane	100	50	$[MnBr(CO)_5]$	$NaBAr^F_4$	0
Cyclohexane	100	50	**Mn-6**	–	0
Cyclohexane	100	50	**Mn-6**	$NaBAr^F_4$	95
Cyclohexane	100	50	**Mn-6**	$AgSbF_6$	27
Cyclohexane	100	50	**Mn-6**	KO^tBu[a]	0
Cyclohexane	100	50	**Mn-6**	Et_3N[a]	0
Toluene	100	50	**Mn-6**	$NaBAr^F_4$	95
Cyclohexane	**60**	**20**	**Mn-6**	**$NaBAr^F_4$**	**94**
Cyclohexane	40	20	**Mn-6**	$NaBAr^F_4$	40
Toluene	40	20	**Mn-6**	$NaBAr^F_4$	6
THF	40	20	**Mn-6**	$NaBAr^F_4$	trace
$CHCl_3$	40	20	**Mn-6**	$NaBAr^F_4$	trace
CH_3CN	40	20	**Mn-6**	$NaBAr^F_4$	0
DMSO	40	20	**Mn-6**	$NaBAr^F_4$	0
MeOH	40	20	**Mn-6**	$NaBAr^F_4$	0

In order to investigate if the stereo- and electronic- properties of the phosphine would significantly influence the catalytic activity, other Mn(I) complexes bearing variously substituted 1,2-bis(phosphino)ethane scaffolds were then tested out as catalyst. For comparison, all the complexes were tested at a loading of 1 mol% in the presence of equimolar $NaBAr^F_4$ in cyclohexane (**Table 8**).

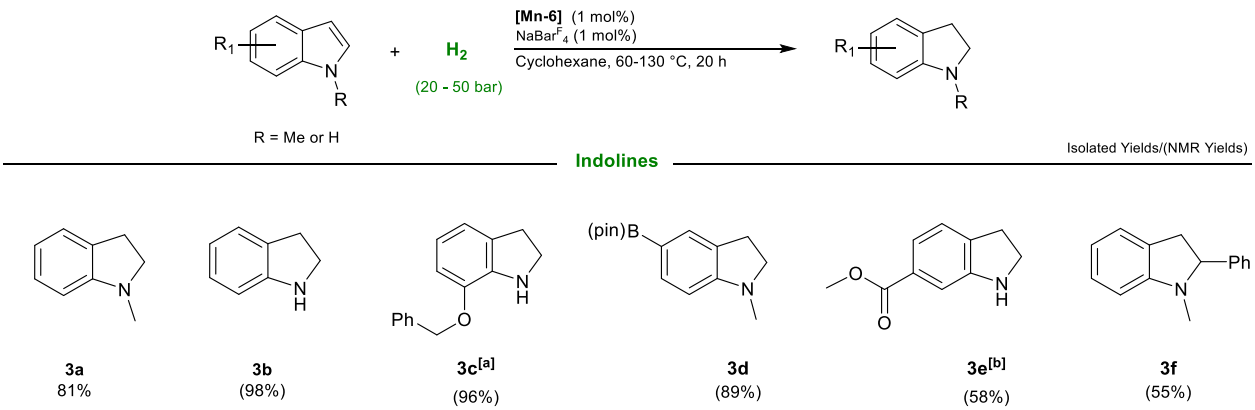
Table 8: Study of the influence of the electro-steric properties of the phosphine on the catalytic performances.



Complex	NMR Yield (3a) (%)
Mn-6	**40**
Mn-8	0
Mn-9	12
Mn-10	45

The analysis revealed that the complexes bearing phosphines with higher electron-donating abilities, such as **Mn-8** or **Mn-9,** exhibited respectively no or lower conversion of the starting material. Conversely, the complex **Mn-10**, coordinating the bulky 1,2-bis(dicyclohexylphosphino)ethane, showed improved performances. However, the similar results obtained by **Mn-6** and **Mn-10**, combined with the significantly lower cost and widespread availability of the dppe ligand, led to the selection of **Mn-6** as the complex of choice for studying the reaction on a range of different indoles.

4.4. Preliminary Reaction Scope

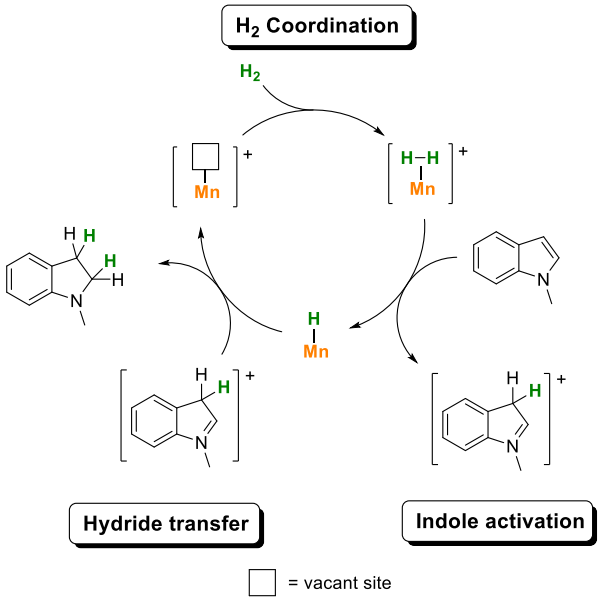


Scheme 45: Scope of the hydrogenation of different indoles to their respective indolines. ^{1}H-NMR yields were determined with respect to 1,3,5-trimethoxybenzene as internal standard. Deviations from the standard conditions are indicated as [a]: T = 100 °C, P(H_2) = 50 bar; [b]: [Mn-6] = $NaBAr^F_4$ = 2 mol%, T = 130 °C and P(H_2) = 50 bar.

A small set of different indoles was screened in the optimized reaction conditions. At 60 °C and 20 bar of H_2, 1-methylindole was reduced to 1-methylindoline and isolated in 81% yield. The absence of a substituent on the nitrogen did not hinder the reaction, since the unprotected indole was successfully reduced to the corresponding indoline in 98% yield. The presence of a boronic acid pinacol ester substituent did also not impede the reaction, allowing for the reduction of the indole to the corresponding indoline in 89% NMR yield and still holding a potential site for future functionalization. The presence of a benzyloxy substituent instead, somehow hindered the reactivity of the indole, requiring 100 °C and 50 bar of H_2 for it to be reduced to the corresponding indoline in 96% of yield. The most drastic reaction conditions were necessary, however, in the presence of an ester functionality, requiring 130 °C, 50 bar of H_2 and twice the amount of catalyst to be converted to the corresponding indoline in a yield above 50%. Instead, the incorporation of a phenyl group at the C-2 position only slightly hindered the reactivity, resulting in a yield of 55% under standard conditions.

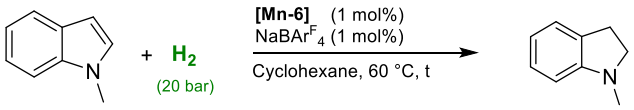
4.5. Mechanistic Investigation

To assist the reader, a preliminary mechanistic scheme will be provided below, helping to follow the subsequent experiments. Based on the initial data, it is plausible to envision that **Mn-6** is activated *in situ* from NaBAr$^F_4$ through bromide abstraction. This activation generates an unsaturated complex from **Mn-6**, able to coordinate H_2 *via* σ-coordination. The binding of H_2 affords a manganese cationic dihydrogen complex, which can subsequently protonate the indole. The protonated indole is then able to react with the resulting manganese hydride, leading to the formation of the first batch of product and regenerating the unsaturated complex that can re-enter the catalytic cycle.



Scheme 46: Preliminary mechanistic scheme.

4.5.1. Yield-time profile



Scheme 47: Various reactions on 1-methylindole analyzed at different time intervals to obtain a yield-time profile of the reaction.

Various reactions on 1-methylindole as model substrate have been performed and analyzed *via* quantitative ^{1}H-NMR at different time intervals. The results of the yield-time profile study are reported in **Figure 17**. Within the first 30 minutes, the yield of 1-methylindoline was below 5%, suggesting the presence of an induction period. This time is likely necessary for the reaction between NaBAr$^F_4$ and the complex **Mn-6** to take place.

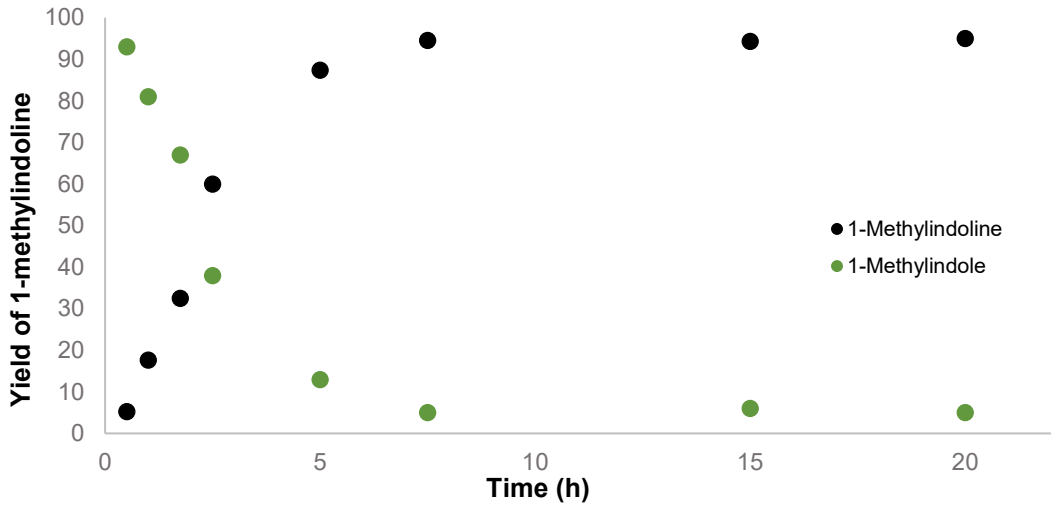


Figure 17: Conversion and Yield-time profile for the hydrogenation of 1-methylindole to 1-methylindoline.

In fact, after a total reaction time of 1 h, the amount of 1-methylindoline in solution notably increased to 18%, reaching 67% after only 2.5 h, 87% after 5 h, and 95% after 7.5 h. When repeating the same investigation using D_2 instead of H_2, it was observed that after the first 30 minutes the yield in 1-methylindoline was also below 5%. This value, very similar to the one obtained with H_2, supports the hypothesis of an induction period. In fact, the differences in rate became way more significant for the following data points. After 2.5 h, the yield in 1-methylindoline was only 21% when running the reaction under D_2 pressure, as opposed to the 67% observed in the case of H_2. Moreover, a time of 7.5 h was necessary to reach a conversion above 50% (**Figure 18**).

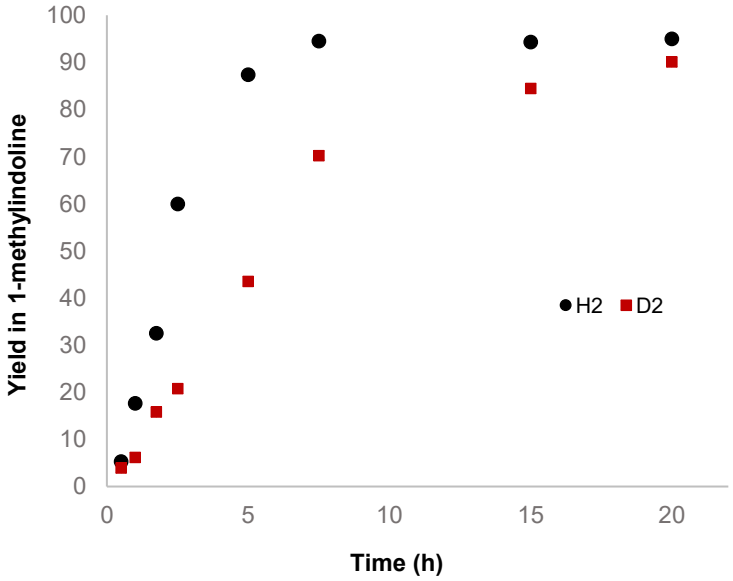


Figure 18: Yield-time profile of the hydrogenation of 1-methylindole to 1-methylindoline respectively using H_2 (in black) and D_2 (in red).

To better quantify the KIE, the first points were analyzed with the initial rates method, showing an apparent initial rate 3.1 times slower for the reaction with D_2 when compared to the one with H_2, leading to an apparent KIE of $k_H/k_D \approx 3.1$ (**Figure 19**). These results suggest that the cleavage of the H_2 bond is involved in the rate determining step.

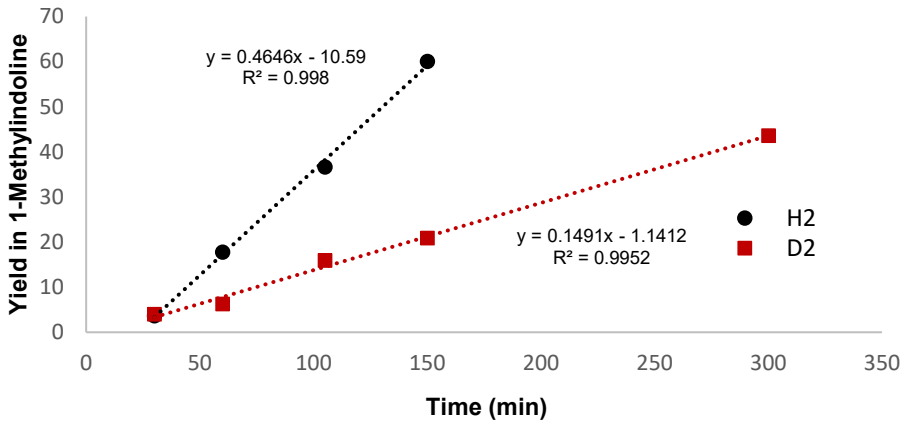
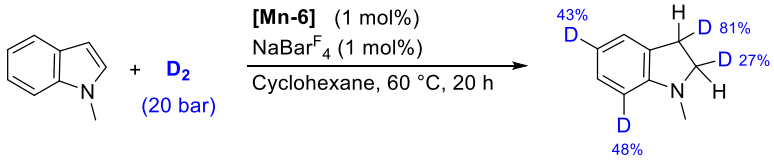


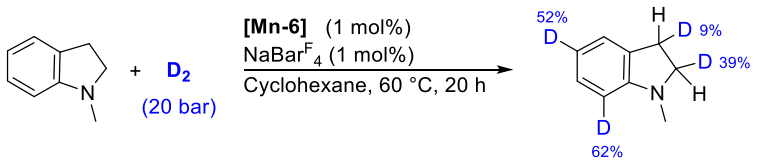
Figure 19: Relative initial rates of the hydrogenation of 1-methylindole to 1-methylindoline respectively using H_2 (in black) and D_2 (in red).

4.5.2. Deuteration analysis



Scheme 48: Hydrogenation reaction of 1-methylindole to 1-methylindoline using D_2 instead of H_2 in the presence of **Mn-6** and NaBAr$^F_4$.

After a reaction with D_2 was run for 20 hours, the deuteration pattern of the corresponding 1-methylindoline was analyzed *via* ^{1}H- and ^{2}H-NMR. The obtained indoline showed deuteration at both the C-2 and C-3 of respectively 27% and 81%. Surprisingly, the indoline was also partially deuterated at the positions C-5 and C-7, respectively in 43% and 48% yield (**Scheme 48**). To figure out whether the scrambling is a direct consequence of the hydrogenation or not, 1-methylindoline was placed in an autoclave and subjected to 20 bar of D_2 under reaction conditions (**Scheme 49**).



Scheme 49: Reaction between 1-Methylindoline and D_2 in the presence of 1 mol% of **Mn-6** and NaBAr$^F_4$.

The resulting indoline showed a similar H-D scrambling also in the same positions (**Figure 20**), suggesting that the deuteration can arise from a reaction mechanism parallel to the indole hydrogenation (like, for example, a *"hydrogenation-dehydrogenation"* mechanism).

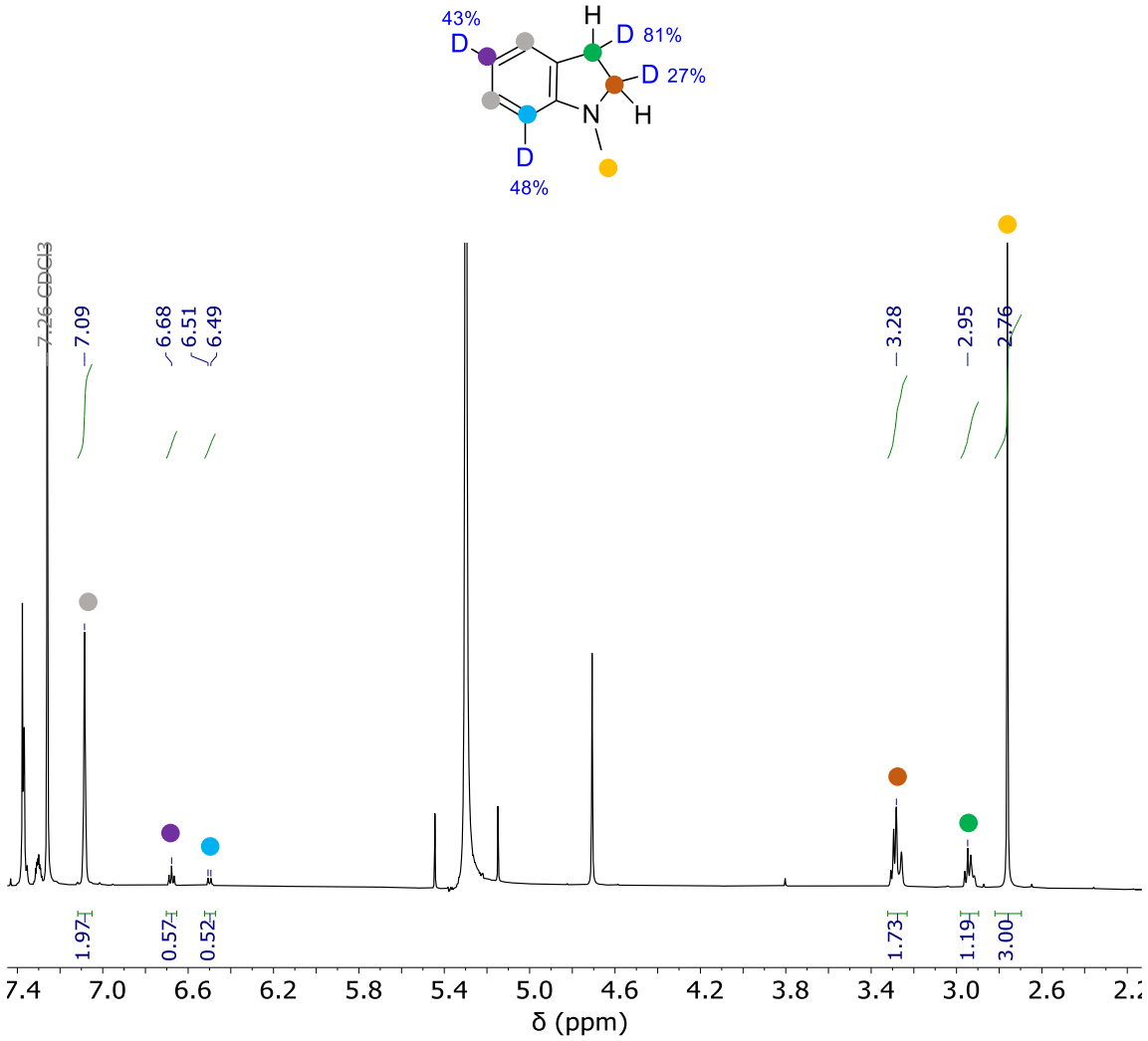
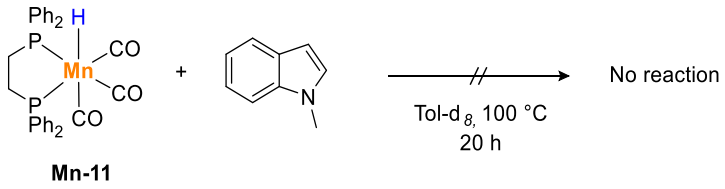


Figure 20: ^{1}H-NMR spectrum of the crude reaction mixture reported in Scheme 48. Benzyl alcohol has been used as internal standard.

4.5.3. Stoichiometric reactions



Mn-11

Scheme 50: Stoichiometric reaction between the complex **Mn-11** and 1-methylindole.

In order to shed light on the reaction mechanism, the complex **Mn-13**, *fac*-[Mn(CO)$_3$(dppe)H] was tested out in a stoichiometric reaction with 1-methylindole, in toluene-d$_8$ at 100 °C. No reaction occurred between 1-methylindole and **Mn-11** even after 20 h (**Figure 21**). This finding indicates that the indole does not undergo direct reduction by the Mn-H, which aligns with some previous literature reports, where the presence of a Brønsted acid in the reaction is essential to activate the electron-rich aromatic ring of the indole.[8-10]

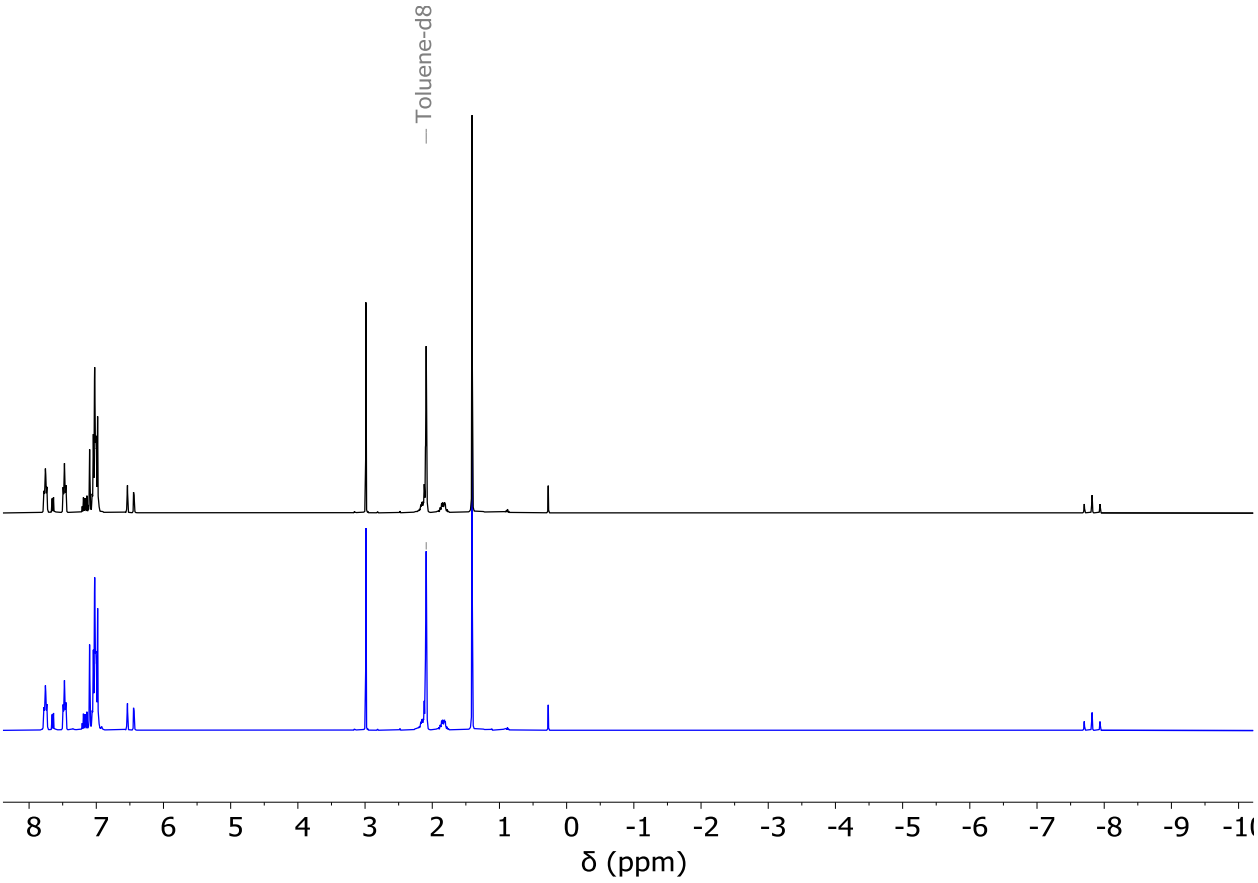
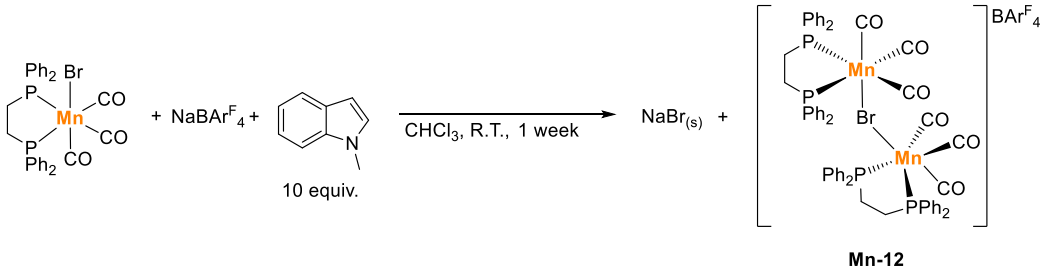


Figure 21: ^{1}H-NMR of the reaction reported in Scheme 50, respectively right after mixing (blue, below) and after 20 h at 100 °C (black, above).

In order to rule out the possibility that the coordination of the indole to the catalyst could be involved in the activation of the substrate, a stoichiometric reaction between **Mn-7** and NaBAr$^F_4$ was run in the presence of 10 equiv. of 1-methylindole (**Scheme 51**). After 1 week at R.T., it was possible to crystallize the dinuclear species **Mn-14** from the crude reaction mixture.



Scheme 51: Reaction between **Mn-6** and NaBAr$^F_4$ in the presence of 10 equiv. of 1-Methylindole.

The structure confirms the ability of NaBAr$^F_4$ to abstract the bromide from the coordination sphere of the starting complex. The generated highly unstable mononuclear cationic 16 electrons complex can then be stabilized forming a bridging dinuclear complex *via* the coordination of a μ-bromido ligand, preferring it over the excess of indole present in solution. Dinuclear structures such as **Mn-12** are likely to be *off-cycle species* of the catalytic cycle.

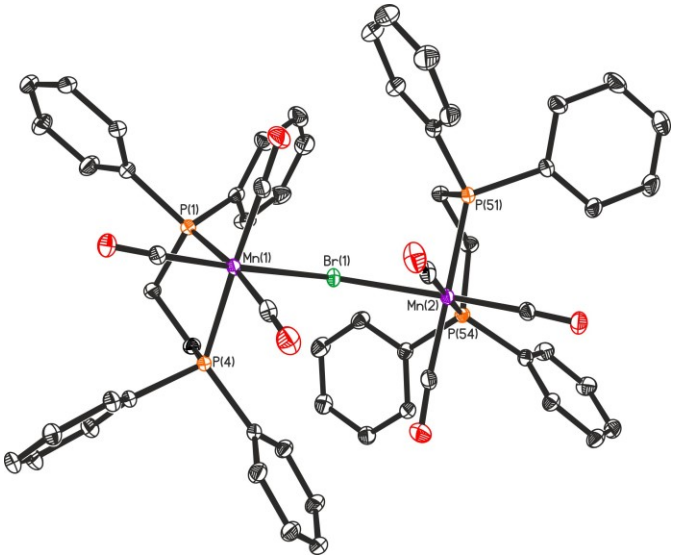
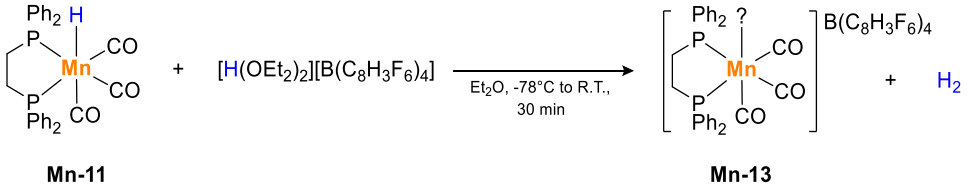


Figure 22: Cationic dinuclear complex [Mn$_2$(CO)$_6$(dppe)$_2$-μ-Br]$^+$ with [BAr$^F_4$]$^-$ as the counterion. The complex was crystallized from the reaction in Scheme 51. The same structure was obtained upon reaction of **Mn-6** with NaBar$^F_4$ in cyclohexane, at 40 °C and with 20 bar of H$_2$.

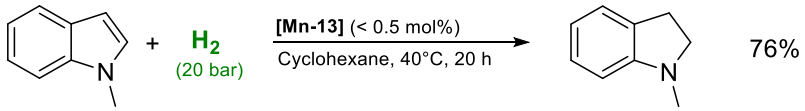
4.5.4. Towards a candidate for the active species



Mn-11 **Mn-13**

Scheme 52: Reaction between the complex **Mn-11** and the acid [H(OEt$_2$)$_2$][B(C$_8$H$_3$F$_6$)$_4$].

In an attempt to generate a mononuclear cationic complex *via* a different synthetic pathway and test it out in catalysis, the hydride complex *fac*-[Mn(CO)$_3$(dppe)H] was reacted with Brookhart's acid ([H(OEt$_2$)$_2$][B(C$_8$H$_3$F$_6$)$_4$]) in Et$_2$O at -78 °C (**Scheme 52**). The color of the solution turned immediately from pale to intense yellow, suggesting the protonation of **Mn-11** and formation of the corresponding Mn(I) complex coordinating H_2 (as already observed in the literature by Kubas[26,27] and Jones;[28] Section 1.2). Once the solution was removed from the -78 °C bath, it was possible to observe intense bubbling before reaching R.T.; the solvent was evaporated under reduced pressure to afford a yellow oil, that was tested for catalytic activity at 40 °C and 20 bar of H_2 pressure, the same conditions used to compare the catalytic activity of differently substituted Mn(I) bis-(phosphino)ethane tricarbonyl complexes in **Table 8**.



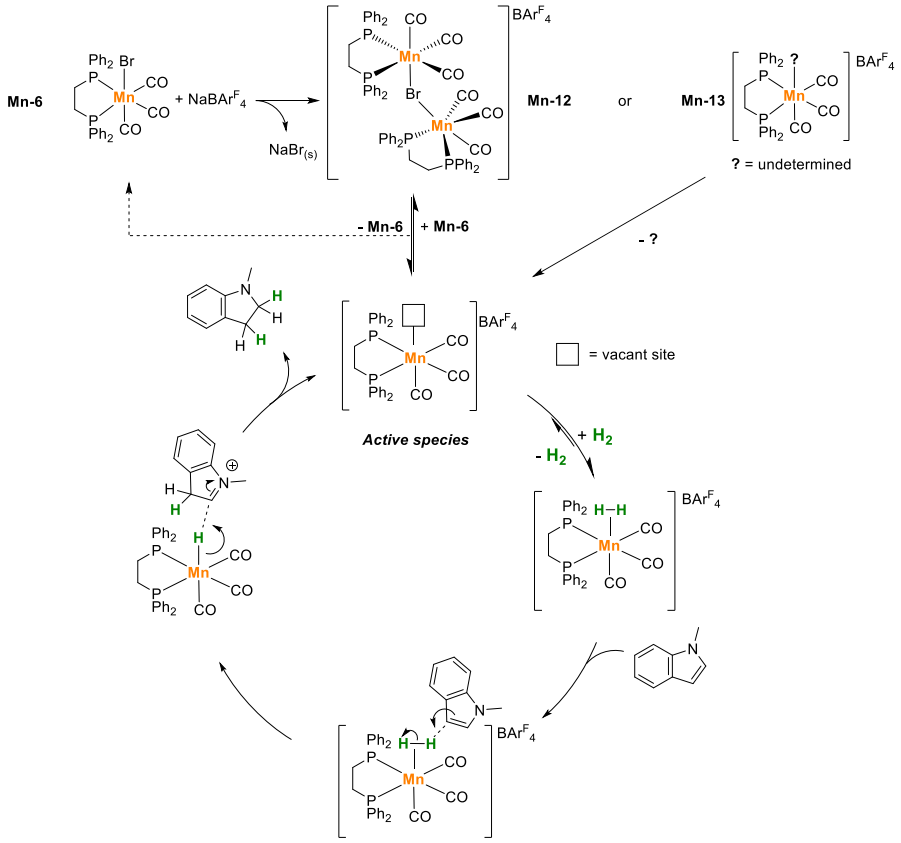
3a

The presence of maximum catalyst loading* of **Mn-13** of 0.5 mol% was enough to convert 1-methylindole to 1-methylindoline in 76% yield, without any further *in situ* activator. This result, compared with the ones obtained in **Table 8**, makes **Mn-13** the most active catalyst among the ones screened. In an attempt to gain more information on the coordination environment of **Mn-13**, the complex was analyzed *via* ^{1}H- and ^{31}P{^{1}H}-NMR. The ^{31}P{^{1}H}-NMR shows only one signal at 75.23 ppm; however, it was not possible to fully elucidate the structure of **Mn-13** yet, and further characterization work is underway.

* = The precise value relies on the exact formula weight of the complex, which is currently unknown. The maximum catalyst loading will be achieved with the lowest possible formula weight, which corresponds to the complex solely stabilized by agostic interactions and with no additional stabilizing ligand.

4.6. Suggested Mechanism

Based on the data collected in this chapter it is possible to suggest a reaction mechanism mediated by a coordinatively unsaturated complex (**Scheme 53**). Initially, the complex **Mn-6** is activated by NaBAr$^F_4$ *via* bromide abstraction to generate **Mn-12**, likely acting as an *off-cycle species* of the catalytic cycle. Under H_2 pressure, a mononuclear complex can coordinate H_2 to form the respective cationic dihydrogen complex that is able to protonate the indole at the C-3 and generate the stabilized iminium ion. The now activated iminium ion can finally be reduced by the resulting *fac*-[Mn(CO)$_3$(dppe)H] that, transferring the hydride, regenerates a monomeric coordinatively unsaturated cationic complex that can coordinate H_2 and continue with the catalytic cycle. A complex which is likely more similar to the suggested active species could be obtained by pre-activation of the complex **Mn-11**, *fac*-[Mn(CO)$_3$(dppe)H], with [H(OEt$_2$)$_2$][B(C$_8$H$_3$F$_6$)$_4$]. The resulting complex **Mn-13**, likely coordinatively unsaturated, is able to carry on the catalytic cycle without any further additive and allowing for even milder reaction conditions.



Scheme 53: Suggested reaction mechanism for the hydrogenation of indoles.

The proposed mechanism seems to align with the observed KIE, in which the cleavage of H_2 is involved in the rate determining step of the reaction. A reasonable speculation for the rate determining step would be

the complete cleavage of the H–H bond at the Mn center in the process of protonating of the indole at the C3, involving the loss of the aromaticity of the five membered ring.

4.7. Conclusions and Outlook

In this final chapter, a catalytic system based on a Mn(I) complex stabilized by the cost-effective ligand dppe was successfully developed for the hydrogenation of indoles. The reaction can be conducted under milder conditions than those employed by the only other complex of Mn(I) reported so far for this reaction. This protocol has, so far, enabled the reduction of a small scope of six indoles variously substituted, demonstrating tolerance to functional groups such as esters, boronic pinacol esters and ethers. It could be demonstrated that the complex *fac*-[MnBr(CO)$_3$(dppe)], which was used as a precatalyst in the reaction, can be activated solely in the presence of a bromide abstractor such as NaBAr$^F_4$. The role of the activator in this case is to generate a coordinatively unsaturated species, likely carrying on the catalytic cycle as for the other chapters. The presence of Mn(I) unsaturated complexes in the reaction mixture is supported by the single crystal obtained of the complex [Mn$_2$Br(CO)$_6$(dppe)$_2$]BAr$^F_4$ from the reaction of *fac*-[MnBr(CO)$_3$(dppe)] with NaBAr$^F_4$.

Catalytic activity in the hydrogenation was also observed by generating a free coordination site on the "Mn(CO)$_3$(dppe)" core *via* reacting *fac*-[Mn(CO)$_3$(dppe)H] with Brookhart's acid. The reaction led to the complex **Mn-13**, which did not require any activator and whose catalytic activity outperformed the one of the complexes generated *in situ*. However, its structure was not fully elucidated yet.

This finding paves the way for the investigation of the catalytic potential of cationic Mn(I) unsaturated complexes for hydrogenation reactions under neutral or acidic conditions, an area that has been relatively underdeveloped in the literature. Additionally, the incorporation of a chelating phosphine in this catalytic system provides a promising avenue for adjusting the electro-steric properties of the catalyst, holding the potential for developing an asymmetric version of this reaction, facilitated by the wide array of commercially available chiral chelating phosphines.

4.8. Experimental Procedure and Characterization Data

To enhance the readability and comprehension of the experimental procedures for this chapter, a detailed list of all the devices employed for measurements is provided in the Appendix, Section 6.1.

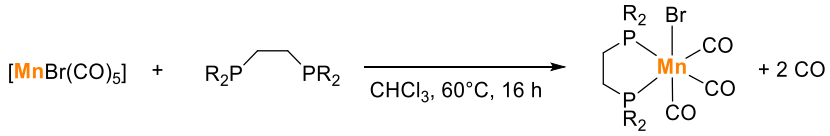
4.8.1. General considerations

Unless otherwise stated, all air-sensitive experiments were conducted under an Ar atmosphere using standard Schlenk techniques or an MBraun inert-gas glovebox. Solvents for air- and moisture-sensitive experiments were purified through a MBraun-SPS-7 system or dried over activated molecular sieves (3 or 4Å) and degassed according to standard laboratory procedure. The indoles used as starting materials and [$Mn_2(CO)_{10}$] were purchased from Sigma Aldrich, abcr, Alfa Aesar, or TCI Europe and used as received. The phosphines for the synthesis of the Mn complexes were purchased from abcr and used as received. [$MnBr(CO)_5$] has been used as received from Thermo Fischer Scientific for the synthesis of the complexes **Mn-6**, **Mn-8**, **Mn-9** and **Mn-10** according to the procedure described below. The chemical shifts (δ) are given in ppm (parts per million) relative to TMS and were assigned taking as a reference the residual solvent signals ($CDCl_3$: $\delta^1H = \delta^2H = 7.26$ ppm, $\delta_C = 77.16$ ppm; DMSO-d_6: $\delta^1H = \delta^2H = 2.50$ ppm, $\delta_C = 39.52$ ppm; Toluene-d_8: $\delta^1H = \delta^2H = 2.08$ ppm, $\delta_C = 20.43$ ppm; C_6D_6: $\delta^1H = \delta^2H = 7.16$ ppm, $\delta_C = 128.06$ ppm) ^{13}C spectra were generally acquired with broadband proton decoupling. The chemical shift (δ) for ^{31}P-NMR spectra is given in ppm with respect to H_3PO_4 (85% in H_2O) as a reference ($\delta^{31}P = 0$ ppm).The peak patterns are indicated as follows: s = singlet; d = doublet; t = triplet; m = multiplet; dd = doublet of doublets; td = triplet of doublets; br = broad. The IR data are given in wavenumbers (cm^{-1}), and the intensity of the bands is indicated as follows: st = strong; me = medium; w = weak.

4.8.2. Synthesis of the non-commercial manganese complexes

All the manganese complexes **Mn-6**, **Mn-8**, **Mn-9** and **Mn-10** were synthetized according to a slightly modified literature procedure.[29] [$MnBr(CO)_5$] and the respective phosphine were weighed in a Schlenk tube equipped with a magnetic stirrer inside the glovebox in a 1:1 stoichiometry. $CHCl_3$ was added (the necessary amount to reach a 0.05 M concentration in [$MnBr(CO)_5$] and the respective phosphine), the Schlenk tube was closed, taken outside the glovebox, covered in Al foil and placed in a pre-heated oil bath at 60 °C for 16 h. The Schlenk tube was cooled down to R.T., the solvent was removed under reduced pressure and the residual solid was washed with pentane 3 times. Pentane was then removed under reduced pressure, yielding a dry yellow powder. Complexes **Mn-8**, **Mn-9** and **Mn-10** were further purified dissolving the complexes in boiling cyclohexane and separating the solution of the complex from inorganic residues *via* cannula filtration.

Table 9: Summary of the conditions used to prepare and isolate the complexes **Mn-6**, **Mn-8**, **Mn-9** and **Mn-10** with the respective purification technique and yield.



Complex	R =	Recrystallized	Yield (%)
Mn-6	Ph	No	98
Mn-8	Me	Yes	43
Mn-9	Et	Yes	39
Mn-10	Cy	Yes	36

4.8.3. Handling of the autoclaves

Experiments with pressurized H_2 must be carried out only with appropriate equipment and under rigorous safety precautions. All high-pressure reactions were carried out in stainless steel finger autoclaves manufactured in-house (V = 20 mL) equipped with a glass inlet **Figure 23**. The experiments performed in this chapter are *highly sensitive* to moisture and oxygen. In order to exclude them, the following precautions while handling the autoclaves have been taken:

1- Each autoclave and inlet has been oven dried (respectively at 60 °C and 120 °C) before being introduced in the glovebox.
2- Once taken out from the glovebox, the hand tight autoclaves have been *rapidly* closed with a wrench
3- The atmosphere inside the arm of the autoclave was exchanged (connecting it to the pressure station) *via* 5 cycles Vacuum/Ar before pressurization.

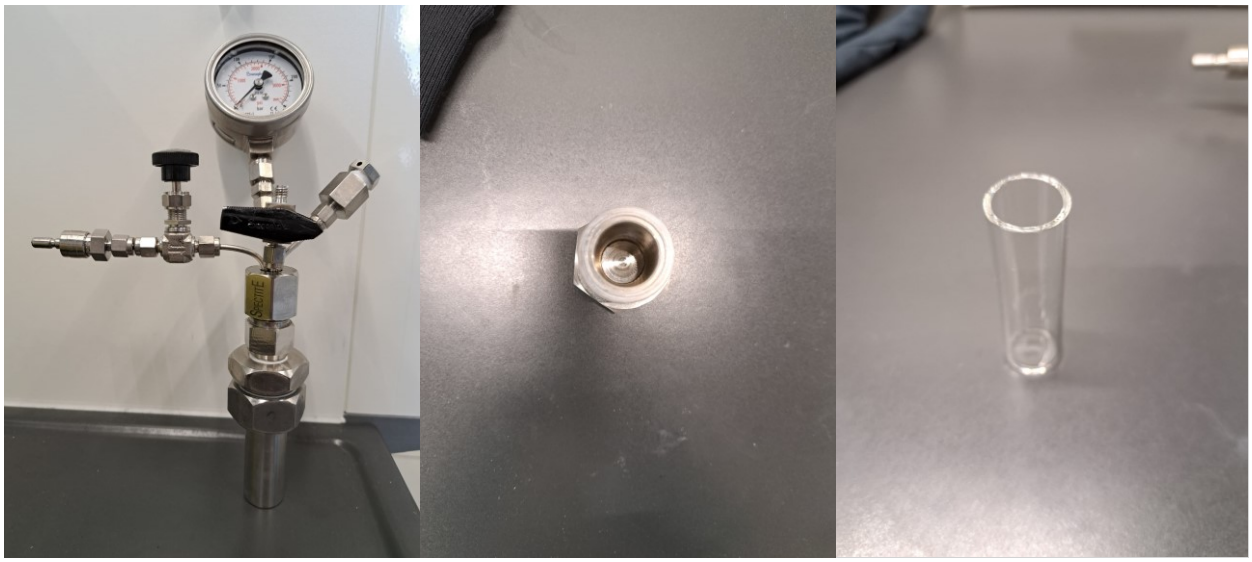


Figure 23: From left to right; Picture of an assembled stainless steel finger autoclave used for the catalytic reactions. Bottom part of the autoclave where the glass inlet is going to be inserted. Glass inlet used as reaction vessel.

4.8.4.General procedure for the optimization

The chosen manganese complex (5 x 10^{-3} mmol), the corresponding additive (5 x 10^{-3} mmol – 0.015 mmol) and 1-methylindole (65.6 mg, 0.5 mmol) were weighed in a glass autoclave inlet inside the glovebox. The inlet was added with a magnetic stirrer and with 2 mL of the solvent of choice. The inlet was placed in an autoclave closed “hand tight”. The autoclave was brought outside the glovebox, fully closed with a wrench and pressurized with the desired H_2 pressure. The autoclave was placed in a pre-heated aluminum cone at the desired temperature for 20 hours, and afterwards put in a water bath to cool down at R.T. for 30 min. The autoclave was then depressurized, the inlet was taken out from the autoclave and the crude reaction mixture was transferred to a 7 mL vial already containing 28.0 mg of 1,3,5-trimethoxybenzene, used as

internal NMR standard. The inlet was washed with DCM (4 x 0.5 mL), and a sample of the crude reaction mixture was transferred to an oven dried NMR tube and added with 0.5 mL of $CDCl_3$. The peaks used to quantify the amount of 1-methylindoline formed in the reaction were the peak at 6.09 ppm for trimethoxybenzene (3H) and 2.76 ppm for 1-methylindoline (3H).

4.8.5. General procedure for the substrate scope

Mn-6 (3.1 mg, 5 x 10^{-3} mmol), $NaBAr^F_4$ (4.4 mg, 5 x 10^{-3} mmol) and the indole of choice (0.5 mmol, or 0.25 mmol for **3e**) were weighed in a glass autoclave inlet inside the glovebox. The inlet was added with a magnetic stirrer and 2 mL of cyclohexane. The autoclave was brought outside the glovebox, fully closed with a wrench and pressurized with the desired H_2 pressure. The autoclave was placed in a pre-heated aluminum cone at the desired temperature for 20 h, and afterwards put in a water bath to cool down at R.T. for 30 minutes. The autoclave was then depressurized and the inlet was taken out from the autoclave. For the NMR Yields, the crude reaction mixture was transferred to a 7 mL vial already containing 28.0 mg of 1,3,5-trimethoxybenzene, used as internal NMR standard. The inlet was washed with DCM (4 x 0.5 mL), and a sample of the crude reaction mixture was transferred to an oven dried NMR tube and added with 0.5 mL of $CDCl_3$. The peaks used to quantify the amount of 1-methylindoline formed in the reaction were the peak at 6.09 ppm for trimethoxybenzene (3H), and the characteristic signals between 3.50-2.50 ppm for the corresponding indoline. For the isolated yields, the crude reaction mixture was transferred directly from the inlet to a round bottom flask, the inlet was washed with DCM (4 x 0.5 mL) and the solvent was removed under reduced pressure. The concentrated crude reaction mixture was then purified *via* column chromatography.

4.8.6. General procedure for the yield-time profile using H_2 or D_2

Mn-6 (3.1 mg, 5 x 10^{-3} mmol), $NaBAr^F_4$ (4.4 mg, 5 x 10^{-3} mmol) and 1-methylindole (65.6 mg, 0.5 mmol) were weighed in a glass autoclave inlet inside the glovebox. The inlet was added with a magnetic stirrer and with 2 mL of cyclohexane. The autoclave was brought outside the glovebox, fully closed with a wrench and pressurized with 20 bar of H_2 (or D_2). The autoclave was placed in a pre-heated aluminum cone at the 60 °C for the desired time, and afterwards put in a water bath to cool down at R.T. for 15 min. The autoclave was then depressurized, the inlet was taken out from the autoclave and the crude reaction mixture was transferred to a 7 mL vial already containing either 28.0 mg of 1,3,5-trimethoxybenzene, or 25.0 mg of benzyl alcohol (in the case of the reactions performed with D_2), used as internal NMR standard. The inlet was washed with 4 x 0.5 mL of DCM, and a sample of the crude reaction mixture was transferred to an oven dried NMR tube and added with 0.5 mL of $CDCl_3$. The peaks used to quantify the amount of 1-methylindoline formed in the reaction were the peak at 6.09 ppm for trimethoxybenzene (3H), 4.71 ppm for benzyl alcohol (2H, in the case of the reaction with D_2), and 2.76 ppm for 1-methylindoline (3H) in both cases.

4.8.7. Synthesis of complex *fac*-[Mn(CO)$_3$(dppe)H]

[$Mn_2(CO)_{10}$] (90.8 mg, 0.25 mmol) and 1,2-bis(diphenylphosphino)ethane (205.1 mg, 0.51 mmol) were weighed in a glass autoclave inlet inside the glovebox. The inlet was added with a magnetic stirrer and with 5 mL of the cyclohexane. The autoclave was brought outside the glovebox, fully closed with a wrench and pressurized with 100 bar of H_2. The autoclave was placed in a pre-heated aluminum cone at the 125 °C for one week, and afterwards put in a water bath to cool down at R.T. for 30 min. The autoclave was then depressurized, the inlet quickly removed from the autoclave and placed inside a 25 mL Schlenk tube (under inert gas) in Ar flow. The inlet was then introduced in the glovebox, and the solution from the inlet was transferred to a 25 mL Schlenk tube. The solution was added with 5 mL of pentane, and a colorless solid started to precipitate from the solution in the Schlenk tube. The solid was decanted, the supernatant solution was poured out and the solid was washed with pentane (3 x 5 mL) and Et_2O (1 x 3 mL). The solvent was evaporated under reduced pressure, affording 116.7 mg (0.22 mmol) of *fac*-[Mn(CO)$_3$(dppe)H] (43% of yield).

4.8.8. Procedure for the reaction between *fac*-[Mn(CO)$_3$(dppe)H] and 1-methylindole

fac-[Mn(CO)$_3$(dppe)H] (6.5 mg, 12,1 μmol) and 1-methylindole (1.8 mg, 13.7 μmol) were weighed in a vial inside the glovebox. The vial was added with 0.5 mL of toluene-d_8, and the solution was transferred to an oven dried (120 °C) J-Young tube. A ^{1}H-NMR was recorded directly after mixing. The J-Young tube was then covered in aluminum foil and placed in an oil bath pre-heated to at 100 °C for 20 h. The J-young tube was removed from the oil bath, cooled down to R.T. and dried from the oil. A ^{1}H-NMR was recorded again for comparison.

4.8.9. Procedure for the reaction between *fac*-[MnBr(CO)$_3$(dppe)] and NaBAr$^F_4$

fac-[MnBr(CO)$_3$(dppe)] (6.1 mg, 0.010 mmol), NaBAr$^F_4$ (8.9 mg, 0.010 mmol) and 1-methylindole (13.9 mg, 0.11 mmol) were weighed in a 4 mL vial equipped with a screw cap and a magnetic stirrer inside the glovebox. The vial was added with 0.75 mL of $CHCl_3$, covered in aluminum foil and left to stir at room temperature for one week inside the glovebox. After one week it was possible to observe that the solution turned from bright yellow to dark red, and the formation of some precipitate has occurred. The suspension was filtered with a syringe filter, added with Et_2O and pentane and placed in the freezer to crystallize. XRD of the single crystals obtained with this procedure led to **Mn-12.**

4.8.10. Procedure for the reaction between *fac*-[MnBr(CO)$_3$(dppe)] and NaBAr$^F_4$ under H_2 pressure

Mn-6 (3.1 mg, 5 x 10^{-3} mmol) and NaBAr$^F_4$ (4.4 mg, 5 x 10^{-3} mmol) were weighed in a glass autoclave inlet inside the glovebox. The inlet was added with a magnetic stirrer and with 2 mL of cyclohexane. The autoclave was brought outside the glovebox, fully closed with a wrench and pressurized with 20 bar of H_2. The autoclave was placed in a pre-heated aluminum cone at the 40 °C for 20 h, and afterwards put to cool

down in a water bath at R.T. for 15 min. The autoclave was then depressurized, the inlet quickly removed from the autoclave and placed inside a 25 mL Schlenk tube (under inert gas) in Ar flow. The inlet was then introduced in the glovebox, and the solution from the inlet was decanted leaving a yellow solid at the bottom of the inlet. The solid was dissolved in DCM, transferred to a vial, added with Et_2O and pentane and placed in the freezer to crystallize. XRD of the single crystals obtained with this procedure, led to **Mn-12.**

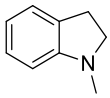
4.8.11. Synthesis of Brookhart's acid

Brookhart's acid $[H(OEt_2)_2][B(C_8H_3F_6)_4]$ was synthetized according to a slightly modified literature procedure.[30] $NaBAr^F_4$ (380 mg, 0.43 mmol) was weighed in a 10 mL Schlenk tube in the glovebox and dissolved in 1 mL of Et_2O. The Schlenk tube was taken outside the glovebox and added dropwise with 1 mL of a 2 M solution of HCl in Et_2O (2.0 mmol) purchased from Acros Organics. It was possible to observe almost instantaneous formation of a white precipitate. The suspension was filtered with a syringe filter into another Schlenk tube under Ar flow. The clear solution was evaporated under reduced pressure to afford an off-white solid. (353 mg, 81% yield).

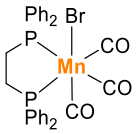
4.8.12. Synthesis of complex Mn-13

Brookhart's acid (39.4 mg, 0.04 mmol) and *fac*-[Mn(CO)$_3$(dppe)H] (22.6 mg, 0.042 mmol) were weighed inside the glovebox in two separate 10 mL Schlenk tubes and added respectively with 2 mL and 5 mL of Et_2O. The Schlenk tube containing $[H(OEt_2)_2][B(C_8H_3F_6)_4]$ was cooled down to -78 °C, and the Et_2O solution of *fac*-[Mn(CO)$_3$(dppe)H] was added dropwise under in Ar flow while stirring. It was possible to observe instantaneous color change to intense yellow. The reaction was stirred at -78 °C for 30 minutes, and it was let warm up at R.T. and stirred for 1 h. During the warming up phase, it was possible to observe intense bubbling. The solvent was evaporated under reduced pressure to afford a viscous oil. The Schlenk tube was brought back into the glovebox, added with 0.5 mL of Et_2O and 2 mL of pentane, forming an oil immiscible with the Et_2O-pentane mixture. The solution supernatant the oil was carefully removed, the yellow oil was washed with pentane (2 x 2mL), and after the residual solvent was under reduced pressure, affording 35.8 mg of the yellow oil. Due to the currently unknown structure of the complex **Mn-13**, it was not possible to deduce a yield from the amount of oil recovered. However, its $^{31}P\{^1H\}$-NMR spectrum is reported in Section 6.8.

4.8.13. Characterization data of isolated compounds

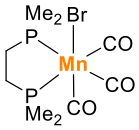


1-Methylindoline,[31] $C_9H_{11}N$, pale yellow oil. **^{1}H NMR** (400 MHz, $CDCl_3$) δ 7.08 (m, 2H), 6.67 (td, J = 7.4, 1.0 Hz, 1H), 6.49 (dd, J = 8.1, 1.0 Hz, 1H), 3.33 – 3.25 (m, 2H), 2.94 (t, J = 8.1 Hz, 2H), 2.76 (s, 3H).**^{13}C{^{1}H} NMR** (101 MHz, $CDCl_3$) δ 153.55, 130.46, 127.45, 124.40, 117.91, 107.37, 56.31, 36.43, 28.88. Isolated *via* column chromatography using pure pentane as the eluent.

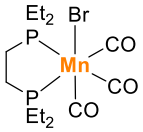


$C_{29}H_{24}BrMnO_3P_2$, yellow solid.[29]

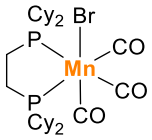
^{1}H NMR (400 MHz, $CDCl_3$) δ 7.74 – 7.61 (m, 4H), 7.55 (m, 4H), 7.48 – 7.30 (m, 12H), 3.14 (m, 2H), 2.78 (m, 2H). **^{31}P NMR** (162 MHz, $CDCl_3$) δ 70.21. **FT-IR** (solid, $\tilde{\nu}$, cm^{-1}) 3055 w, 2011 st, 1949 st, 1905 st, 1483 w, 1434 me, 1097 me, 690 me.



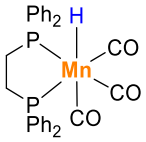
$C_9H_{16}BrMnO_3P_2$, yellow solid.[32] **^{1}H NMR** (500 MHz, $CDCl_3$) δ 2.20 – 2.06 (m, 2H), 1.93 – 1.67 (m, 8H), 1.67 – 1.48 (m, 6H). **^{31}P{^{1}H} NMR** (202 MHz, $CDCl_3$) δ 56.77. **FT-IR** (solid, $\tilde{\nu}$, cm^{-1}) = 2922 me, 2006 st, 1930 st, 1880 st, 1418 me, 1287 w, 949 me, 936 me, 845 w, 791 w, 746 w, 717 me, 670 me, 640 me, 613 me.



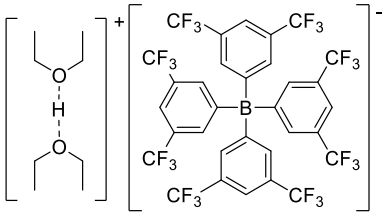
$C_{13}H_{24}BrMnO_3P_2$, yellow solid.[33] **^{1}H NMR** (500 MHz, $CDCl_3$) δ 2.29 – 2.10 (m, 4H), 2.05 – 1.88 (m, 4H), 1.85 – 1.68 (m, 4H), 1.19 (m, 12H). **^{31}P{^{1}H} NMR** (202 MHz, $CDCl_3$) δ 72.02. **FT-IR** (solid, $\tilde{\nu}$, cm^{-1}) = 2966 w, 2935 w, 2879 w, 2006 s, 1946 s, 1914 s, 1461 w, 1420 w, 1031 w, 877 w, 742 me, 725 me, 664 me, 616 me.



$C_{29}H_{48}BrMnO_3P_2$, yellow solid.[33] **^{1}H NMR** (400 MHz, $CDCl_3$) δ 2.41 (s, 2H), 2.11 (s, 2H), 2.02 – 0.92 (m, br, 44H). **^{31}P{^{1}H} NMR** (162 MHz, $CDCl_3$) δ 72.50. **FT-IR** (solid, $\tilde{\nu}$, cm^{-1}) = 2926 st, 2851 st, 2006 s, 1935 s, 1886 s, 1447 me, 669 me, 635 w, 615 w.



$C_{29}H_{25}BrMnO_3P_2$, colorless solid.[34] **^{1}H NMR** (400 MHz, Benzene-d_6) δ 7.79 (m, 4H), 7.49 (m, 4H), 7.09 – 6.93 (m, 12H), 2.11 (m, 2H), 1.91 – 1.72 (m, 2H), -7.73 (t, J = 46.9 Hz, 1H).**^{31}P{^{1}H} NMR** (162 MHz, Benzene-d_6) δ 95.51 **FT-IR** (solid, $\tilde{\nu}$, cm^{-1}) = 3054 w, 2961 w, 1986 st, 1895 st, 1483 w, 1433 me, 1261 w, 1097 me, 814 me, 693 st.



Brookhart's acid**,** $C_{40}H_{33}BF_{24}O_2$, colorless solid.[30] **^{1}H NMR** (400 MHz, DMSO-d_6) δ 8.39 (s, br, 1H), 7.72 (s, br, 4H), 7.61 (s, br, 8H), 3.37 (q, J = 7.0 Hz, 8H), 1.08 (t, J = 7.0 Hz, 12H).

4.9. References

1. Wei, H.; Li, B.; Wang, N.; Ma, Y.; Yu, J.; Wang, X.; Su, J.; Liu, D., Development and Application of Indolines in Pharmaceuticals. *ChemistryOpen* **2023,** *12* (2).

2. Ndongo, J. T.; Mbing, J. N.; Tala, M. F.; Monteillier, A.; Pegnyemb, D. E.; Cuendet, M.; Laatsch, H., Indoline alkaloids from Tabernaemontana contorta with cancer chemopreventive activity. *Phytochemistry* **2017,** *144*, 189-196.

3. Wilson, J. E.; Kurukulasuriya, R.; Reibarkh, M.; Reiter, M.; Zwicker, A.; Zhao, K.; Zhang, F.; Anand, R.; Colandrea, V. J.; Cumiskey, A.-M.; Crespo, A.; Duffy, R. A.; Murphy, B. A.; Mitra, K.; Johns, D. G.; Duffy, J. L.; Vachal, P., Discovery of Novel Indoline Cholesterol Ester Transfer Protein Inhibitors (CETP) through a Structure-Guided Approach. *ACS Med. Chem. Lett.* **2016,** *7* (3), 261-265.

4. Tercel, M.; Marnane, R. N.; Tatnell, M. A.; Stevenson, R. J.; Halim, A.; Lu, G. L.; Duchesnes, C.; Truong, M.; Denny, W. A.; Wilson, W. R.; Mountjoy, K. G., An indoline-derived compound that markedly reduces mouse body weight. *Int. J. Obes.* **2013,** *37* (5), 685-692.

5. Chaffman, M.; Heel, R. C.; Brogden, R. N.; Speight, T. M.; Avery, G. S. Indapamide. *Drugs* **1984**, *28* (3), 189–235.

6. Roumeguere, T.; Maxime Rossi. Silodosin in the Treatment of Benign Prostatic Hyperplasia. *DDDT* **2010**, 291.

7. Silva, T. S.; Rodrigues, M. T.; Santos, H.; Zeoly, L. A.; Almeida, W. P.; Barcelos, R. C.; Gomes, R. C.; Fernandes, F. S.; Coelho, F., Recent advances in indoline synthesis. *Tetrahedron* **2019,** *75* (14), 2063-2097.

8. Wang, D.-S.; Chen, Q.-A.; Li, W.; Yu, C.-B.; Zhou, Y.-G.; Zhang, X., Pd-Catalyzed Asymmetric Hydrogenation of Unprotected Indoles Activated by Brønsted Acids. *J. Am. Chem. Soc.* **2010,** *132* (26), 8909-8911.

9. Núñez-Rico, J. L.; Fernández-Pérez, H.; Vidal-Ferran, A., Asymmetric hydrogenation of unprotected indoles using iridium complexes derived from P–OP ligands and (reusable) Brønsted acids. *Green Chem.* **2014,** *16* (3), 1153-1157.

10. Saito, A.; Yoshioka, S.; Naruto, M.; Saito, S., Catalytic Hydrogenation of N-protected α-Amino Acids Using Ruthenium Complexes with Monodentate Phosphine Ligands. *Adv. Synth. Catal.* **2020,** *362* (2), 424-429.

11. Bianchini, C.; Meli, A.; Vizza, F., Hydrogenation of Arenes and Heteroaromatics. In *The Handbook of Homogeneous Hydrogenation*, 2006; pp 455-488.

12. Touge, T.; Arai, T., Asymmetric Hydrogenation of Unprotected Indoles Catalyzed by η6-Arene/N-Me-sulfonyldiamine–Ru(II) Complexes. *J. Am. Chem. Soc.* **2016,** *138* (35), 11299-11305.

13. Yang, Z.; Chen, F.; He, Y.; Yang, N.; Fan, Q.-H., Highly Enantioselective Synthesis of Indolines: Asymmetric Hydrogenation at Ambient Temperature and Pressure with Cationic Ruthenium Diamine Catalysts. *Angew. Chem. Int. Ed.* **2016,** *55* (44), 13863-13866.

14. Wen, J.; Fan, X.; Tan, R.; Chien, H.-C.; Zhou, Q.; Chung, L. W.; Zhang, X., Brønsted-Acid-Promoted Rh-Catalyzed Asymmetric Hydrogenation of N-Unprotected Indoles: A Cocatalysis of Transition Metal and Anion Binding. *Org. Lett.* **2018,** *20* (8), 2143-2147.

15. Duan, Y.; Chen, M.-W.; Ye, Z.-S.; Wang, D.-S.; Chen, Q.-A.; Zhou, Y.-G., An Enantioselective Approach to 2,3-Disubstituted Indolines through Consecutive Brønsted Acid/Pd-Complex-Promoted Tandem Reactions. *Chem. Eur. J.* **2011,** *17* (26), 7193-7197.

16. Wang, D.-S.; Tang, J.; Zhou, Y.-G.; Chen, M.-W.; Yu, C.-B.; Duan, Y.; Jiang, G.-F., Dehydration triggered asymmetric hydrogenation of 3-(α-hydroxyalkyl)indoles. *Chem. Sci.* **2011,** *2* (4), 803-806.

17. Duan, Y.; Chen, M.-W.; Chen, Q.-A.; Yu, C.-B.; Zhou, Y.-G., Pd-Catalyzed asymmetric hydrogenation of 3-(toluenesulfonamidoalkyl)indoles. *Org. Biomol. Chem.* **2012,** *10* (6), 1235-1238.

18. Li, C.; Chen, J.; Fu, G.; Liu, D.; Liu, Y.; Zhang, W., Highly enantioselective hydrogenation of N-unprotected indoles using (S)-C10–BridgePHOS as the chiral ligand. *Tetrahedron* **2013,** *69* (33), 6839-6844.

19. Duan, Y.; Li, L.; Chen, M.-W.; Yu, C.-B.; Fan, H.-J.; Zhou, Y.-G., Homogenous Pd-Catalyzed Asymmetric Hydrogenation of Unprotected Indoles: Scope and Mechanistic Studies. *J. Am. Chem. Soc.* **2014,** *136* (21), 7688-7700.

20. Lyubimov, S. E.; Ozolin, D. V.; Davankov, V. A., Asymmetric iridium-catalyzed hydrogenation of 2-methylindole using phosphite ligands. *Tetrahedron Lett.* **2014,** *55* (26), 3613-3614.

21. Kim, A. N.; Stoltz, B. M., Recent Advances in Homogeneous Catalysts for the Asymmetric Hydrogenation of Heteroarenes. *ACS Catal.* **2020,** *10* (23), 13834-13851.

22. Chakraborty, S.; Brennessel, W. W.; Jones, W. D., A Molecular Iron Catalyst for the Acceptorless Dehydrogenation and Hydrogenation of N-Heterocycles. *J. Am. Chem. Soc.* **2014,** *136* (24), 8564-8567.

23. Xu, R.; Chakraborty, S.; Yuan, H.; Jones, W. D., Acceptorless, Reversible Dehydrogenation and Hydrogenation of N-Heterocycles with a Cobalt Pincer Catalyst. *ACS Catal.* **2015,** *5* (11), 6350-6354.

24. Papa, V.; Cao, Y.; Spannenberg, A.; Junge, K.; Beller, M., Development of a practical non-noble metal catalyst for hydrogenation of N-heteroarenes. *Nat. Catal.* **2020,** *3* (2), 135-142.

25. Zubar, V.; Borghs, J. C.; Rueping, M., Hydrogenation or Dehydrogenation of N-Containing Heterocycles Catalyzed by a Single Manganese Complex. *Org. Lett.* **2020,** *22* (10), 3974-3978.

26. King, W. A.; Luo, X.-L.; Scott, B. L.; Kubas, G. J.; Zilm, K. W., Cationic Manganese(I) Dihydrogen and Dinitrogen Complexes Derived from a Formally 16-Electron Complex with a Bis-Agostic Interaction, $[Mn(CO)(Ph_2PC_2H_4PPh_2)_2]^+$. *J. Am. Chem. Soc.* **1996,** *118* (28), 6782-6783.

27. Fang, X.; Huhmann-Vincent, J.; Scott, B. L.; Kubas, G. J., H2 binding to and silane alcoholysis on an electrophilic Mn(I) fragment with tied-back phosphite ligands. X-ray structure of a Mn–CH_2Cl_2 complex. *J. Organomet. Chem.* **2000,** *609* (1), 95-103.

28. Perthuisot, C.; Fan, M.; Jones, W. D., Catalytic thermal carbon-hydrogen activation with Manganese complexes: evidence for .η^2-H_2 coordination in a neutral Manganese complex and its role in carbon-hydrogen activation. *Organometallics* **1992,** *11* (11), 3622-3629.

29. J. A. Pope, S.; Reid, G., Phosphine, arsine and stibine complexes of Manganese(I) carbonyl halides: synthesis, multinuclear NMR spectroscopic studies, redox properties and crystal structures. *Journal of the Chemical Society, Dalton Trans.* **1999,** (10), 1615-1622.

30. Brookhart, M.; Grant, B.; Volpe, A. F., Jr., $[(3,5\text{-}(CF_3)_2C_6H_3)_4B]^-[H(OEt_2)_2]^+$: a convenient reagent for generation and stabilization of cationic, highly electrophilic organometallic complexes. *Organometallics* **1992,** *11* (11), 3920-3922.

31. Li, Y.; Fang, X.; Junge, K.; Beller, M., A General Catalytic Methylation of Amines Using Carbon Dioxide. *Angew. Chem. Int. Ed.* **2013,** *52* (36), 9568-9571.

32. Connor, J. A.; Hudson, G. A., Studies of chelation: II. Phosphine complexes of molybdenum and Manganese. *J. Organomet. Chem.* **1974,** *73* (3), 351-358.

33. Hinzmann, A.; Gröger, H., Selective Hydrogenation of Fatty Nitriles to Primary Fatty Amines: Catalyst Evaluation and Optimization Starting from Octanenitrile. *Eur. J. Lipid Sci. Technol.* **2020,** *122* (1), 1900163.

34. Orchin, M.; Mandal, S. K.; Feldman, J.; Lee, W.-Z.; Darensbourg, D. J., Tricarbonyl(Hydrido) [1,2-Bis (Diphenyl-phosphino)Ethane]Manganese as Precursor to Labile Site Derivatives. In *Inorganic Syntheses*, Darensbourg, Marcetta. Y., Ed.; John Wiley & Sons, Inc.: Hoboken, NJ, USA, 2007; pp 298–302.

5. Conclusion and Outlook

In the pursuit of a more environmentally friendly chemical industry, the development of novel catalytic systems based on earth-abundant metals holds significant importance. One promising approach is substituting Ru(II) pincer complexes with their Mn(I) analogues in hydrogenation and dehydrogenation reactions. In fact, the use of cooperative ligands on Mn(I) pincer complexes significantly enhanced their catalytic activity, enabling them to compete with, and sometimes even surpass, similar Ru(II) complexes. Although the use of Metal-Ligand Cooperation has been viewed so far as essential for achieving good catalytic performances, revisiting Mn(I) organometallic chemistry reveals that there can be alternative approaches. In this study, we focused on investigating the catalytic performances of Mn(I) complexes capable of activating E–H bonds (where E = Si or H) through σ-coordination for (de)hydrogenation reactions.

It was shown that Mn(I) non-pincer complexes can offer good catalytic performances, and that the use of pincer ligands can even be detrimental to catalytic activity in some cases. In Chapter 2, we demonstrated that the commercially available complex $[MnBr(CO)_5]$ exhibited superior performance compared to several other pincer Mn(I) complexes in the activation of Si–H bonds for hydrosilylation reactions. We established that a crucial prerequisite for achieving catalytic turnover in Si–H bond activation is the ability of the catalyst to generate a vacant coordination site. This characteristic, which was challenging to achieve for Mn(I) pincer complexes under reaction conditions, was an easily accessible pathway for $[MnBr(CO)_5]$ through the dissociation of CO, leading to species with at least one vacant coordination site. This finding was verified through GC-TCD and $^{31}P\{^1H\}$-NMR analyses. Leveraging the catalytic activity demonstrated by $[MnBr(CO)_5]$, we proceeded to perform the reductive hydrosilylation of various unprotected carboxylic acids to their corresponding alcohols. During the course of the mechanistic studies, a silyl ester was generated *via* the formation of a dehydrogenative bond between RCO_2–H and R_3Si–H using $[MnBr(CO)_5]$ as the catalyst. This silyl ester was then isolated and subsequently reduced to the corresponding alcohol in standard reaction conditions, confirming its nature as a plausible reaction intermediate.

In Chapter 3, the $[MnBr(CO)_5]$ catalyzed dehydrogenative coupling of Si–H bonds with protic nucleophiles was further investigated using H_2O as the coupling partner. Once again, the necessity for a free coordination site was observed. Additionally, an unreported pathway for the activation of Si–H bonds *via* σ-coordination at a Mn(I) center was discovered. This activation involves the metathesis of the Mn–Br and Si–H bonds to form the corresponding Si–Br and Mn–H, that were identified and confirmed *via* ^1H- and ^{29}Si-NMR spectroscopy. Furthermore, the study yielded the initial evidence that the catalytic cycle is carried on by a coordinatively unsaturated species, which was deduced through kinetic investigations of the reaction.

Specifically, the kinetic equation of the reaction between H_2O and $PhMe_2SiH$ resulted in:

$$K_{obs} = K\,[MnBr(CO)_5]^{0.9}\,[H_2O]^{-0.6}\,[PhMe_2SiH]^{0.8}$$

This result led to the interpretation that the active species, which is coordinatively unsaturated, engages in a coordinative pre-equilibrium with H_2O, functioning as a reversible inhibitor for the catalyst. As a result, the negative order in H_2O is observed. Finally, with the help of flow FT-IR studies, GC-TCD studies and the crystal structure of a manganese complex grown from a crude reaction mixture, it was possible to partially elucidate the structure of the active species, composed of "$Mn(CO)_3$" units.

In Chapter 4, the knowledge gained on the activation of Si–H bonds *via* σ-coordination was transferred to the investigation of H–H bond activation. After several attempts, suitable conditions were identified to develop a stabilized Mn(I) catalytic system able to activate H_2 for the hydrogenation of indoles. Catalytic activity was observed when utilizing either the complex *fac*-[$MnBr(CO)_3$(dppe)] in the presence of $NaBAr^F{}_4$ as the *in situ* activator, or the complex generated from the reaction of the *fac*-[$Mn(CO)_3$(dppe)H] and Brookhart's acid. Both of these approaches, likely generating a stabilized Mn(I) cationic unsaturated complex, exhibit catalytic activity in the hydrogenation of indoles. This activity was demonstrated so far on a small scope of 6 indoles, showing good functional group tolerance.

The activation mechanism of the precatalyst *fac*-[$MnBr(CO)_3$(dppe)] by the activator $NaBAr^F{}_4$ was found to be bromide abstraction. This conclusion was supported by the observation that the reaction between the two resulted in the complex $[Mn_2Br(CO)_6(dppe)_2]BAr^F{}_4$ for which a crystal structure could be obtained. The activation of H_2 by the catalyst was further supported by performing a yield-time profile study both with H_2 and D_2, resulting in a KIE = 3.1 and indicating that the H–H bond is likely to be cleaved in the rate determining step of the reaction.

This work concludes that the potential for activating σ-bonds using Mn(I) non-MLCve catalysts is still largely untapped in the literature. Specifically, there is ample room for the development of efficient and scalable Mn(I) catalysts for the dehydrogenative coupling of Si–H bonds with various substrates, as well as other base-free hydrogenation reactions that have only been scarcely explored so far.

A potential future direction for this ongoing work is the exploration of an asymmetric version of the reaction. The wide availability of chiral chelating phosphines and the diverse applications of chiral indolines in the field of medicinal chemistry make this an appealing avenue to pursue. Another outlook for this research could be to apply the developed catalysts to the deuteration of anilines and other organic molecules. Although it was serendipitously observed as an unintended side reaction in Chapter 4, it could be an interesting reaction to study more in detail.

Beyond that, an important aspect is to thoroughly characterize the complex responsible for the hydrogenation of indoles arising from the protonation of the complex *fac*-[$Mn(CO)_3$(dppe)H] with

Brookhart's acid. A better understanding of the structure of this complex could lead to improved design and testing in hydrogenation reactions so far underexplored with Mn(I) complexes. Specifically, this would be of particular significance since it would pave the way for the development of hydrogenation reactions that are incompatible with bases, or require acidic conditions to be performed. These conditions are mostly inaccessible to MLCve-Mn(I) complexes, due to the need for a basic environment to activate MLCve mechanisms. Therefore, a breakthrough in this direction could facilitate the rise of a new class of Mn(I)-catalysts able to catalyze hydrogenation reactions under complementary conditions to the ones currently employing Metal–Ligand Cooperation.

6. Appendix

In the following appendix, all the necessary electronic supplementary material will be included to support the experimental findings presented in the chapters above.

6.1. Analytical Instrumentation

A list of the analytical instruments used to analyze the data in the previous chapters is reported below

6.1.1. NMR spectrometers

NMR spectra were recorded on a Bruker AVANCE NEO 400 MHz, a Bruker AVANCE III HD 500 MHz NMR spectrometer with a Bruker Prodigy probe, or Bruker AVANCE NEO 600 MHz NMR spectrometer with a BBO cryoprobe. The kinetic studies were performed on a Bruker AVANCE III HD 400 MHz NMR spectrometer equipped with a BBO probe.

6.1.2. GC for headspace analysis

Gas-phase analyses have been performed on a Shimadzu GC Nexis 2030 *via* manual injection (100 µL) equipped with a Restek Q-Bond column (Length: 30m; inner Diameter: 0.32 mm; film thickness: 10 µm) and a TCD detector using $He_{(g)}$ as a carrier gas.

6.1.3. FT-IR spectrometers

FT-IR characterization has been performed with a Nicolet™ iS™ 5 FT-IR-Spectrometer equipped with a ATR-iD7. The flow FT-IR was a Bruker Vertex 70v with a Harrick Scientific high-pressure demountable liquid cell equipped with diamond windows with a path length of 100 µm. A 1/16'' tubing connected the IR device to a Fischer-Porter tube. The sample was continuously pumped through the loop to the FT-IR spectrometer during sample measurement by a WADose Lite HP HPLC pump.

6.1.4. Polarimeter

Optical rotations were measured with an A-Krüss Otronic Model P8000-t polarimeter at a wavelength of 589 nm.

6.1.5. Photochemistry setup

The blue light "Evoluchem™" (450 nm) was purchased from Hepatochem and used in combination with the PhotoRedOx Box TC.

6.1.6. X-Ray Diffraction

A Bruker D8 Venture diffractometer equipped with an IµS3 Diamond Mo-source (Mo-Kα radiation; λ=0.71073 Å) and an IµS3 Cu-source (Cu-Kα radiation; λ=1.54178 Å), INCOATEC Helios mirror optics, and Photon III detector was used for data collection.

6.1.7. Mass spectrometry

HR-MS have been recorded *via* an “LTQ-FT-Ultra” provided by Thermo Scientific, while APCI-MS have been recorded on an “expression CMS” device by Advion.

6.2. Supplementary Electronic Characterization Data

New molecules, or compounds for which it was not possible to find a literature reference supporting their identity, are shown here with supplementary electronic characterization data.

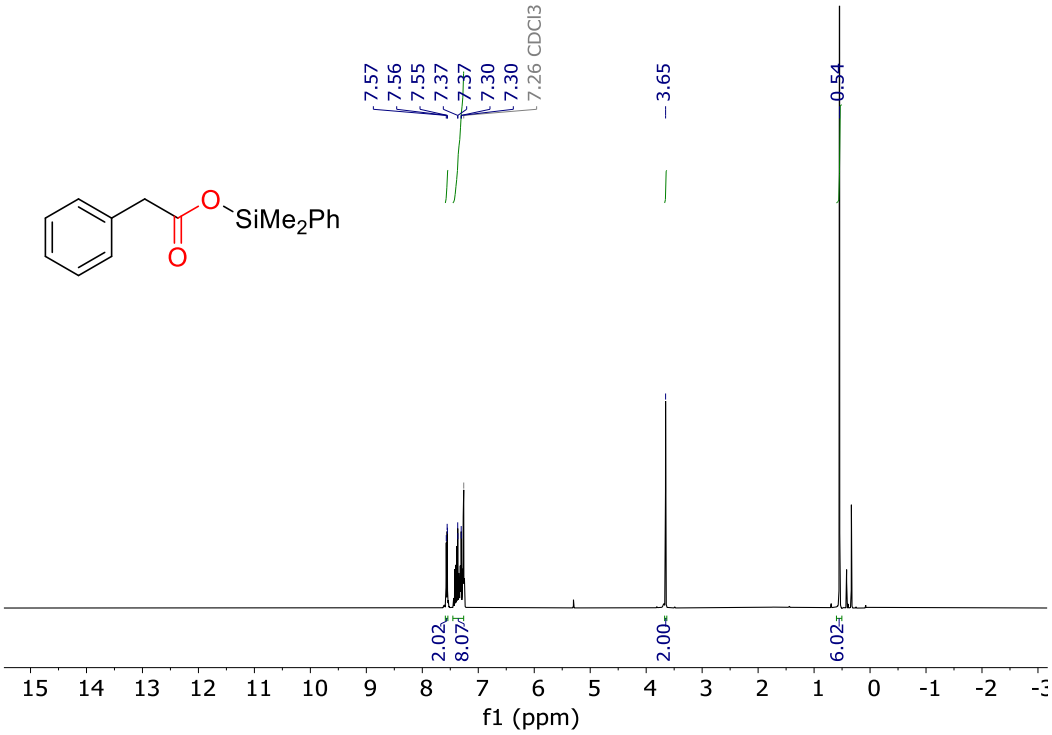


Figure 24: ^{1}H-NMR (400 MHz, $CDCl_3$, 296 K) spectrum of the silyl ester (Sections 2.5.1 and 2.8.5).

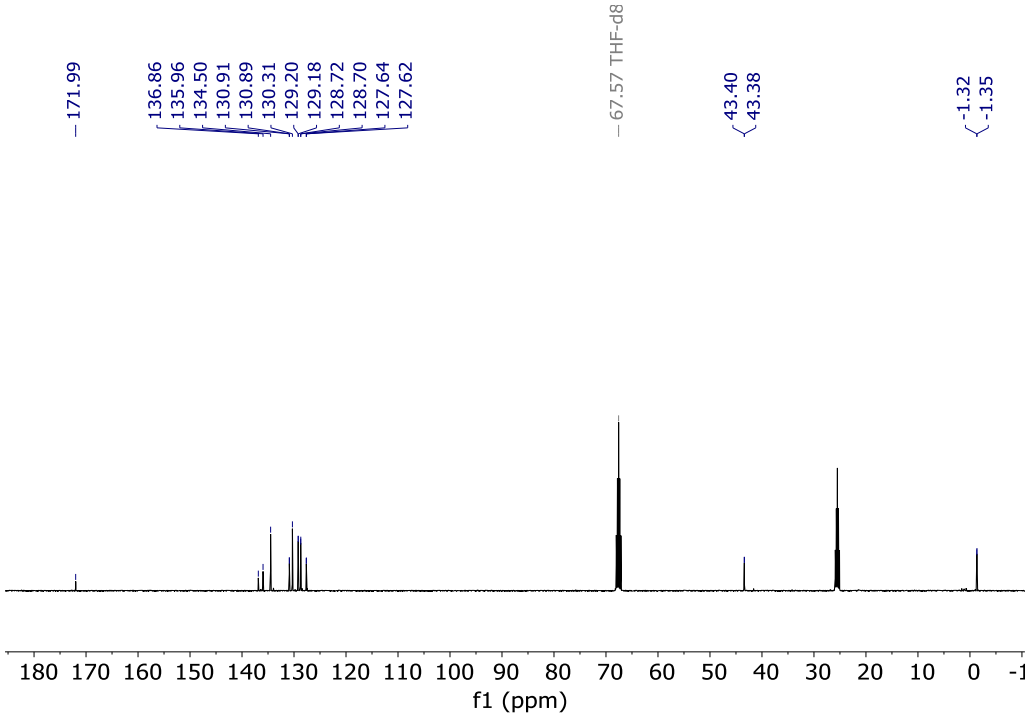


Figure 25: $^{13}C\{^{1}H\}$-NMR (101 MHz, THF-d_8, 296 K) spectrum of the silyl ester (Sections 2.5.1 and 2.8.5).

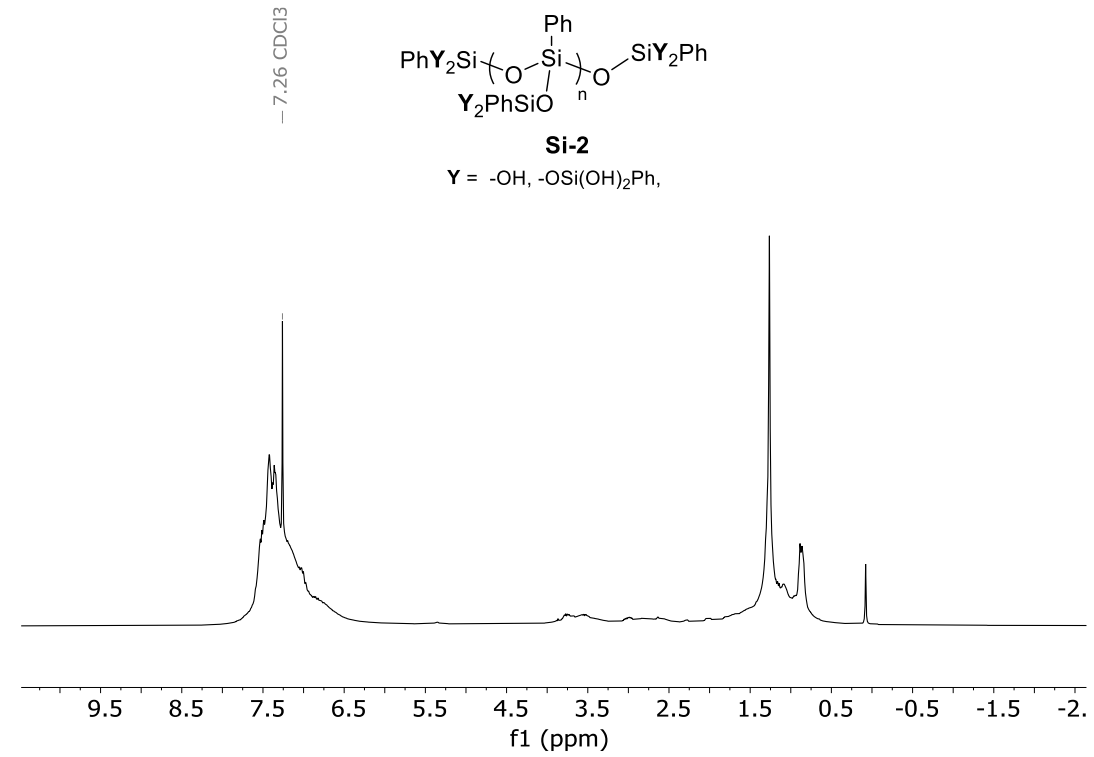


Figure 26: ^{1}H-NMR (400 MHz, $CDCl_3$, 296 K) spectrum of the silicon-based byproducts obtained after isolation via Kugelrohr distillation (Section 2.5.3).

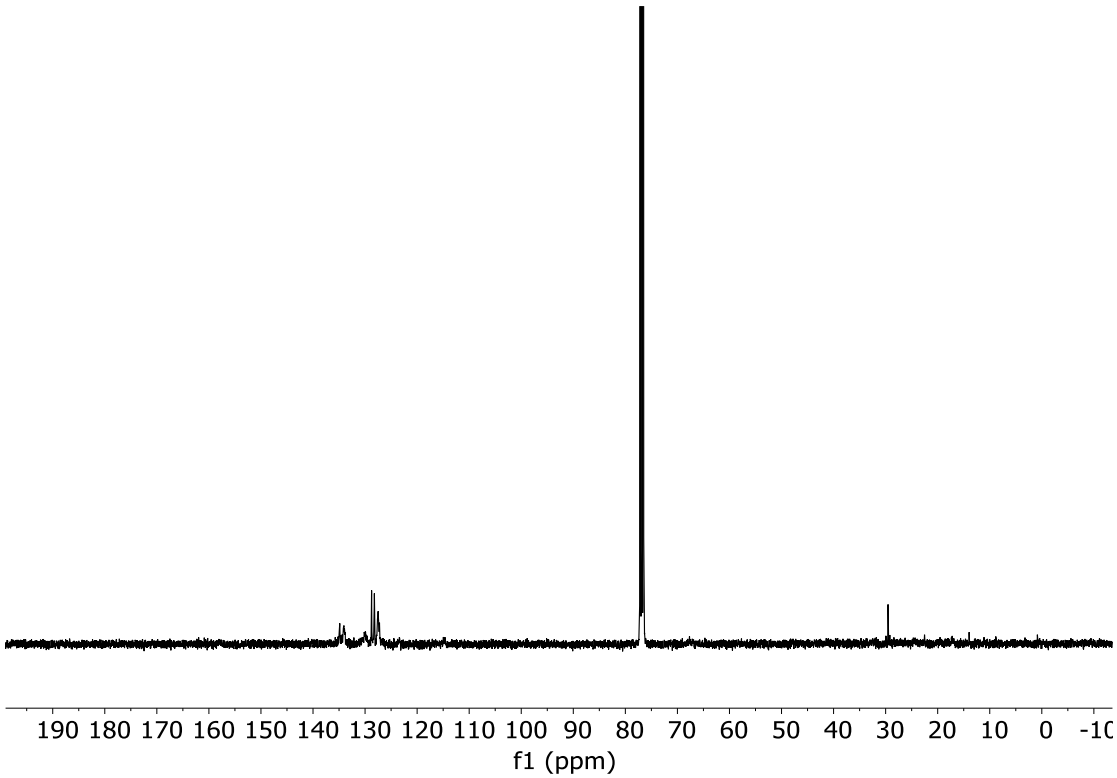


Figure 27: ^{13}C{^{1}H}-NMR (400 MHz, CDCl3, 296 K):) spectrum of the silicon-based byproducts obtained after isolation via Kugelrohr distillation (Section 2.5.3).

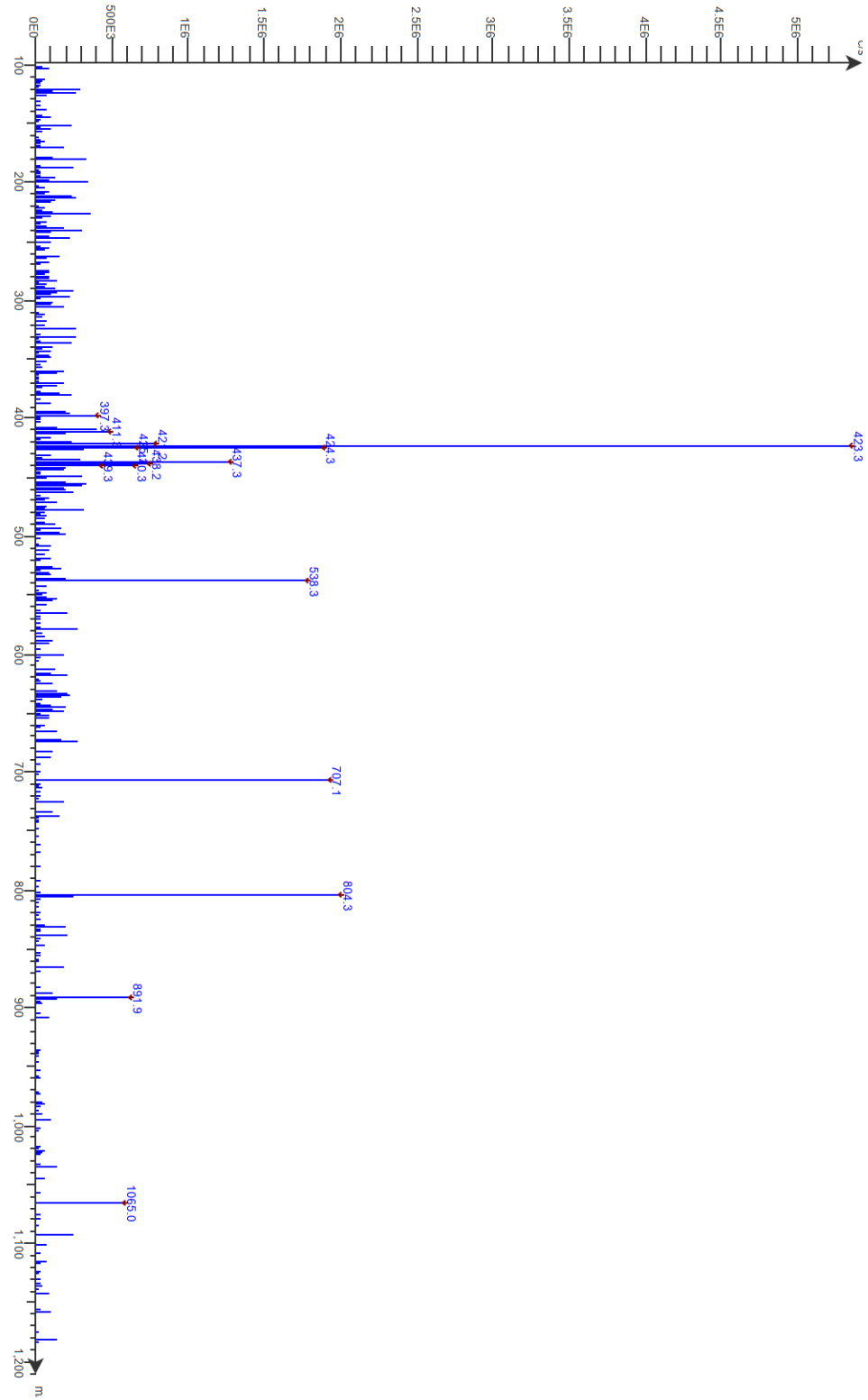


Figure 28: Anionic APCI-MS of spectrum of the silicon-based byproducts obtained after isolation via Kugelrohr distillation (Section 2.5.3).

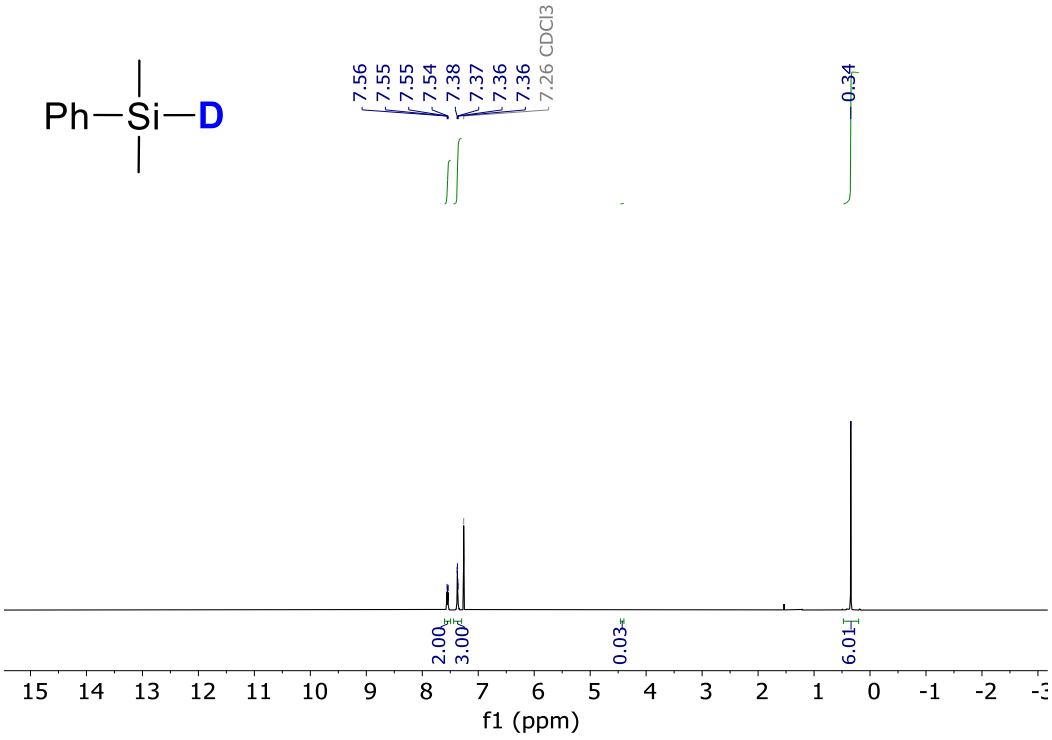


Figure 29: ^{1}H-NMR (400 MHz, $CDCl_3$, 296 K) spectrum of $PhMe_2SiD$ (Section 3.7.5).

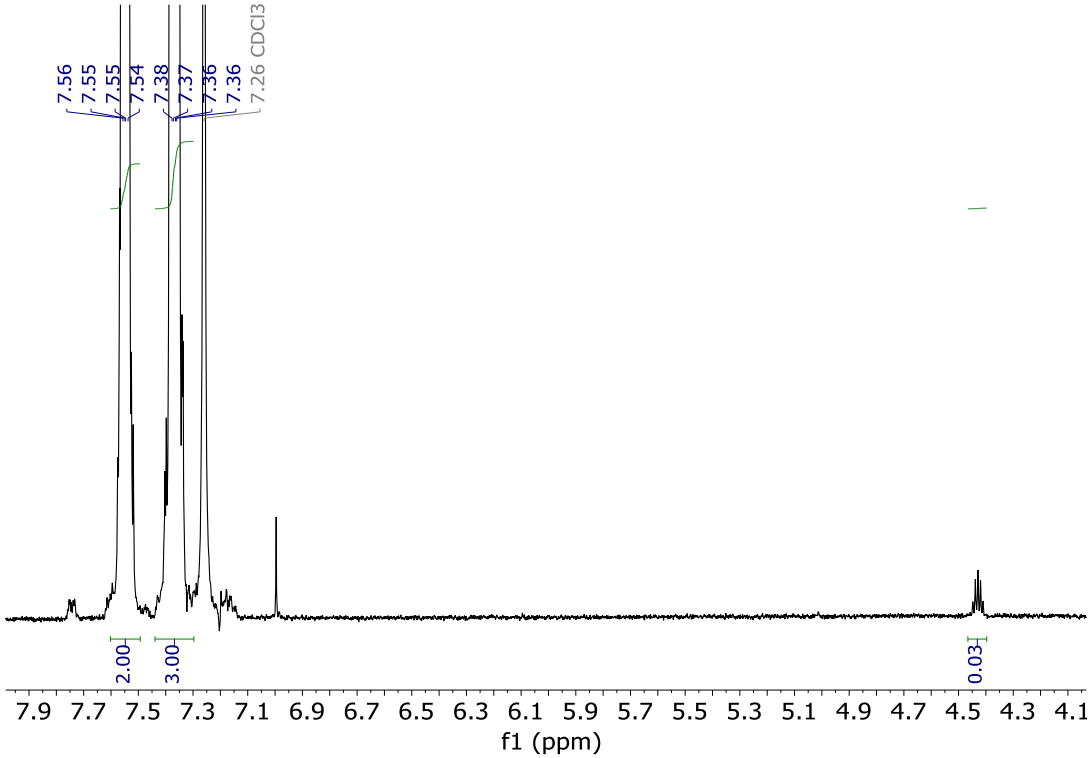


Figure 30: ^{1}H-NMR (400 MHz, $CDCl_3$, 296 K) spectrum. Detail of the spectrum of $PhMe_2SiD$ (Section 3.7.5).

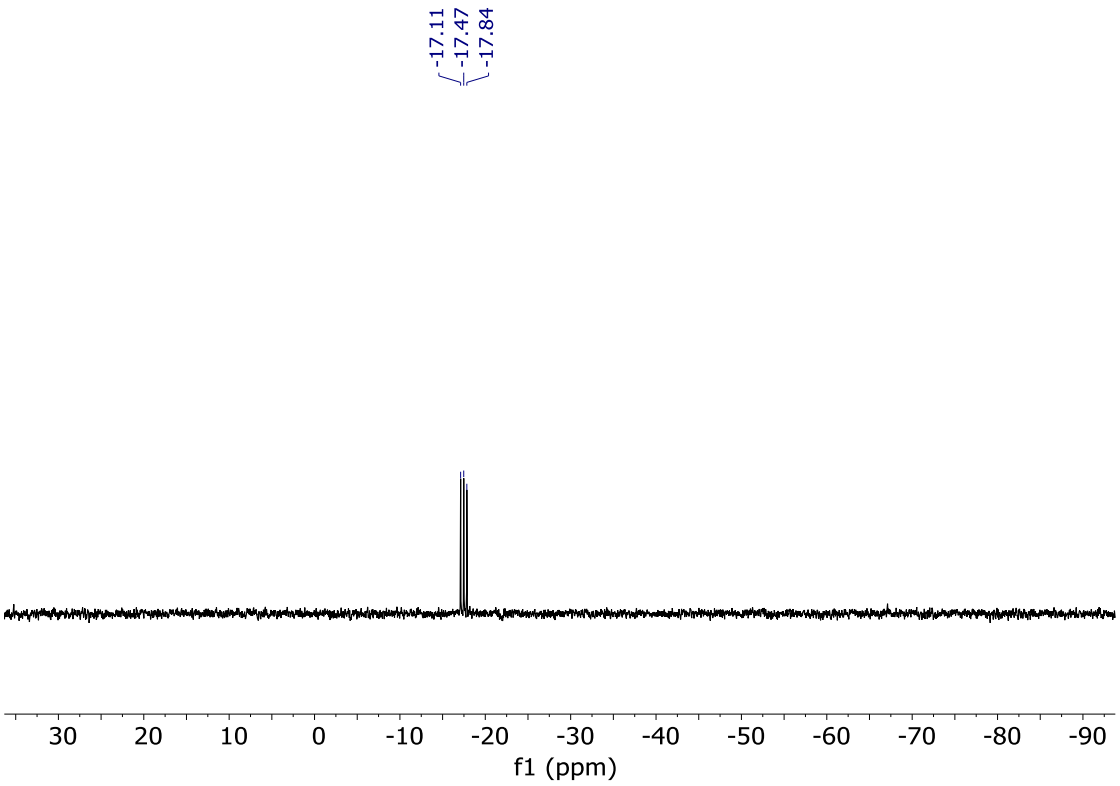


Figure 31: : ^{29}Si-NMR (79 MHz, $CDCl_3$ 296 K) spectrum of $PhMe_2SiD$ (Section 3.7.5).

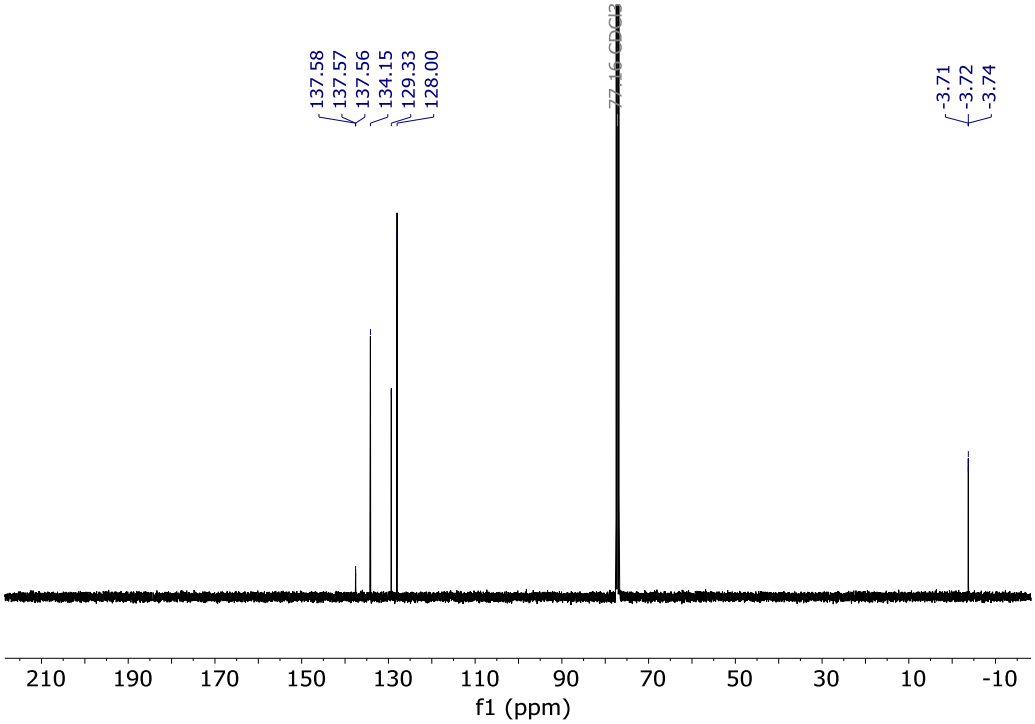


Figure 32: $^{13}C\{^1H\}$-NMR (101 MHz, $CDCl_3$, 296 K) spectrum of $PhMe_2SiD$ (Section 3.7.5).

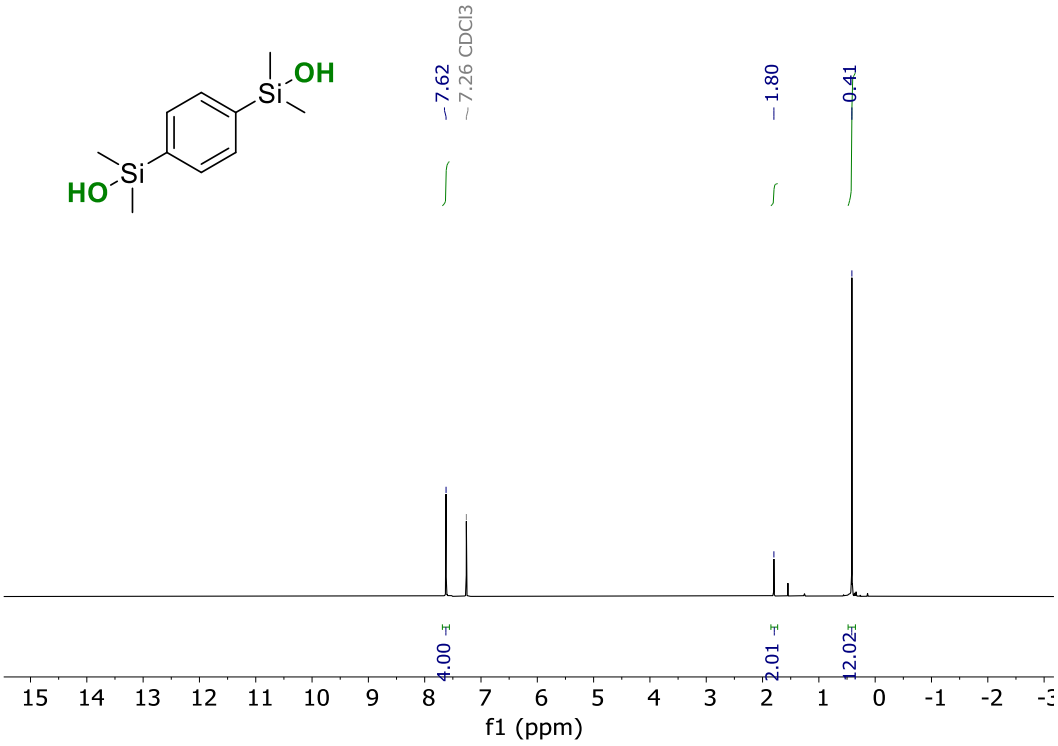


Figure 33: : ^{1}H-NMR (400 MHz, $CDCl_3$, 296 K) spectrum of compound **2n** (Section 3.3).

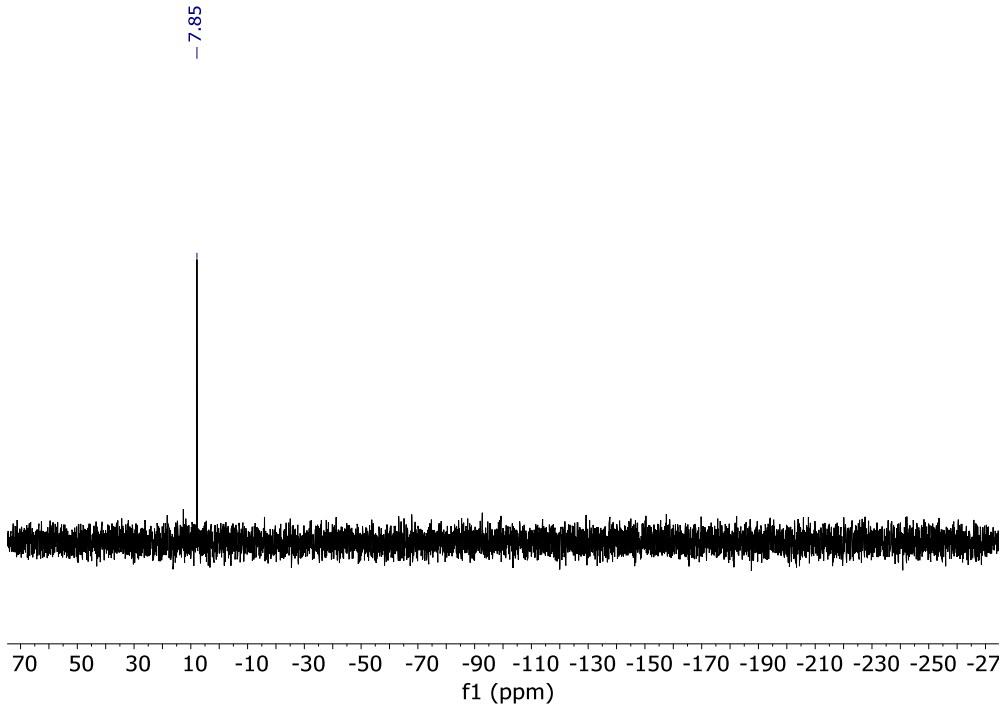


Figure 34: ^{29}Si-NMR (79 MHz, $CDCl_3$, 296K) spectrum of compound **2n** (Section 3.3).

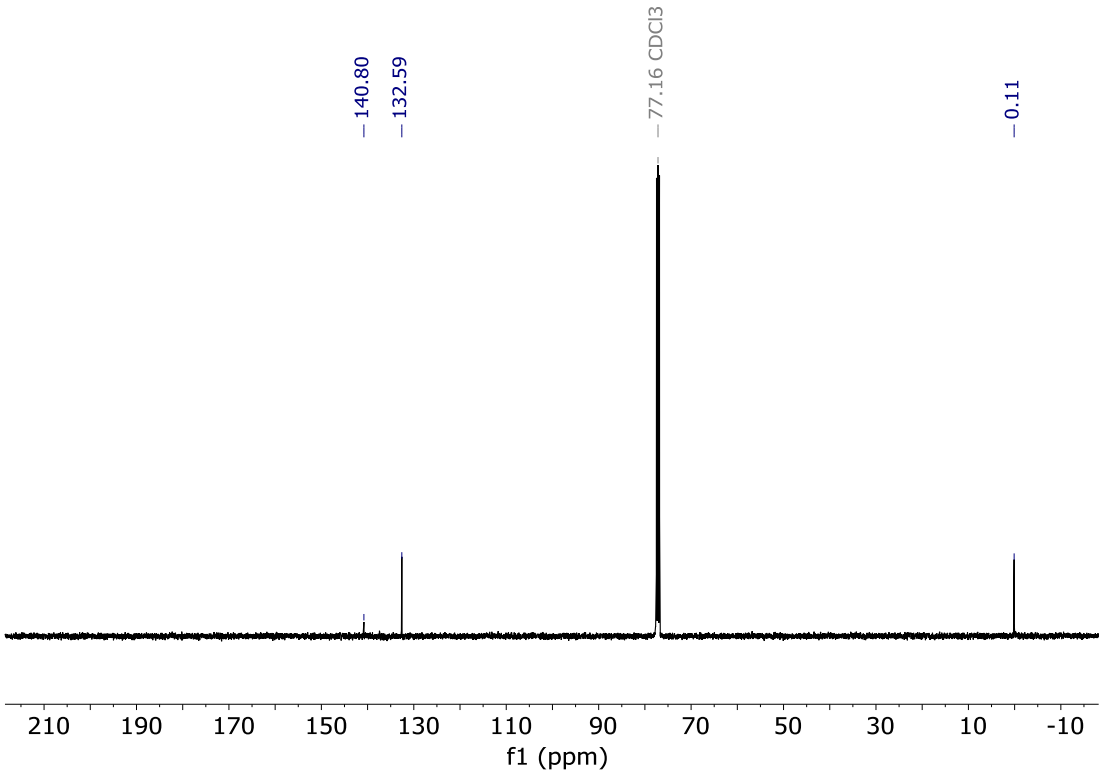


Figure 35: $^{13}C\{^{1}H\}$-NMR (101 MHz, $CDCl_3$, 296 K) spectrum of compound **2n** (Section 3.3).

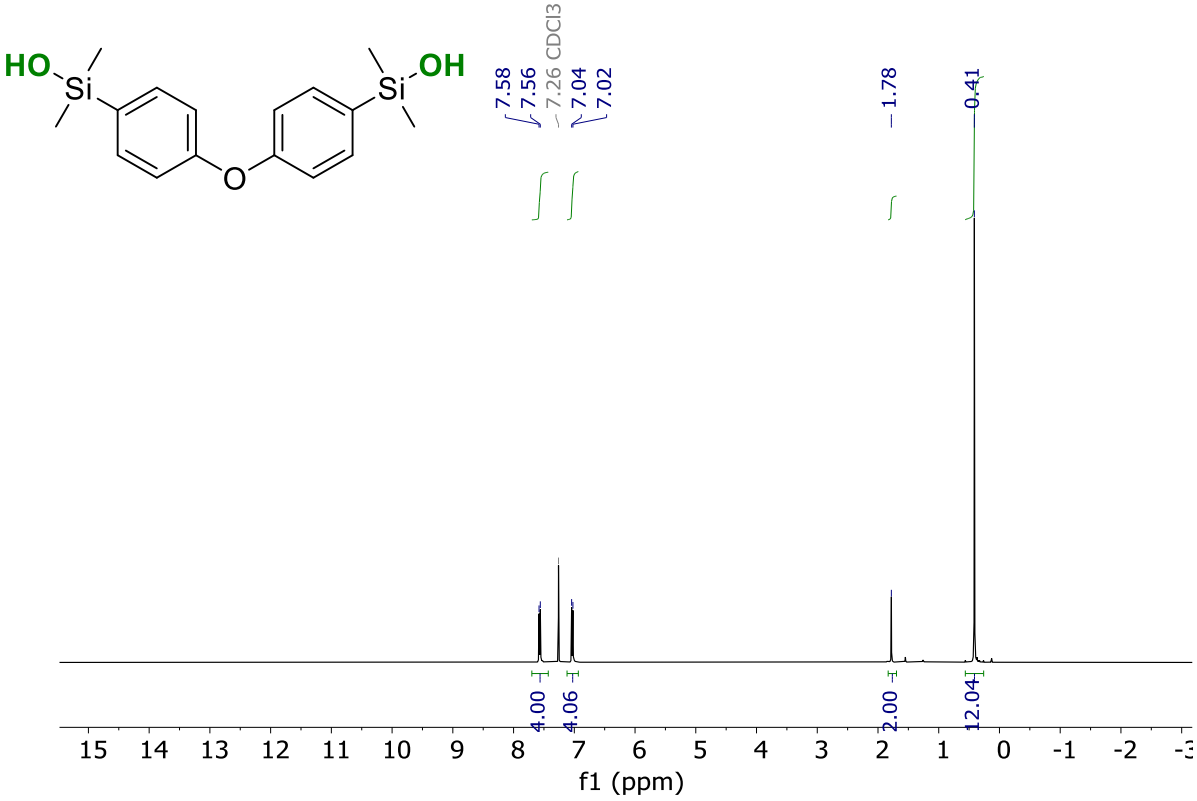


Figure 36: ^{1}H-NMR (400 MHz, $CDCl_3$, 296 K) spectrum of compound **2o**.

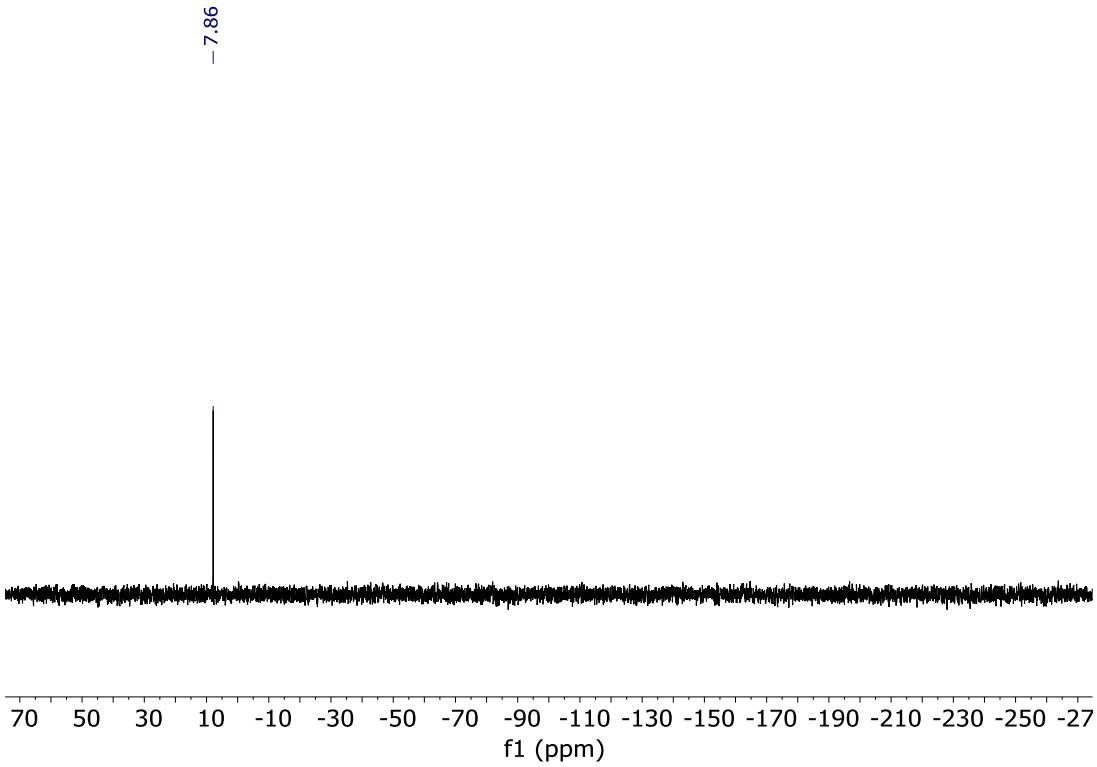


Figure 37: ^{29}Si-NMR (79 MHz, $CDCl_3$, 296K) spectrum of compound **2o** (Section 3.3).

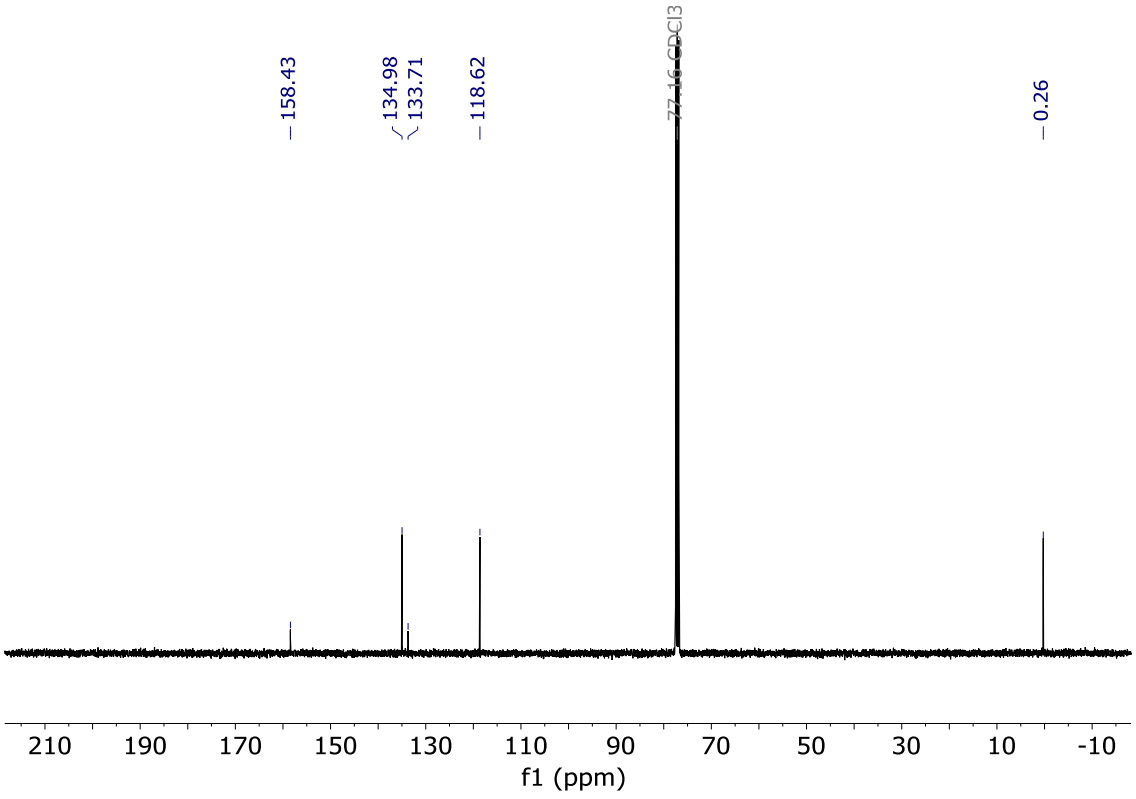


Figure 38: $^{13}C\{^1H\}$-NMR (101 MHz, $CDCl_3$, 296 K) spectrum of compound **2o** (Section 3.3).

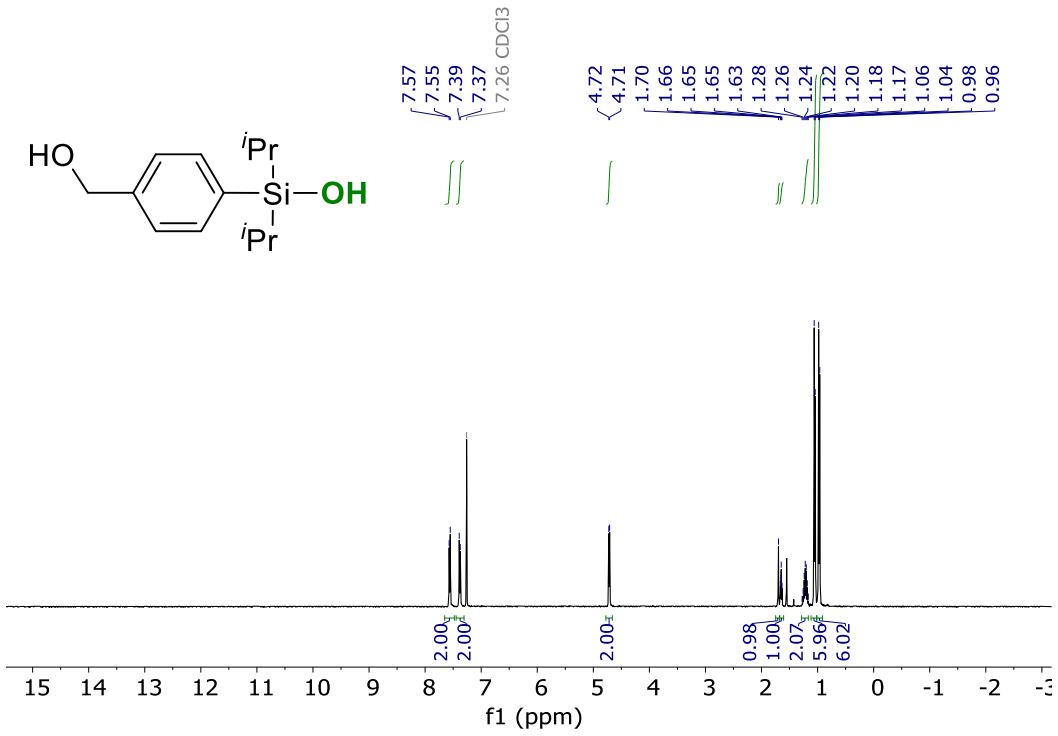


Figure 39: ^{1}H-NMR (400 MHz, $CDCl_3$, 296 K) spectrum of compound **2p** (Section 3.3).

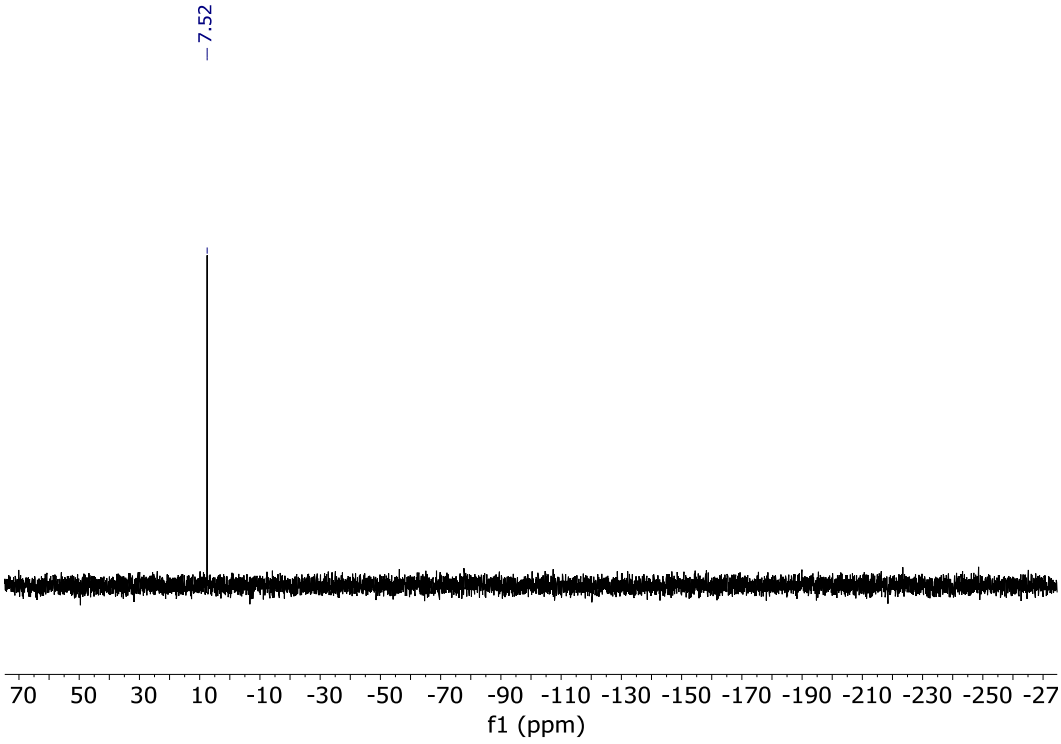


Figure 40: ^{29}Si-NMR (79 MHz, $CDCl_3$, 296K) spectrum of compound **2p** (Section 3.3).

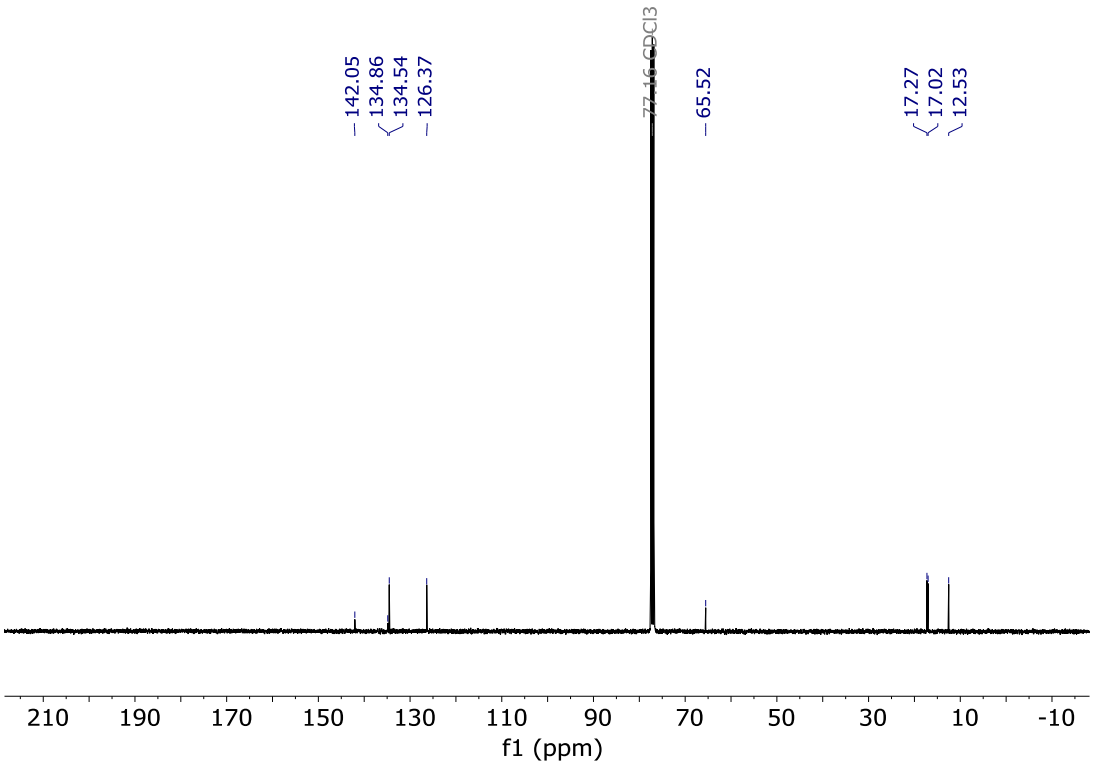


Figure 41: $^{13}C\{^{1}H\}$-NMR (101 MHz, $CDCl_3$, 296 K) spectrum of compound **2p** (Section 3.3).

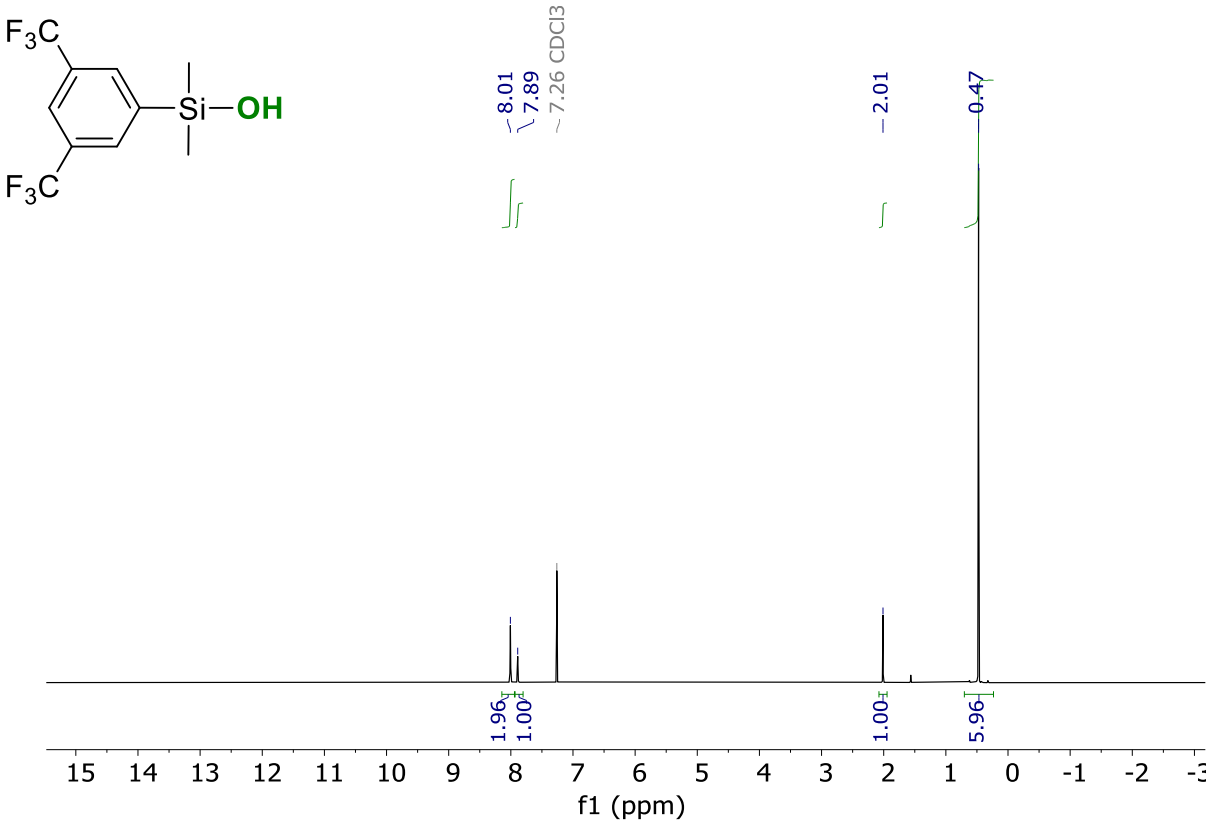


Figure 42: ^{1}H-NMR (400 MHz, $CDCl_3$, 296 K) spectrum of compound **2e**.

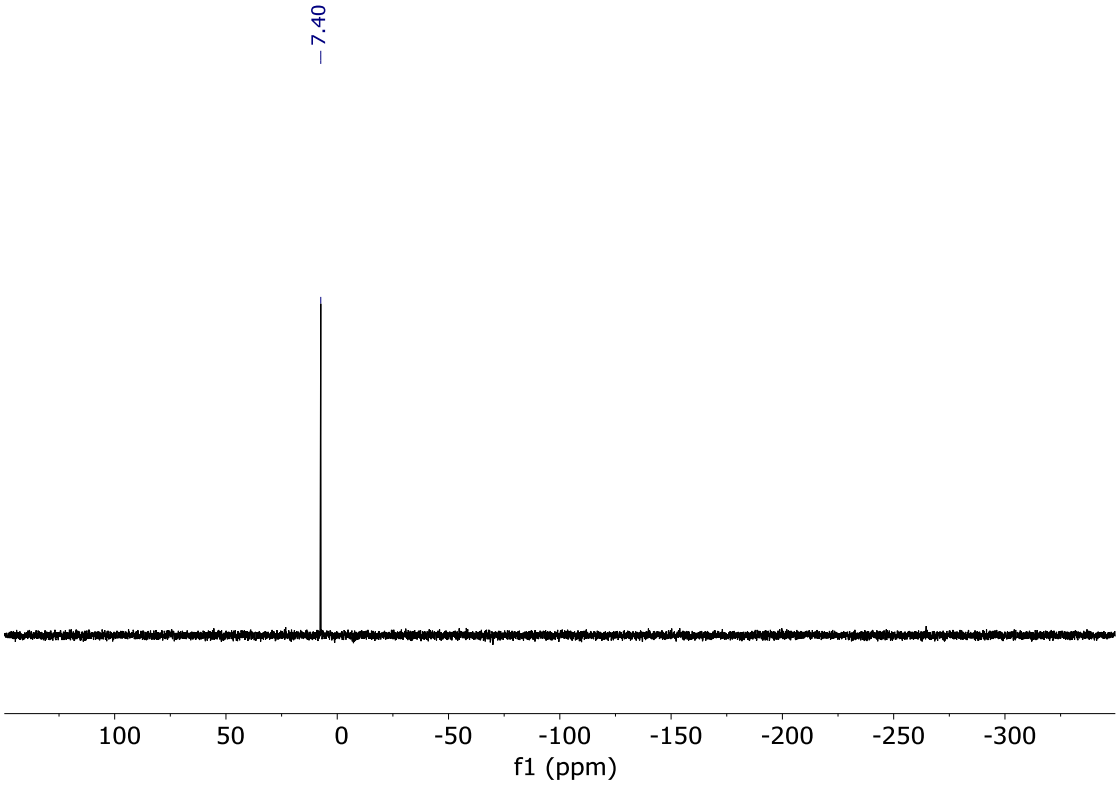


Figure **43**: ^{29}Si-NMR (79 MHz, $CDCl_3$, 296K) spectrum of compound **2e**.

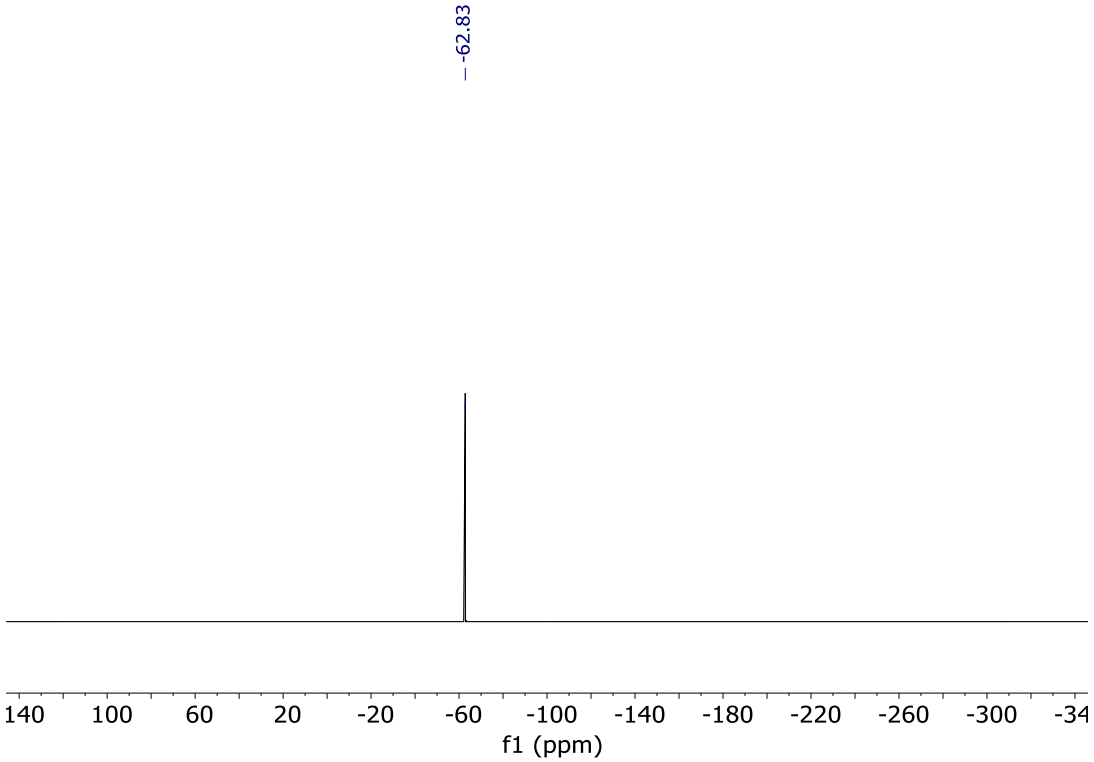


Figure 44: ^{19}F-NMR (376 MHz, $CDCl_3$, 296K): spectrum of compound **2e**.

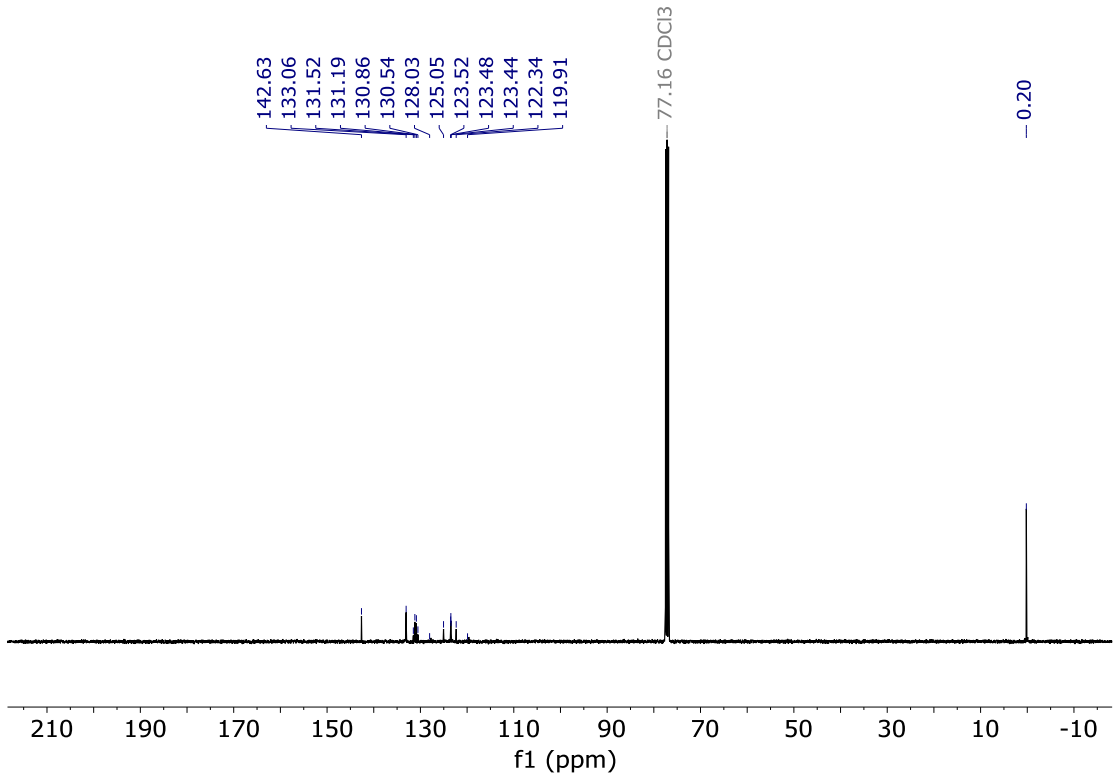


Figure 45: $^{13}C\{^{1}H\}$-NMR (101 MHz, $CDCl_3$, 296 K) spectrum of compound **2e**.

6.3. Supplementary NMR Data for Section 3.4.1

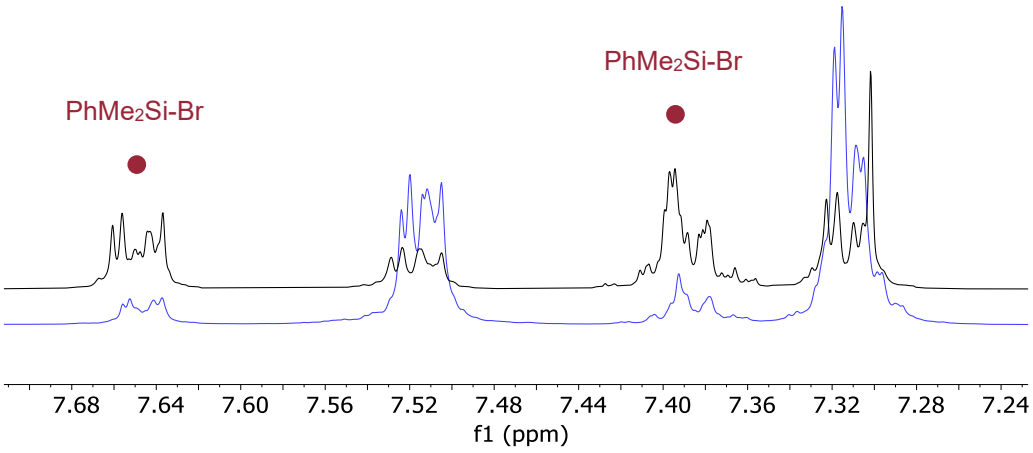


Figure 46: Detail of the ^{1}H spectra reported in Section 3.4.1. In particular, region between 7.70 – 7.23 ppm. Comparison of the crude reaction mixture between $PhMe_2SiH$ and Br_2 in black, with the reaction $PhMe_2SiH$ and $[MnBr(CO)_5]$ after 15 minutes in blue.

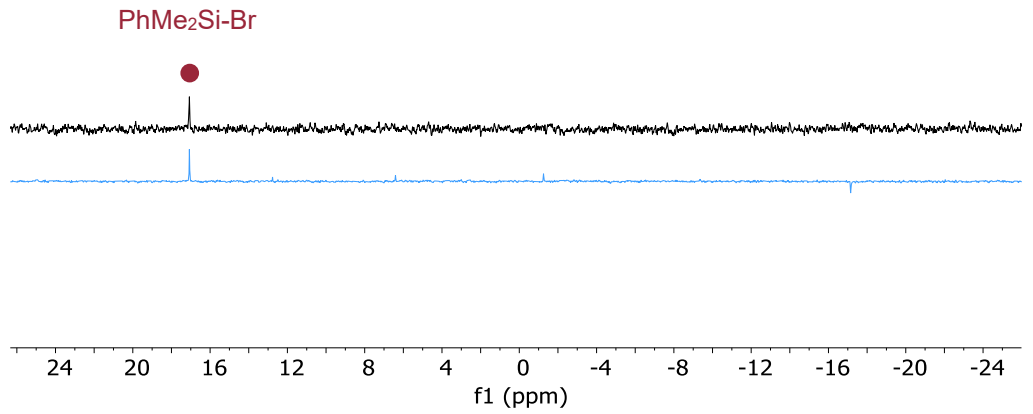


Figure 47: ^{29}Si-NMR (79 MHz, THF-d_8, 296 K) spectra reported in Section 3.4.1. Comparison of the crude reaction mixture between $PhMe_2SiH$ and Br_2 in black, with the reaction $PhMe_2SiH$ and $[MnBr(CO)_5]$ after 15 minutes in blue.

6.4. Novel Crystal Structures of Compounds Reported in the Work

6.4.1. Procedure for the X-Ray crystallography and the refinement of structures

Single crystals were selected by Dr. Thomas Weyhermüller, Bernd Mienert or Helena Randel under a microscope in polarized light with an applied nitrogen cryostream at approx. -40 °C and were covered with polyfluorinated polyether. The crystals were picked up with nylon loops and rap-idly mounted in the nitrogen cold gas stream of the diffractometer at 100 K to prevent solvent loss. Intensity data were corrected for absorption using intensities of redundant reflections using SADABS[1]. The structures were readily solved by Direct methods and subsequent difference Fourier techniques. Data were processed using the BRUKER APEX 3[2] software suite. Final cell constants, are based upon the refinement of the XYZ-centroids of several thousand reflections above 20 σ(I). Structures were solved and refined using the embedded BRUKER SHELXTL soft-ware package. All non-hydrogen atoms were anisotropically refined and hydrogen atoms were placed at calculated positions and refined as riding atoms with isotropic displacement parameters.

6.4.2. Crystallographic data and structure refinement for the molecule 2o

Table 10: Crystallographic data and structure refinement for the molecule **2o**.

	2o
Formula	$C_{16}H_{22}O_3Si_2$
M_r in g mol^{-1}	318.52
Colour	colorless
Crystal system	monoclinic
Space group	$P2_1/n$
a in Å	12.9559(7)
b in Å	10.4977(6)
c in Å	28.982(2)
α in °	90
β in °	95.735(2)
γ in °	90
V in Å^3	3922.0(4)
Z	8
T in K	85(2)
Crystal size in mm^3	0.155 × 0.140 × 0.035
ρ_c in g cm^{-3}	1.241
F(000)	1360
Diffractometer	Bruker-D8 Venture
$\lambda_{MoK\alpha}$ in Å	0.71073
θ_{min} in °	2.06
θ_{max} in °	31.08
Index range	$-13 \le h \le 18$ $-15 \le k \le 15$ $-42 \le l \le 42$
μ in mm^{-1}	0.187
Abs. correction	multi-Scan
Reflections collected	112870
Reflections unique	12536
R_{int}	0.0420
Reflections obs. [F>2σ(F)]	10539
Residual density in e Å^{-3}	0.943/-0.357
Params/restraints	391/0
GOOF	1.054
R_1 [I>2σ(I)]	0.0530
wR_2 (all data)	0.1426
CCDC	2190210

6.4.3. Crystallographic data and structure refinement for the molecule 2p

Table 11: Crystallographic data and structure refinement for the molecule **2p**.

	2p
Formula	$C_{13}H_{22}O_2Si$
M_r in g mol^{-1}	238.39
Colour	colorless
Crystal system	orthorhombic
Space group	Pbca
a in Å	8.0671(2)
b in Å	15.0932(4)
c in Å	22.4852(6)
α in °	90
β in °	90
γ in °	90
V in Å^3	2737.76(12)
Z	8
T in K	233(2)
Crystal size in mm^3	0.14 × 0.08 × 0.02
ρ_c in g cm^{-3}	1.157
F(000)	1040
Diffractometer	Bruker-D8 Venture
$\lambda_{MoK\alpha}$ in Å	0.71073
θ_{min} in °	2.699
θ_{max} in °	29.999
Index range	$-11 \le h \le 10$ $-21 \le k \le 21$ $-31 \le l \le 31$
μ in mm^{-1}	0.157
Abs. correction	multi-Scan
Reflections collected	47682
Reflections unique	3992
R_{int}	0.0722
Reflections obs. [F>2σ(F)]	2998
Residual density in e Å^{-3}	0.357/-0.199
Params/restraints	151/0
GOOF	1.082
R_1 [I>2σ(I)]	0.0444
wR_2 (all data)	0.1205
CCDC	2190209

6.4.4. Crystallographic data and structure refinement for the complex Mn-7

Table 12: Crystallographic data and structure refinement for the complex **Mn-7**.

	Mn-7
Formula	$C_{44}H_{68}Br_6Mn_5O_{22}$
M_r in g mol^{-1}	1703.14
Colour	yellow
Crystal system	triclinic
Space group	P-1
a in Å	10.9650(7)
b in Å	11.6978(7)
c in Å	13.6443(9)
α in °	111.740(3)
β in °	101.903(3)
γ in °	90.098(3)
V in Å^3	1584.8(2)
Z	1
T in K	100(2)
Crystal size in mm^3	0.13 × 0.10 × 0.08
ρ_c in g cm^{-3}	1.785
F(000)	843
Diffractometer	Bruker-D8 Venture
$\lambda_{MoK\alpha}$ in Å	0.71073
θ_{min} in °	1.881
θ_{max} in °	29.998
Index range	$-15 \le h \le 15$ $-16 \le k \le 16$ $-19 \le l \le 19$
μ in mm^{-1}	4.819
Abs. correction	multi-Scan
Reflections collected	71687
Reflections unique	9245
R_{int}	0.0825
Reflections obs.[F>2σ(F)]	7237
Residual density in e Å^{-3}	2.340/-0.680
Params/restraints	355/2
GOOF	1.092
R_1 [I>2σ(I)]	0.0477
wR_2 (all data)	0.1428
CCDC	2190208

6.4.5.Crystallographic data and structure refinement for the complex Mn-10

Table 13: Crystallographic data and structure refinement for the complex **Mn-10**.

	CEC0243
Formula	$C_{32.5}H_{52}BrMnO_3P_2$
M_r in g mol^{-1}	687.53
Color	yellow-orange
Crystal system	monoclinic
Space group	$P2_1/n$
a in Å	11.0201(3)
b in Å	21.0464(5)
c in Å	14.3056(4)
α in °	90
β in °	100.8950(10)
γ in °	90
V in Å^3	3258.1(2)
Z	4
T in K	85(2)
Crystal size in mm^3	0.22 × 0.09 × 0.07
ρ_c in g cm^{-3}	1.402
F(000)	1444
Diffractometer	Bruker-D8 Venture
$\lambda_{MoK\alpha}$ in Å	0.71073
θ_{min} in °	1.94
θ_{max} in °	36.45
Index range	$-18 \le h \le 16$ $-35 \le k \le 35$ $-23 \le l \le 23$
μ in mm^{-1}	1.761
Abs. correction	multi-Scan
Reflections collected	179375
Reflections unique	15851
R_{int}	0.0437
Reflections obs. [F>2σ(F)]	13132
Residual densityin e Å^{-3}	1.144/-1.665
Params/restraints	425/34
GOOF	1.173
R_1 [I>2σ(I)]	0.0437
wR_2 (all data)	0.0944

6.4.6. Crystallographic data and structure refinement for the complex Mn-12

Table 14: Crystallographic data and structure refinement for the complex **Mn-12**.

	Mn-12
Formula	$C_{90}H_{60}BBrF_{24}Mn_2O_6P_4$
M_r in g mol^{-1}	2017.88
Color	yellow
Crystal system	monoclinic
Space group	$P2_1/c$
a in Å	15.0901(6)
b in Å	32.4529(12)
c in Å	19.0269(7)
α in °	90
β in °	96.706(2)
γ in °	90
V in Å^3	9254.1(6)
Z	4
T in K	85(2)
Crystal size in mm^3	0.26 × 0.09 × 0.07
ρ_c in g cm^{-3}	1.448
F(000)	4056
Diffractometer	Bruker-D8 Venture
$\lambda_{MoK\alpha}$ in Å	0.71073
θ_{min} in °	1.85
θ_{max} in °	36.36
Index range	$-25 \le h \le 25$ $-54 \le k \le 54$ $-31 \le l \le 30$
μ in mm^{-1}	0.873
Abs. correction	multi-Scan
Reflections collected	556831
Reflections unique	44872
R_{int}	0.0586
Reflections obs. [F>2σ(F)]	35761
Residual densityin e Å^{-3}	1.244/-0.908
Params/restraints	1179/804
GOOF	1.049
R_1 [I>2σ(I)]	0.0452
wR_2 (all data)	0.1247

6.4.7. Graphical representation of the molecular structures of the crystallized compounds

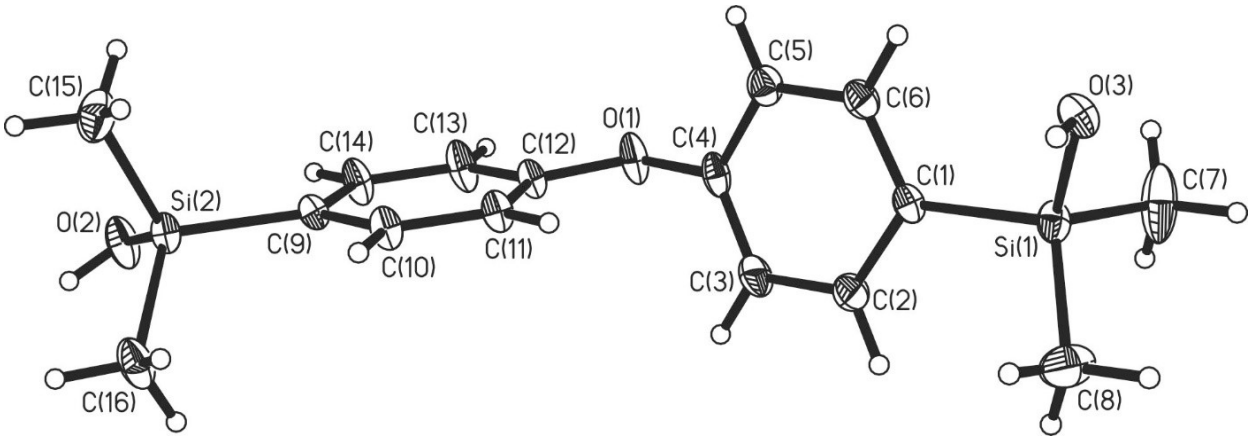


Figure 48: Molecular structure of **2o** (CCDC 2190210). It contained two crystallographically independent molecules of $C_{16}H_{22}O_3Si_2$ and a severely disordered chloroform molecule.

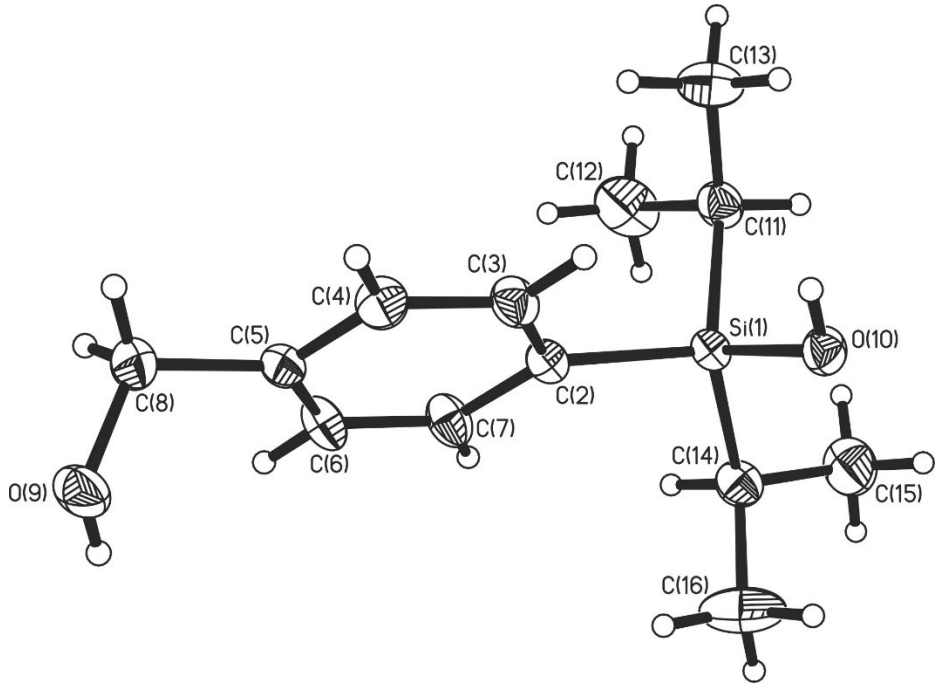


Figure 49: Molecular structure of the silanol **2p**.

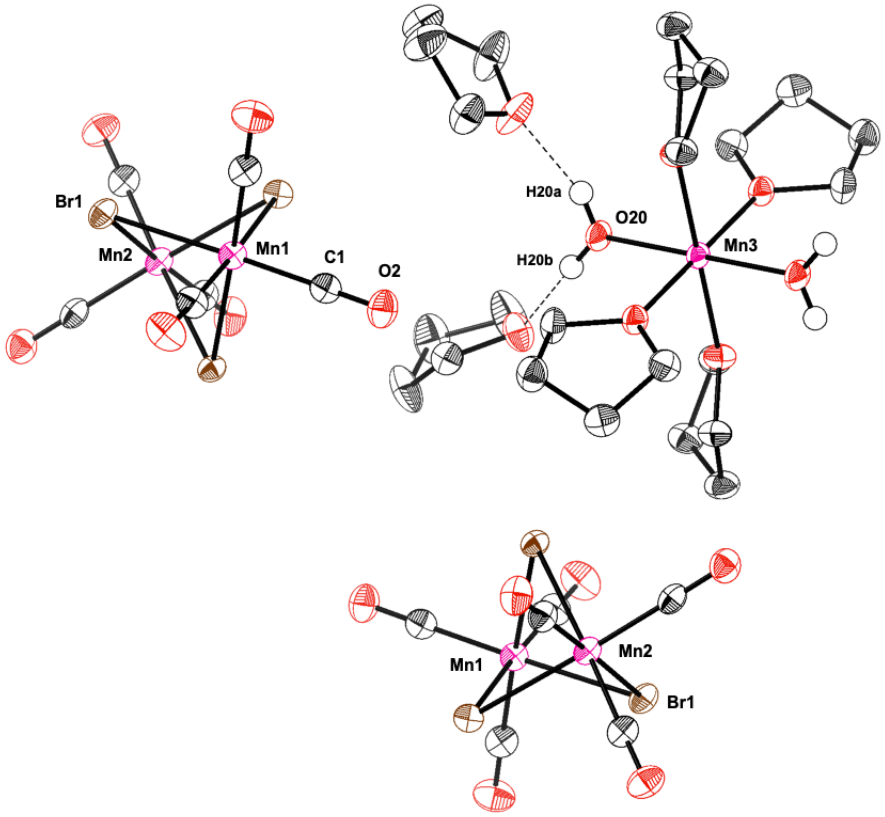


Figure 50: Complete molecular structure of complex **Mn-7**.

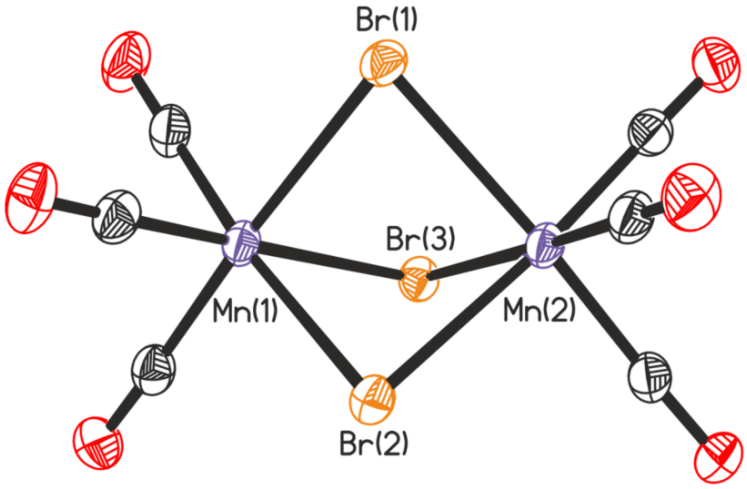


Figure 51: Detail of the dinuclear anion of **Mn-7**.

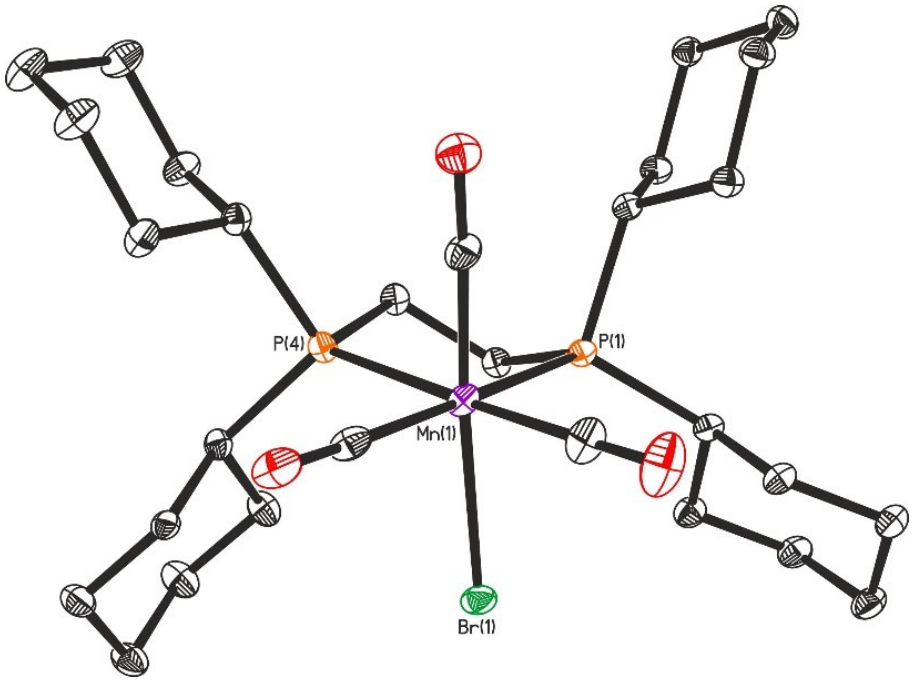


Figure 52: Molecular structure of the complex **Mn-10.**

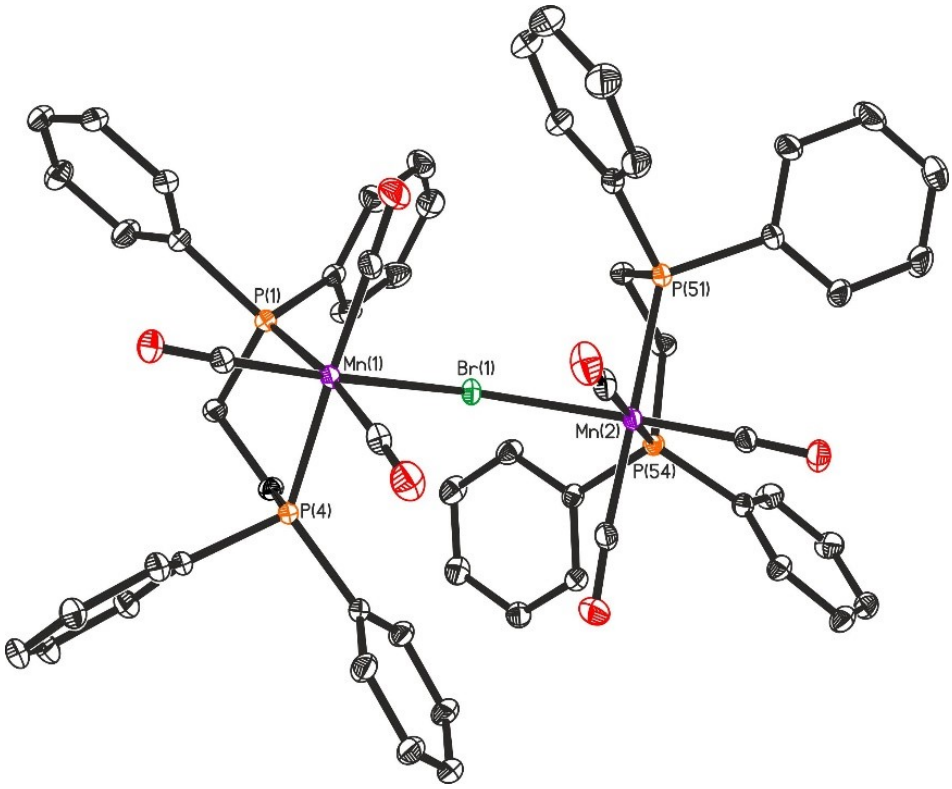


Figure 53: Molecular structure of the complex **Mn-12**.

The asymmetric unit of **Mn-12** contains a complex dimanganese cation, a barf-anion and severely disordered dichloromethane molecules located in a solvent accessible volume of about 291 Å.[3] The scattering contribution of the solvent was removed using the Platon/SQUEEZE program package[3] since an

attempt to model the disorder was not completely satisfying. A total of 86 electrons per void was found which corresponds to the calculated number of electrons of two dichloromethane molecules. Two CF_3-groups in the barf-anion were treated by a split atom model. EADP, SIMU, ISOR and SADI instructions of ShelXL were used for refinement of the corresponding atom positions.

6.5. Supplementary Kinetic Section

The data presented in Section 3.4.2 have been analyzed according to the Variable Time Normalization Analysis method.[4-6] It is a graphical method for analyzing kinetic data, and it can be applied to each component of a reaction to study its order in the kinetic equation.

Mathematically, the concentration profiles in (in the case analyzed, of $PhMe_2SiOH$) in different experiments differing in the concentration of a reactant **A**, will overlap only when the time axis (t) is replaced by the time integral of the concentration of **A** raised to the correct power alpha, order of **A** in the reaction. The approximation that this method applies, is the one reported in **Figure 54**.

$$\int_{t=0}^{t=n} [\mathrm{A}]^{\alpha} \mathrm{d}t = \sum_{i=1}^{n} \left(\frac{[\mathrm{A}]_i - [\mathrm{A}]_{i-1}}{2} \right)^{\alpha} (t_i - t_{i-1})$$

Figure 54: Trapezoid rule applied to approximate the integral value of the function [A](t) between t = 0 and the desired t = n**.**

The complete set of data of each component of the reaction are reported here in the Appendix, together with the same data analyzed using the more traditional *initial rates method* for completeness and showing a very similar result.

6.5.1.Order in [MnBr(CO)$_5$]

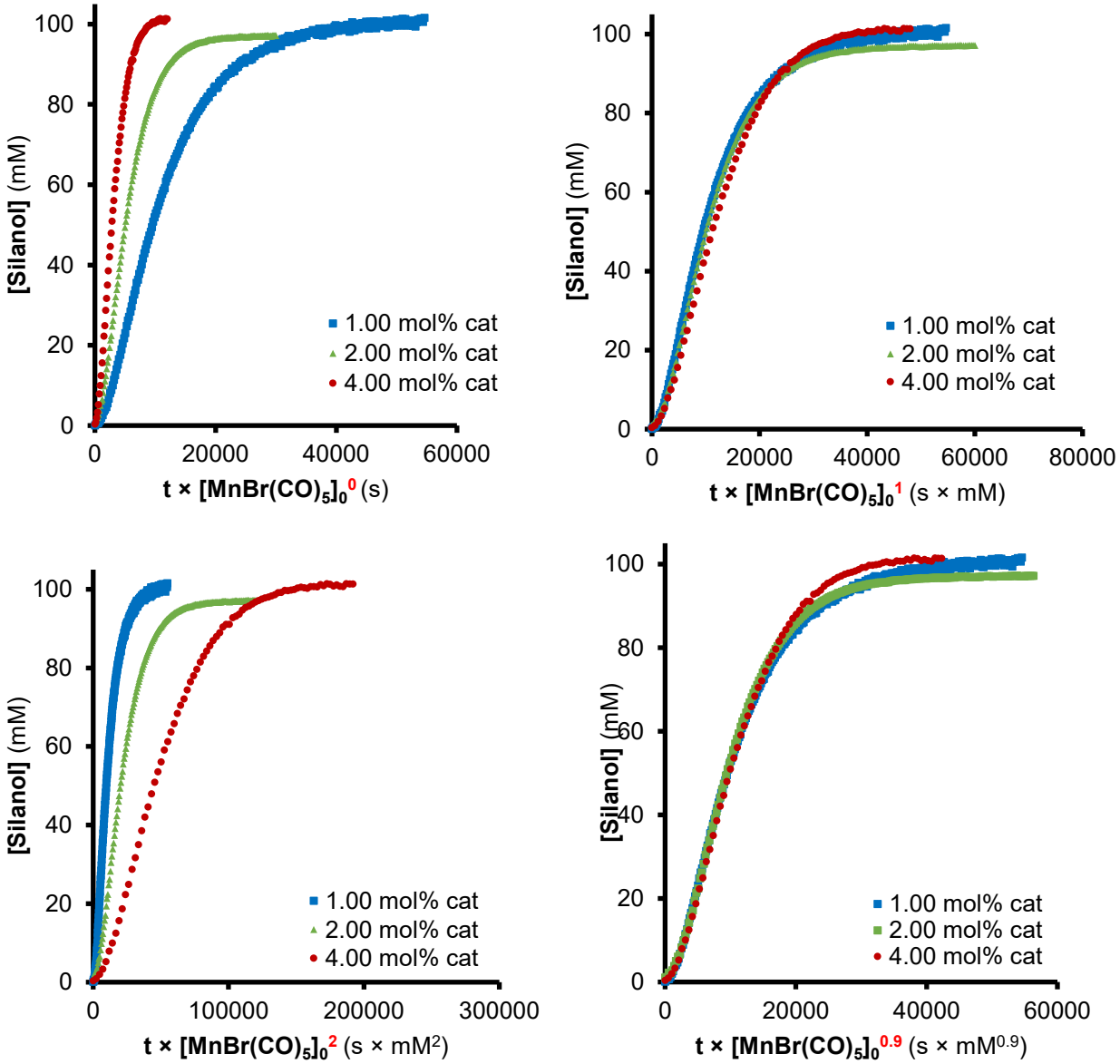
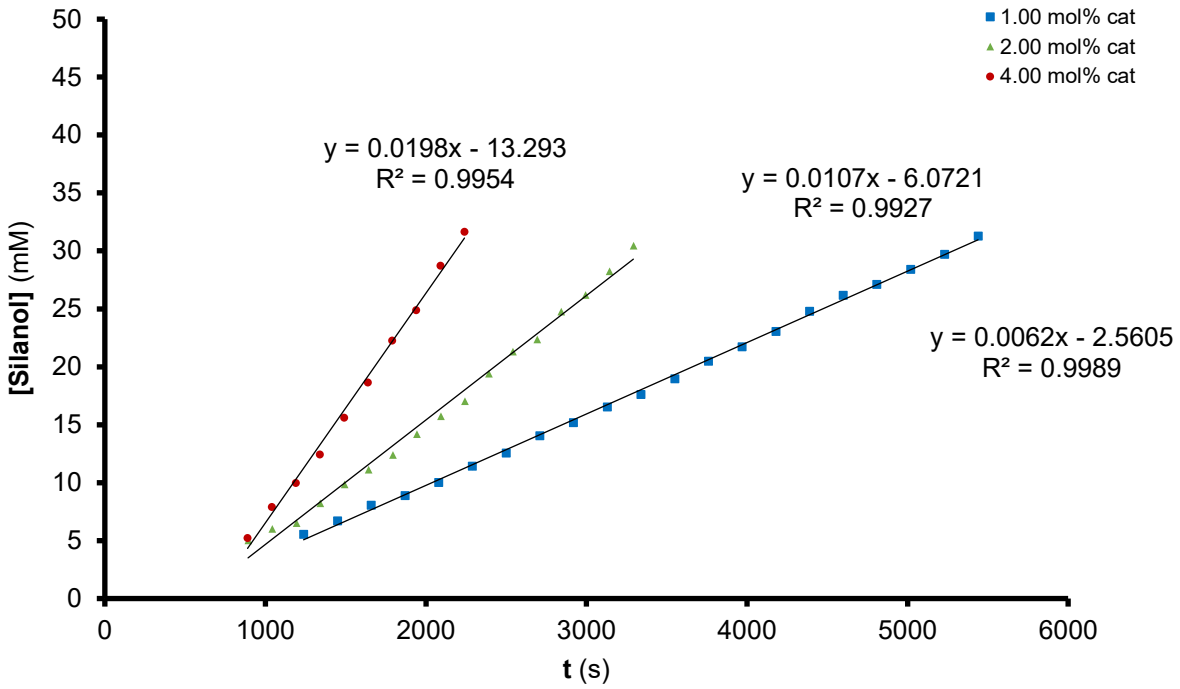
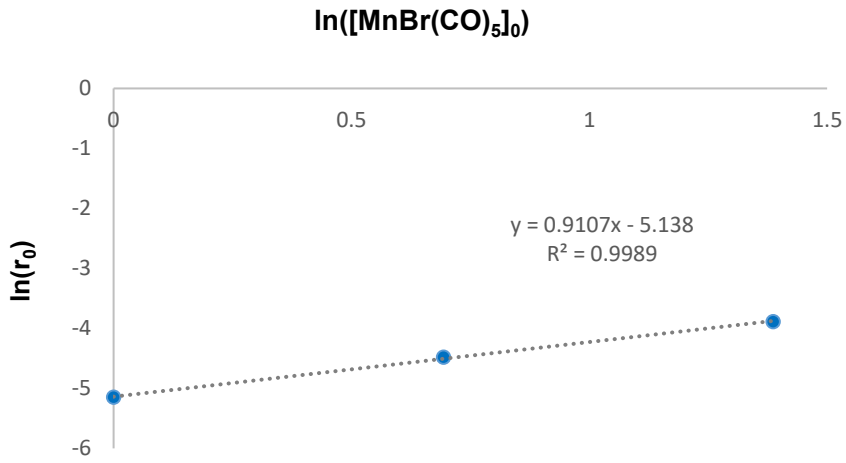


Figure 55: Plots obtained *via* VTNA of the NMR data where the initial concentration of [MnBr(CO)$_5$], **[MnBr(CO)$_5$]$_0$**, is elevated to different exponents, as described in the above paragraph.

.





[MnBr(CO)$_5$] (mM)	r_0 (mM/s)	ln([MnBr(CO)$_5$]$_0$)	ln(r_0)
1	0.0062	0	-5.1499
2	0.0107	0.693147181	-4.48295
4	0.0198	1.386294361	-3.88733

Figure 56: Results obtained with the initial rates method to determine the order of [MnBr(CO)$_5$] in the initial reaction rate.

6.5.2. Order in $PhMe_2SiH$

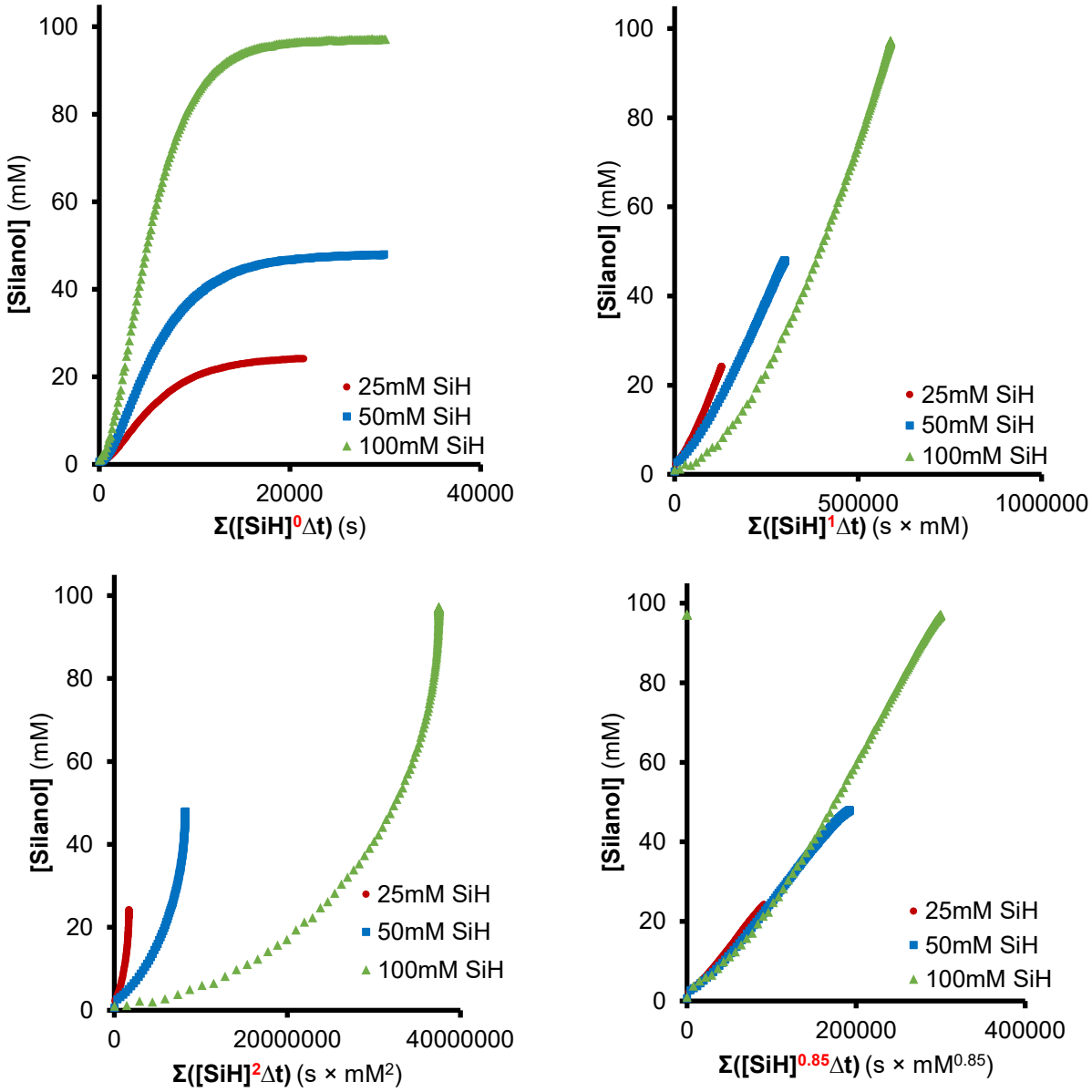
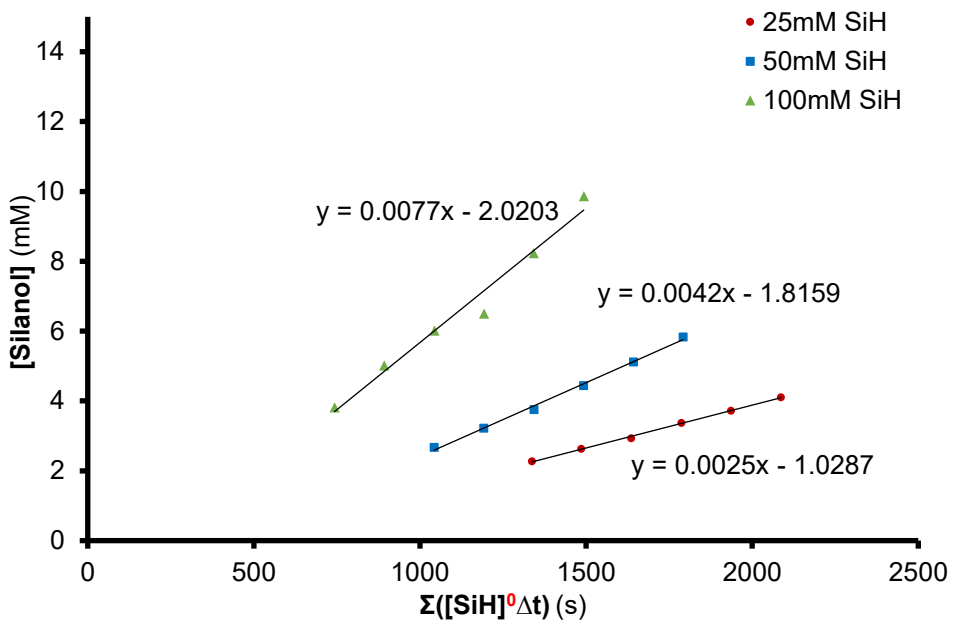
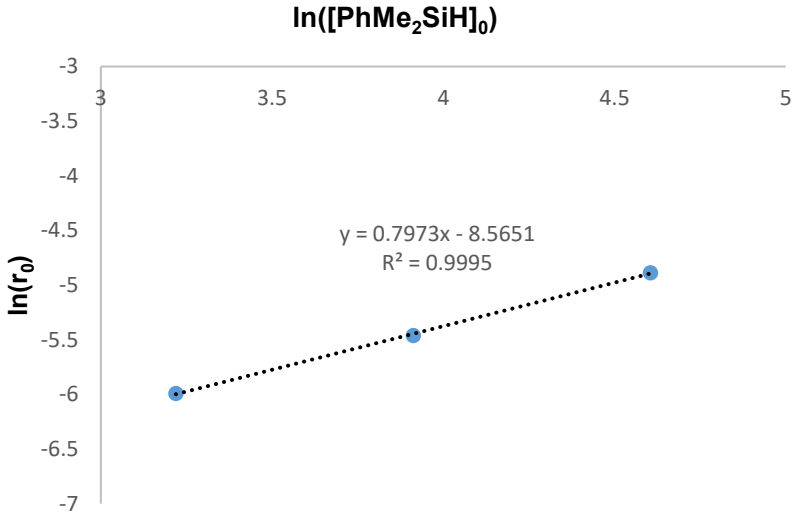


Figure 57: Plots obtained *via* VTNA of the NMR data where the concentration of $PhMe_2SiH$ is elevated to different exponents as described in the above paragraph.





$[PhMe_2SiH]_0$	r_{01} (mM/s)	r_{02} (mM/s)	r_0 (mM/s)	$\ln([PhMe_2SiH]_0)$	$\ln(r_0)$
100	0.0077	0.0074	0.00755	4.60517	-4.88621
50	0.0042	0.0043	0.00425	3.912023	-5.46084
25	0.0025	0.0025	0.0025	3.218876	-5.99146

Figure 58: Results obtained with the initial rates method to determine the order of $PhMe_2SiH$ in the initial reaction rate.

6.5.3.Order in H_2O

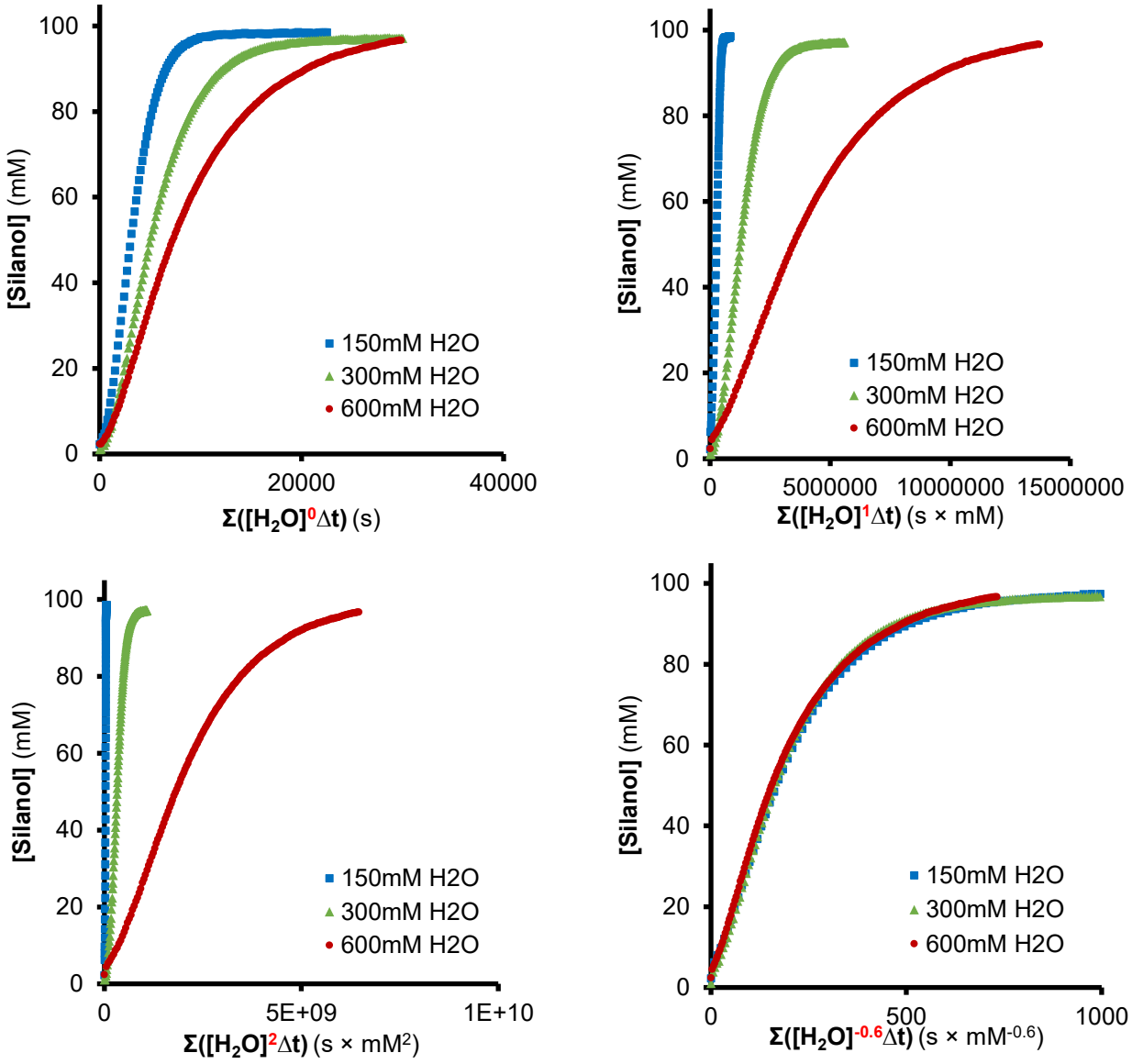
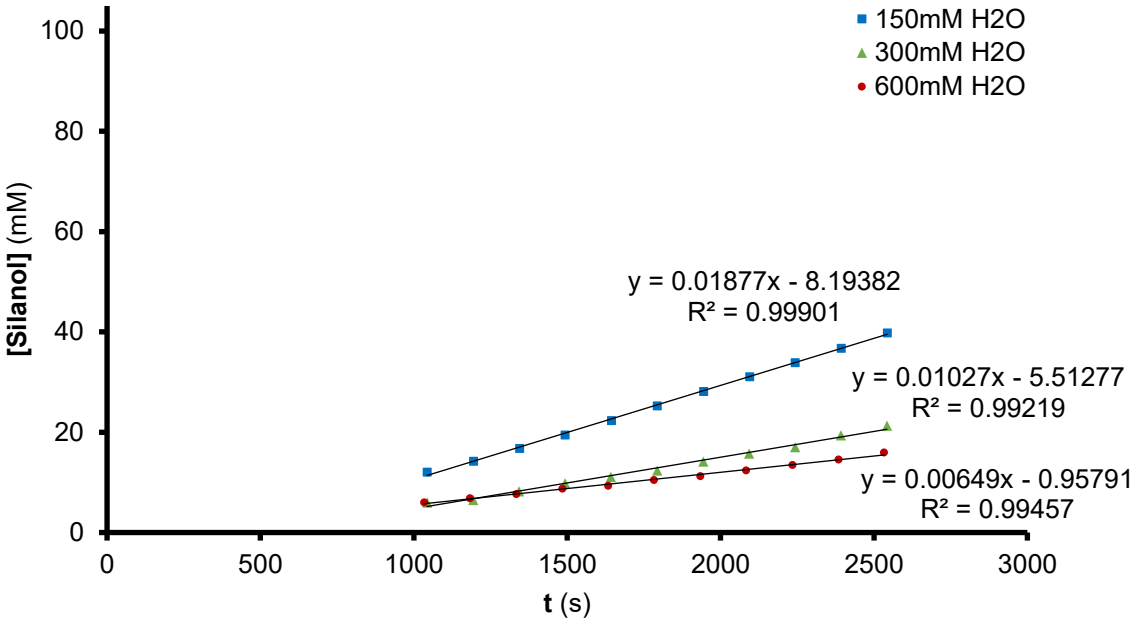
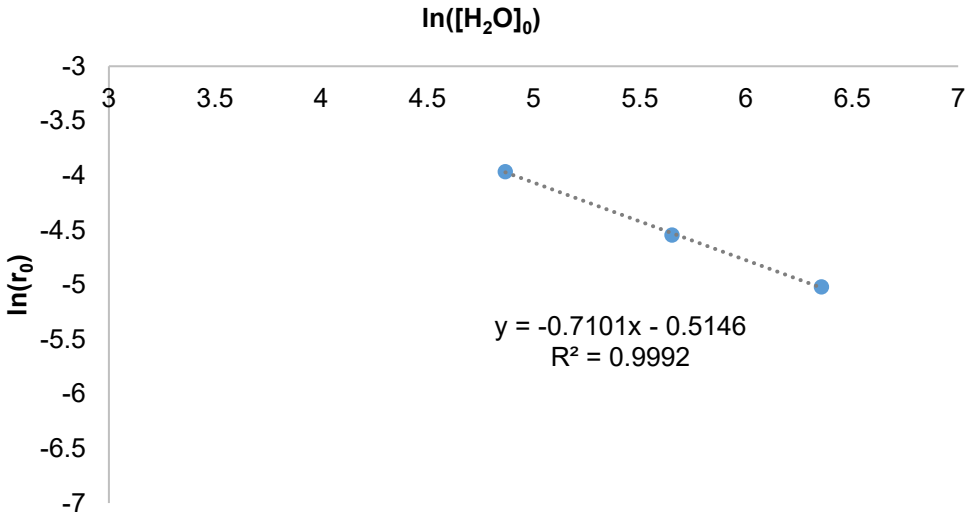


Figure 59: Plots obtained *via* VTNA of the NMR data where the concentration of H_2O is elevated to different exponents, as described in the above paragraph.





$[H_2O]_0$ (mM)	r_0 (mM/s)	$\ln([H_2O]_0)$	$\ln(r_0)$
130	0.01872	4.867534	-3.97816
285	0.01096	5.652489	-4.5135
576	0.00649	6.356108	-5.03749

Figure 60: : Results obtained with the initial rates method to determine the order of H_2O in the initial reaction rate.

6.6. Relevant Spectra for Flow FT-IR

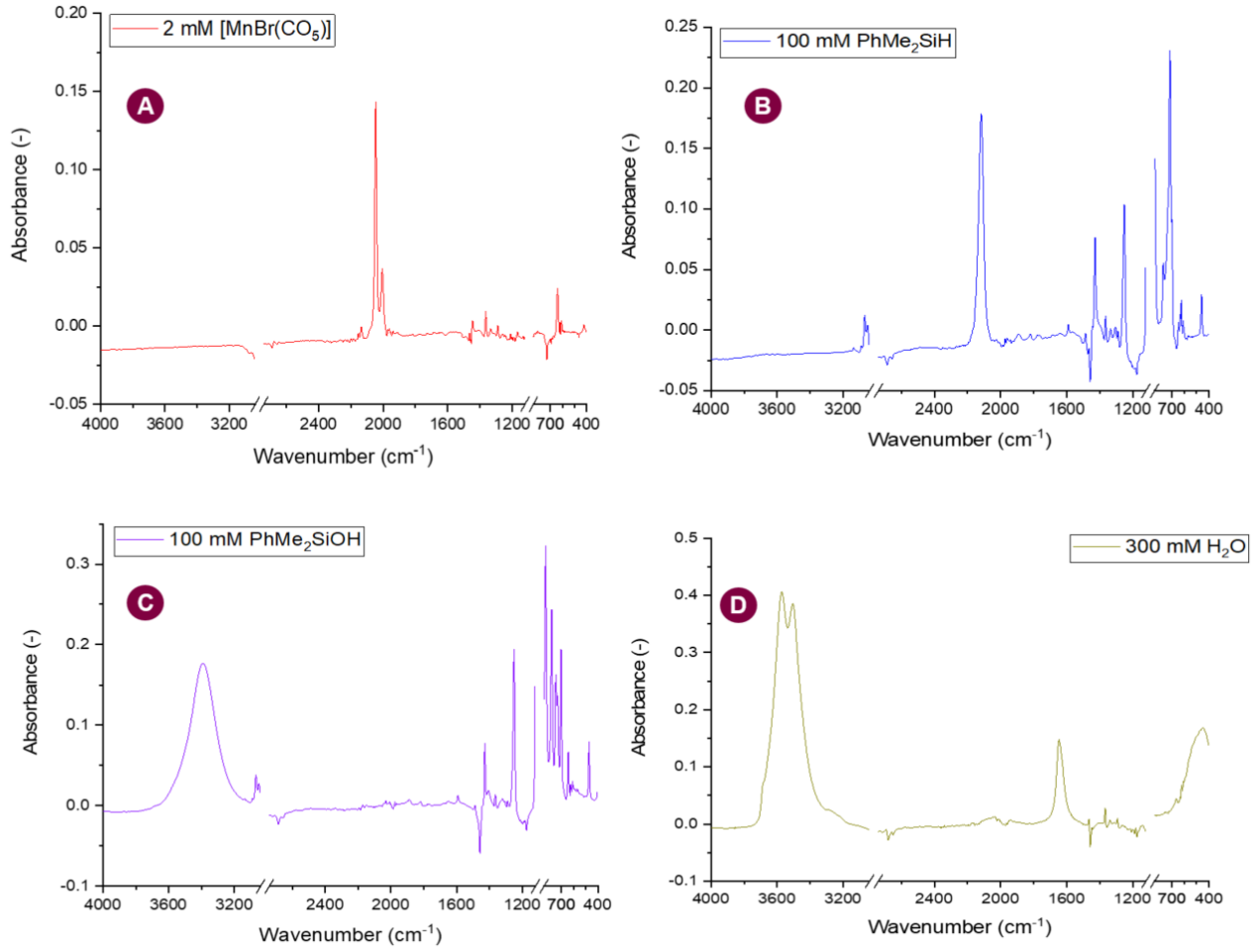


Figure 61: Selected spectra of the reaction components studied in the reaction at the respective concentrations used in the experiment. The areas where the THF-solvent cutoff is present have been removed.

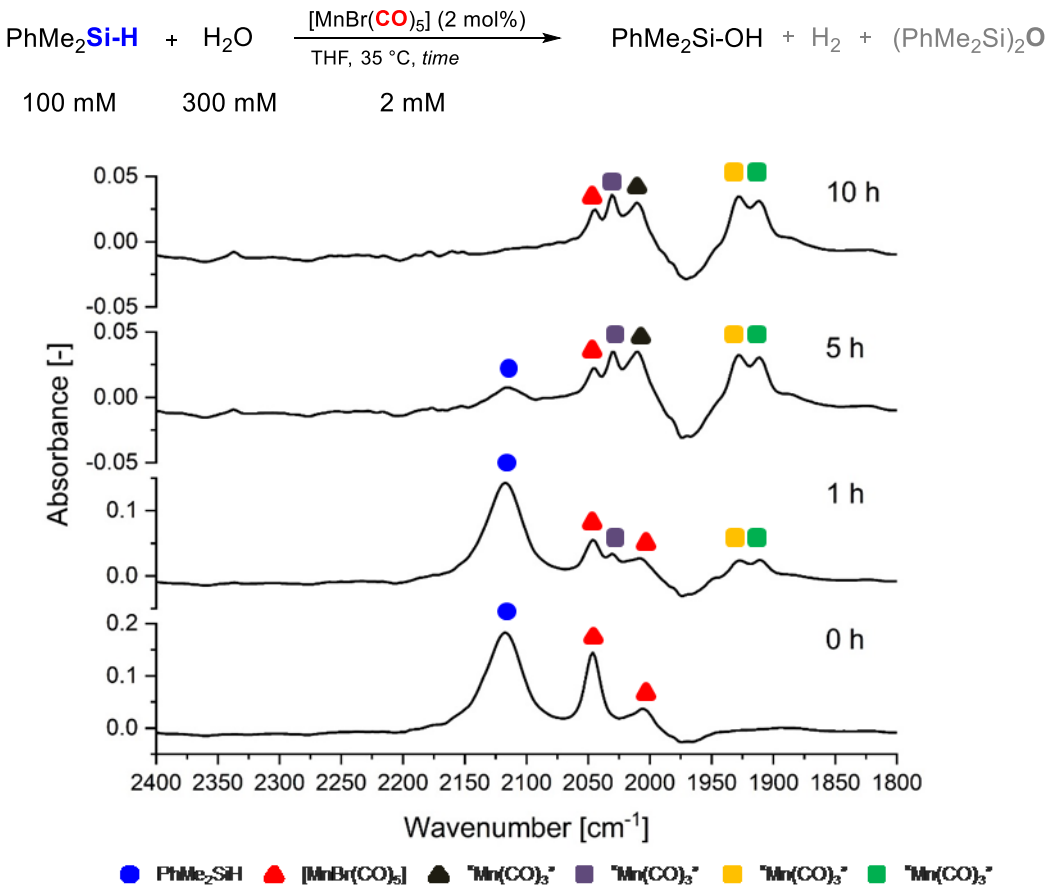


Figure 62: Selected spectra since the beginning of the reaction above.

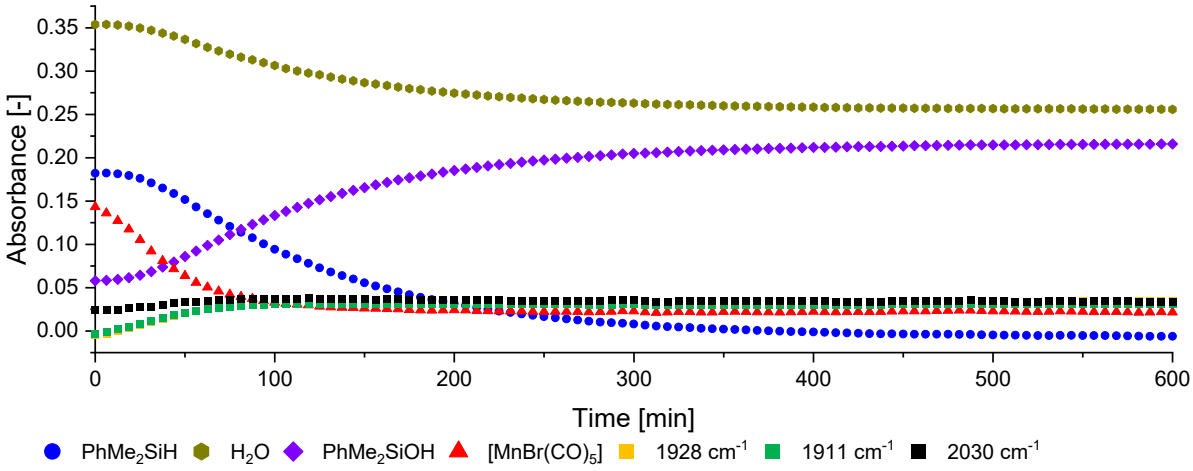
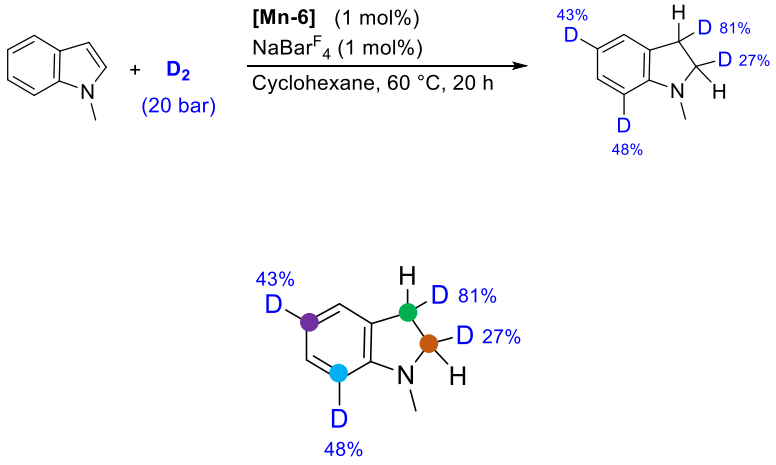


Figure 63: Plot reporting the absorbance of a specific wavelength over time for the reaction reported in **Figure 62**.

6.7. Supplementary Spectra for the Deuteration of 1-methylindole and 1-methylindoline



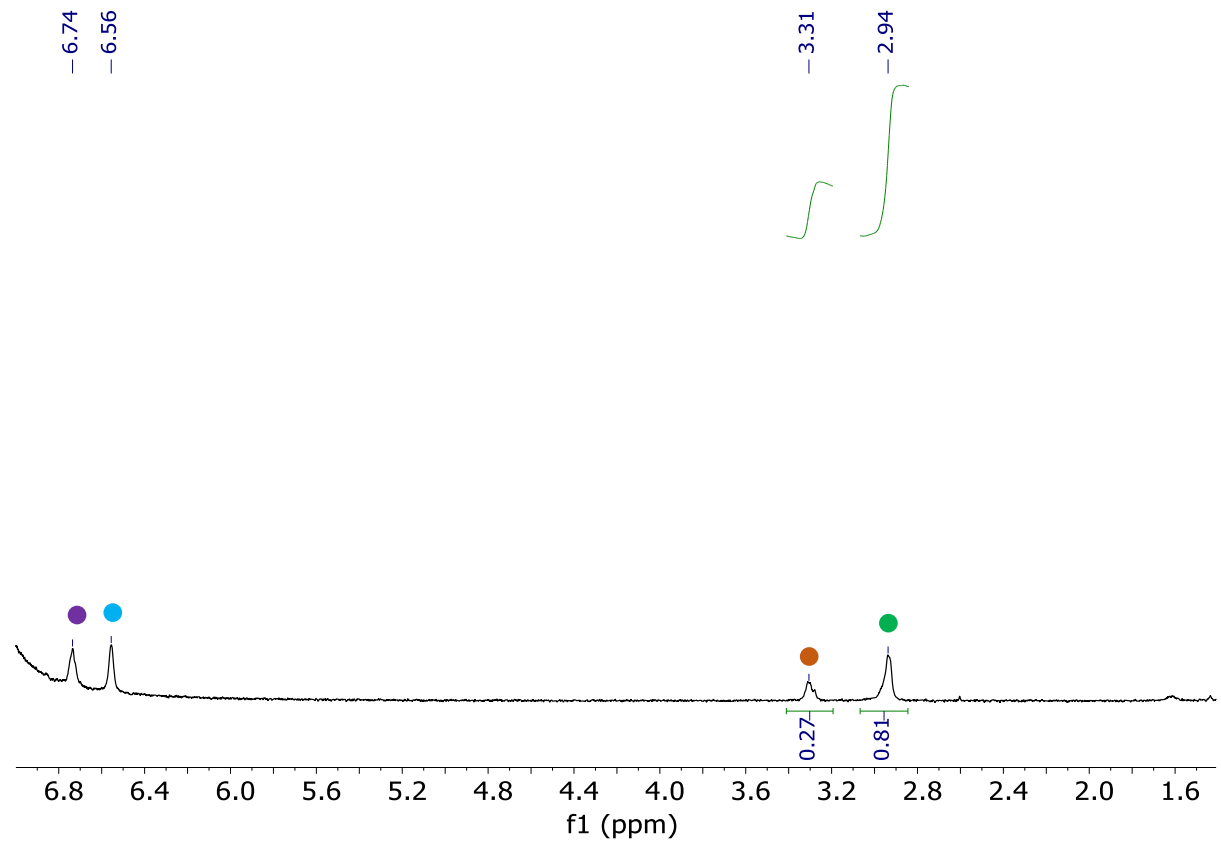


Figure 64: ^{2}H-NMR (92 MHz, $CDCl_3$) spectrum of the crude reaction mixture reported above in the presence of Benzyl alcohol as NMR standard.

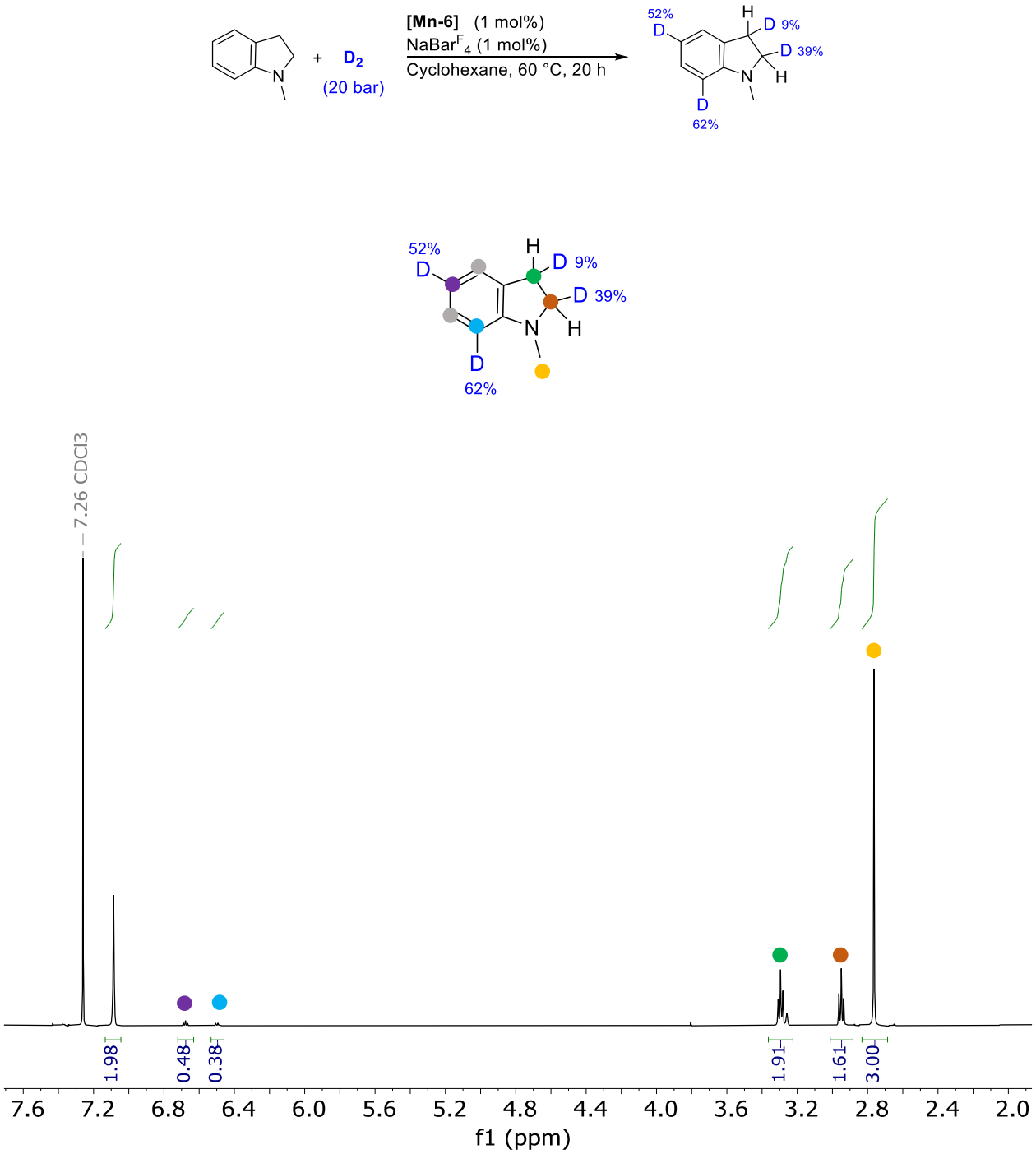


Figure 65: ^{1}H-NMR (600 MHz, $CDCl_3$) spectrum of the crude reaction mixture reported in Scheme 49.

6.8. Characterization Data of the Complex Mn-13

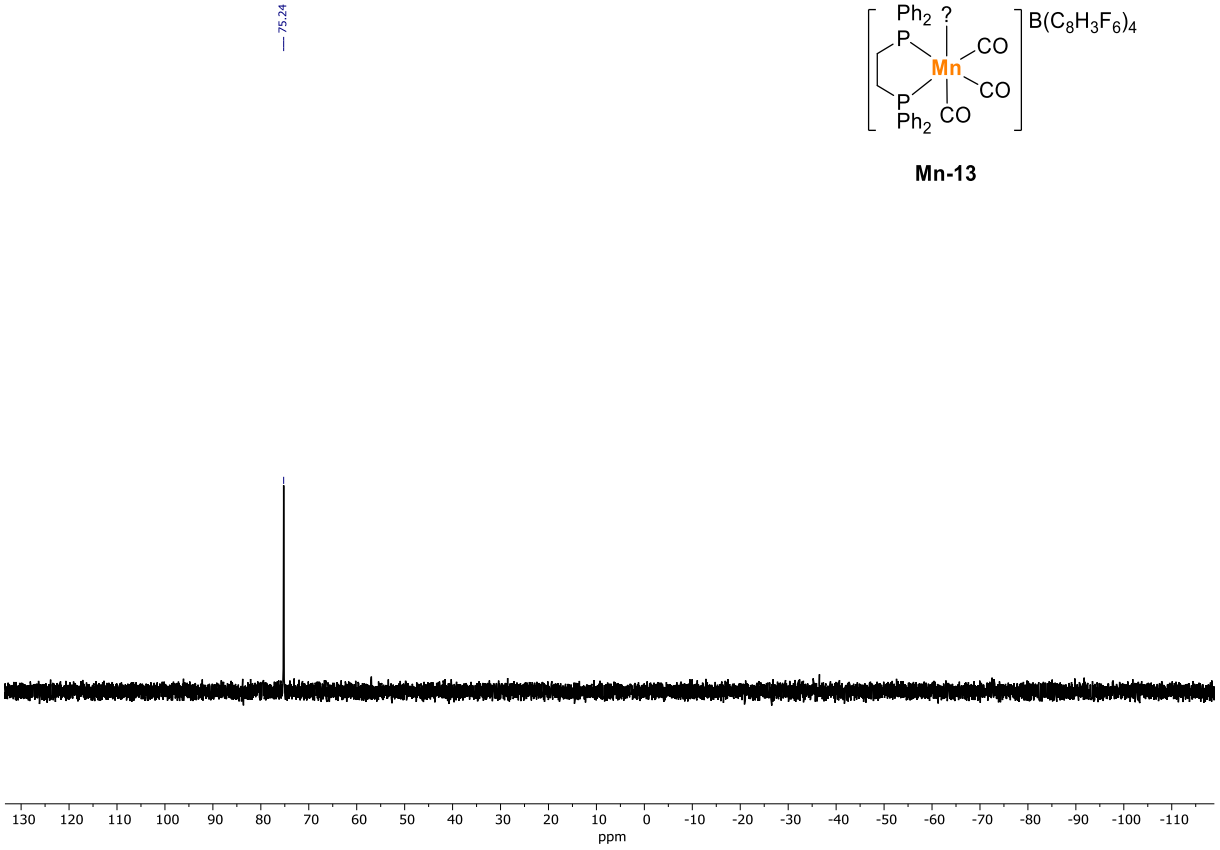


Figure 66: $^{31}P\{^{1}H\}$-NMR (162 MHz, Benzene-d_6) spectrum of the complex **Mn-13**.

6.9. References

1. Krause, L.; Herbst-Irmer, R.; Sheldrick, G. M.; Stalke, D. Comparison of Silver and Molybdenum Microfocus X-Ray Sources for Single-Crystal Structure Determination. *J. Appl. Cryst.* **2015**, *48* (1), 3–10.

2. APEX4 v2022.1-1 program package, Bruker AXS, Karlsruhe, Germany, 2022

3. Spek, A. L. PLATON SQUEEZE: A Tool for the Calculation of the Disordered Solvent Contribution to the Calculated Structure Factors. *Acta Cryst. C* **2015**, *71* (1), 9–18.

4. Burés, J., Variable Time Normalization Analysis: General Graphical Elucidation of Reaction Orders from Concentration Profiles. *Angew. Chem. Int. Ed.* **2016,** *55* (52), 16084-16087.

5. Burés, J., A Simple Graphical Method to Determine the Order in Catalyst. *Angew. Chem. Int. Ed.* **2016,** *55* (6), 2028-2031.

6. Nielsen, C. D. T.; Burés, J., Visual kinetic analysis. *Chem. Sci.* **2019,** *10* (2), 348-353.